2019

How are Interannual Variations of Land Surface Phenology in the Highland Pastures of Kyrgyzstan Modulated by Terrain, Snow Cover Seasonality, and Climate Oscillations? An Investigation Using Multi-Source Remote Sensing Data

Monika Anna Tomaszewska
South Dakota State University

HOW ARE INTERANNUAL VARIATIONS OF LAND SURFACE PHENOLOGY IN THE HIGHLAND PASTURES OF KYRGYZSTAN MODULATED BY TERRAIN, SNOW COVER SEASONALITY, AND CLIMATE OSCILLATIONS? AN INVESTIGATION USING MULTI-SOURCE REMOTE SENSING DATA

BY

MONIKA ANNA TOMASZEWSKA

A dissertation submitted in partial fulfillment of the requirements for the

Doctor of Philosophy

Major in Geospatial Science and Engineering

Specialization in Remote Sensing Geography

South Dakota State University

2019

DISSERTATION ACCEPTANCE PAGE

Monika Anna Tomaszewska

This dissertation is approved as a creditable and independent investigation by a candidate for the Doctor of Philosophy degree and is acceptable for meeting the dissertation requirements for this degree. Acceptance of this does not imply that the conclusions reached by the candidate are necessarily the conclusions of the major department.

Geoffrey M Henebry
Advisor Date

Robert Watrel
Department Head Date

Dean, Graduate School Date

This dissertation is dedicated to my beloved parents.

ACKNOWLEDGEMENTS

I would like to express my sincere gratitude to all of those who supported me and helped throughout the last four years on my path for PhD degree.

At first, I would like to thank my parents, Anna and Janusz, who have always cheered for me and have been the first to support. Dziękuję Najlepsi!

I am especially grateful to my dissertation advisor Professor Geoffrey M. Henebry for his limitless patience, incredible guidance and all the chances to develop, improve and reach higher. I wish that every graduate student would have an opportunity for such an amazing mentorship. Professor Henebry supported me not only in pursuing PhD degree but also in my private life, by taking great care of me, which I will never forget and will always be indebted.

I would like to acknowledge my former and current PhD advisory committee members, Dr. David Roy (Michigan State University), Dr. Michael Wimberly (University of Oklahoma), Dr. Rasmus Houborg (Planet Labs, CA), Dr. Xiaoyang Zhang (SDSU), Dr. Christopher J. Crawford (USGS/EROS) and Graduate Faculty Representative Dr. Robin Brown (SDSU).

For his great help with data processing and coding, words of recognition go to Dr. Lan H. Nguyen (University of Calgary), a former PhD student at Geospatial Science Center of Excellence, SDSU.

I am very thankful for all the encouragement and support from Professor Katarzyna Dąbrowska-Zielińska (Institute of Geodesy and Cartography Warsaw, Poland) for being my mentor and inspiring me to make big decisions about my life and career. I also

appreciate much all the cheering and help from former colleagues from IGiK, especially Dr. Agata Hościło and Dr. Przemysław Dykowski.

Although I cannot name all family members and friends who always supported me, thus, I will express it in persona, but at least, I want to highlight here, how much grateful I am.

This acknowledgement would not be full if I did not thank my South Dakota's family (Mr. and Mrs. Ruane) who have been of great importance to me during the last year of the PhD program, and will be always in my heart.

Finally, I would like to thank all medical and nursing staff from Prairie Center at Avera McKennan in Sioux Falls, SD for their hard work on my health, so I was able to focus entirely on this research and dissertation.

TABLE OF CONTENTS

ABBREVIATIONS

AATSR	Advanced Along-Track Scanning Radiometer
ADB	Asian Development Bank
AGDD	Accumulated Growing Degree-Days
AMO	Atlantic Multidecadal Oscillation
AO	Arctic Oscillation
ATSR-2	Along-Track Scanning Radiometer 2
AUC	Area Under the Curve
AVHRR	Advanced Very High Resolution Radiometer
Bsk	Cold semi-arid climate
BWk	Cold desert climate
CACILM	Central Asia Countries Initiative for Land Management
CV	Cross-validation
CxQ	Convex Quadratic function
DEM	Digital Elevation Model
Dfa	Warm continental/humid continental climate
Dfb	Temperate continental/humid continental climate
DJF	December-January-February
DoSS	Duration of Snow Season
DOY	Day of Year
Dsa	Warm continental climate
Dsb	Temperate continental climate/Mediterranean continental climate
EA/WR	East Atlantic/West Russia
ENSO	El Niño-Southern Oscillation

EOS	End of growing Season
EROS	Earth Resources Observation and Science
EROS	USGS Earth Resources Observation and Science
ERS-2	European Remote sensing Satellite 2
ESA DUE	European Space Agency Data User Element
ESPA	EROS Center Science Processing Architecture (ESPA) On Demand Interface
ETM+	Enhanced Thematic Mapper Plus
EVI	Enhanced Vegetation Index
EVI2	two-band Enhanced Vegetation Index
FAO	Food and Agriculture Organization of the United Nations
$\mathbf{F_{calc}}$	calculated F-value
$\mathbf{F_{crit}}$	critical value for the F distribution
FDoS	First Date of Snow
GDD	Growing Degree-Days
GIMMS	Global Inventory Modeling and Mapping Studies
GlobSnow	Global Snow Monitoring for Climate Research
GMTED2010	Global Multi-resolution Terrain Elevation Data 2010
HP	Highly Persistent pastures
HTV	Half-Time Value
IMS	Interactive Multisensor Snow and Ice Mapping System
IPCC	Intergovernmental Panel on Climate Change
JJA	June-July-August
KGZ	Kyrgyzstan
L1TP	Landsat Collection 1 Level-1 Precision and Terrain

LDoS	Last Date of Snow
LOS	Length of growing Season
LSP	Land Surface Phenology
LST	Land Surface Temperature
MAM	March-April-May
MEI	Multivariate ENSO Index
MLR	Multiple linear regression
MOD10A1	MODIS/Terra Snow Cover Daily L3 Global 500m SIN Grid
MOD10A2	MODIS/Terra Snow Cover 8-Day L3 Global 500m SIN Grid
MOD11A1	MODIS/Terra Land Surface Temperature/Emissivity Daily L3 Global 1 km SIN Grid
MOD11A2	MODIS/Terra Land Surface Temperature/Emissivity 8-Day L3 Global 1 km SIN Grid
MODIS	MODerate resolution Imaging Spectroradiometer
MYD11A1	MODIS/Aqua Land Surface Temperature/Emissivity Daily L3 Global 1 km SIN Grid
MYD11A2	MODIS/Aqua Land Surface Temperature/Emissivity 8-Day L3 Global 1 km SIN Grid
NaN	Not a Number
NAO	North Atlantic Oscillation
nd	No data
NDVI	Normalized Difference Vegetation Index
NIR	Near-InfraRed
NOAA	National Oceanic and Atmospheric Administration
ns	not significant
OLI	Operational Land Imager
OLR	Outgoing Longwave Radiation
P	Persistent pastures

PCA	Principal Component Analysis
PH	Peak Height
PLS	Partial Least Squares
POL/EUR	Polar–Eurasian oscillation
QTP	Qinghai-Tibetan Plateau
RA	Rarely Available pastures
RC	Regression Coefficient method
Red	red reflectance
RMSD	Root Mean Square Difference
RMSE	Root Mean Square Error
SCAND	Scandinavian oscillation
SCD	Snow Cover Dates
SLP	Sea Level Pressure
SON	September-October-November
SOS	Start of growing Season
SR	Selectivity Ratio
SRTMGL	Shuttle Radar Topography Mission Global 1 arc-second
SST	Sea Surface Temperature
S-NPP	Suomi National Polar-orbiting Partnership
SWE	Snow Water Equivalent
SWIR	ShortWave InfraRed
TM	Thematic Mapper
TRASP	Topographic Solar-Radiation Aspect Index
TTP	Thermal Time to Peak

USGS	United States Geological Survey
VIP	Variable Importance in Projection
VIIRS	Visible Infrared Imaging Radiometer Suite
VIS	Visible reflectance
WGS-1984	World Geodetic System 1984
WRS-2	Worldwide Reference System 2

LIST OF FIGURES

LIST OF TABLES

ABSTRACT

HOW ARE INTERANNUAL VARIATIONS IN LAND SURFACE PHENOLOGY IN THE HIGHLAND PASTURES OF KYRGYZSTAN MODULATED BY TERRAIN, SNOW COVER SEASONALITY, AND CLIMATE OSCILLATIONS?

AN INVESTIGATION USING MULTI-SOURCE REMOTE SENSING DATA

MONIKA ANNA TOMASZEWSKA

2019

In the semiarid, continental climates of montane Central Asia, with its constant moisture deficit and low relative humidity, agropastoralism constitutes the foundation of the rural economy. In Kyrgyzstan, an impoverished, landlocked republic in Central Asia, herders of the highlands practice vertical transhumance—the annual movement of livestock to higher elevation pastures to take advantage of seasonally available forage resources. Dependency on pasture resource availability during the short mountain growing season makes herds and herders susceptible to changing weather and climate patterns. This dissertation focuses on using remote sensing observations over the highland pastures in Kyrgyzstan to address five interrelated topics: (i) changes in snow cover and its seasonality from 2002 through 2016; (ii) pasture phenology from the perspective of land surface phenology using multi-scale data from 2001 through 2017; (iii) relationships between snow cover seasonality and subsequent land surface phenology; (iv) terrain effects on the snow-phenology interrelations; and (v) the influence of atmospheric teleconnections on modulating the relationships between snow cover seasonality, growing season duration, and pasture phenology.

Results indicate that more territory has been experiencing earlier snow onset than earlier snowmelt, and around equivalent areas with longer and shorter duration of snow seasons. Significant shifts toward earlier snow onset (snowmelt) occurred in western and central (eastern) Kyrgyzstan, and significant duration of the snow season shortening (extension) across western and eastern (northern and southwestern) Kyrgyzstan. Below 3400 m, there was a general trend of significantly earlier snowmelt, and this area of earlier snowmelt was 15 times greater in eastern than western rayons. In terms of land surface phenology, there was a predominant and significant trend of increasing peak greenness, and a significant positive relationship between snow covered dates and modeled peak greenness. While there were more negative correlations between snow cover onset and peak greenness, there were more positive correlations between snowmelt timing and peak greenness, meaning that a longer snow cover season increased the amplitude of peak greenness. The amount of thermal time (measured in accumulated growing degree-days) to reach peak greenness was significantly negatively correlated both with the number of snow covered dates and the snowmelt date. Thus, more snow covered dates translated into fewer growing degree-days accumulated to reach peak greenness in the subsequent growing season. Terrain features influenced the timing of snowmelt more strongly than the number of snow covered dates. Slope was more important than aspect, but the strongest effect appeared from the interaction of aspect and the steepest slopes. The influence of atmospheric teleconnection arising from climate oscillation modes was marginal at the spatial resolutions of this study. Thermal time accumulation could be largely explained with Partial Least Squares (PLS) regression models by elevation and snow cover metrics. However, explanation of peak greenness was less susceptible to terrain and snow cover variables. This research study

provides a comprehensive evaluation of the spatial variation of interannual phenology in the highland pastures that serve as the foundation of rural Kyrgyz economy. Finally, it contributes to a better understanding of recent environmental changes in remote highland Central Asia.

CHAPTER 1

INTRODUCTION

1.1. Background

Agropastoralism relates to a practice of both growing crops and keeping livestock as a livelihood strategy. In the semiarid, continental climate of montane Central Asia with its constant moisture deficit and low relative humidity, agropastoralism serves as the foundation of the rural economy. Specifically, in countries such as Kyrgyzstan, where rangelands constitute 87% of the agricultural land area (FAO, 2015), the extensive herbaceous grasslands form the basis for highlanders' livelihood. A highly mountainous republic, Kyrgyzstan is located in the eastern part of Central Asia and shares borders with Kazakhstan, China, Tajikistan, and Uzbekistan. The total area is just shy of 200,000 km^2 (comparable with the USA states of Nebraska or South Dakota, or with Belarus—the largest landlocked country in Europe) of which 191,801 km^2 is in land and 8,150 km^2 is open water. In 2018, the population of Kyrgyzstan was approximately 6.3M. For comparison, the populations of Nebraska, South Dakota, and Belarus were 1.92M, 0.88M, and 9.45M, respectively. Kyrgyzstan is divided into in seven oblasts or provinces, of which only 36% of the population resides in urban areas with the largest city being the capital Bishkek (WorldBank, 2018).

Mobile pastoralism has been embedded in the cultures of Central Asia for millennia: the first traces of pastoralism in the region are dated to at least 8,000 years ago. During the Soviet era, collectivization ended the traditional nomadic pastoralism in the region. In early 1990s, a daily "home-pasture-home" system was introduced, with herds grazing in the

communal pastures near the settlements, as a replacement for remote grazing (Bekturova and Romanova, 2007; Kerven et al., 2011; Mirzabaev et al., 2016).

Nevertheless, herders of the highlands continue to practice vertical transhumance—the annual movement of livestock to higher elevation pastures to take advantage of seasonally available forage resources (Schillhorn Van Veen, 1995).

In Kyrgyzstan, pastures are classified by distance from the settlements into (i) near-village (winter use, ~23% of the total area of pasture land), (ii) intensive (spring and autumn use, ~32%), or (iii) distant (summer use, ~45%) (SAEPF, 2007). Dependency on pasture resource availability during the short growing season in the mountains makes both herds and herders susceptible to changing weather patterns. In this semi-arid region, precipitation variability is a critical driver of pasture resource dynamics, thus the pastoral livelihoods are especially vulnerable to variability in environmental conditions, such as changes in precipitation that may shift forage availability, quantity, and quality (Hoppe et al., 2016; Vetter, 2005; Zhumanova et al., 2016).

1.1.1. Climate projections and their effects in mountainous Central Asia

The ability of global climate projections to capture the complex dynamics of mountainous environments is particularly limited (Reyer et al., 2017). Moreover, there remains a scarcity of climate change impact studies for Central Asia (Hijioka et al., 2014; Xenarios et al., 2018), despite the region showing special sensitivity to climatic changes (Lioubimtseva and Henebry, 2009; Luo et al., 2018; Yu et al., 2018).

Temperature increases are projected to be higher in summer and fall seasons (Hijioka et al., 2014; Lioubimtseva and Henebry, 2009), and lower in winter (Xu et al., 2017), with a

decrease in precipitation for late spring and summer (Hijioka et al., 2014; Yuan-An et al., 2013), but strong increase in precipitation during winter and early spring (Luo et al., 2018; Yu et al., 2018). Increasing temperatures accelerate shrinkage of glacial ice and snow, and projected warming is expected to change significantly glacier and snow melt timing and magnitude (Luo et al., 2018; Wang et al., 2014). Melt characteristics are particularly important, since seasonal and longer-term water storage are critical ecosystem services provided by mountains, especially in drier climates. Meltwater from glaciers and snow in Tien Shan and Pamir mountains drive river flow and are the main water supply in the region. Recent studies have shown a shift in precipitation from snow to rain, which decreases snowfall fraction and results in less accumulation of snow and glacial ice during the winter (Chen et al., 2016). Changes in snow cover and shrinkage of glaciers lead to alterations in the local water cycle and water storage (Bai et al., 2019; Dedieu et al., 2014) than may further affect vegetation dynamics.

However, there is a substantial uncertainty in precipitation projections due to the scarcity of observational data coupled with the coarse spatial resolution of models that perform poorly over mountainous terrain (Christensen et al., 2013; Reyer et al., 2017). There also remain shortcomings in the models' handling of precipitation due to limited observational data for validation, interpolation methods that tend to smooth the climatological patterns, and comparisons using cross-scale data, e.g., model projections frequently have higher resolutions than the available observational data (Mannig et al., 2013; Rhoades et al., 2018; Stocker et al., 2013).

While increased temperatures may result in an extended growing season that could benefit certain plant species and vegetation communities, enhanced variation in precipitation

timing and amount of water availability (Chen et al., 2016; Immerzeel et al., 2010), and increased incidence of drought may negatively affect vegetation phenology and pasture productivity (Marshall et al., 2019; Petersky et al., 2019). Snowfall dominates the annual precipitation total in montane Central Asia (Aizen et al., 1995; Apel et al., 2018; Sorg et al., 2012); thus, changes in timing and/or magnitude could be especially impactful, since snowmelt is the main contributor to early growing season soil moisture, and most of the seasonal biomass accumulation in pastures relies on this initial store of moisture. Variation in the duration of snow cover and snow depth may affect soil-vegetation interactions. Increased snow cover duration and/or depth could add soil moisture, slow down soil heat exchange, and affect soil heat and moisture preservation that might protect over-winter survival of vegetation from low air temperatures and desiccating winds. It may also influence soil microbial activity and the transformation of soil organic matter and nutrient availability (Groffman et al., 2001; Qiao and Wang, 2019). Earlier snow cover could shield vegetation from lower temperatures by keeping the subniveal temperature at a favorable level and protecting the activity of the soil microorganisms during the winter, which could lead to increased vegetation growth during the following growing season (Qiao and Wang, 2019). On the other hand, lack of snow cover or just a shallow snowpack may increase the frequency of soil freeze-thaw events and, consequently, alter soil nutrient cycling and aboveground productivity (Choler, 2015).

Evaluation of past interactions between snow cover and pasture vegetation and the impacts of snow cover change on pasture dynamics will help to identify where in the Kyrgyz landscape of highland pastures that land surface phenology was sensitive to variable and changing environmental conditions. That knowledge may provide another perspective for

pasture sustainable management programs that address ecological and socioeconomic problems associated with environmental changes, especially in the light of the loss of pasture productivity due to high pasture degradation (Sabyrbekov, 2019).

1.1.2. Remote sensing of snow cover seasonality and highland pasture phenology

Due to the current paucity of ground level data and the fact that most weather stations are located in valleys far from the pastures of interest, satellite remote sensing provides the best avenue for spatially comprehensive observations, albeit at relatively coarse spatial resolutions. Remote sensing products offer the ability to evaluate changes in snow cover extent, snow cover duration, snow cover timing, and land surface temperature, and to monitor land surface phenology that provides a window on vegetation phenology and productivity in highland pastures.

Spatial, temporal, and elevational variations in snow seasonality in Central Asia have been detected and quantified at multiple spatial extents (Dietz et al., 2014, 2013; Liu et al., 2017; Tang et al., 2017; Zhou et al., 2013). Dietz et al. (2013) processed daily MODIS snow cover products between 2000 and 2011 to characterize interannual variation in snow cover across Central Asia with a view to estimating the water content in major regional catchments contributed by snowmelt. They found high spatial and temporal variation in snow cover and no discernible trend in the start, end, or duration of the snow season at this broad scale of analysis. Zhou et al. (2013) used AVHRR (Advanced Very High Resolution Radiometer and MODIS (Moderate Resolution Imaging Spectroradiometer) data to study snow cover trends across the basin of the Amu Darya from 1986 to 2008. They found statistically significant negative trends in snow cover duration, date of snow cover onset, and date of snowmelt across most of the basin, except a significant trend of later snow

onset and a non-significant trend of snow melt in the Central Pamir, especially at elevations greater than 4,000 m. Tang et al. (2017) using simple linear regression to identify and characterize trends in the Tien Shan range using MODIS daily snow products, found decreases in the mean snow-covered area in each of four seasons in the Central Tien Shan ranging from a minimum of -8% in autumn to maximum of -14% in spring, but no trend was statistically significant at $p<0.05$. They also calculated a decrease of -12% in the duration of snow cover in the Central Tien Shan from 2001 to 2015, but it was also not significant.

There are many methods to simulate the temporal variation of vegetation index time series so as to characterize land surface phenology, including threshold, derivative, smoothing algorithms, and model fit (de Beurs and Henebry, 2010a). Those methods use one or more remotely sensed vegetation indices (VIs), such as the Normalized Difference Vegetation Index (NDVI), the most common remotely sensed vegetation index, which usesthe differential reflectance at the visible and near infrared parts of the spectrum as a proxy for active green vegetation (Myneni et al., 1995; Tucker, 1979). Land surface phenology (LSP) metrics are many, but some of the most common are (i) onset of greening (start of growing season, SOS), (ii) end of greenness (end of growing season, EOS), (iii) timing of the growing season maximum, and (iv) growing season length (de Beurs and Henebry, 2010a). The simplest method to determine LSP metrics is based on threshold values: for SOS, the date of year when the NDVI crossed the specified threshold first time in upward direction, while EOS, when NDVI crossed the threshold values in downward direction. Threshold values can be set arbitrarily (Fischer, 1994; Lloyd, 1990; Myneni et al., 1997; Reed et al., 2003; Zhou et al., 2003) or calculated based on long-term mean of NDVI (Karlsen et al.,

2006; Piao et al., 2006), a baseline year (Shabanov et al., 2002), NDVI ratios (White et al., 1997), or using another remote sensing index (Delbart et al., 2005). Other authors have been using derivatives of NDVI curves, and defined the SOS as the time of the greatest increase of NDVI, and the lowest negative derivative as EOS (Moulin et al., 1997; Tateishi and Ebata, 2004). Smoothing algorithms include using an autoregressive moving average function that determines SOS and EOS as the dates, when a smoothed time series of VI crosses a curve established from moving average models (Archibald and Scholes, 2007; Reed et al., 1994). Another approach has been to apply Fourier analysis that approximates complex curves with a sum of sinusoidal waves of multiple frequencies (de Jong et al., 2011; Jakubauskas et al., 2001; Moody and Johnson, 2001; Zhou et al., 2015).There are multiple approaches to model fitting, especially more commonly used the piecewise logistic curve (and its modification) (Zhang, 2015; Zhang et al., 2003). It has been widely utilized to generate global phenology products delivered from MODIS Collection 5 (Ganguly et al., 2010), AVHRR dataset (Zhang et al., 2014) and NPP VIIRS (Zhang et al., 2018) or used for a basis of other algorithms e.g. Landsat phenology algorithm (Melaas et al., 2013).However, there is an argument that the logistic curve seems to be better suited to woody vegetated landscapes (Ahl et al., 2006; Baumann et al., 2017; Nguyen et al., 2018; Zhang et al., 2003). For the more recent MODIS Collection 6 (Gray et al., 2019), the smoothing penalized cubic spline method has been used for phenological phase detection. This approach uses prescribed thresholds in the amplitude of variation in two-band Enhanced Vegetation Index (EVI2; Jiang et al., 2008) for each phenological cycle (Moon et al., 2019).

For modeling the LSP of herbaceous vegetation outside of the tropics, studies have shown that a good approximation of the temporal vegetation development, observed using the NDVI or the Enhanced Vegetation Index EVI (Huete et al., 2002), can be achieved using a downward-arching convex quadratic (CxQ) model that links the VI to accumulated growing degree-days (AGDD), which measure thermal time using either air temperature orland surface temperature (LST). Since spatially comprehensive remotely sensed LST products are available, they are preferable to interpolated air temperature because growing season LST is highly correlated with insolation and it better approximates the thermal environment experienced by short-statured herbaceous vegetation (Henebry, 2013; Still et al., 2014).

For modeling the LSP of herbaceous vegetation outside of the tropics, studies have shown that a good approximation of the temporal vegetation development, observed using the NDVI or the Enhanced Vegetation Index EVI (Huete et al., 2002), can be achieved using a downward-arching convex quadratic (CxQ) model that links the VI to accumulated growing degree-days (AGDD), which measure thermal time using either air temperature orland surface temperature (LST). Since spatially comprehensive remotely sensed LST products are available, they are preferable to interpolated air temperature because growing season LST is highly correlated with insolation and it better approximates the thermal environment experienced by short-statured herbaceous vegetation (Henebry, 2013; Still et al., 2014). The CxQ model, that captures well the seasonal course of insolation and temperature, has been used successfully for analyzing LSP dynamics at various spatial extents and resolutions as well as temporal durations and resolutions across and within Central Asia (de Beurs et al., 2018; de Beurs and Henebry, 2008b, 2004; Henebry et al.,

2005), Eurasia (de Beurs et al., 2009; de Beurs and Henebry, 2008a, 2005), and North America (Henebry and de Beurs, 2013; Krehbiel et al., 2017; Krehbiel and Henebry, 2016; Nguyen et al., 2018; Walker et al., 2015).

There are recent studies that analyze snow cover impact on pasture phenology using remote sensing products over specific regions in Central Asia and High Mountain Asia, although none of them is focusing specifically on Kyrgyzstan. Paudel and Andersen (2013) explored the response of rangeland vegetation to snow cover dynamics in Nepal Trans Himalayas; whereas, Wan et al. (2014) explored relationships between changes in snow cover and its impact on alpine vegetation in Qinghai-Tibetan Plateau (QTP). More recently, Wang et al. (2018) studied snow cover effects on alpine vegetation growth dynamics over Tibetan Plateau. Relationships between winter snow cover dynamics, climate, and spring grassland phenology in Inner Mongolia (China) were analyzed by Qiao and Wang (2019). Each study found changes in snow cover affecting the length of the growing season and, especially, the start of the growing season, which also influences aboveground net primary production as viewed through NDVI.

Since the interest here is on highland pastures, terrain characteristics cannot be neglected. Terrain complexity affects the pasture phenology dynamics and the relationship between snow seasonality and pasture phenology. In general, longer snow cover favors higher elevations, but terrain features can modify that relationship. Findings of An et al. (2018) over QTP indicate that in complex terrain at high elevations, the shaded locations differ from sun-exposed locations in terms of insolation and thus soil thereby strongly shaping the land surface phenology, with slope playing a key role in the vegetation development. They also showed that the magnitude of terrain modulation depends on vegetation

community characteristics. For example, green-up onset dates of meadow areas across QTP were later over shaded than sun-exposed slopes, while steppe areas did not show any significant aspect effect. Further, both meadow and steppe areas showed earlier dormancy onset dates over shaded slopes.

In semi-arid to arid environments, vegetation dynamics are strongly dependent on weather patterns. Both temperature and precipitation are influenced in part by large-scale climate teleconnections. Previous studies have shown that fluctuations in land surface phenology over the northern hemisphere can be linked to the Northern Annular Mode through the North Atlantic Oscillation and the Arctic Oscillation indices (de Beurs and Henebry, 2010b, 2008a). A more recent study (de Beurs et al., 2018) demonstrates that land surface phenology over Central Asia has been significantly affected by several climate oscillations, which makes the region a "climate change hotspot" (a region in which climate is specially responsive to global change and), where the teleconnections produce strong spatial variations in weather patterns (Bothe et al., 2012; Giorgi, 2006). For example, the winter Multivariate ENSO Index (MEI) is strongly linked to spring and summer precipitation in southeastern Central Asia: SE Kazakhstan, all of Kyrgyzstan, and eastern Tajikistan (de Beurs et al., 2018). In addition, these teleconnections may partially explain why the CMIP5 models did not likely improve upon the precipitation projections from the previous model generation (Flato et al., 2013).

All those environmental complex conditions lead to interannual variation in land surface phenology of highland pastures in Central Asia. Thus, in this study I focus on five interrelated topics that are describe climate-induced impacts on pasture phenology and its variation over 17 years, from 2001 to 2017 across the highlands of Kyrgyzstan.

1) analysis of trends in the seasonality of snow cover
2) analysis of land surface phenology
3) evaluation of relationships between snow cover seasonality and subsequent land surface phenology
4) assessment of the modulation effect of terrain features on the snow cover relationship with land surface phenology
5) investigation of the role of atmospheric teleconnections on modulating relationships between snow cover seasonality, growing season duration, and pasture phenology

Analysis in Task 1 spans across whole area of Kyrgyzstan from 2002 through 2016; Tasks 2-4 are limited to the pastureland areas of Kyrgyz Republic mapped based on updated Soviet maps (Asian Development Bank, 2010a, 2010b); and Task 5 focuses on pastureland areas located in five districts (or rayons) important for livestock production: Chong-Alay, Alay, Kara-Kulja, At-Bashy, and Naryn. Study period of Tasks 2-5 extends from 2001 through 2017.

Let me clearly acknowledge and state that I do not account for human impacts on pasture phenology that may arise from stocking rates and herd management, pasture maintenance and control of invasive species. Each management issue may add to uncertainties that may potentially affect the generalizability of some findings of this study. I do not investigate the rangeland degradation issue; instead, my focus is on climate-induced impacts on pasture vegetation. Moreover, I have focused on the early season green-up dynamics when differential effects from grazing management are expected to be minimal.

1.2. Research studies

I have divided this broad topic into three distinct complementary research studies:

Research study #1

In the research study #1, I analyzed various aspects of snow cover seasonality to detect whether significant changes had occurred in Kyrgyzstan during the early 21st century. Therefore, I asked two questions:

(1.1) Where across Kyrgyzstan have there been significant changes in snow cover seasonality (onset, melt, and duration) from 2002 through 2016?

(1.2) Where significant trends did occur, how were they associated to terrain features?

The results were published in 2018:

Tomaszewska, M.A., Henebry, G.M., 2018. Changing snow seasonality in the highlands of Kyrgyzstan. ***Environmental Research Letters*** 13, 065006. https://doi.org/10.1088/1748-9326/aabd6f

Research study #2

The second research study focused on land surface phenology of highland pastures and its relationships with snow cover seasonality by asking three questions:

(2.1) How does snow cover seasonality relate to subsequent land surface phenology in highland pastures?

(2.2) How does the mountainous terrain modulate snow cover effects?

(2.3) What can recent changes in snow cover seasonality tell us about possible futures for highland pasture phenology and productivity?

These results are in a manuscript that has been reviewed by ***Remote Sensing of Environment***. The manuscript is currently under revision (reviews received 07OCT2019, RSE-D-19-01373, with a revision deadline of 90 days):

Tomaszewska M.A, Nguyen L.H., Henebry G.M., *In revision following review*. Land surface phenology in the highland pastures of montane Central Asia: Interactions with snow cover seasonality and terrain characteristics. ***Remote Sensing of Environment***. (reviews received 07OCT19, RSE-D-19-01373).

Research study #3

In the third research study, I analyzed whether the impacts of oscillation anomalies are detectable and significant in the mountain pastures using LSP metrics based on fine spatial resolution data by asking a question:

(3.1) How much more explanatory power information about oscillation modes might add to explain LSP in mountain pastures of Kyrgyzstan?

These results are in a manuscript that was reviewed by ***International Journal of Applied Earth Observation and Geoinformation***. The manuscript is currently under review following revision (revised manuscript submitted 25NOV2019).

Tomaszewska M.A, Henebry, G.M., *In review following revision.* How much variation in land surface phenology can climate oscillations explain at the scale of mountain pastures in Kyrgyzstan? ***International Journal of Applied Earth Observation and Geoinformation*** (revision submitted 25NOV2019, JAG-2019-1051-R1).

1.3. Significance of the research

My dissertation research provides an advancement of knowledge about 17 years of interannual variability in pasture phenology over the mountainous landscapes of Kyrgyzstan. It is a first study that exclusively focuses on montane pasture phenology in Kyrgyzstan at large scale using remote sensing data. Advanced technical approach, particularly, the use of more than 13K moderate (30 m) spatial resolution images over 17 years for modeling land surface phenology provides uniquely detailed insight into highland pastures and the critical linkage with snow cover seasonality. The study also demonstrates that this large scale, conversely, may not be suitable for linking phenology changes with large and regional-scale atmospheric circulations, even if on the smaller scale they showed significant relationships. I hope this research study will find a use in sustainable mountain development programs by contributing to the explanation of complicated and contingent relationships between pasture, snow, and terrain, especially within the context of ongoing climatic changes in the region.

1.4. Structure of the Dissertation

The dissertation consists of five chapters, where this introduction belongs to chapter one. In the second chapter, I focus on the research study #1, where I analyzed snow cover seasonality to detect whether and where across Kyrgyzstan significant changes have occurred in snow cover onset and snowmelt dates, and snow cover duration. The third chapter (research study #2), which partially uses methods from Chapter Two, provides analyses of land surface phenology in highland pastures from 2001 through 2017 and the relationships between phenological metrics (phenometrics) and aspects of snow cover seasonality, as well as exploring how those relationships differ due to terrain

characteristics. In Chapter Four (research study #3), I focus on the explanatory and predictive power of seasonal climatic oscillation modes that influence weather patterns in the region, on land surface phenology in highland pastures in five rayons of Kyrgyzstan between 2001 and 2017 to determine if the impacts of climatic oscillation modes are detectable at moderate spatial resolution scale. In the final chapter, I summarize the key findings of the research studies, present their conclusions, discuss the various study limitations, and provide recommendations for potential future studies.

1.5. References

Ahl, D.E., Gower, S.T., Burrows, S.N., Shabanov, N. V., Myneni, R.. B., Knyazikhin, Y., 2006. Monitoring spring canopy phenology of a deciduous broadleaf forest using MODIS. https://doi.org/10.1016/j.rse.2006.05.003

Aizen, V.B., Aizen, E.M., Melack, J.M., 1995. Climate, snow cover, glaciers, and runoff in the Tien Shan. J. Am. Water Resour. Assoc. 31, 1113–1129. https://doi.org/10.1111/j.1752-1688.1995.tb03426.x

An, S., Zhang, X., Chen, X., Yan, D., Henebry, G.M., 2018. An Exploration of Terrain Effects on Land Surface Phenology across the Qinghai–Tibet Plateau Using Landsat ETM+ and OLI Data. Remote Sens. 10, 1069. https://doi.org/10.3390/rs10071069

Apel, H., Abdykerimova, Z., Agalhanova, M., Baimaganbetov, A., Gavrilenko, N., Gerlitz, L., Kalashnikova, O., Unger-Shayesteh, K., Vorogushyn, S., Gafurov, A., 2018. Statistical forecast of seasonal discharge in Central Asia using observational records: development of a generic linear modelling tool for operational water resource management. Hydrol. Earth Syst. Sci 22, 2225–2254. https://doi.org/10.5194/hess-22-2225-2018

Archibald, S., Scholes, R.J., 2007. Leaf green-up in a semi-arid African savanna-separating tree and grass responses to environmental cues. J. Veg. Sci. 18, 583–594.

Asian Development Bank, 2010a. Central Asian Countries Initiative for Land Management (CACILM) Multicountry Partnership Framework Support Project [WWW Document]. URL https://www.adb.org/projects/38464-012/main

Asian Development Bank, 2010b. Central Asia Atlas of Natural Resource. Central Asian Countries Initiative for Land Management and Asian Development Bank, Manila, Philippines.

Bai, J., Shi, H., Yu, Q., Xie, Z., Li, L., Luo, G., Jin, N., Li, J., 2019. Satellite-observed vegetation stability in response to changes in climate and total water storage in Central Asia. Sci. Total Environ. 659, 862–871.

https://doi.org/10.1016/J.SCITOTENV.2018.12.418

Baumann, M., Ozdogan, M., Richardson, A.D., Radeloff, V.C., 2017. Phenology from Landsat when data is scarce: Using MODIS and Dynamic Time-Warping to combine multi-year Landsat imagery to derive annual phenology curves. Int. J. Appl. Earth Obs. Geoinf. 54, 72–83. https://doi.org/10.1016/j.jag.2016.09.005

Bekturova, G., Romanova, S., 2007. Traditional Land Management Knowledge in Central Asia: Resource Pack.

Bohovic, R., Dobrovolny, P., Klein, D., 2016. The Spatial and Temporal Dynamics of Remotely-sensed Vegetation Phenology in Central Asia in the 1982–2011 Period. Eur. J. Remote Sens. 49, 279–299. https://doi.org/10.5721/EuJRS20164916

Bothe, O., Fraedrich, K., Zhu, X., 2012. Precipitation climate of Central Asia and the large-scale atmospheric circulation. Theor. Appl. Climatol. 108, 345–354. https://doi.org/10.1007/s00704-011-0537-2

Chen, Y., Li, W., Deng, H., Fang, G., Li, Z., 2016. Changes in Central Asia's Water Tower: Past, Present and Future. Sci. Rep. 6, 35458. https://doi.org/10.1038/srep35458

Choler, P., 2015. Growth response of temperate mountain grasslands to inter-annual variations in snow cover duration. Biogeosciences 12, 3885–3897. https://doi.org/10.5194/bg-12-3885-2015

Christensen, J.H., Kumar, K.K., Aldrian, E., An, S., Cavalcanti, I.F.A., De Castro, M., Dong, W., Goswami, P., Hall, A., Kanyanga, J.K., Kitoh, A., Kossin, J., Lau, N.C., Renwick, J., Stephenson, D.B., Xie, S.P., Zhou, T., 2013. Climate Phenomena and their Relevance for Future Regional Climate Change. In: Climate Change 2013: The Physical Sci- ence Basis. Contribution of Working Group I to the Fifth Assessment Report of the Intergovernmental Panel on Climate Change Coordinating L.

de Beurs, K.. M., Wright, C.K., Henebry, G.M., 2009. Dual scale trend analysis for evaluating climatic and anthropogenic effects on the vegetated land surface in Russia and Kazakhstan. Environ. Res. Lett. 4, 045012. https://doi.org/10.1088/1748-9326/4/4/045012

de Beurs, K.M., Henebry, G.M., 2010a. Spatio-Temporal Statistical Methods for Modelling Land Surface Phenology, in: Hudson, I.L., Keatley, M.R. (Eds.), Phenological Research. Springer Science+Business Media B.V., Dordrecht, pp. 177–208. https://doi.org/10.1007/978-90-481-3335-2_9

de Beurs, K.M., Henebry, G.M., 2010b. A land surface phenology assessment of the northern polar regions using MODIS reflectance time series. Can. J. Remote Sens. 36, S87–S110. https://doi.org/10.5589/m10-021

de Beurs, K.M., Henebry, G.M., 2008a. Northern annular mode effects on the land surface phenologies of northern Eurasia. J. Clim. 21, 4257–4279. https://doi.org/10.1175/2008JCLI2074.1

de Beurs, K.M., Henebry, G.M., 2008b. War, Drought, and Phenology: Changes in the land

surface phenology of Afghanistan since 1982. J. Land Use Sci. 3, 95–111. https://doi.org/10.1109/IGARSS.2006.630

de Beurs, K.M., Henebry, G.M., 2005. Land surface phenology and temperature variation in the International Geosphere-Biosphere Program high-latitude transects. Glob. Chang. Biol. 11, 779–790. https://doi.org/10.1111/j.1365-2486.2005.00949.x

de Beurs, K.M., Henebry, G.M., 2004. Land surface phenology, climatic variation, and institutional change: Analyzing agricultural land cover change in Kazakhstan. Remote Sens. Environ. 89, 497–509. https://doi.org/10.1016/J.RSE.2003.11.006

de Beurs, K.M., Henebry, G.M., Owsley, B.C., Sokolik, I.N., 2018. Large scale climate oscillation impacts on temperature, precipitation and land surface phenology in Central Asia. Environ. Res. Lett. 13, 065018. https://doi.org/10.1088/1748-9326/aac4d0

de Beurs, K.M., Henebry, G.M., Owsley, B.C., Sokolik, I.N., 2015. Using multiple remote sensing perspectives to identify and attribute land surface dynamics in Central Asia 2001-2013. Remote Sens. Environ. 170, 48–61. https://doi.org/10.1016/j.rse.2015.08.018

de Jong, R., de Bruin, S., de Wit, A., Schaepman, M.E., Dent, D.L., 2011. Analysis of monotonic greening and browning trends from global NDVI time-series. Remote Sens. Environ. 115, 692–702. https://doi.org/10.1016/j.rse.2010.10.011

Dedieu, J.P., Lessard-Fontaine, A., Ravazzani, G., Cremonese, E., Shalpykova, G., Beniston, M., 2014. Shifting mountain snow patterns in a changing climate from remote sensing retrieval. Sci. Total Environ. 493, 1267–1279. https://doi.org/10.1016/J.SCITOTENV.2014.04.078

Delbart, N., Kergoat, L., Le Toan, T., Lhermitte, J., Picard, G., 2005. Determination of phenological dates in boreal regions using normalized difference water index. Remote Sens. Environ. 97, 26–38. https://doi.org/10.1016/j.rse.2005.03.011

Dietz, A.J., Conrad, C., Kuenzer, C., Gesell, G., Dech, S., 2014. Identifying changing snow cover characteristics in central Asia between 1986 and 2014 from remote sensing data. Remote Sens. 6, 12752–12775. https://doi.org/10.3390/rs61212752

Dietz, A.J., Kuenzer, C., Conrad, C., 2013. Snow-cover variability in central Asia between 2000 and 2011 derived from improved MODIS daily snow-cover products. Int. J. Remote Sens. 34, 3879–3902. https://doi.org/10.1080/01431161.2013.767480

FAO, 2015. FAOStats: Statistics page of the Food and Agriculture Organisation (FAO) [WWW Document]. URL http://www.fao.org/faostat/en/#data/RL

Fischer, A., 1994. A model for the seasonal variations of vegetation indices in coarse resolution data and its inversion to extract crop parameters. Remote Sens. Environ. 48, 220–230. https://doi.org/10.1016/0034-4257(94)90143-0

Flato, G., Marotzke, J., Abiodun, B., Braconnot, P., Chou, S.C., Collins, W., Cox, P., Driouech, F., Emori, S., Eyvring, V., Forest, C., Gleckler, P., Guilyardi, E., Jakob, C.,

Kattsov, V., Reason, C., Rummukainen, M., 2013. Evaluation of Climate Models, in: Stocker, T.F., Qin, D., Plattner, G.K., Tignor, M., Allen, S.K., Boschung, J., Nauels, A., Xia, Y., Bex, V., Midgley, P.M. (Eds.), Climate Change 2013: The Physical Science Basis. Contribution of Working Group I to the Fifth Assessment Report of the Intergovernmental Panel on Climate Change. Cambridge University Press, Cambridge, United Kingdom and New York, NY, USA, pp. 741–866.

Ganguly, S., Friedl, M.A., Tan, B., Zhang, X., Verma, M., 2010. Land surface phenology from MODIS: Characterization of the Collection 5 global land cover dynamics product. Remote Sens. Environ. 114, 1805–1816. https://doi.org/10.1016/j.rse.2010.04.005

Giorgi, F., 2006. Climate change hot-spots. Geophys. Res. Lett. 33, 1–4. https://doi.org/10.1029/2006GL025734

Gray, J., Sulla-Menashe, D., Friedl, M.A., 2019. User Guide to Collection 6 MODIS Land Cover Dynamics (MCD12Q2) Product.

Groffman, P.M., Driscoll, C.T., Fahey, T.J., Hardy, J.P., Fitzhugh, R.D., Tierney, G.L., 2001. Colder soils in a warmer world: A snow manipulation study in a northern hardwood forest ecosystem. Biogeochemistry 56, 135–150. https://doi.org/10.1023/A:1013039830323

Henebry, G.M., 2013. Phenologies of North American Grasslands and Grasses, in: Schwartz, M.D. (Ed.), Phenology: An Integrative Environmental Science. Springer Netherlands, Dordrecht, pp. 197–210. https://doi.org/10.1007/978-94-007-6925-0

Henebry, G.M., de Beurs, K.M., 2013. Remote Sensing of Land Surface Phenology: A Prospectus, in: Phenology: An Integrative Environmental Science. Springer Netherlands, Dordrecht, pp. 385–411. https://doi.org/10.1007/978-94-007-6925-0_21

Henebry, G.M., de Beurs, K.M., Gitelson, A.A., 2005. Land surface phenologies of Uzbekistan and Turkmenistan between 1982 and 1999. Arid Ecosyst. 11, 25–32.

Hijioka, Y., Lin, E., Pereira, J.J., Corlett, R.T., Cui, X., Insarov, G.E., Lasco, R.D., Lindgren, E., Surjan, A., 2014. Asia.

Hoppe, F., Zhusui Kyzy, T., Usupbaev, A., Schickhoff, U., 2016. Rangeland degradation assessment in Kyrgyzstan: vegetation and soils as indicators of grazing pressure in Naryn Oblast. J. Mt. Sci. 13, 1567–1583. https://doi.org/10.1007/s11629-016-3915-5

Huete, A., Didan, K., Miura, T., Rodriguez, E.P., Gao, X., Ferreira, L.G., 2002. Overview of the radiometric and biophysical performance of the MODIS vegetation indices. Remote Sens. Environ. 83, 195–213. https://doi.org/10.1016/S0034-4257(02)00096-2

Immerzeel, W.W., van Beek, L.P.H., Bierkens, M.F.P., 2010. Climate Change Will Affect the Asian Water Towers. Science (80-.). 328, 1382–5. https://doi.org/10.1126/science.1183188

Jakubauskas, M.E., Legates, D.R., Kastens, J.H., 2001. Harmonic Analysis of Time-Series

AVHRR NDVI Data. Photogramm. Eng. Remote Sens. 67, 461–470.

Jiang, L., Guli·J., Bao, A., Guo, H., Ndayisaba, F., 2017. Vegetation dynamics and responses to climate change and human activities in Central Asia. Sci. Total Environ. 599–600, 967–980. https://doi.org/10.1016/J.SCITOTENV.2017.05.012

Jiang, Z., Huete, A.R., Didan, K., Miura, T., 2008. Development of a two-band enhanced vegetation index without a blue band. Remote Sens. Environ. 112, 3833–3845. https://doi.org/10.1016/j.rse.2008.06.006

Kariyeva, J., van Leeuwen, W.J.D., 2011. Environmental Drivers of NDVI-Based Vegetation Phenology in Central Asia. Remote Sens. 3, 203–246. https://doi.org/10.3390/rs3020203

Kariyeva, J., van Leeuwen, W.J.D., Woodhouse, C.A., 2012. Impacts of climate gradients on the vegetation phenology of major land use types in Central Asia (1981–2008). Front. Earth Sci. 6, 206–225. https://doi.org/10.1007/s11707-012-0315-1

Karlsen, S.R., Elvebakk, A., Høgda, K.A., Johansen, B., 2006. Satellite-based mapping of the growing season and bioclimatic zones in Fennoscandia. Glob. Ecol. Biogeogr. 15, 416–430. https://doi.org/10.1111/j.1466-822X.2006.00234.x

Kerven, C., Steimann, B., Ashley, L., Dear, C., Ur Rahim, I., 2011. Pastoralism and Farming in Central Asia's Mountains: A Research Review (No. 1), MSRC Background Paper. Bishkek, Kyrgyzstan.

Krehbiel, C., Henebry, G., 2016. A Comparison of Multiple Datasets for Monitoring Thermal Time in Urban Areas over the U.S. Upper Midwest. Remote Sens. 8, 297. https://doi.org/10.3390/rs8040297

Krehbiel, C., Zhang, X., Henebry, G., 2017. Impacts of Thermal Time on Land Surface Phenology in Urban Areas. Remote Sens. 9, 499. https://doi.org/10.3390/rs9050499

Lioubimtseva, E., Henebry, G.M., 2009. Climate and environmental change in arid Central Asia: Impacts, vulnerability, and adaptations. J. Arid Environ. 73, 963–977. https://doi.org/10.1016/j.jaridenv.2009.04.022

Liu, J., Zhang, W., 2017. Long term spatio-temporal analyses of snow cover in Central Asia using ERA-Interim and MODIS products. IOP Conf. Ser. Earth Environ. Sci. 57. https://doi.org/10.1088/1755-1315/57/1/012033

Lloyd, D., 1990. A phenological classification of terrestrial vegetation cover using shortwave vegetation index imagery. Int. J. Remote Sens. 11, 2269–2279. https://doi.org/10.1080/01431169008955174

Lu, L., Guo, H., Kuenzer, C., Klein, I., Zhang, L., Li, X., 2014. Analyzing phenological changes with remote sensing data in Central Asia. IOP Conf. Ser. Earth Environ. Sci. 17, 012005. https://doi.org/10.1088/1755-1315/17/1/012005

Luo, M., Liu, T., Meng, F., Duan, Y., Bao, A., Frankl, A., De Maeyer, P., 2018. Spatiotemporal characteristics of future changes in precipitation and temperature in Central Asia. Int. J. Climatol. https://doi.org/10.1002/joc.5901

Mannig, B., Müller, M., Starke, E., Merkenschlager, C., Mao, W., Zhi, X., Podzun, R., Jacob, D., Paeth, H., 2013. Dynamical downscaling of climate change in Central Asia. Glob. Planet. Change 110, 26–39. https://doi.org/10.1016/J.GLOPLACHA.2013.05.008

Marshall, A.M., Link, T.E., Abatzoglou, J.T., Flerchinger, G.N., Marks, D.G., Tedrow, L., 2019. Warming Alters Hydrologic Heterogeneity: Simulated Climate Sensitivity of Hydrology-Based Microrefugia in the Snow-to-Rain Transition Zone. Water Resour. Res. 55, 2122–2141. https://doi.org/10.1029/2018WR023063

Melaas, E.K., Friedl, M.A., Zhu, Z., 2013. Detecting interannual variation in deciduous broadleaf forest phenology using Landsat TM/ETM + data. Remote Sens. Environ. 132, 176–185. https://doi.org/10.1016/J.RSE.2013.01.011

Mirzabaev, A., Ahmed, M., Werner, J., Pender, J., Louhaichi, M., 2016. Rangelands of Central Asia: challenges and opportunities. J Arid L. 8, 93–108. https://doi.org/10.1007/s40333-015-0057-5

Moody, A., Johnson, D.M., 2001. Land-surface phenologies from AVHRR using the discrete fourier transform. Remote 75, 305–323.

Moon, M., Zhang, X., Henebry, G.M., Liu, L., Gray, J.M., Melaas, E.K., Friedl, M.A., 2019. Long-term continuity in land surface phenology measurements: A comparative assessment of the MODIS land cover dynamics and VIIRS land surface phenology products. Remote Sens. Environ. 226, 74–92. https://doi.org/10.1016/j.rse.2019.03.034

Moulin, S., Kergoat, L., Viovy, N., Dedieu, G., 1997. Global-Scale Assessment of Vegetation Phenology Using NOAA/AVHRR Satellite Measurements. J. Clim. 10, 1154–1170. https://doi.org/10.1175/1520-0442(1997)010<1154:GSAOVP>2.0.CO;2

Myneni, R.B., Hall, F.G., Sellers, P.J., Marshak, A.L., 1995. The interpretation of spectral vegetation indexes. IEEE Trans. Geosci. Remote Sens. 33, 481–486. https://doi.org/10.1109/TGRS.1995.8746029

Myneni, R.B., Keeling, C.D., Tucker, C.J., Asrar, G., Nemani, R.R., 1997. Increased plant growth in the northern high latitudes from 1981 to 1991. Nature 386, 698–702. https://doi.org/10.1038/386698a0

Nguyen, L.H., Joshi, D.R., Clay, D.E., Henebry, G.M., 2018. Characterizing land cover/land use from multiple years of Landsat and MODIS time series: A novel approach using land surface phenology modeling and random forest classifier. Remote Sens. Environ. https://doi.org/10.1016/J.RSE.2018.12.016

Paudel, K.P., Andersen, P., 2013. Response of rangeland vegetation to snow cover dynamics in Nepal Trans Himalaya. Clim. Change 117, 149–162. https://doi.org/10.1007/s10584-012-0562-x

Petersky, R.S., Shoemaker, K.T., Weisberg, P.J., Harpold, A.A., 2019. The sensitivity of snow ephemerality to warming climate across an arid to montane vegetation gradient. Ecohydrology 12, e2060. https://doi.org/10.1002/eco.2060

Piao, S., Fang, J., Zhou, L., Ciais, P., Zhu, B., 2006. Variations in satellite-derived phenology in China's temperate vegetation. Glob. Chang. Biol. 12, 672–685. https://doi.org/10.1111/j.1365-2486.2006.01123.x

Qiao, D., Wang, N., 2019. Relationship between Winter Snow Cover Dynamics, Climate and Spring Grassland Vegetation Phenology in Inner Mongolia, China. ISPRS Int. J. Geo-Information 8, 42. https://doi.org/10.3390/ijgi8010042

Reed, B.C., Brown, J.F., VanderZee, D., Loveland, T.R., Merchant, J.W., Ohlen, D.O., 1994. Measuring phenological variability from satellite imagery. J. Veg. Sci. 5, 703–714. https://doi.org/10.2307/3235884

Reed, B.C., White, M., Brown, J.F., 2003. Remote Sensing Phenology, in: Schwartz, M.D. (Ed.), Phenology: An Integrative Environmental Science. Tasks for Vegetation Science. Kluwer Academic Publishers, Dordrecht,The Netherlands, pp. 365–381. https://doi.org/10.1007/978-94-007-0632-3_23

Reyer, C.P.O., Otto, I.M., Adams, S., Albrecht, T., Baarsch, F., Cartsburg, M., Coumou, D., Eden, A., Ludi, E., Marcus, R., Mengel, M., Mosello, B., Robinson, A., Schleussner, C.F., Serdeczny, O., Stagl, J., 2017. Climate change impacts in Central Asia and their implications for development. Reg. Environ. Chang. 17, 1639–1650. https://doi.org/10.1007/s10113-015-0893-z

Rhoades, A.M., Ullrich, P.A., Zarzycki, C.M., Johansen, H., Margulis, S.A., Morrison, H., Xu, Z., Collins, W.D., 2018. Sensitivity of Mountain Hydroclimate Simulations in Variable-Resolution CESM to Microphysics and Horizontal Resolution. J. Adv. Model. Earth Syst. 10, 1357–1380. https://doi.org/10.1029/2018MS001326

Sabyrbekov, R., 2019. Income diversification strategies among pastoralists in Central Asia: Findings from Kyrgyzstan. Pastoralism 9. https://doi.org/10.1186/s13570-019-0152-x

SAEPF, 2007. Environment and Natural Resources for Sustainable Development. Bishkek, Kyrgyzstan.

Schillhorn Van Veen, T.W., 1995. The Kyrgyz Sheep Herders at a Crossroads. Overseas Dev. Institute. Pastor. Dev. Netw. Ser.

Shabanov, N. V., Zhou, L., Knyazikhin, Y., Myneni, R.B., Tucker, C.J., 2002. Analysis of Interannual Changes in Northern Vegetation Activity Observed in AVHRR Data From 1981 to 1994. IEEE Trans. Geosci. Remote Sens. 40, 115–130.

Sorg, A., Bolch, T., Stoffel, M., Solomina, O., Beniston, M., 2012. Climate change impacts on glaciers and runoff in Tien Shan (Central Asia). Nat. Clim. Chang. 2. https://doi.org/10.1038/NCLIMATE1592

Still, C.J., Pau, S., Edwards, E.J., 2014. Land surface skin temperature captures thermal environments of C 3 and C 4 grasses. Glob. Ecol. Biogeogr. 3, 286–296. https://doi.org/10.1111/geb.12121

Stocker, T.F., Qin, D., Plattner, G.-K., Tignor, M.M.B., Allen, S.K., Boschung, J., Nauels,

A., Xia, Y., Bex, V., Midgley, P.M., 2013. Climate Change 2013 The Physical Science Basis Working Group I Contribution to the Fifth Assessment Report of the Intergovernmental Panel on Climate Change. Cambridge University Press, Cambridge, United Kingdom and New York, NY, USA.

Tang, Z., Wang, X., Wang, J., Wang, X., Li, H., Jiang, Z., 2017. Spatiotemporal Variation of Snow Cover in Tianshan Mountains , Central Asia , Based on Cloud-Free. Remote Sens. 9, 2001–2015. https://doi.org/10.3390/rs9101045

Tateishi, R., Ebata, M., 2004. Analysis of phenological change patterns using 1982–2000 Advanced Very High Resolution Radiometer (AVHRR) data. Int. J. Remote Sens. 25, 2287–2300. https://doi.org/10.1080/01431160310001618455

Tucker, C.J., 1979. Red and photographic infrared linear combinations for monitoring vegetation. Remote Sens. Environ. 8, 127–150. https://doi.org/10.1016/0034-4257(79)90013-0

Vetter, S., 2005. Rangelands at equilibrium and non-equilibrium: recent developments in the debate. J. Arid Environ. 62, 321–341. https://doi.org/10.1016/J.JARIDENV.2004.11.015

Walker, J.J., de Beurs, K.M., Henebry, G.M.M., 2015. Land surface phenology along urban to rural gradients in the U.S. Great Plains. Remote Sens. Environ. 165, 42–52. https://doi.org/10.1016/j.rse.2015.04.019

Wan, Y., Gao, Q., Li, Y., Qin, X., Zhang, W., Ma, X., Liu, S., 2014. Change of Snow Cover and Its Impact on Alpine Vegetation in the Source Regions of Large Rivers on the Qinghai-Tibetan Plateau. Arctic, Antarct. Alp. Res. 46, 632–644. https://doi.org/10.1657/1938-4246-46.3.632

Wang, L., Li, Z., Wang, F., Edwards, R., 2014. Glacier shrinkage in the Ebinur lake basin, Tien Shan, China, during the past 40 years. J. Glaciol. 60, 245–254. https://doi.org/10.3189/2014JoG13J023

Wang, X., Wu, C., Peng, D., Gonsamo, A., Liu, Z., 2018. Snow cover phenology affects alpine vegetation growth dynamics on the Tibetan Plateau: Satellite observed evidence, impacts of different biomes, and climate drivers. Agric. For. Meteorol. 256–257, 61–74. https://doi.org/10.1016/J.AGRFORMET.2018.03.004

White, M.A., Thomton, P.E., Running, S.W., 1997. A continental phenology model for monitoring vegetation responses to interannual climatic variability, Global Biogeochemical Cycles.

WorldBank, 2018. Kyrgyzstan; Population 2018 [WWW Document]. URL https://data.worldbank.org/country/kyrgyz-republic

Xenarios, S., Gafurov, A., Schmidt-Vogt, D., Sehring, J., Manandhar, S., Hergarten, C., Shigaeva, J., Foggin, M., 2018. Climate change and adaptation of mountain societies in Central Asia: uncertainties, knowledge gaps, and data constraints. Reg. Environ. Chang. 1–14. https://doi.org/10.1007/s10113-018-1384-9

Xu, Y., Zhou, B., Wu, Ji, Han, Z., Zhang, Y., Wu, J, 2017. Asian climate change under 1.5–4 °C warming targets. Adv. Clim. Chang. Res. 8, 99–107. https://doi.org/10.1016/J.ACCRE.2017.05.004

Yu, X., Zhao, Y., Ma, X., Yao, J., Li, H., 2018. Projected changes in the annual cycle of precipitation over central Asia by CMIP5 models. Int. J. Climatol. 38, 5589–5604. https://doi.org/10.1002/joc.5765

Yuan-An, J., Ying, C., Yi-Zhou, Z., Peng-Xiang, C., Xing-Jie, Y., Jing, F., Su-Qin, B., 2013. Analysis on Changes of Basic Climatic Elements and Extreme Events in Xinjiang, China during 1961–2010. Adv. Clim. Chang. Res. 4, 20–29. https://doi.org/10.3724/SP.J.1248.2013.020

Zhang, X., 2015. Reconstruction of a complete global time series of daily vegetation index trajectory from long-term AVHRR data. Remote Sens. Environ. 156, 457–472. https://doi.org/10.1016/j.rse.2014.10.012

Zhang, X., Friedl, M.A., Schaaf, C.B., Strahler, A.H., Hodges, J.C.F., Gao, F., Reed, B.C., Huete, A., 2003. Monitoring vegetation phenology using MODIS. Remote Sens. Environ. 84, 471–475. https://doi.org/10.1016/S0034-4257(02)00135-9

Zhang, X., Liu, L., Liu, Y., Jayavelu, S., Wang, J., Moon, M., Henebry, G.M., Friedl, M.A., Schaaf, C.B., 2018. Generation and evaluation of the VIIRS land surface phenology product. Remote Sens. Environ. 216, 212–229. https://doi.org/10.1016/j.rse.2018.06.047

Zhang, X., Tan, B., Yu, Y., 2014. Interannual variations and trends in global land surface phenology derived from enhanced vegetation index during 1982-2010. Int. J. Biometeorol. 58, 547–564. https://doi.org/10.1007/s00484-014-0802-z

Zhou, H., Aizen, E., Aizen, V., 2013. Deriving long term snow cover extent dataset from AVHRR and MODIS data: Central Asia case study. Remote Sens. Environ. 136, 146–162. https://doi.org/10.1016/J.RSE.2013.04.015

Zhou, J., Jia, L., Menenti, M., 2015. Reconstruction of global MODIS NDVI time series: Performance of Harmonic ANalysis of Time Series (HANTS). Remote Sens. Environ. 163, 217–228. https://doi.org/10.1016/j.rse.2015.03.018

Zhou, L., Kaufmann, R.K., Tian, Y., Myneni, R.B., Tucker, C.J., 2003. Relation between interannual variations in satellite measures of northern forest greenness and climate between 1982 and 1999. J. Geophys. Res. D Atmos. 108. https://doi.org/10.1029/2002jd002510

Zhumanova, M., Wrage-Mönnig, N., Darr, D., 2016. Farmers' Decision-making and Land Use Changes in Kyrgyz Agropastoral Systems. Mt. Res. Dev. 36, 506–517. https://doi.org/10.1659/MRD-JOURNAL-D-16-00030.1

CHAPTER 2

CHANGING SNOW SEASONALITY IN THE HIGHLANDS OF KYRGYZSTAN

Paper #1:

Tomaszewska, M.A., Henebry, G.M., 2018. Changing snow seasonality in the highlands of Kyrgyzstan. *Environmental Research Letters*. 13, 065006. https://doi.org/10.1088/1748-9326/aabd6f

2.0. Abstract

Few studies have examined changing snow seasonality in Central Asia. Here, we analyzed changes in the seasonality of snow cover across Kyrgyzstan (KGZ) over 14 years from 2002/03 to 2015/16 using the recent version (v006) of MODIS Terra and Aqua 8-day snow cover composites (MOD10A2/MYD10A2). We focused on three metrics of snow seasonality—first date of snow (FDoS), last date of snow (LDoS), and duration of snow season (DoSS)—and used nonparametric trends tests to assess the significance and direction of trends. We evaluated trends at three administration scales and across elevation. We used two techniques to assure that our identification of significant trends were not resulting from random spatial variation. First, we report only significant trends (positive or negative) that are at least twice as prevalent as the converse trends. Second, we use a two-stage analysis at the national scale to identify asymmetric directional changes in snow seasonality. Results show more territory has been experiencing earlier onset of the snow than earlier snowmelt, and roughly equivalent areas have been experiencing longer and shorter duration of snow seasons in the past 14 years. The changes are not uniform across KGZ, with significant shifts toward earlier snow arrival in western and central KGZ and significant shifts toward earlier snowmelt in eastern KGZ. Duration of snow season has

significantly shortened in western and eastern KGZ and significantly lengthened in north and southwestern KGZ. DoSS is significantly longer where the snow onset was significantly earlier or the snowmelt significantly later. There is general trend of significantly earlier snowmelt below 3,400 m and the area of earlier snowmelt is 15 times greater in eastern than western districts. Significant trends in Aqua product were less prevalent than in Terra product, but the general trend toward earlier snowmelt were also evident in Aqua data.

2.1. Introduction

Snow cover extent has been observed to be changing for more than three decades using both in-situ data (Groisman et al. 2006, Bulygina et al. 2010, 2011) and remote sensing products (Schanda et al. 1983, Hall et al. 2002, Brown and Robinson 2011). Remote sensing techniques for monitoring of snow cover extent have advanced substantially in the past three decades (Robinson et al. 1993, Armstrong and Brodzik 2001, Painter et al. 2009, Rittger et al. 2013, Morriss et al.. 2016). Much of the change analysis has focused on broad scales—from hemispheric to subcontinental—at coarse spatial resolution (Robinson and Dewey 1990, Groisman et al. 1994b, Brown 2000, Robinson and Frei 2000, Dye 2002, Déry and Brown 2007, Hori et al. 2017).

Impacts of climate change are exacerbated in mountainous regions (Beniston 2003, Fischlin et al. 2007, Immerzeel et al. 2010, Rangwala and Miller 2012, Kohler et al. 2014). However, the ability of global climate projections to capture the complex dynamics of mountain climates is limited (Christensen et al. 2013), particularly over mountainous Central Asia (Hijioka et al. 2014, Reyer et al. 2017).

Studies in montane Central Asia are relatively few, especially at higher spatial resolutions, but they have all shown significant changes, whether in snow cover (Dietz et al. 2013, 2014, Zhou et al. 2013, Tang et al. 2017), glacial extent (Aizen et al. 1995, Narama et al. 2010), or meltwater runoff (Aizen et al. 1997, Chevallier et al. 2014). Still, there is a notable paucity of studies on the changing environment across montane Central Asia (Hijioka et al. 2014, Reyer et al. 2017).

Here we evaluate trends in the seasonality of snow cover across Kyrgyzstan since 2002 using the latest version of the MODIS (MODerate Resolution Imaging Spectrometer) snow cover composites. Our need to quantify changing snow cover seasonality arises from our interest in highland pasture conditions in rural Kyrgyzstan. Kyrgyz livelihoods based on montane agropastoralism are particularly vulnerable to changing environmental conditions, due to a reliance on the seasonal movement of livestock to higher elevation pastures, a practice also called vertical transhumance (Schillhorn Van Veen 1995). We assess at multiple scales whether and where the snow cover timing and duration have changed significantly in the recent past: at the scale of oblasts (provinces); in four rayons (districts); and at elevational bands within these selected rayons. We compare results from MODIS snow cover products generated from different overpass times (late morning and early afternoon), and two product versions.

2.2. Study Area

The study area is the territory of Kyrgyzstan (Kyrgyz Republic), a highly mountainous country in the eastern part of Central Asia. Kyrgyzstan shares borders with, moving clockwise from due north: Kazakhstan, China, Tajikistan, and Uzbekistan. The total area of the country is just shy of 200,000 km^2, of which 191,801 km^2 is in land and 8,150 km^2

is in open water. In 2017, the population was approximately 5.8 million living in seven oblasts or provinces (Figure 2.1a), of which only 36% are in urban areas with the largest city being the capital Bishkek.

Kyrgyzstan is among the poorer nations, with an estimated per capita gross domestic production in 2016 based on purchasing power parity of just US$3,551 (WorldBank 2017a). Moreover, the country is heavily dependent on remittances from workers aboard; World Bank projects remittance inflows of US$2.5 billion for 2017 (WorldBank 2017b). Poverty, particularly rural poverty, limits adaptive capacity to respond to impacts on livelihoods arising with climate change (Lioubimtseva and Henebry 2009, Reyer et al. 2017).

More than 56% of the territory occurs above 2,500 m (Azykova 2002). Mountains ranges cover more than 90% of the land area. These ranges include parts of the Pamir and the Alatau, and a large portion of the Tien Shan that divides the country into two zones. The northern zone holds three oblasts—Talas, Chuy (including the capital Bishkek), and Issyk-Kul—and the southern zone has four oblasts—Jalal-Abad, Naryn, Osh, and Batken (Asian Development Bank 2010).

The climate of Kyrgyzstan is influenced by country's inland location between temperate and sub-tropical zone, high elevation, the distance from oceans, and proximity to the deserts. It results in intense solar radiation, low precipitation, and a continental climate (Akimaliev et al. 2013). The mountain relief causes elevational climatic zonation of temperature and moisture. In the hot months of July and August, the mean air temperature over lowlands ranges between 17 to 40 °C and only ~4°C in the mountains. During winter months, the lowest temperatures are recorded in the mountain valleys and depressions

(Kulikov and Schickhoff 2017), but frost can occur in every oblast. Annual precipitation varies from 144 mm in some parts of Issyk-Kul to 1,090 mm in the lowlands of the Fergana valley, but precipitation is unevenly distributed across the country. Vegetation types are scattered along distinct elevational zones, influenced by vertical gradients of climatic variables. Less than 10% of land area is appropriate for crops, forests cover ~5%, and more than 50% of the land is used as pastoral rangelands (Asian Development Bank 2010).

2.3. Methods

2.3.1. Satellite data

To characterize snow seasonality, we used the most recent Version 6 of the MODIS Terra snow cover 8-day composites with a nominal spatial resolution of 500 m (MOD10A2/MYD10A2) for the period of 14 years starting in 2002. Both datasets (Terra and Aqua) report the maximum snow cover extent observed during an 8-day period by compositing 500 m observations from the MODIS daily snow cover products (MOD10A1/MYD10A1) generated by The National Snow and Ice Data Center (https://nsidc.org/). Snow cover information is derived from the Normalized Difference Snow Index (NDSI) (Hall et al. 2002). Snow cover typically has very high visible (VIS) reflectance and very low shortwave infrared (SWIR) reflectance. The algorithm uses a threshold test for spectral band ratios of a difference in VIS (band 4: 0.555 μm) and SWIR (band 6: 1.650 μm) reflectance.

$$NDSI = \frac{(R_{vis} - R_{SWIR})}{(R_{vis} + R_{SWIR})} \quad \text{(Equation 2.1)}$$

NDSI > 0.0 indicates the presences of some snow within the pixel, while a pixel with NDSI < 0.0 indicates a snow-free land surface (Riggs and Hall 2015).

Although snow always has NDSI > 0.0, not all surface features with positive NDSI values are snow covered (i.e., salt pans or cloud contaminated pixels at cloud edges). Thus, additional screening procedures are required to reduce commission error. In the MODIS products, a pixel will be mapped as snow if the NDSI > 0.4 and the MODIS band 2 (red) reflectance exceeds 0.11 to discriminate snow from water (Riggs and Hall 2015). These MODIS snow cover products (MOD10A1/MYD10A1) have undergone extensive peer-review evaluation and validation processes (Hall et al. 2002; Riggs and Hall 2015), and no effort was made in this retrospective study to conduct additional product evaluations. We postprocessed the products by mosaicking two MODIS tiles (h23v04 and h23v05), reprojecting into WGS-1984, and extracting all pixels flagged as "snow". There were 46 composited images per year per product. We chose to work with the 8-day composited products instead of the daily products for two reasons: (1) so that the statistical power for the trend analyses would be constant across scales, and (2) because far fewer studies have worked with the composited data.

For terrain information, we used the 15 arc-second (~450m) mean elevation product of Global Multi-resolution Terrain Elevation Data 2010 (GMTED2010) developed by the U.S. Geological Survey and the National Geospatial-Intelligence Agency.

2.3.2. Trend Analysis

To analyze changes in snow cover seasonality, we defined the observation season for each year to start on day of the year (DOY) 169—approximately the summer solstice—and extend to DOY 168 of the following year (DOY169year through DOY168year+1). Thus, we analyzed a 14-year time series starting in the middle of 2002 and ending in middle of 2016. For each snow season, we tracked three snow cover variables: the First Date of Snow

(FDoS), the Last Date of Snow (LDoS), and the Duration of Snow Season (DoSS). FDoS was the composite date when the snow pixel is marked as 1 (snow on) first time for each snow season. LDoS was calculated inversely, the composite date of the last appearance of snow during the snow season. The DoSS was the simple difference between the LDoS and the FDoS. For each of snow variables, we calculated mean, standard deviation, and coefficient of variation for the series of 14 snow seasons from 2002/03 through 2015/16.

Note that since we are interested in the potential impact of changes in snow seasonality on pastoralism, we have purposefully chosen to characterize the snow cover season by its temporal extremities: the first occurrence of snow appearing in a composite during the observation season (FDoS) and the last occurrence of snow appearing in a composite (LDoS). We understand that snowmelt can occur after FDoS and before LDoS, even multiple times. Were our purpose to evaluate snow cover duration to estimate the regional hydrological budget or the surface energy balance, then these outer bounds of snow occurrence could overestimate snow cover influence. However, our motivation in characterizing snow season timing is different. We are more interested in pasture dynamics than in high mountain snow processes.

Simple linear regression has been used by remote sensing scientists to estimate trends (de Beurs and Henebry 2008). However, it is better to use non-parametric tests since they provide higher statistical power in case of nonnormality and are robust against outliers (de Beurs and Henebry 2004). To evaluate the change in snow season metrics, we applied the non-parametric Mann-Kendall trend test and the Theil-Sen linear trend estimator. The non-parametric test is based on the rank correlation coefficient statistic τ (Kendall 1938) with modification (Mann 1945), which requires an observation series y and an accompanying

time vector x of length n to detect monotonic changes over time. The Mann-Kendall trend test calculates difference between later-measured data to all earlier-measured data, ($y_j - y_i$), where j > i are the jth and ith year in the time series, and assigns an integer value of 1, 0, or -1 (positive difference, no difference, and negative difference, respectively) (Meals et al 2011). The Mann-Kendall score S is computed as the sum of the integer scores:

$$S = \sum_{i=1}^{n-1} \sum_{j=i+1}^{n} \begin{cases} 1, & if\ y_j - y_i > 0 \\ 0, & if\ y_j - y_i = 0 \\ -1, & if\ y_j - y_i < 0 \end{cases} \quad \text{(Equation 2.2)}$$

Then the Mann-Kendall test statistic τ is measured by dividing S by the total of n×(n-1)/2 possible pairs of data, where n is the total number of observations for trend direction and strength. Kendall's τ ranges from -1.0 to 1.0, analogous to a correlation coefficient.

We estimated the monotonic rate of change in the time series using the Theil-Sen slope, which computes the slope for all pairs of observations and selects the median value as the robust estimate of the trend's slope (Hirsch et al. 1982):

$$\beta_1 = median\left(\frac{y_j - y_i}{x_j - x_i}\right) \quad \text{(Equation 2.3)}$$

We calculated the area of Theil-Sen slope values associated at a significance level of $p<0.05$ for positive and negative trends for each of the seven oblasts of Kyrgyzstan and focused on four rayons (districts). To analyze elevational effects, we divided the area of the focal rayons into five classes: $1{,}400 \leq x < 1{,}900$ m; $1{,}900 \leq x < 2{,}400$ m; $2{,}400 \leq x < 2{,}900$ m; $2{,}900 \leq x < 3{,}400$ m; and $x \geq 3{,}400$ m. Note there are no elevations below 1,900 m in At-Bashy and Chong-Alay rayons. Note also that Alay and Chong-Alay are adjacent rayons located in the southwest of the country and Naryn and At-Bashy are adjacent rayons in central Kyrgyzstan located to the east of the other pair of focal rayons.

A negative (positive) trend in FDoS indicates earlier (later) onset of snow. A negative (positive) trend in LDoS indicates earlier (later) snowmelt. A negative (positive) trend in DoSS indicates a shorter (longer) snow season.

To highlight areas of significant change and to attenuate the risk of finding a significant difference where none exists (i.e., a Type I inferential error), we calculated the ratio of area of significant negative trends to the area of the significant positive trends for each administrative unit. We interpreted a factor of >2.0 (or <0.5) in the ratio of significant trends to indicate the predominant direction of change over the study period. We report here only the significant trends showing the predominant direction of change at the level of administrative unit or elevation class. Pixel totals can vary among metrics due to exclusion of pixels exhibiting no variation in snow cover and thereby generating NaNs (i.e., Not a Number) in the trend analyses.

Finally, at the national level only, we tracked the trend status (positive at $p<0.05$ or negative at $p<0.05$ or not significant at $p\geq0.05$) of every pixel for the three metrics at two sequential stages yielding 3^2 combinations for each of the three metrics as follows:

FDoS = {+ | - | ns} AND DoSS = {+ | - | ns}
LDoS = {+ | - | ns} AND DoSS = {+ | - | ns}
FDoS = {+ | - | ns} AND LDoS = {+ | - | ns}

Random spatial variation should yield approximately equal proportion of positive and negative trends. Accordingly, deviations from equal proportions are particularly interesting, especially when the deviations occur in two sequential stages.

2.4. Results

We first present the areal extent in each oblast associated with the predominant trend direction and compare the results from the most recent MODIS snow product from Terra (MOD10A2 v006) with the similar MODIS product from Aqua (MYD10A2 v006). Since these satellites have different equatorial daytime overpass times (10:30 and 13:30, respectively), we expect to see some areal differences. We then focus on the four rayons in the southern zone where we have conducted summer field work in pastures—Alay and Chong-Alay rayons in Osh oblast and At-Bashy and Naryn rayons in Naryn oblast—and compare the areal extent of the predominant trends by elevation class in the Terra product only. (Some tables appear in the supplementary materials.)

For visual display only, we identified pixels from Terra with values of Theil-Sen slope that were significantly different from zero at three significance levels ($p< 0.1$, $p<0.05$, and $p<0.01$). The areal analyses are limited to those data significant at $p<0.05$.

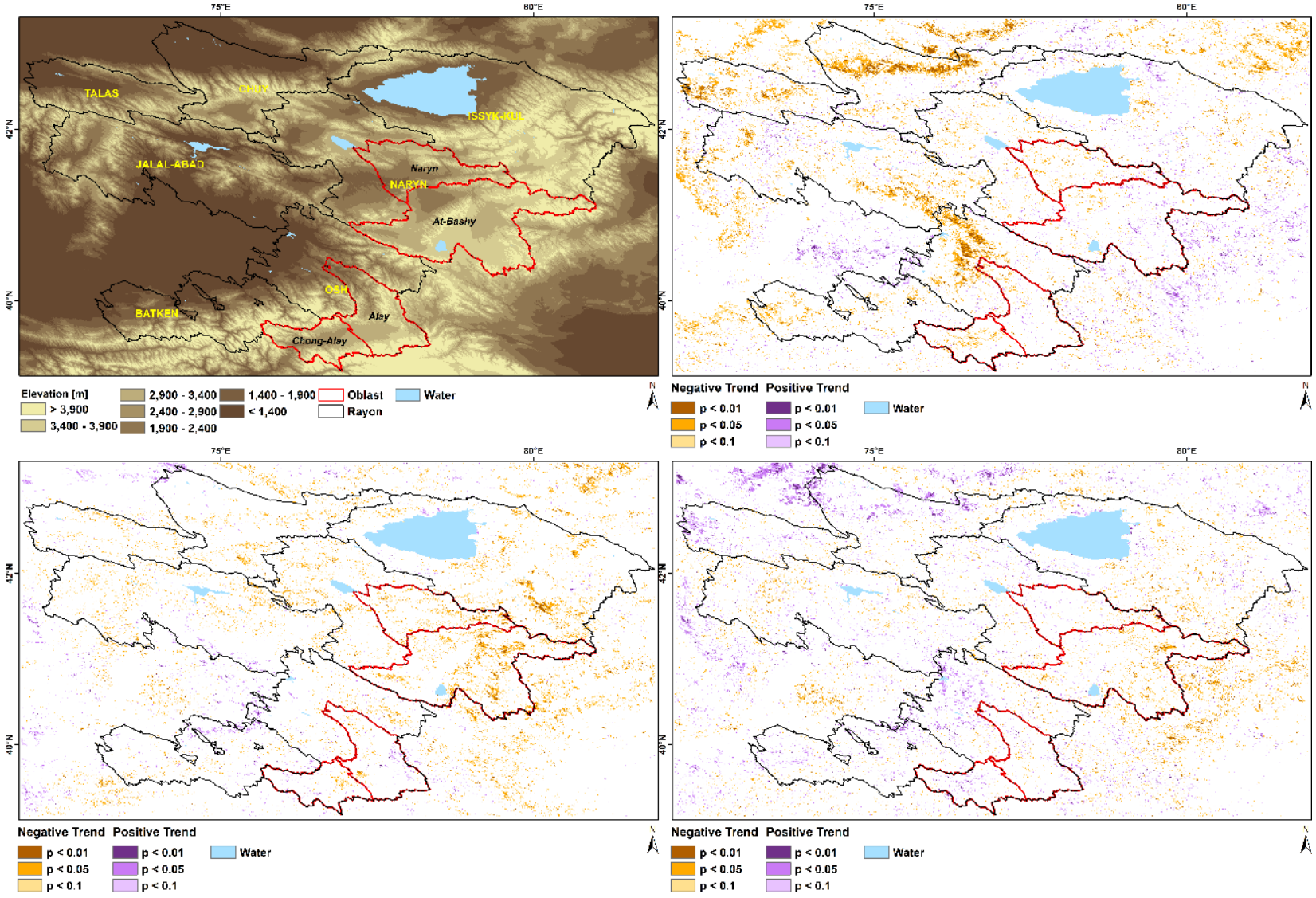
75°E
80°E
42°N
40°N
TALAS
CHUY
ISSYK-KUL
JALAL-ABAD
Naryn
NARYN
At-Bashy
OSH
BATKEN
Alay
Chong-Alay
Elevation [m]
> 3,900
3,400 - 3,900
2,900 - 3,400
2,400 - 2,900
1,900 - 2,400
1,400 - 1,900
< 1,400
Oblast
Rayon
Water
N
Negative Trend
Positive Trend
p < 0.01
p < 0.05
p < 0.1

Figure 2.1. Study area and results: (a) map of Kyrgyzstan with oblast borders in black and the four focal rayons outlined in red over the GMTED2010 elevation map stratified by elevation class used in the analyses; and (b) First Date of Snow (FDoS), (c) Last Date of Snow (LDoS), and (d) Duration of Snow Season (DoSS) from the Terra MODIS snow cover product version 6 from 2002/03 to 2015/16 at three significance levels ($p \leq 0.01$, $p \leq 0.05$, $p \leq 0.1$). Shades of brown (purple) indicate negative (positive) significant trends.

Earlier snow arrival corresponds to a negative trend in the FDoS, and it appears prevalent across Kyrgyzstan (Figure 2.1b), particularly in the oblasts of Chuy (2,079 km2), Jalal-Abad (1,534 km2) and Osh (2,021 km2), for almost 8,000 km2 in total (Table 2.1, column 1). Only Issyk-Kul oblast does not exhibit a significant predominant trend of earlier snow arrival. Some patches of significant positive trends in FDoS (later snow arrival) are evident in eastern Kyrgyzstan (Figure 2.1a), but they are not predominant, resulting in no entry ("--") in Table 2.1.

Earlier snowmelt corresponds to a negative trend in the LDoS, and it appears prevalent across Kyrgyzstan (Figure 2.1c), particularly in the oblasts of Naryn (2,227 km^2) and Issyk-Kul (1,376 km^2), for almost 5,000 km^2 in total (Table 2.1, column 3). Note, however, that neither Batken nor Osh oblast exhibits snowmelt that is either significantly earlier or significantly later.

A shorter (longer) snow season corresponds to a negative (positive) trend in the DoSS, and the results are mixed across Kyrgyzstan (Figure 2.1d). A shorter snow season is apparent in Naryn (872 km^2) and Issyk-Kul (884 km^2) oblasts, totaling 1,757 km^2 (Table 2.1, column 5). In contrast, a longer snow season appears in parts of four oblasts to the west: Batken (325 km^2), Chuy and Osh (each at 701 km^2), and Talas (357 km^2), totaling 2,084 km^2 (Table

2.1, column 6). Only Jalal-Abad oblast exhibits no predominant change in areal extent of DoSS.

Table 2.1. Area in predominant significant ($p<0.05$) trends from Terra and Aqua during 2002/03-2015/16 by oblast for snow season metrics: First Date of Snow (FDoS), Last Date of Snow (LDoS), and Duration of Snow Season (DoSS). "--" indicates no prevalent trend.

oblast	Terra FDoS earlier (km^2)	Aqua FDoS earlier (km^2)	Terra LDoS earlier (km^2)	Aqua LDoS earlier (km^2)	Terra DoSS shorter (km^2)	Terra DoSS longer (km^2)
Batken	**526**	**179**	**--**	**--**	**--**	**325**
Chuy	**2,079**	**682**	**401**	**375**	**--**	**701**
Issyk-Kul	**--**	**--**	**1,376**	**823**	**884**	**--**
Jalal-Abad	**1534**	**--**	**759**	**645**	**--**	**--**
Naryn	**839**	**--**	**2,227**	**1,242**	**872**	**--**
Osh	**2,021**	**648**	**--**	**--**	**--**	**701**
Talas	**972**	**--**	**222**	**213**	**--**	**357**
TOTAL	**7,971**	**1,510**	**4,985**	**3,298**	**1,757**	**2,084**

Trend analysis with the Aqua product (MYD10A2) shows predominant trends in fewer oblasts and much smaller areas than in the Terra product (MOD10A2) (Table 2.1, columns 2 and 4). There are no oblasts with predominant positive trends in FDoS, LDoS, or DoSS as well as no predominant negative trends in DoSS (Table 2.1). Earlier snow arrival is evident in just three oblasts in the Aqua product: Chuy (682 km^2), Osh (648 km^2), and Batken (179 km^2) (Table 2.1, column 2). These areal extents are less than the corresponding areas in the Terra product by 67%, 68%, and 66%, respectively. Total area with earlier onset of snow is 1,510 km^2 for Aqua versus 7,971 km^2 for Terra, or a decrease of 81%. Earlier snowmelt (negative trend in LDoS) is evident in five of seven oblasts in the Aqua product, but the proportional decreases in area are less than seen with the FDoS: Chuy (6%), Issyk-Kul (40%), Jalal-Abad (15%), Naryn (44%), Talas (4%), and 34% overall (Table 2.1, column 4).

Based on the Terra data, elevational patterns are consistent across the four focal rayons for LDoS. In both Naryn and At-Bashy, earlier snowmelt occurs at every elevational stratum, with an increase area with increasing elevation most apparent in At-Bashy (Table 2.2, column 1-2). In Alay and Chong-Alay, there are predominant areas of later snowmelt only above 3,400 m, but earlier snowmelt below 3,400 m (Table 2.2, columns 3-4). The area of earlier snowmelt is greater in the eastern than the western rayons by a factor of 15.

Table 2.2. Area in predominant significant trends from Terra for Last Date of Snow (LDoS) by elevation class in the four focal rayons. Bold entries indicate significant ($p<0.05$) negative trends at least twice as prevalent as significant positive trends. *Italicized underlined entries* indicate significant ($p<0.05$) positive trends at least twice as prevalent as significant negative trends. Negative (positive) trends in LDoS correspond to earlier (later) snowmelt. "nd" = no data as lowest elevation in rayon is >1,900 m. "--" indicates no prevalent trend.

elevation class	**Naryn** (km^2)	**At-Bashy** (km^2)	**Alay** (km^2)	**Chong-Alay** (km^2)
1,400-1,900 m	**2.6**	nd	**2.1**	nd
1,900-2,400 m	**38.0**	**57.5**	**25.1**	--
2,400-2,900 m	**137.8**	**93.2**	**23.8**	**18.5**
2,900-3,400 m	**182.0**	**441.8**	**47.7**	--
> 3,400 m	**47.2**	**720.0**	*49.2*	*18.7*
Total earlier	**407.6**	**1,312.4**	**98.7**	**18.5**
Total later	--	--	*49.2*	*18.7*

In contrast to the LDoS, the FDoS shows elevational variation across rayons. In Naryn, 167 km^2 show earlier snow onset and all of it occurs below 3,400 m (Table S2.1, column 1). In the neighboring rayon of At-Bashy, there is both earlier snow onset and later snow onset, with the latter appearing between 2,900-3,400 m (Table S2.1, column 2). Alay exhibits earlier snow onset below 2,900 m and above 3,400 m (Table S2.1, column 3). Chong-Alay rayon, in contrast, shows earlier snow onset particularly between 2,900-3,400 m, but not above 3,400 m (Table S2.1, column 4).

The DoSS show both longitudinal and elevational patterns of significant change. The two eastern rayons (Naryn and At-Bashy) exhibit areas with shorter snow season duration, with a clear pattern of increasing area with increasing elevation above 2,400 m in At-Bashy, but only at the highest elevation class in Naryn (Table S2.2). The two western rayons (Alay and Chong-Alay) show areas of longer snow season duration, with Chong-Alay's duration highest between 2,400-2,900 m but absent above 3,400 m (Table S2.2).

We conducted the two-stage trend analyses only at the national scale and used only the Terra dataset, since it had larger areas of significant change. Varying amount of total pixels in the first stage metrics arises from exclusion of pixels exhibiting no variation in snow cover, which generated NaNs (Not a Number) in the trend analyses.

Two-stage trend analysis for FDoS followed by DoSS shows substantially more area in significantly earlier FDoS than significantly later and, of those significantly earlier FDoS pixels, substantially more area (19.8%) exhibits significantly longer DoSS than shorter (Table 2.3, row 1). In contrast, there is substantially more area (60.1%) showing significantly shorter DoSS associated with pixels with significantly later FDoS (Table 2.3, row 2). No predominant trend in DoSS was evident in those pixels with no significant trends in FDoS (Table 2.3, row 3).

Table 2.3. Two-stage trend analysis for FDoS and DoSS. **Bold entries** indicate at least twice the area of the significant ($p<0.05$) pair.

Trend of 1st metric: FDoS	Area in 1st metric (%)	Area in 1st metric (km^2)	Trend of 2nd metric: DoSS	Area in 2nd metric (%)	Area in 2nd metric (km^2)
FDoS earlier	**4.9**	**8,555**	DoSS shorter	0.0	0
			DoSS longer	**19.8**	**1,693**
			DoSS ns	80.2	6,862
FDoS later	0.9	1,635	DoSS shorter	**60.1**	**983**
			DoSS longer	0.8	13
			DoSS ns	39.1	639
FDoS ns	94.2	166,832	DoSS shorter	1.1	1,878
			DoSS longer	0.8	1,307
			DoSS ns	98.1	163,197

Two-stage trend analysis for LDoS following by DoSS shows substantially more area (3.2%) in significantly earlier LDoS than significantly later and, of those significantly earlier LDoS pixels, substantially more area (8.2%) exhibits significantly shorter DoSS than shorter (Table S2.3, row 1). In contrast, there is substantially more area (19.9%) showing significantly longer DoSS associated with pixels with significantly later LDoS (Table S2.3, row 2). No predominant trend in DoSS was evident in those pixels with no significant trends in LDoS (Table S2.3, row 3).

Two-stage trend analysis of FDoS followed by LDoS shows substantially more area (4.8%) in significantly earlier FDoS than significantly later and, of those significantly earlier FDoS pixels, substantially more area (2.3%) exhibits significantly earlier LDoS than later (Table S2.4, row 1). Likewise, there is substantially more area showing significantly earlier LDoS associated with pixels with significantly later FDoS (0.9%) or no significant trend in FDoS (91.3%) (Table S2.4, rows 2-3).

2.5. Discussion

Our results, based primarily on the most recent version of Terra MODIS snow cover composites, indicate that snow seasonality has been changing in recent years in each of the seven oblasts of the Kyrgyz Republic: specifically, more territory has been experiencing earlier onset of the snow than earlier snowmelt, and roughly equivalent areas have been experiencing longer and shorter duration of snow seasons in the past 14 years (Table 2.1). Significant trends apparent in the Aqua data were less prevalent (Table 2.1). This discrepancy between the Terra and Aqua results may arise from the early afternoon overpass of Aqua, when imaging geometry, cloudiness, and surface temperature may differ. However, the general trend toward earlier snowmelt seen in the Terra product was also evident in the Aqua product.

Zooming into the rayon level and stratifying by broad elevational bands within the focal rayons revealed trend variation in snow cover metrics. We found elevational variation in each snow metric: (1) earlier onset of snow below 2,900 m in all four rayons, but divergence above 2,900 m, including later onset of snow in At-Bashy between 2,900 and 3,400 m (Table S2.1); (2) earlier snowmelt below 3,400 m in all rayons except Chong-Alay, but later snowmelt above 3,400 m in Alay and Chong-Alay (Table 2.2); and (3) occurrence of shorter snow seasons in At-Bashy above 2,400 m and longer snow seasons in Chong-Alay below 3,400 m (Table S2.2).

At the national level, there are ~8,600 km^2 with significantly earlier snow onset (Tables 2.3, S2.4) and ~5,500 km^2 with significantly earlier snowmelt (Table S2.3). Regardless of trend status in first date of snow, there is substantially more area in exhibiting significantly earlier snowmelt across Kyrgyzstan (Table S2.4). Snow season duration is significantly

longer across ~1,700 km^2 where snow onset is significantly earlier (Table 2.3). However, snow season duration is significantly shorter across 980 km^2 where snow onset is significantly later (Table 2.3). Snow season duration is significantly shorter across 452 km^2 where snowmelt is significantly earlier (Table S2.3). In contrast, snow season duration is significantly longer in 155 km^2 where snowmelt is significantly later (Table S2.3). Each of these two-stage trends exhibits strong asymmetry in the area associated with the pair of significant trends, strengthening the interpretation that these trends are not a result of random spatial variation.

Spatial, temporal, and elevational variations in snow seasonality in Central Asia have been detected and quantified in earlier studies at multiple spatial extents. (We summarize the results of the following studies and ours in Table S2.5) (Dietz et al. 2013) processed daily MODIS snow cover products between 2000 and 2011 to characterize interannual variation in snow cover across Central Asia with a view to estimating the water content in major regional catchments contributed by snowmelt. They found high spatial and temporal variation in snow cover and no discernable trend in the start, end, or duration of the snow season at this broad scale of analysis.

In a follow-on study, Dietz et al. (2014) expanded the temporal scope of the analysis from 1986 to 2014 by adding coarser spatial resolution AVHRR (Advanced Very High Resolution Radiometer) data to the MODIS data. They divided the snow cover duration into early (01SEP-15JAN) and later (16JAN-31AUG) seasons to detect trends within nine major catchments in Central Asia and by 100 m elevational increments across Central Asia. They found significant positive trends in early season snow cover duration for most catchments, but mixed results for later season snow cover duration, with five of the nine

catchments had no significant trend and the remaining four showed significant negative trends. A similar pattern was apparent in their elevational analysis: significant increasing snow cover duration in the early season at most elevations, but more than half the trends in the later season were not significant. Of those that were significant, there was decreasing later season snow duration between 2,500 m and 3,300 m (Dietz et al. 2014). This elevational range is significant: most of the highland pastures on which Kyrgyz agropastoralism depends fall into this band. However, the scale of their analysis was broad, encompassing all of Central Asia.

Zhou et al. (2013) used AVHRR and MODIS data to study snow cover trends across the basin of the Amu Darya from 1986 to 2008. They found statistically significant negative trends in snow cover duration, date of snow cover onset, and date of snowmelt across most of the basin, except trends of earlier snow onset in the Central Pamir, especially at elevations greater than 4,000 m (Zhou et al. 2013).

Tang et al. (2017) found that maps of snow cover days based on cloud-screened MODIS daily snow products exhibited a high mean (> 85%) consistency with in-situ observations of snow cover days. Their analysis focused on the Tien Shan range divided into four regions of which the Central Tien Shan corresponds most closely to our study area. Using simple linear regression to identify and characterize trends, Tang et al. (2017) found in the mean snow-covered area in each of four seasons in the Central Tien Shan ranging from a minimum of -8% in autumn to maximum of -14% in spring, but no trend was statistically significant at $p<0.05$. They also calculated a decrease of -12% in the duration of snow cover in the Central Tien Shan from 2001 to 2015, but it was also not significant.

Despite substantial spatio-temporal variation within Kyrgyzstan and across the rest of Central Asia, significant trends in snow seasonality exist and these changes have the potential to disrupt herder livelihoods. We took along preliminary maps of the snow season analyses during a field campaign in Osh oblast during July 2017 to sample pastures. The longtime head of the pasture committee for Chong-Alay rayon studied our trend maps and commented that earlier onset of snow season had indeed become a serious problem for herders in recent years by limiting the use of the fall and winter pastures (Paizylad Maatkarimov, personal communication, July 25, 2017). Note that when we speak of trends, we are talking retrospectively about changes that have already occurred. We are not inferring changes to the local or regional climates using 14 years of data. However, there have been sufficient observations gathered through remote sensing to document significant trends in snow seasonality across large areas in Kyrgyzstan and elsewhere in montane Central Asia.

Recent studies over the Central Asia region show a shift in precipitation from snow to rain. It causes a decrease in snowfall fraction, reducing snow and glacier accumulation during winter (Chen et al. 2016). Moreover, changes in snow cover and substantial shrinkage of glaciers induce alterations in the local water cycle, changing runoff and groundwater storage. Less precipitation in the form of snow leads to earlier melting of snow, which can eventually shift peak runoff and river flow toward earlier in the year instead during the summer when demand for water is highest (Barnett et al 2005, Tang et al. 2017). Higher increases of temperature are projected for summer and fall seasons, while lower increases during winter (Xu et al. 2017), and a significant decrease in precipitation in spring and summer (Hijioka et al. 2014, Yuan-An et al. 2013). However, these precipitation

projections are highly uncertain (Flato et al. 2013, Hijioka et al. 2014). The assessment of climate change effects on snow cover is particularly difficult (Tang et al. 2017) because those effects strongly vary with geographic context and elevation. Complex terrain generates many local microclimates with different feedbacks making them harder to compare. Sunshine duration, vapor pressure, wind velocity, and their interactions may also enhance spatial and temporal variation in snow cover.

Snow cover affects surface climate, including subsequent vegetation growth (Groisman et al. 1994a, Dye and Tucker 2003). Changes in the timing of snow arrival and snowmelt may also have impacts on montane vegetation (Inouye 2000, 2008). Changes in vegetation community composition at higher elevations occur as cold-adapted species decrease in abundance while warm-adapted species increase in a process called thermophilization (Gottfried et al. 2012). Furthermore, pasture degradation, including the spread of weedy and unpalatable species, is already a concern in the highland pastures of Kyrgyzstan (Hoppe et al. 2016, Eddy et al. 2017). A logical next step is to link snow cover seasonality—timing of snow onset, snowmelt, and duration of snow season—with subsequent land surface phenology to detect moisture-induced vegetation stress in highland pastures.

2.6. Conclusions

Climate change impacts threaten the prospects for economic development across Central Asia, but especially rural livelihoods that depend on natural resources (Reyer et al. 2017). One possible consequence is increased rural to urban migration (Reyer et al. 2017). Yet, Central Asia in general and Kyrgyzstan in particular, are lagging in institutional preparation for climate change adaptation (Ford et al. 2015, Lesnikowski et al. 2015).

The Working Group II of the IPCC Fifth Assessment report noted that there are manifold knowledge gaps about the impacts of climate change in Central Asia (*cf.* Table 24-2 in Hijioka et al. 2014). This study attempts to help address some of these gaps at a scale finer than most of the literature to date. By using the most recent MODIS snow cover composited product at multiple scales relevant to herder livelihoods in Kyrgyzstan, we have identified areas where snow season timing and duration have already significantly changed in the past 14 years.

Significant shifts toward earlier onset of snow have been identified in nearly 8,000 km^2 in six of seven oblasts and significant shifts toward earlier onset of snowmelt in nearly 5,000 km^2 in five of seven oblasts. In the past 14 years, the duration of snow season has significantly shortened in two oblasts and significantly lengthened in four oblasts. At finer scales, changes in snow seasonality have varied by elevation and rayon, and the changes detected may impact the montane agropastoralism that forms the basis of the economy in much of rural Kyrgyzstan. The next step is an assessment of how these recent changes in snow seasonality have affected the highland pastures upon which rural livelihoods depend.

2.7. Acknowledgements

We appreciate the assistance and feedback from A.A. Aidaraliev, K. Kelgenbaeva, and P. Maatkarimov. We thank for the two anonymous reviewers for their useful feedback that helped us to improve the article's clarity. This research was supported, in part, by the NASA Land Cover / Land Use Change Program (NNX15AP81G) How Environmental Change in Central Asian Highlands Impacts High Elevation Communities.

2.8. References

Aizen, V.B., Aizen, E.M., Melack, J.M., 1995. Climate, snow cover, glaciers, and runoff in the Tien Shan. J. Am. Water Resour. Assoc. 31, 1113–1129. https://doi.org/10.1111/j.1752-1688.1995.tb03426.x

Aizen, V.B., Aizen, E.M., Melack, J.M., Dozier, J., 1997. Climatic and Hydrologic Changes in the Tien Shan, Central Asia. J. Clim. 10, 1393–1404. https://doi.org/10.1175/1520-0442(1997)010<1393:CAHCIT>2.0.CO;2

Akimaliev, D.A., Zaurov, D.E., Eisenman, S.W., 2013. The Geography, Climate and Vegetation of Kyrgyzstan, in: Medicinal Plants of Central Asia: Uzbekistan and Kyrgyzstan. Springer New York, New York, NY, pp. 1–4. https://doi.org/10.1007/978-1-4614-3912-7_1

Armstrong, R.L., Brodzik, M.J., 2001. Recent Northern Hemisphere snow extent: A comparison of data derived from visible and microwave satellite sensors. Geophys. Res. Lett. 28, 3673–3676. https://doi.org/10.1029/2000GL012556

Asian Development Bank, 2010. Central Asia Atlas of Natural Resource. Central Asian Countries Initiative for Land Management and Asian Development Bank, Manila, Philippines.

Azykova, E.K., 2002. Geographyical and landscape characteristics of mountain territories, in: Aidaraliev, A.A. (Ed.), Mountains of Kyrgyzstan. Technology, Bishkek.

Barnett, T.P., Adam, J.C., Lettenmaier, D.P., 2005. Potential impacts of a warming climate on water availability in snow-dominated regions. Nature 438, 303–309. https://doi.org/10.1038/nature04141

Beniston, M., 2003. Climatic Change in Mountain Regions: A Review of Possible Impacts. Clim. Change 59, 5–31. https://doi.org/10.1023/A:1024458411589

Brown, R.D., 2000. Northern Hemisphere Snow Cover Variability and Change, 1915–97. J. Clim. 13, 2339–2355. https://doi.org/10.1175/1520-0442(2000)013<2339:NHSCVA>2.0.CO;2

Brown, R.D., Robinson, D.A., 2011. Northern Hemisphere spring snow cover variability and change over 1922–2010 including an assessment of uncertainty. Cryosph. 5, 219–229. https://doi.org/10.5194/tc-5-219-2011

Bulygina, O.N., Groisman, P.Y., Razuvaev, V.N., Korshunova, N.N., 2011. Changes in snow cover characteristics over Northern Eurasia since 1966. Environ. Res. Lett. 6, 045204. https://doi.org/10.1088/1748-9326/6/4/045204

Bulygina, O.N., Groisman, P.Y., Razuvaev, V.N., Radionov, V.F., 2010. Snow cover basal ice layer changes over Northern Eurasia since 1966. Environ. Res. Lett. 5, 015004. https://doi.org/10.1088/1748-9326/5/1/015004

Chen, Y., Li, W., Deng, H., Fang, G., Li, Z., 2016. Changes in Central Asia's Water Tower: Past, Present and Future. Sci. Rep. 6, 35458. https://doi.org/10.1038/srep35458

Chevallier, P., Pouyaud, B., Mojaïsky, M., Bolgov, M., Olsson, O., Bauer, M., Froebrich, J., 2014. River flow regime and snow cover of the Pamir Alay (Central Asia) in a changing climate. Hydrol. Sci. J. 59, 1491–1506. https://doi.org/10.1080/02626667.2013.838004

Christensen, J.H., Kumar, K.K., Aldrian, E., An, S., Cavalcanti, I.F.A., De Castro, M., Dong, W., Goswami, P., Hall, A., Kanyanga, J.K., Kitoh, A., Kossin, J., Lau, N.C., Renwick, J., Stephenson, D.B., Xie, S.P., Zhou, T., 2013. Climate Phenomena and their Relevance for Future Regional Climate Change. In: Climate Change 2013: The Physical Sci- ence Basis. Contribution of Working Group I to the Fifth Assessment Report of the Intergovernmental Panel on Climate Change Coordinating L.

de Beurs, K.M., Henebry, G.M., 2008. War, Drought, and Phenology: Changes in the land surface phenology of Afghanistan since 1982. J. Land Use Sci. 3, 95–111. https://doi.org/10.1109/IGARSS.2006.630

de Beurs, K.M., Henebry, G.M., 2004. Trend analysis of the pathfinder AVHRR land (PAL) NDVI data for the deserts of central Asia. IEEE Geosci. Remote Sens. Lett. 1, 282–286. https://doi.org/10.1109/LGRS.2004.834805

Déry, S.J., Brown, R.D., 2007. Recent Northern Hemisphere snow cover extent trends and implications for the snow-albedo feedback. Geophys. Res. Lett. 34, L22504. https://doi.org/10.1029/2007GL031474

Dietz, A.J., Conrad, C., Kuenzer, C., Gesell, G., Dech, S., 2014. Identifying changing snow cover characteristics in central Asia between 1986 and 2014 from remote sensing data. Remote Sens. 6, 12752–12775. https://doi.org/10.3390/rs61212752

Dietz, A.J., Kuenzer, C., Conrad, C., 2013. Snow-cover variability in central Asia between 2000 and 2011 derived from improved MODIS daily snow-cover products. Int. J. Remote Sens. 34, 3879–3902. https://doi.org/10.1080/01431161.2013.767480

Dye, D.G., 2002. Variability and trends in the annual snow-cover cycle in Northern Hemisphere land areas, 1972-2000. Hydrol. Process. 16, 3065–3077. https://doi.org/10.1002/hyp.1089

Dye, D.G., Tucker, C.J., 2003. Seasonality and trends of snow-cover, vegetation index, and temperature in northern Eurasia. Geophys. Res. Lett. 30. https://doi.org/10.1029/2002GL016384

Eddy, I.M.S., Gergel, S.E., Coops, N.C., Henebry, G.M., Levine, J., Zerriffi, H., Shibkov, E., 2017. Integrating remote sensing and local ecological knowledge to monitor rangeland dynamics. Ecol. Indic. 82, 106–116. https://doi.org/10.1016/J.ECOLIND.2017.06.033

Fischlin, A., Midgley, G.F., Price, J.T., Leemans, R., Gopal, B., Turley, C., Rounsevell, M.D.A., Dube, O.P., Tarazona, J., Velichko, A.A., 2007. Ecosystems, their properties, goods, and services, in: Climate Change 2007: Impacts, Adaptation and Vulnerability. Contribution of Working Group II to the Fourth Assessment Report of the Intergovernmental Panel on Climate Change. Cambridge University Press, pp. 211–

272.

Flato, G., Marotzke, J., Abiodun, B., Braconnot, P., Chou, S.C., Collins, W., Cox, P., Driouech, F., Emori, S., Eyvring, V., Forest, C., Gleckler, P., Guilyardi, E., Jakob, C., Kattsov, V., Reason, C., Rummukainen, M., 2013. Evaluation of Climate Models, in: Stocker, T.F., Qin, D., Plattner, G.K., Tignor, M., Allen, S.K., Boschung, J., Nauels, A., Xia, Y., Bex, V., Midgley, P.M. (Eds.), Climate Change 2013: The Physical Science Basis. Contribution of Working Group I to the Fifth Assessment Report of the Intergovernmental Panel on Climate Change. Cambridge University Press, Cambridge, United Kingdom and New York, NY, USA, pp. 741–866.

Ford, J.D., Berrang-Ford, L., Bunce, A., McKay, C., Irwin, M., Pearce, T., 2015. The status of climate change adaptation in Africa and Asia. Reg. Environ. Chang. 15, 801–814. https://doi.org/10.1007/s10113-014-0648-2

Gottfried, M., Pauli, H., Futschik, A., Akhalkatsi, M., Barančok, P., Benito Alonso, J.L., Coldea, G., Dick, J., Erschbamer, B., Fernández Calzado, M., Kazakis, G., Krajči, J., Larsson, P., Mallaun, M., Michelsen, O., Moiseev, D., Moiseev, P., Molau, U., Merzouki, A., Nagy, L., Nakhutsrishvili, G., Pedersen, B., Pelino, G., Puscas, M., Rossi, G., Stanisci, A., Theurillat, J., Tomaselli, M., Villar, L., Vittoz, P., Vogiatzakis, I., Grabherr, G., 2012. Continent-wide response of mountain vegetation to climate change. Nat. Clim. Chang. 2, 111–115. https://doi.org/10.1038/nclimate1329

Groisman, P.Y., Karl, T.R., Knight, R.W., 1994a. Observed Impact of Snow Cover on the Heat Balance and the Rise of Continental Spring Temperatures. Science (80-.). 263, 198–200. https://doi.org/10.1126/science.263.5144.198

Groisman, P.Y., Karl, T.R., Knight, R.W., Stenchikov, G.L., 1994b. Changes of Snow Cover, Temperature, and Radiative Heat Balance over the Northern Hemisphere. J. Clim. 7, 1633–1656. https://doi.org/10.1175/1520-0442(1994)007<1633:COSCTA>2.0.CO;2

Groisman, P.Y., Knight, R.W., Razuvaev, V.N., Bulygina, O.N., Karl, T.R., 2006. State of the Ground: Climatology and Changes during the Past 69 Years over Northern Eurasia for a Rarely Used Measure of Snow Cover and Frozen Land. J. Clim. 19, 4933–4955. https://doi.org/10.1175/JCLI3925.1

Hall, D.K., Riggs, G.A., Salomonson, V. V., DiGirolamo, N.E., Bayr, K.J., 2002. MODIS snow-cover products. Remote Sens. Environ. 83, 181–194. https://doi.org/10.1016/S0034-4257(02)00095-0

Hijioka, Y., Lin, E., Pereira, J.J., Corlett, R.T., Cui, X., Insarov, G.E., Lasco, R.D., Lindgren, E., Surjan, A., 2014. Asia.

Hirsch, R.M., Slack, J.R., Smith, R.A., 1982. Techniques of trend analysis for monthly water quality data. Water Resour. Res. 18, 107–121. https://doi.org/10.1029/WR018i001p00107

Hoppe, F., Zhusui Kyzy, T., Usupbaev, A., Schickhoff, U., 2016. Rangeland degradation assessment in Kyrgyzstan: vegetation and soils as indicators of grazing pressure in

Naryn Oblast. J. Mt. Sci. 13, 1567–1583. https://doi.org/10.1007/s11629-016-3915-5

Hori, M., Sugiura, K., Kobayashi, K., Aoki, T., Tanikawa, T., Kuchiki, K., Niwano, M., Enomoto, H., 2017. A 38-year (1978–2015) Northern Hemisphere daily snow cover extent product derived using consistent objective criteria from satellite-borne optical sensors. Remote Sens. Environ. 191, 402–418. https://doi.org/10.1016/J.RSE.2017.01.023

Immerzeel, W.W., van Beek, L.P.H., Bierkens, M.F.P., 2010. Climate Change Will Affect the Asian Water Towers. Science (80-.). 328, 1382–5. https://doi.org/10.1126/science.1183188

Inouye, D.W., 2008. Effects of climate change on phenology, frost damage, and floral abundance of montane wildflowers. Ecology 89, 353–62.

Inouye, D.W., 2000. The ecological and evolutionary significance of frost in the context of climate change. Ecol. Lett. 3, 457–463. https://doi.org/10.1046/j.1461-0248.2000.00165.x

Kendall, M.G., 1938. A new measure of rank correlation. Biometrika 30, 81. https://doi.org/10.2307/2332226

Kohler, T., Wehrli, A., Jurek, M., 2014. Mountains and Climate Change A Global Concern, in: Sustainable Mountain Development Series. Bern Swiss Centre for Development and Environment (CDE), Swiss Agency for Development and Cooperation (SDC) and Geographica Bernensia.

Kulikov, M., Schickhoff, U., 2017. Vegetation and climate interaction patterns in Kyrgyzstan: spatial discretization based on time series analysis. Erdkunde 71, 143–165. https://doi.org/10.3112/erdkunde.2017.02.04

Lesnikowski, A.C., Ford, J.D., Berrang-Ford, L., Barrera, M., Heymann, J., 2015. How are we adapting to climate change? A global assessment. Mitig. Adapt. Strateg. Glob. Chang. 20, 277–293. https://doi.org/10.1007/s11027-013-9491-x

Lioubimtseva, E., Henebry, G.M., 2009. Climate and environmental change in arid Central Asia: Impacts, vulnerability, and adaptations. J. Arid Environ. 73, 963–977. https://doi.org/10.1016/j.jaridenv.2009.04.022

Mann, H.B., 1945. Nonparametric Tests Against Trend. Econometrica 13, 245. https://doi.org/10.2307/1907187

Meals, D.W., Spooner, J., Dressing, S.A., Harcum, J.B., 2011. Statistical Analysis for Monotonic Trends. Tech Notes 6.

Morriss, B.F., Ochs, E., Deeb, E.J., Newman, S.D., Daly, S.F., Gagnon, J.J., 2016. Persistence-based temporal filtering for MODIS snow products. Remote Sens. Environ. 175, 130–137. https://doi.org/10.1016/J.RSE.2015.12.030

Narama, C., Kääb, A., Duishonakunov, M., Abdrakhmatov, K., 2010. Spatial variability of recent glacier area changes in the Tien Shan Mountains, Central Asia, using Corona (~ 1970), Landsat (~ 2000), and ALOS (~ 2007) satellite data. Glob. Planet. Change

71, 42–54. https://doi.org/10.1016/J.GLOPLACHA.2009.08.002

Painter, T.H., Rittger, K., McKenzie, C., Slaughter, P., Davis, R.E., Dozier, J., 2009. Retrieval of subpixel snow covered area, grain size, and albedo from MODIS. Remote Sens. Environ. 113, 868–879. https://doi.org/10.1016/J.RSE.2009.01.001

Rangwala, I., Miller, J.R., 2012. Climate change in mountains: a review of elevation-dependent warming and its possible causes. Clim. Change 114, 527–547. https://doi.org/10.1007/s10584-012-0419-3

Reyer, C.P.O., Otto, I.M., Adams, S., Albrecht, T., Baarsch, F., Cartsburg, M., Coumou, D., Eden, A., Ludi, E., Marcus, R., Mengel, M., Mosello, B., Robinson, A., Schleussner, C.F., Serdeczny, O., Stagl, J., 2017. Climate change impacts in Central Asia and their implications for development. Reg. Environ. Chang. 17, 1639–1650. https://doi.org/10.1007/s10113-015-0893-z

Riggs, G.A., Hall, D.K., 2015. MODIS Snow Products Collection 6 User Guide.

Rittger, K., Painter, T.H., Dozier, J., 2013. Assessment of methods for mapping snow cover from MODIS. Adv. Water Resour. 51, 367–380. https://doi.org/10.1016/j.advwatres.2012.03.002

Robinson, D.A., Dewey, K.F., 1990. Recent secular variations in the extent of Northern Hemisphere snow cover. Geophys. Res. Lett. 17, 1557–1560. https://doi.org/10.1029/GL017i010p01557

Robinson, D.A., Dewey, K.F., Heim, R.R.J., 1993. Global Snow Cover Monitoring: An Update. Bull. Am. Meteorol. Soc. 74, 1689–1696. https://doi.org/10.1175/1520-0477(1993)074<1689:GSCMAU>2.0.CO;2

Robinson, D.A., Frei, A., 2000. Seasonal Variability of Northern Hemisphere Snow Extent Using Visible Satellite Data*. Prof. Geogr. 52, 307–315.

Schanda, E., Matzler, C., Kunzi, K., 1983. Microwave remote sensing of snow cover. Int. J. Remote Sens. 4, 149–158. https://doi.org/10.1080/01431168308948536

Schillhorn Van Veen, T.W., 1995. The Kyrgyz Sheep Herders at a Crossroads. Overseas Dev. Institute. Pastor. Dev. Netw. Ser.

Tang, Z., Wang, X., Wang, J., Wang, X., Li, H., Jiang, Z., 2017. Spatiotemporal Variation of Snow Cover in Tianshan Mountains , Central Asia , Based on Cloud-Free. Remote Sens. 9, 2001–2015. https://doi.org/10.3390/rs9101045

WorldBank, 2017a. Kyrgyzstan; GDP per capita; PPP (current international $) [WWW Document]. URL https://data.worldbank.org/indicator/NY.GDP.PCAP.PP.CD?end=2016&locations=KG&start=1990

WorldBank, 2017b. Migration and Remittances Data [WWW Document]. URL http://www.worldbank.org/en/topic/migrationremittancesdiasporaissues/brief/migration-remittances-data

Xu, Y., Zhou, B., Wu, Ji, Han, Z., Zhang, Y., Wu, J, 2017. Asian climate change under 1.5–4 °C warming targets. Adv. Clim. Chang. Res. 8, 99–107. https://doi.org/10.1016/J.ACCRE.2017.05.004

Yuan-An, J., Ying, C., Yi-Zhou, Z., Peng-Xiang, C., Xing-Jie, Y., Jing, F., Su-Qin, B., 2013. Analysis on Changes of Basic Climatic Elements and Extreme Events in Xinjiang, China during 1961–2010. Adv. Clim. Chang. Res. 4, 20–29. https://doi.org/10.3724/SP.J.1248.2013.020

Zhou, H., Aizen, E., Aizen, V., 2013. Deriving long term snow cover extent dataset from AVHRR and MODIS data: Central Asia case study. Remote Sens. Environ. 136, 146–162. https://doi.org/10.1016/J.RSE.2013.04.015

2.9. Supplementary materials

Table S2.1. Area in predominant significant trends from Terra for First Date of Snow by elevation class in selected rayons. **Bold entries** indicate significant ($p<0.05$) negative trends at least twice as prevalent as significant positive trends. *Italicized underlined entries* indicate significant ($p<0.05$) positive trends at least twice as prevalent as significant negative trends. Negative (positive) trends in FDoS correspond to earlier (later) onset of snow cover. "nd" = no data as lowest elevation in rayon is >1,900 m. "--" indicates no prevalent trend.

elevation class	**Naryn** (km^2)	**At-Bashy** (km^2)	**Alay** (km^2)	**Chong-Alay** (km^2)
1,400-1,900 m	**2.8**	nd	**13.1**	nd
1,900-2,400 m	**58.0**	**45.5**	**45.5**	**1.7**
2,400-2,900 m	**41.0**	**33.1**	**33.1**	**7.7**
2,900-3,400 m	**64.8**	*116.6*	**--**	**20.8**
> 3,400 m	**--**	**--**	**109.7**	**--**
Total earlier	**166.6**	**78.6**	**201.4**	**30.3**
Total later	**--**	*116.6*	**--**	**--**

Table S2.2. Area in predominant significant trends from Terra for Duration of Snow Season (DoSS) by elevation class in selected rayons. **Bold entries** indicate significant ($p<0.05$) negative trends at least twice as prevalent as significant positive trends. *Italicized underlined entries* indicate significant ($p<0.05$) positive trends at least twice as prevalent as significant negative trends. Negative (positive) trends in DoSS correspond to shorter (longer) snow season. "nd" = no data as lowest elevation in rayon is >1,900 m. "--" indicates no prevalent trend.

elevation class	**Naryn** (km^2)	**At-Bashy** (km^2)	**Alay** (km^2)	**Chong-Alay** (km^2)
1,400-1,900 m	--	nd	*4.3*	nd
1,900-2,400 m	--	--	*15.7*	*5.4*
2,400-2,900 m	--	**38.0**	--	*57.1*
2,900-3,400 m	--	**222.0**	--	*38.6*
> 3,400 m	**23.4**	**331.4**	*24.3*	--
Total shorter	**23.4**	**591.4**		
Total longer	--	--	*44.3*	*101.1*

Table S2.3. Two-stage trend analysis for LDoS and DoSS. **Bold entries** indicate at least twice the area of the significant ($p<0.05$) pair.

Trend of 1st metric: LDoS	Area in 1st metric (%)	Area in 1st metric (km^2)	Trend of 2nd metric: DoSS	Area in 2nd metric (%)	Area in 2nd metric (km^2)
LDoS earlier	**3.2**	**5,514**	DoSS shorter	**8.2**	**452**
			DoSS longer	0.1	8
			DoSS ns	91.7	5,054
LDoS later	0.4	778	DoSS shorter	<0.1	<1
			DoSS longer	**19.9**	**155**
			DoSS ns	80.1	623
LDoS ns	96.4	168,131	DoSS shorter	1.4	2,408
			DoSS longer	1.7	2,850
			DoSS ns	96.9	162,873

Table S2.4. Two-stage trend analysis for FDoS and LDoS. **Bold entries** indicate at least twice the area of the significant ($p<0.05$) pair.

Trend of 1st metric: FDoS	Area in 1st metric (%)	Area in 1st metric (km^2)	Trend of 2nd metric: LDoS	Area in 2nd metric (%)	Area in 2nd metric (km^2)
FDoS earlier	**4.8**	**8,555**	LDoS earlier	**2.3**	**196**
			LDoS later	0.2	21
			LDoS ns	97.5	8,338

FDoS later	0.9	1,634	LDoS earlier	**3.2**	**54**
			LDoS later	1.0	15
			LDoS ns	95.8	1,565
FDoS ns	91.3	161,225	LDoS earlier	**3.3**	**5,264**
			LDoS later	0.5	742
			LDoS ns	96.2	155,219

Table S2.5. Summary of trend results from recent research studies.

		Dietz *et al.* (2013)	Dietz *et al.* (2014)	Zhou *et al.* (2013)	Tang *et al.* (2017)	Tomaszewska & Henebry (2018)
Time		2000 – 2011	1986 – 2014	1986 – 2008	2001 – 2015	2002/03 – 2015/16
Data		Daily snow cover Terra/Aqua MODIS at 500m	Daily snow cover Terra/Aqua MODIS at 500 m, and daily AVHRR at 1km	Daily and 8-day snow cover composites Terra MODIS at 500m, and daily AVHRR at 1km	Daily snow cover Terra MODIS at 500m	8-day snow cover composites Terra/Aqua MODIS at 500m
Area		Central Asia	Central Asia (results for Syr Darya upstream sub-catchment)	Central Asia (Amu Darya catchment)	Tien Shan Mountains	Kyrgyzstan
Snow Season Metrics		Snow cover duration (SCD) Snow cover start (SCS) Snow cover melt (SCM) Snow cover index (SCI)	Snow cover duration (SCD) Snow cover duration in early season (SCD_{ES}) Snow cover duration in later season (SCD_{LS})	Snow covering days (SCD) Snow cover onset date (SCOD) Snow cover melting date (SCMD)	Snow covered area (SCA) Snow covered days (SCD)	First date of snow (FDoS) Last date of snow (LDoS) Duration of snow season (DoSS)
Results	Snow Arrival	No discernable trend recognized	Negative trend of snow arrival	Negative trend of snow arrival (>3,000 m) Slightly positive trend > 4,000 m in Central Pamirs	Did not analyze snow arrival	Negative trends of snow arrival in western and central KGZ
	Snow Departure	No discernable trend recognized.	Negative trend of snow departure	Negative trend of snow departure (> 3,000 m) No significant trend >4,000 m in Central Pamirs	Did not analyze snow departure	Negative trends of snow departure in eastern KGZ

	Snow Duration	Positive trend increases with elevation	Positive trend in early season increases with elevation Generally negative trends in later season, but varies with elevation: <1,800 m positive; 1,800–2,500 m not significant; and >2,500 m negative	Did not analyze duration	Negative trend in central and eastern Tien Shan Positive trend northern and western Tien Shan	Negative trends in western and eastern KGZ Positive trends in north and southwestern KGZ

CHAPTER 3

LAND SURFACE PHENOLOGY IN THE HIGHLAND PASTURES OF MONTANE CENTRAL ASIA: INTERACTIONS WITH SNOW COVER SEASONALITY AND TERRAIN CHARACTERISTICS

Paper #2:

Tomaszewska, M.A., Nguyen, L.N., Henebry, G.M., *In revision following review*. Land Surface Phenology in the Highland Pastures of Montane Central Asia: Interactions with Snow Cover Seasonality and Terrain Characteristics. *Remote Sensing of Environment*. (reviews received 07OCT19, RSE-D-19-01373)

3.0. Abstract

Many studies have shown that high elevation environments are among very sensitive to climatic changes, and where impacts are exacerbated. Across Central Asia, the ability of global climate projections to capture the complex dynamics of mountainous environments is particularly limited. Agropastoralism constitutes the major portion of agriculture in montane Central Asia. Extensive herbaceous vegetation forms the basis of rural economies in Kyrgyzstan. Here we focus on snow cover seasonality and terrain effects on highland pasture phenology using remote sensing data for 2001-2017. First, we described the thermal regime of growing season using MODerate Resolution Imaging Spectrometer (MODIS) land surface temperature (LST) data, analyzing the modulation by elevation, slope, and aspect. We then characterized the phenology in highland pastures with metrics derived from modeling the land surface phenology using Landsat NDVI time series together with MODIS LST data. Next, using rank correlations, we analyzed the influence of four metrics of snow cover seasonality calculated from MODIS snow cover composites—first date of snow, late date of snow, duration of snow season, and the number snow covered dates—on metrics of land surface phenology, specifically, peak height (PH)

and thermal time to peak (TTP), in the subsequent growing season. Then we evaluated the role of terrain features in shaping the relationships between snow cover and pasture phenology using exact multinomial tests for equivalence. Results revealed a positive relationship between snow covered dates (SCD) and PH occurred in over 1,664 km^2 at $p < 0.01$ and 5,793 km^2 at $p < 0.05$, which account for more than 8% of 68,881 km^2 of pasturelands analyzed in Kyrgyzstan. Also, more negative than positive correlations were found between snow cover onset and PH, and more positive correlations were observed between snowmelt timing and PH. Thus, a longer snow season can positively influence PH. Significant negative correlations between TTP and SCD appeared in 1,840 km^2 at $p < 0.01$ and 6,208 km^2 at $p < 0.05$, and a comparable but smaller area showed negative correlations between TTP and snowmelt date (1,538 km^2 at $p < 0.01$ and 5,188 km^2 at $p < 0.05$). Furthermore, terrain had a stronger influence on the timing of snowmelt than on the number of snow covered dates, with slope being more important than aspect, and the strongest effect appearing from the interaction of aspect with steeper slopes. In this study, we characterized the snow-phenology interactions in highland pastures and revealed strong dependencies of pasture phenology on timing of snowmelt and snow onset and snow cover duration and. Under changing climatic conditions toward earlier spring warming, decreased duration of snow cover may lead to lower pasture productivity threatening the sustainability of montane agropastoralism.

3.1. Introduction

Studies have shown that high elevation environments are among the most sensitive to climatic changes (Diaz et al., 2003; Pepin et al., 2015; Thompson, 2000), where impacts are exacerbated (Chen et al., 2016; Immerzeel et al., 2010). Over Central Asia, which is

especially vulnerable to climate changes, (Lioubimtseva and Henebry, 2009; Luo et al., 2018; Yu et al., 2018) the ability of global climate projections to capture the complex dynamics of mountainous environments is particularly limited (Reyer et al., 2017). There remains a scarcity of climate change impact studies for Central Asia (Hijioka et al., 2014; Xenarios et al., 2018).

In a semiarid, continental climate, agropastoralism constitutes the foundation of agriculture in montane Central Asia. According to FAO statistics from 2015, rangelands constitute 87% of the agricultural land in Kyrgyzstan, the Central Asia country that is mostly mountainous (>90% of land area) (FAO, 2015). Extensive herbaceous vegetation lands form a basis of rural economies in Kyrgyzstan, which makes the foundation of highlanders' livelihoods. For centuries, the herders of the highlands have been practicing vertical transhumance — the annual movement of livestock to higher elevation pastures to take advantage of seasonally available forage resources (Schillhorn Van Veen, 1995). Dependency on pasture resource availability during the short montane growing season makes herders susceptible to changes in climate and weather patterns.

In Central Asia, the Syr Darya and the Amu Darya are the region's major rivers that flow into the Aral Sea Basin (Bernauer and Siegfried, 2012). River flow is driven by meltwater from glaciers and snow cover in the Tien Shan and Pamir mountains as well as runoff from across the Basin (Sorg et al., 2012). Increasing temperatures trigger accelerated glacier massloss and snow cover extent shrinkage, and projected warming is expected to affect significantly melt timing and magnitude (Luo et al., 2018; Wang et al., 2014). Recent studies over the region have shown a shift in precipitation from snow to rain, which decreases snowfall fraction and results in less accumulation of snow and glacier ice during

the winter (Chen et al., 2016). Moreover, changes in snow cover and shrinkage of glaciers lead to alterations in the local water cycle and water storage (Bai et al., 2019; Dedieu et al., 2014). Temperature increases are projected to be particularly high in summer and fall seasons but lower in winter (Xu et al., 2017), with a decrease in precipitation for late spring and summer (Hijioka et al., 2014; Yuan-An et al., 2013), but strong increase in winter and early spring (Luo et al., 2018; Yu et al., 2018).

There is substantial uncertainty in precipitation projections due to the scarcity of observational data coupled with the coarse spatial resolution of models that cannot resolve the complex mountainous terrain (Christensen et al., 2013; Reyer et al., 2017). There remain shortcomings in models to simulate interacting dynamical influences on precipitation due to observational data limitation for validation, interpolation methods that tend to smooth the climatological patterns, and comparison using multiscale data (Mannig et al., 2013; Rhoades et al., 2018; Stocker et al., 2013). While increased temperatures may result in an extended growing season that could benefit certain vegetation types and communities, enhanced variation in precipitation timing and amount of water availability (Chen et al., 2016; Immerzeel et al., 2010), and increased incidence of drought may negatively affect vegetation phenology and pasture productivity (Marshall et al., 2019; Petersky et al., 2019).

Here we address three open questions regarding snow cover seasonality and terrain effects on pasture phenology:

1) How does snow cover seasonality relate to subsequent land surface phenology in highland pastures?
2) How does mountainous terrain modulate snow cover effects?

3) What can recent changes in snow cover seasonality tell us about possible futures for highland pasture phenology and productivity?

Why focus on snow cover instead of precipitation or soil moisture to describe the moisture regime? First, snow dominates in the annual precipitation totals in montane Central Asia (Aizen et al., 1995; Apel et al., 2018; Sorg et al., 2012). Second, snowmelt is the critical contributor to early growing season soil moisture, and most of the seasonal biomass accumulation in pastures relies on this initial store of moisture. Third, the spatial resolution of remote sensing snow cover products is significantly higher than what is available for either precipitation or soil moisture, and the higher spatial resolution is critical to capture the complex effects of terrain.

There are recent studies that analyze snow cover impact on pasture phenology using remote sensing products over specific regions in Central Asia and High Mountain Asia. Paudel and Andersen (2013) explored the response of rangeland vegetation to snow cover dynamics in Nepal Trans Himalayas; whereas, Wan et al. (2014) explored relationships between changes in snow cover and its impact on alpine vegetation in Qinghai-Tibetan Plateau. More recently, Wang et al. (2018) studied snow cover effects on alpine vegetation growth dynamics over Tibetan Plateau. Relationships between winter snow cover dynamics, climate, and spring grassland phenology in Inner Mongolia, China was analyzed by Qiao and Wang (2019). Each study found changes in snow cover affecting the length of the growing season and, especially, the start of the growing season, which also influences aboveground net primary production as viewed through the normalized difference vegetation index (NDVI).

Due to the scarcity of ground-level data, an inability to access much data from the Soviet era, and the fact that most weather stations are located in valleys far from the pastures of interest, we relied on remote sensing datasets for measurement and indicators of snow and pasture phenology.

We framed this study using three key aspects of the highland environment (thermal regime, moisture regime, and terrain attributes) that drive and constrain the growth and development of pasture vegetation. The study period corresponds to the MODIS era: 2001-2017, and the study area encompasses pastures across Kyrgyzstan. Here we describe the thermal regime of growing season using MODIS Land Surface Temperature (LST) dataset and analyze how it is modulated by mountainous terrain. The moisture regime and its changes have already been described using snow cover metrics and trends in snow cover seasonality (Tomaszewska and Henebry, 2018).

First, we explored pasture phenology characteristics via modeling of land surface phenology (LSP) by combining Landsat surface NDVI and MODIS LST data. Phenological modeling has previously provided evidence of changes in land surface dynamics and phenology in Central Asia (Bohovic et al., 2016; de Beurs et al., 2015, 2018; de Beurs and Henebry, 2008a; Kariyeva and Van Leeuwen, 2011; Lu et al., 2014). Second, we analyzed the influence of snow cover seasonality on the phenological development in pastures using Spearman's rank correlation and asymmetry analysis. Finally, we investigated the role of terrain features—elevation, slope, and aspect—in modulating the thermal regime and in shaping relations between snow cover and subsequent phenology and productivity in highland pastures. Each of those steps prepared us to address the bigger picture of pasture vegetation dynamics to identify where in the landscape of pastures the

phenology were more sensitive to variable and changing climatic conditions. Pastures are for grazing animals, but we did not explicitly address grazing dynamics in this synoptic study because (1) vertical transhumance is the key livestock management technique in these agropastoralist communities and (2) we were addressing all pasture areas across the country without regard to the seasonality of use.

3.2. Study Area

The study area falls within the territory of Kyrgyzstan (Kyrgyz Republic), a land-locked republic in Central Asia. A highly mountainous country, it is bordered on the north and northwest by Kazakhstan, on the east and southeast by China, on the southwest by Tajikistan, and on the west by Uzbekistan. With a population of about 6 million, the total area of Kyrgyzstan is 199,951 km^2, of which nearly 96% is land with 8,150 km^2 in lakes and reservoirs (WorldBank, 2018). More than 56% of the territory lies above 2,500 m, where mountains ranges of the Tien Shan, the Pamir, and the Alatau cover more than 90% of the total land area (Azykova, 2002). The country is divided into seven *oblasts* or provinces—Talas, Chuy (including the capital Bishkek), and Issyk-Kul on the northern part of the country, and Jalal-Abad, Naryn, Osh, and Batken in the southern part—and 40 *rayons* or districts (Asian Development Bank, 2010b).

The climate of Kyrgyzstan is continental with low precipitation and intense solar radiation. Weather patterns are influenced by the high elevation, mountain ranges, distance from oceans, adjacency to the deserts, and the country's inland location in the temperate and sub-tropical zone (Akimaliev et al., 2013). Due to the high relief of the terrain, there is significant variability in daily and seasonal averages of air temperature and moisture, which result in climatic zonation by elevation. During summer months (June through August) the

average air temperature can reach from 17 to 40 °C over lowlands, while dropping to -4 °C in the mountains. The lowest average air temperatures during winter are registered in the high mountain valleys; whereas, frost occurs over the entire country (Kulikov and Schickhoff, 2017). Precipitation is unequally distributed across the country, with the lowest annual precipitation of less than 150 mm in some areas of Issyk-Kul oblast in northeastern Kyrgyzstan to more than 1,000 mm over the lowlands of the Ferghana valley to the west. More than 50% of the land area is used as pastoral rangelands, which constitutes 87% (according to 2015 FAO statistics) of the agricultural lands in Kyrgyzstan. Less than 10% of the land is suitable for crops, while forests cover only about 5%. Our focal area are the pastures of Kyrgyzstan, and our study period extends from 2000/2001 to 2017 (Figure 3.1).

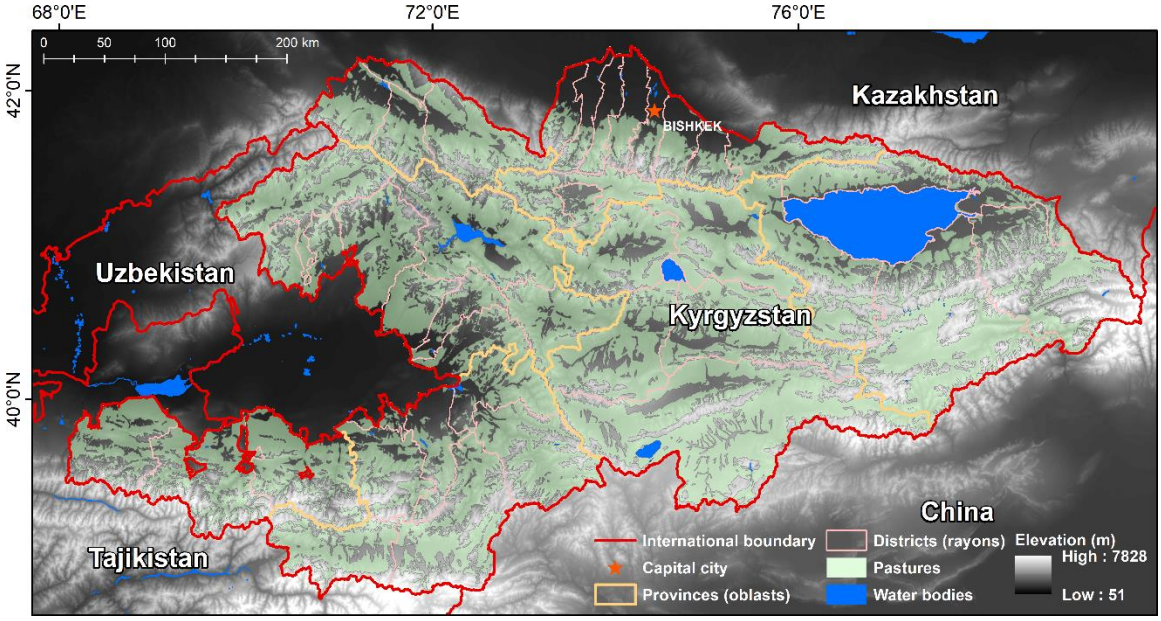

Figure 3.1. Study area: pasture land use in Kyrgyzstan is displayed in light green from (Asian Development Bank, 2010a, 2010b) and draped over the SRTM 30 m DEM (Projected coordinate system: Albers Conic Equal Area).

3.3. Geospatial Data

We used three remote sensing datasets: two MODIS Version 6 Products (i) Snow Cover at 500 m, and (ii) Land Surface Temperature at 1 km; and 30 m surface reflectance products from the Landsat Collection 1 Tier 1. Other geospatial data included Digital Elevation Model (DEM) at 1 arc-second spatial resolution (NASA JPL, 2013), the Global Multi-resolution Terrain Elevation Data 2010 (GMTED2010) mean product at 30 arc-seconds (Danielson and Gesch, 2011), and pasture land use information from a Soviet-era land use map that was updated in 2008 using Landsat 7 Enhanced Thematic Mapper Plus (ETM+) images and MODIS datasets for the CACILM project (Central Asian Countries Initiative for Land Management; Asian Development Bank, 2010a, 2010b).

3.3.1. MODIS Snow Cover Product

We used the most recent version of the MODIS Terra snow cover 8-day composites (MOD10A2 V006; Riggs and Hall, 2015) distributed by the National Snow and Ice Data Center (https://nsidc.org/). The nominal spatial resolution is 500 m, and the data are provided in a sinusoidal projection. MOD10A2 product reports the maximum snow cover extent observed during 8-day period by compositing observations from the MODIS/Terra Snow Cover Daily L3 Global 500 m Grid product (MOD10A1 V006), where the snow cover information is derived using the Normalized Difference Snow Index (NDSI) (Hall et al., 2002; Riggs and Hall, 2004). The annual dataset contains 46 8-day composites. We downloaded two MODIS tiles (h23v04 and h23v05) from 2000 to the end of 2017, merged them, then projected them into the Albers Conic Equal Area coordinate system with pixel resampling to 30 m using nearest neighbors. We then extracted in each composite all pixels flagged as “snow” (*i.e.*, pixel value = "200").

3.3.2. MODIS Land Surface Temperature Products

We used the MODIS/Terra and MODIS/Aqua Land Surface Temperature/Emissivity products at 1 km spatial resolution (MOD11A2/MYD11A2 V006), which provide an average 8-day land surface temperature (LST) for all MOD11A1/MYD11A1 LST pixels collected within the 8-day time frame (Wan et al., 2015). We downloaded two MODIS tiles (h23v04 and h23v05) of MODIS/Terra from 2001 and MODIS/Aqua from 2002 through the end of 2017. We filtered out invalid pixels using the quality bits in each product, converted temperature from Kelvin to °C, and projected the data into the Albers Conic Equal Area coordinate system with 30 m pixel resolution using bilinear resampling. We created a second dataset in which we reprojected data to the Albers Conic Equal Area coordinate system using the bilinear method, but left the spatial resolution at the nominal 1 km. This second dataset was used to characterize the thermal regimes as a function of terrain (*cf.* sections 3.4.2, 3.5.2, and 3.6.2). In contrast, the first dataset was used for land surface phenology modeling (*cf.* sections 3.4.3, 3.5.3, and 3.6.3).

3.3.3. Landsat Surface Reflectance Product

We worked with the Landsat Collection 1 Tier 1 Level-1 Precision and Terrain (L1TP) corrected product from 2001 to the end of 2017. The Collection consists of Level-1 data products generated from Landsat 8 Operational Land Imager (OLI), Landsat 7 ETM+, and Landsat 5 Thematic Mapper (TM) (USGS EROS, 2017). Surface reflectance NDVI data were obtained by downloading 13,285 images in 33 unique tiles (WRS-2 Paths 147 to 155 and Rows 30 to 33; Table S3.1) from the USGS Earth Resources Observation and Science (EROS) Center Science Processing Architecture (ESPA) On Demand Interface (https://espa.cr.usgs.gov/). We masked out invalid pixels (as cloud/snow or cloud shadows)

by applying pixel quality bits delivered with each product, and projected the data into the Albers Conic Equal Area coordinate system. The NDVI from Landsat 8 OLI surface reflectance data is greater, on average, than the NDVI from Landsat 7 ETM+ surface reflectance data (Roy et al., 2016). Thus, we also used an inter-calibration equation to adjust Landsat 7 ETM+ surface NDVI and Landsat 5 TM surface NDVI to the surface Landsat 8 OLI NDVI (Roy et al., 2016):

$$NDVI_{OLI} = 0.0235 + 0.9723 \times \{NDVI_{TM} | NDVI_{ETM+}\} \quad \text{(Equation 3.1)}$$

We used the equation [3.1] on both datasets since the differences between surface NDVI from Landsat 7 ETM+ and Landsat 5 TM are very small. Moreover, these datasets have been used together successfully in studies of land surface phenology (*e.g.*, Fisher et al., 2006; Melaas et al., 2013).

In areas with terrain complexity, differential illumination remains a controlling factor on the radiometric properties of remotely sensed data. Slope surfaces directly oriented to the sun receive more insolation than those surfaces without direct illumination. The difference of illumination and variation of the proportion of light reflected from the ground to the sensor may yield variable spectral responses even in homogeneous land covers (Allen, 2000; Vázquez-Jiménez et al., 2017). We investigated different topographic correction methods to evaluate whether these corrections would significantly affect the NDVI data in our study area. Based on exploratory analysis (*cf.* Supplementary Materials 3.11.1), we concluded a topographic normalization method was not necessary, given our questions and the demonstrated ability of the NDVI to attenuate a large amount of the variation induced by changing sun angles, topography, clouds or shadows, and atmospheric conditions (Huete et al., 1999; Matsushita et al., 2007).

3.3.4. Other Geospatial Data

For representation of the terrain, we used two digital elevation datasets. At the finer resolution, we used the SRTMGL1, the NASA Shuttle Radar Topography Mission Global 1 arc-second (~30 m) V003 product. We downloaded 133 tiles from USGS Earth Explorer (https://earthexplorer.usgs.gov/). Then we merged them and projected into the Albers Conic Equal Area coordinate system using bilinear resampling technique to 30 m spatial resolution. Further, we generated two layers—slope (in degrees) and aspect (in degrees)—and reclassified them into groups for subsequent analysis: five slope classes (0-5°, 5-10°, 10-15°, 15-30°, >30°), and nine aspect classes (N, NE, E, SE, S, SW, W, NW, and flat).

The second was the Global Multi-resolution Terrain Elevation Data 2010 (GMTED2010) mean product at 30 arc-seconds (~1 km) developed by the US Geological Survey and the National Geospatial-Intelligence Agency (Danielson and Gesch, 2011). We projected the data into the Albers Conic Equal Area coordinate system with pixel resampling to 1 km using bilinear resampling. We again created two layers—slope (in degrees) and aspect (in degrees)—and reclassified them into groups: four slope classes (0-5°, 5-10°, 10-15°, 15-30°) and just two aspect classes for aspect: Northern (NE+N+NW) and Southern (SE+S+SW). Due to its coarser spatial resolution, there is no >30° slope class in the GMTED2010.

3.4. Methods – data processing

Figure 3.2 offers an overview of the study's technical workflows to aid navigation of the multitude of data and multiple analysis steps.

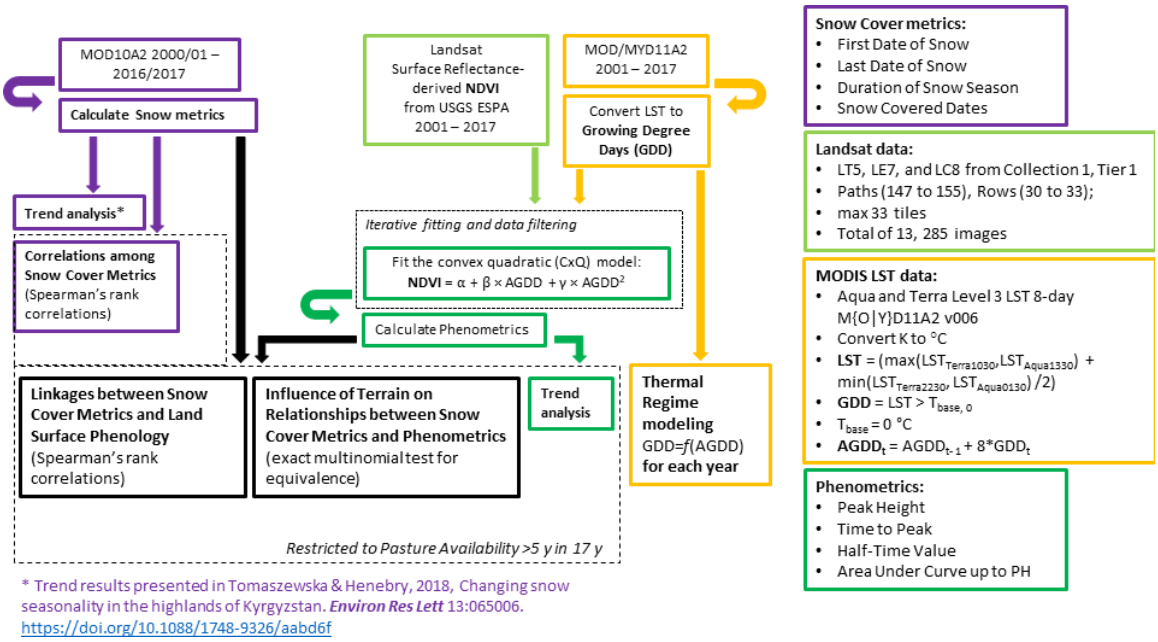

Figure 3.2. Overview of technical workflows.

3.4.1. Metrics of Snow Seasonality

We described snow seasonality by generating four temporal metrics for each snow season. We defined our observation window to bound the snow cover season each year by starting on the day of year (DOY) 169 (approximately the summer solstice) and extending to DOY 168 in the following year ($DOY169_{year}$ through $DOY168_{year+1}$). This approach enabled us to identify the first and last appearances of snow cover during the cold season. We generated four snow cover metrics: First Date of Snow (FDoS), Last Date of Snow (LDoS), Duration of Snow Season (DoSS), and the number of Snow Covered Dates (SCD). FDoS is the composite date when the pixel is flagged as snow for the first time each snow cover season. LDoS is the composite date of the last composite with snow cover during the snow season. DoSS is the difference in composite dates between LDoS and FDoS multiplied by 8 [(LDoS – FDoS+1)*8]; SCD is a number of composites with snow cover present between FDoS and LDoS, also multiplied by 8 (Tomaszewska and Henebry, 2018). The

multiplication by 8 enabled the scaling of dates across the calendar year and simplified interpretation of the metrics. Note, that we have purposefully chosen to characterize the snow cover season by its temporal extremities. Since we were interested in highland pastures, we characterized the snow cover season by the first and last detected snow cover event during the season, even though we realized that this approach could over-estimate the period of time that snow cover persisted. In terms of pasture access and grazing use, our definition of snow season is reasonable. However, we also look at the number of snow cover dates (SCD) as another way to characterize snow seasonality.

We used 8-day composites rather than daily data to obtain consistent statistical power across trend analyses, a significant advantage over daily time series.

Figure 3.3 illustrates the mean LDoS across 17 years of observations across those pasture areas with at least one year of successful LSP fitting.

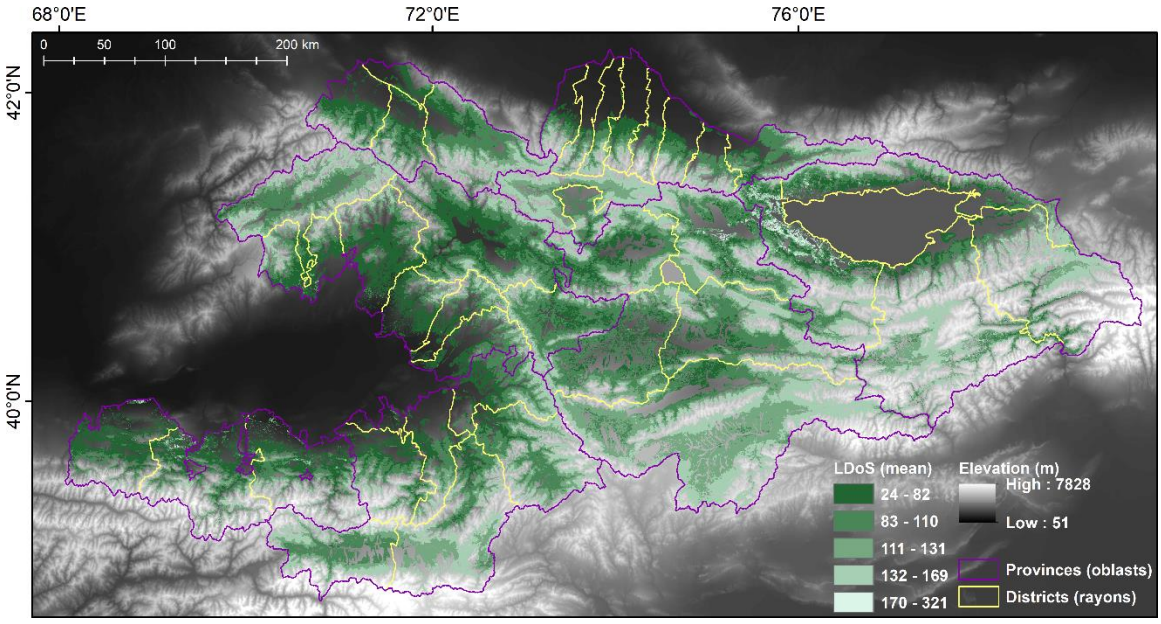

Figure 3.3. Mean values of Last Date of Snow (LDoS). Map draped over the SRTM 30 m DEM displays data only for pasture land use (Projected coordinate system: Albers Conic Equal Area).

The earlier mean LDoS during the snow season occurs mostly over western lowlands near the Ferghana Valley, in the interior at lower elevations, and around Issyk-Kul (the large lake of the endorheic basin in northeastern Kyrgyzstan). The latest snowmelt occurs at higher pastures in central Kyrgyzstan, and over the southern and southeastern parts of the Tien-Shan mountains. (Note how well mean LDoS corresponds with MODIS LST-derived mean annual AGDD shown in Figure 3.5) The average snow covered dates appear in Figure 3.4. Higher values of SCD occur over the southern area of the country, close to the northern range of the Pamirs, and over the higher ridges of the Tien-Shan in central Kyrgyzstan. The least SCD occur at the edges of the Ferghana Valley, and along the lower elevated areas around Issyk-Kul. See Appendix for the maps of mean FDoS (Figure S.31) and mean DoSS (Figure S3.2).

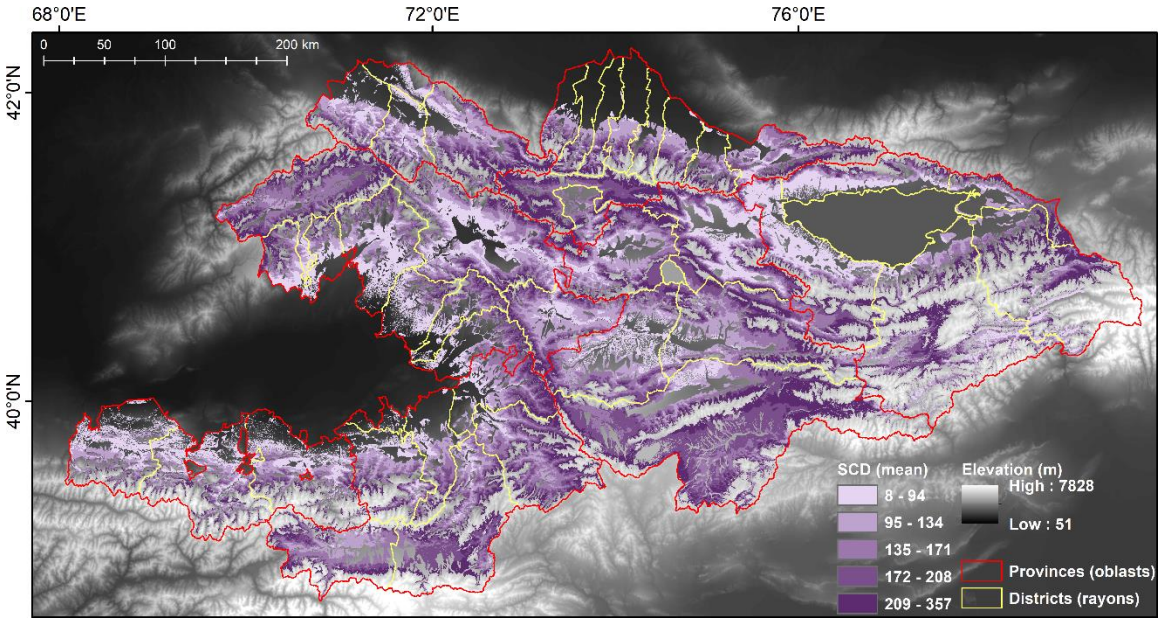

Figure 3.4. Mean values of Snow Cover Days (SCD). Map draped over the SRTM 30 m DEM displays data only for pasture land use (Projected coordinate system: Albers Conic Equal Area).

3.4.2. Metrics of Thermal Time

We calculated accumulated growing degree-days (AGDD) to characterize the progression of thermal time during the year. Growing degree-days (GDD) can be interpreted as a proxy of insolation, potentially useful for growth and development of herbaceous vegetation in the temperate mid-latitudes (de Beurs and Henebry, 2010a; Henebry, 2003). We modified an algorithm developed by Krehbiel and Henebry (2016), and subsequently revised (Krehbiel et al., 2017; Nguyen et al., 2018) to calculate AGDD from MODIS LST time series. The transformation of two daytime and nighttime observations from Terra and Aqua into mean MODIS LST was based on equation [3.2], where the highest and the lowest LST values were selected to calculate the mean MODIS LST:

$$\text{mean MODIS LST} = [\max(LST_{1030}, LST_{1330}) + \min(LST_{2230}, LST_{0130})]/2 \quad \text{(Equation 3.2)}$$

For the year 2001 and part of 2002, we used only MODIS/Terra images. To fill gaps due to missing or excluded pixels by filtering, we used Seasonally Decomposed Missing Value Imputation (Moritz and Bartz-Beielstein, 2017), which first removed the seasonal component from the time series, was conducted using the weighted moving average with k = 4 (8 observations with 4 left, and 4 right), determined the exponential weighting based on the deseasonalized series, and then added back the seasonal component. We further filtered out mean MODIS LST below 0°C, and calculated the GDD [3.3] at composite period t as the maximum between mean LST and T_{base}, which was set to 0 °C (Goodin and Henebry, 1997; Henebry 2013). Each of 46 GDD composites was then multiplied by 8 to account for the 8-day compositing time frame of the MODIS product and accumulated across the year [3.4]. $AGDD_0$ was set to zero at the start of each year.

$$GDDt = \max(\text{mean MODIS } LST_t - T_{base}, 0) \quad \text{(Equation 3.3)}$$

$$AGDDt = AGDD_{t-1} + (GDD_t \times 8) \quad \text{(Equation 3.4)}$$

In total, we generated 17 years of time series of accumulated growing degree-days (AGDD in °C). Figure 3.5 illustrates the average annual AGDD across the pasture areas of Kyrgyzstan. Note the higher mean AGDD (in reds) occur over western lowlands near the Ferghana Valley in Uzbekistan, in the interior of the country at lower elevations, and around Issyk-Kul. The lowest average AGDD occur over southern Kyrgyzstan, which is higher in elevation.

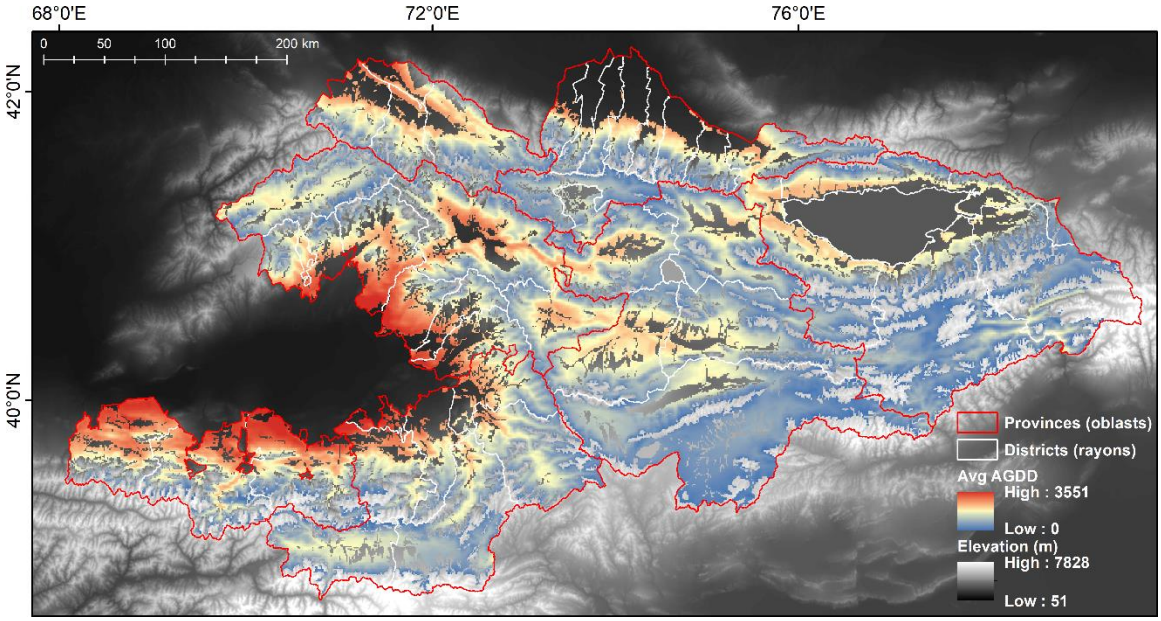

Figure 3.5. MODIS LST-derived (2001–2017) mean annual AGDD for pasture land use in Kyrgyzstan. Map draped over the SRTM 30 m DEM displays data only for pasture land use (Projected coordinate system: Albers Conic Equal Area).

3.4.3. Land Surface Phenology

There are many methods to characterize land surface phenology (*cf.* de Beurs and Henebry, 2010a). We used a downward-arching convex quadratic (CxQ) function to model LSP (de Beurs and Henebry, 2004; Henebry and de Beurs, 2013) as follows:

$$NDVI = \alpha + \beta \times AGDD + \gamma \times AGDD^2 \quad \text{(Equation 3.5)}$$

where the fitted coefficient of the quadratic parameter (γ) was required to be negative. Landsat surface reflectance data served to calculate NDVI as a proxy for active green vegetation, and MODIS LST for AGDD as a proxy for insolation, since the land surface temperature in grasslands during the growing season is highly correlated with insolation (Henebry, 2003; Still et al., 2014). The CxQ model has been successfully used in analyses of LSP dynamics at various scales in Central Asia (de Beurs et al., 2018; de Beurs and Henebry, 2008b, 2004; Henebry et al., 2005) elsewhere in Eurasia (de Beurs et al., 2009; de Beurs and Henebry, 2008a, 2005) and in North America (Henebry and de Beurs, 2013; Krehbiel et al., 2017; Walker et al., 2015).

For each pixel in the study area, we used the fitted parameter coefficients—intercept (α), slope (β), and quadratic (γ)—to calculate four phenological metrics (phenometrics) for each year from 2001 to 2017. These phenometrics provide indications of pasture condition.

Table 3.1. Phenology metrics (phenometrics) used in the study.

Phenometrics	**Equation**	**Description**
Peak Height	$PH = \alpha - (\beta^2/4\gamma)$	the maximum modeled NDVI
Thermal Time to Peak	$TTP = -\beta/2\gamma$	the quantity of AGDD required to reach PH; corresponds to duration of modeled green-up phase
Half-Time Value	$HTV = \alpha - (3\beta^2)/(16\gamma)$	NDVI at half-TTP; corresponds to green-up rate
Area Under the Curve up to PH and TTP	$AUC = \Sigma_{i=1,t} (NDVI_t+NDVI_{t-1})\times(AGDD_t-AGDD_{t-1})$	numerically integrating by trapezoidal method the NDVI time series as a function of thermal time, serves as a proxy of pasture productivity during the green-up phase

It was necessary to process the pixel time series to reduce noise and spurious data prior to model fitting and then to evaluate the quality of each fit. For each period spanning the 8-day AGDD composites, we used the corresponding Landsat observation with the highest NDVI value. We filtered out observations with NDVI<0.1 and AGDD<100 to avoid including non-vegetated pixels. In addition, to account for cloud contamination that might not have been eliminated through quality masking, we looked for unusual dips in the NDVI time series. We first calculated the simple average of NDVI observations on either side of the focal observation. We then calculated the percentage difference between the average NDVI and the focal observation, and then excluded observations that were greater than or equal to 15% than the average of the two neighboring observations. We further excluded pixels from model fitting where the number of Landsat observations in a particular year were fewer than seven.

For each pixel in each year, we fitted the filtered NDVI and associated AGDD time series to the downward-arching CxQ LSP model shown in [3.5]. We accepted the fitted model into further analysis only if it passed all six of the following criteria:

1) the quadratic parameter (γ) was less than 0;
2) the TTP greater than the AGDD of the first observation;
3) the adjusted R^2 greater than 0.7;
4) the Root Mean Square Difference (RMSD) less than 0.08;
5) the PH below 1.0; and
6) at least three observations were distributed before and at least three after the PH.

If any criterion was not fulfilled during the fitting, then the last observation was removed from the filtered dataset, and the model fitting was rerun over the newly filtered dataset. We repeated this fitting procedure to contract the length of the time series until either a fitted model that passed all criteria or the length of the time series was fewer than 7 observations. In the latter case, the model fit for that pixel was labeled as a failure in that year and no phenometrics were calculated. Finally, for the successfully fit models, we calculated the AUC up to PH using a baseline of AGDD=100 and NDVI=0.10 using trapezoidal integration. Figure S3.3 shows the total number of observations over 17 years used for successful fits.

3.5. Methods – data analysis

3.5.1. Pasture Availability Classes

We summarized each annual fit with a binary variable (0=no fit, 1=fit) to generate a final map of the total number of years with successful fits for each pixel. Then we divided these results into three pasture availability classes: (i) Highly Persistent (HP) pastures with 11-17 years of successful fits out of 17 years of observations, (ii) Persistent (P) pastures with 5-10 years, and (iii) Rarely Available (RA) pastures with just 1-4 years of successful fits. We based all subsequent analyses only on those pixels in either the HP or P pasture availability classes, because these locations host the natural resources that provide the foundation of the pastoralist economy.

3.5.2. Thermal Regime of Growing Season

To understand thermal regime of the growing season over pasture areas over Kyrgyzstan, we fitted mean GDD values for 1000 randomly selected pixels as a quadratic function of AGDD (at 1 km spatial resolution) varying by elevation, slope gradient (in four classes: 0-5°, 5-10°, 10-15°, 15-30°), and contrasting aspects (northern: NE+N+NW, southern: SE+S+SW). We used fitted parameter coefficients of quadratic curves from modeling and calculated PH for GDD and TTP for AGDD.

3.5.3. Land Surface Phenology

Based on the successful model fits, we calculated basic descriptive statistics (mean, standard deviation, and coefficient of variation) for each of the four phenometrics (*viz.*, PH, TTP, HTV, and AUC) for the series of 17 seasons from 2001 through 2017. We also applied the non-parametric Mann-Kendall trend test and the Theil-Sen linear trend

estimator (Hirsch et al., 1982; Kendall, 1938)—the same approach as in Tomaszewska and Henebry (2018)—to detect directional changes in PH and TTP over the 17 year study period.

3.5.4. Spearman's Rank Correlation to Link Snow Cover Seasonality with Phenometrics

To estimate the association of the metrics of snow cover seasonality with phenometrics from the subsequent growing season, we used Spearman's rank correlations (Fieller et al., 1957; Lehmann and D'Abrera, 2006), which assesses whether a monotonic relationship—not necessarily linear—occurs between two variables. The method is robust against outliers and works for data exhibiting non-normality. We used rank correlations in two ways: (1) to evaluate the relationships among the four snow cover temporal metrics (*viz.*, FDoS, LDoS, DoSS, and SCD); and (2) to evaluate the relationships between the four snow cover temporal metrics and four phenometrics (*viz.*, TTP, PH, HTV, AUC) for the Highly Persistent (HP) and Persistent (P) pasture availability classes, separately. Note that we consider FDoS to precede the growing season; thus, we did not evaluate the relationship between the phenometrics and FDoS of the subsequent snow season, even though it may occur in the same calendar year. We calculated the areal percentage of pixels exhibiting significant positive or negative correlations at $p<0.01$ and $p<0.05$. Finally, we calculated the ratio of pixels with positive correlations to pixels with negative correlations to identify the predominant direction of the detected significant relationships. We used threshold values of >2.0 to indicate a strong asymmetry favoring significant positive correlations and of <0.5 to indicate a strong asymmetry favoring significant negative correlations.

3.5.5. Exact Test for Multinomial Equivalence of Terrain Effects

Statistical tests of the difference (inequality) are typically used in remote sensing studies to determine whether differences between groups are statistically significant (Foody, 2009). Here we instead conducted a series of equivalence tests to evaluate the influence of terrain on the associations between snow seasonality and phenometrics, due to the very large sample size and non-negligible spatial autocorrelation (de Beurs et al., 2015; Foody, 2009; Frey, 2009; Wellek, 2010). Equivalence testing works through evaluating two one-sided tests against the null hypothesis that the distributions are different in the sense that the distance between the distributions is greater than or equal to the specified value Δ:

$$H_0: d(p,p0) \geq \Delta \text{ against } H_1: d(p,p0) < \Delta$$

where d(p,p0) is the observed Euclidean distance between two probability densities (distributions), and the 95% upper bound for d(p,p0) corresponds to a p-value of 0.05. Posed another way: if the distance between the two distributions is less than Δ (*viz.*, failing to reject both one-sided tests), then we conclude the distributions are equivalent. We used a conservative version of the exact multinomial test for equivalence since the sample sizes were large, and we selected $\Delta = 0.025$ as the standard for equivalence (Frey, 2009).

To investigate the influence of terrain on the linkage between snow cover seasonality and land surface phenology, we focused on nine hotspots in HP pastures where spatial clusters of significant correlations between particular snow cover temporal metrics and phenometrics were evident (Figure S3.4). We reasoned that the influence of terrain on the relationships would be more evident in HP pastures, where there are more years of successful fits. The null hypothesis for our equivalence testing is that terrain plays a major

role in shaping the relationship between snow cover seasonality and the phenometrics in the subsequent warm season in that hotspot. Rejecting H_0 deems the two distributions as equivalent, indicating that no effect of the terrain feature is evident.

For each hotspot, we calculated the proportions of pixels over the entire area hosting the hotspot in different terrain feature classes. These data were the "potential" distribution. We also calculated the proportion of pixels exhibiting significant correlations between the snow cover temporal metrics and the phenometrics in different terrain feature classes. This subset of pixels was the "observed" distribution. We tabulated proportions in aspect in nine classes, slope in five classes, and slope × aspect interactions, giving a total of eight terrain feature groups: aspect; slope; 0-5° × aspect; 5-10° × aspect; 10-15° × aspect; 15-30° x aspect; >30° × aspect; and slope × aspect. For each terrain feature group, we ran a separate exact multinomial test for equivalence. We generated "observed" distributions as follows: for positive correlations between SCD and PH for nine hotspots; positive correlations between LDoS and PH for hotspots 1-8; negative correlations between LDoS and PH for hotspot 9 only; and, for all nine hotspots, negative correlations between SCD and TTP, negative correlations between LDoS and TTP; and positive correlations between SCD and HTV.

3.6. Results

3.6.1. Pasture Availability Classes

We generated 115,551,865 pixels (103,997 km^2) with successful fits over pasture areas for the 17-year period. This area covers 52% of the country's land area and 85% of the pasture land use area. Highly Persistent (HP) pastures covered 15,261 km^2 or 12.5% of pasture land use area, Persistent (P) pastures covered 53,620 km^2 or 43.8%, and Rarely Available

(RA) pastures covered 35,114 km^2 or 28.7% of the area indicated as pasture land use (Figure 3.6). The total area of unsuccessful fits covered 18,412 km^2 or 15% of pasture land use. Table 3.2 shows the distribution of pasture availability classes by elevation in areal percentage. Note, in Figure 3.6, the purple stripes that arise, in part, from data availability. While it is not possible to disentangle data availability from *in situ* pasture suitability, the segregation of the pixels into different temporal classes helps to focus the subsequent analyses of linkages between variables to locations with more data.

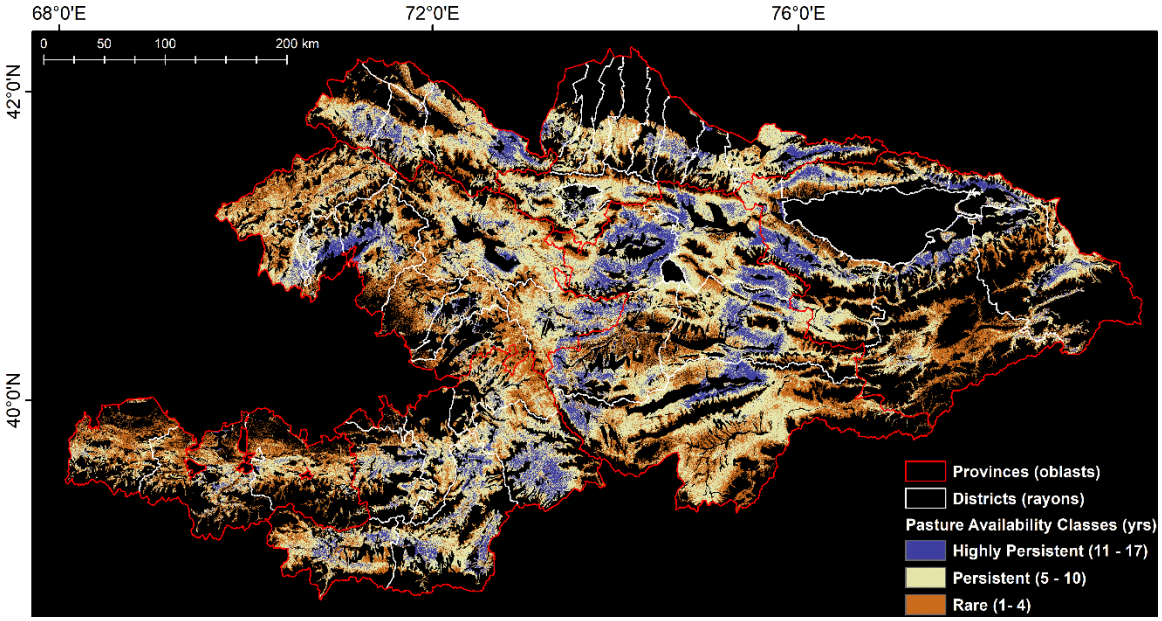

Figure 3.6. Pasture Availability classes: Highly Persistent pastures (available during 11-17 years of the 17-year study period) in dark purple; Persistent pastures (5–10 years) in light yellow; and Rarely Available pastures (1–4 years) in orange. Map displays data only for pasture land use areas (Projected coordinate system: Albers Conic Equal Area).

Table 3.2. Total area in pasture availability class and percentage distribution by elevation class.

Elevation Class (m)	Pasture Area (km^2)	Highly Persistent (%)	Persistent (%)	Rarely Available (%)	No Fit (%)
< 1800	23,593	16.0	15.5	21.8	28.1
1800–2400	25,487	27.2	25.0	18.9	7.0
2400–2900	21,597	32.9	21.2	13.2	3.4
2900–3400	27,221	21.7	26.8	22.1	9.7
3400–4000	22,038	2.2	11.5	23.6	39.3
> 4000	2,469	<0.01	<0.1	0.4	12.5
Total	122,405	100.0	100.0	100.0	100.0

Highly persistent pastures are prevalent from 1800-2400 m, with nearly one-third found between 2400 m and 2900 m and 27% from 1800 m to 2400 m. In contrast, there are more persistent pastures above 2900 m and roughly the same proportion below 2400 m: 43% in HP vs. 41% in P (Table 3.2) Rarely Available pastures occur at different elevations in comparable proportion, except in the 2400 – 2900 m elevation band, where there are many more HP pastures. Most unsuccessful fits occur at the lowest elevation range below 1800 m (28%) and above 3400 (52%). We based our subsequent analyses only on the HP and P pasture availability classes.

3.6.2. Thermal Regime of Growing Season

The Thermal regimes in highland pastures can be summarized by the shape of GDD as a function of AGDD changes due to elevation (Figure 3.7). It is clear from Figure 3.7 and from Table 3.3 that (1) the patterns of GDD as a function of AGDD during the warm season are well-approximated by the same kind of downward-arching parabolic shape used to model LSP, and (2) the seasonal amplitudes (PH_{GDD}) and durations (TTP_{AGDD}) change smoothly as a function of elevation. PH_{GDD} and TTP_{AGDD} are greater at the lower elevations (Table 3.3). The annual variation represented by the error bars (± 2 SEM) across the 17

years of observation is much higher during beginning and end of the warm season than the seasonal peak at lower elevations; however, at higher elevations, variation is much larger just before peak values (Figure 3.7). Some asymmetries in the seasonal curves are evident and documented by the pattern of adjusted R^2 values, which reach a relative low point in the 2400-2900 m elevation class (Table 3.3).

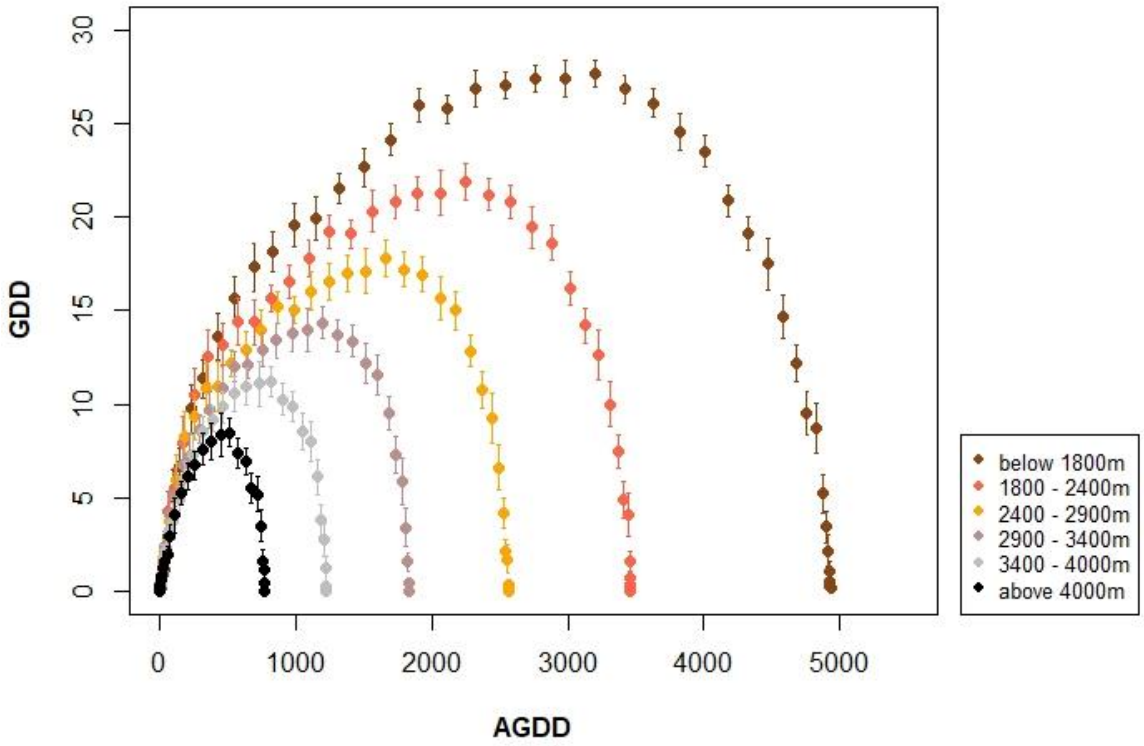

Figure 3.7. Mean annual Growing Degree-Days (GDD) with ± 2 SEM (Standard Errors of Mean) vs. mean annual Accumulated Growing Degree-Days (AGDD) for 1000 randomly selected pixels within six elevation classes: (i) below 1800 m (brown), (ii) 1800–2400 m (orange) , (iii) 2400–2900 m (golden), (iv) 2900–3400 m (rosy brown), (v) 3400–4000 m (gray), and (vi) above 4000 m (black).

Table 3.3. Modeled PH and TTP, adjusted R^2 values on GDD – AGDD quadratic curve at different elevation ranges.

Elevation Class (m)	PH_{GDD}	TTP_{AGDD}	adjusted R^2
below 1800	29.5	2527	0.94
1800-2400	23.1	1774	0.92
2400-2900	18.8	1313	0.91
2900-3400	15.3	937	0.92
3400-4000	11.9	625	0.94
above 4000	8.8	392	0.95

Figure 3.8 shows the mean annual progression of thermal time during the warm season as a function of both slope and aspect for the six elevation classes. Four patterns are notable. First, at the beginning of the warm season there is very little distinction in the progression of thermal time among terrain features. As the season progresses, divergence among slope×aspect classes becomes more pronounced. Second, the divergences between contrasting aspects (northern vs. southern) are more pronounced in steeper slope classes. Third, interactions of slope and aspect result in virtually interchangeable thermal time profiles, especially at higher elevations, but these interactions can produce counter-intuitive results. Two examples: (1) in the 2900-3400 m class, the southern aspect pixels on 15-30° slopes (open yellow) show a comparable seasonal profile to the northern aspect pixels on 0-5° slopes (solid black); and (2) in the 3400-4000 m class, the southern aspect pixels on 5-10° slopes (open magenta) track similarly to northern aspect pixels on 15-30° slopes (solid yellow). The patterns in PH_{GDD} and TTP_{AGDD} across elevations, slopes, and aspects are expected. Downward-arching quadratic curves fit well, with all adjusted R^2 values greater than 0.90; decreasing values of PH_{GDD} and TTP_{AGDD} as elevation increases; and increased differences between phenometrics by aspect as slopes increase (Table 3.4). Moreover, southern aspect slopes are proportionally warmer than northern aspect slopes

averaged across elevations, but the magnitudes of the differences increase as slopes become steeper, and TTP_{AGDD} increases more quickly than PH_{GDD} (Table 3.5).

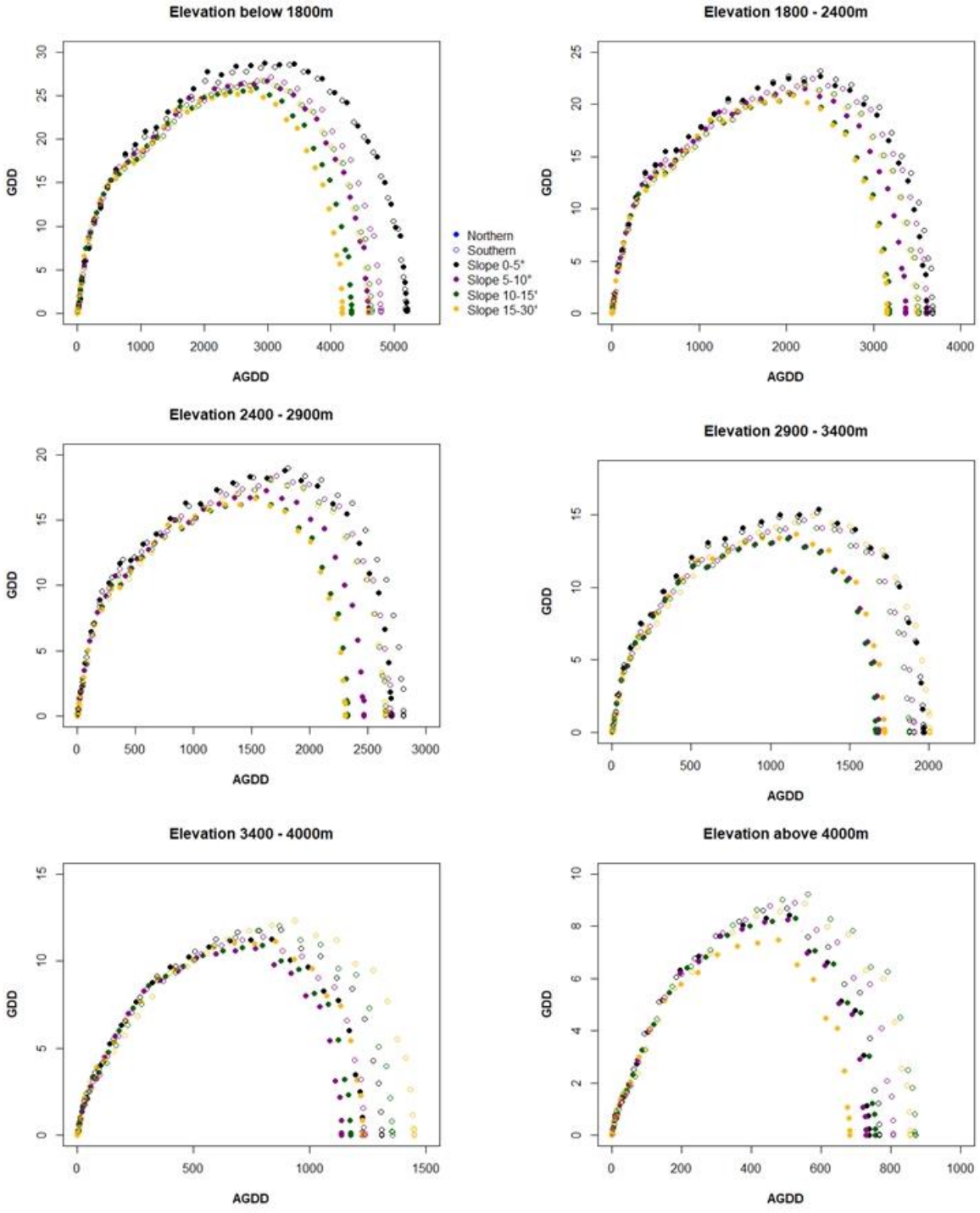

Figure 3.8. Mean annual Growing Degree Days (GDD) vs. mean annual Accumulated Growing Degree Days for 1000 randomly selected pixels at six elevation ranges: (i) below 1800m, (ii) 1800 – 2400m , (iii) 2400 – 2900 m, (iv) 2900 – 3400m, (v) 3400 – 4000m, and (vi) above 4000m, for northern (filled circle) and southern (open circle) aspects at four slope classes: (i) 0-5°, (ii) 5-10°, (iii) 10-15°, (iv) 15-30°. Note that the scaling of the y-axes varies between panels.

Table 3.4. PH, TTP, and adjusted R^2 values from fitting quadratic thermal time patterns at different elevation classes as a function of slope (four classes) and two contrasting aspects (northern and southern).

	Slope 0 -5°			*Slope 5-10°*			*Slope 10-15°*			*Slope 15-30°*		
Elevation Class (m) and aspect	**PH_{GDD}**	**TTP_{AGDD}**	**adj. R^2**	**PH_{GDD}**	**TTP_{AGDD}**	**adj. R^2**	**PH_{GDD}**	**TTP_{AGDD}**	**adj. R^2**	**PH_{GDD}**	**TTP_{AGDD}**	**adj. R^2**
below 1800 **N**	30.9	2665	0.94	28.3	2352	0.94	27.5	2216	0.93	27.2	2142	0.93
below 1800 **S**	30.3	2661	0.94	28.5	2460	0.93	27.9	2384	0.93	27.9	2360	0.92
1800-2400 **N**	24.3	1846	0.92	22.9	1725	0.92	22.0	1629	0.92	22.1	1617	0.92
1800-2400 **S**	24.6	1884	0.92	23.5	1857	0.92	22.7	1807	0.92	22.7	1799	0.92
2400-2900 **N**	20.1	1383	0.91	18.4	1261	0.91	17.8	1191	0.91	17.8	1179	0.92
2400-2900 **S**	20.1	1439	0.91	19.3	1384	0.91	18.9	1364	0.91	18.8	1365	0.92
2900-3400 **N**	16.5	1004	0.92	14.5	860	0.92	14.4	851	0.92	14.7	878	0.93
2900-3400 **S**	16.3	1006	0.92	15.4	977	0.92	15.2	964	0.92	15.6	1030	0.92
3400-4000 **N**	12.1	626	0.94	11.5	579	0.94	11.7	600	0.93	11.9	626	0.94
3400-4000 **S**	12.6	669	0.94	12.0	632	0.93	12.5	694	0.93	12.7	743	0.93
above 4000 **N**	8.7	376	0.94	8.6	371	0.94	8.6	385	0.94	7.8	347	0.94
above 4000 **S**	9.0	391	0.95	9.1	411	0.94	9.4	445	0.94	9.0	438	0.94

Table 3.5. Percent differences, calculated as (southern-northern)/northern×100), in PH and TTP values for contrasting aspects averaged across elevation classes.

Slope Class	Aspect Difference in PH_{GDD} (%)	Aspect Difference in TTP_{AGDD} (%)
0<5°	0.94	2.84
5<10°	4.10	9.26
10<15°	5.42	12.93
15<30°	6.52	16.57

3.6.3. Land Surface Phenology

We calculated averages (over 17 years) for the four phenometrics (PH, TTP, AUC, HTV) derived from the successful fits over the pasture land use areas. Figure 3.9 displays maps of the mean values of PH and TTP. Note that the strips apparent in Figure 3.6 are not evident in Figure 3.9 since the former shows the frequency, and the latter shows average fitted values. Higher PH values (in green) occur at higher elevations over western, northern, and central parts of Kyrgyzstan; whereas, lower PH (in brown) occurs in the central lowlands and over the drier higher elevations in southern Kyrgyzstan. West of Issyk-Kul PH values are low, while they are higher east of the lake. The pattern for TTP is different. In the west near the Ferghana Valley at lower elevations, the TTP mean values are high (in red), and TTP decreases as elevation increases. Over the lowlands in central Kyrgyzstan, where PH is low, TTP is high, and conversely, TTP is low where PH is high. The spatial pattern of mean HTV values closely track PH (data not shown).

Figure S3.5 shows mean AUC values over the 17 years. Over western Kyrgyzstan, where PH and TTP values are high, AUC is also high (dark green). In contrast, over areas where PH is high but TTP is low at northern highlands, AUC values are lower. However, in the central highlands, where PH is high but TTP is low, mean AUC reaches high values. The

lowest AUC values occur over dry southern Kyrgyzstan. Mean TTP more closely follows an elevational gradient compared to PH, since air temperature and moisture exhibit lapse rates as a function of altitude, and land surface temperature is related to, but distinct from, air temperature. In contrast, since PH and AUC are driven by abiotic factors (climate, terrain, recent weather), biotic influences (vegetation community, grazing pressure, unpalatable species), and disturbance history (time since landslide, time since grazing, time since drought), they can interact with elevation in complicated ways.

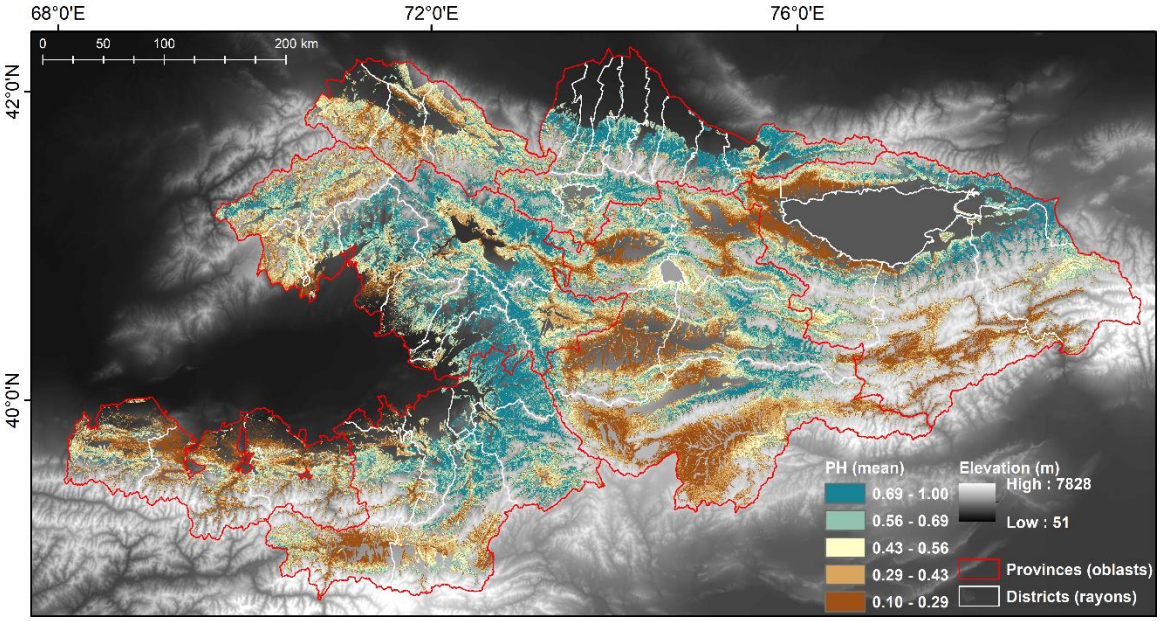

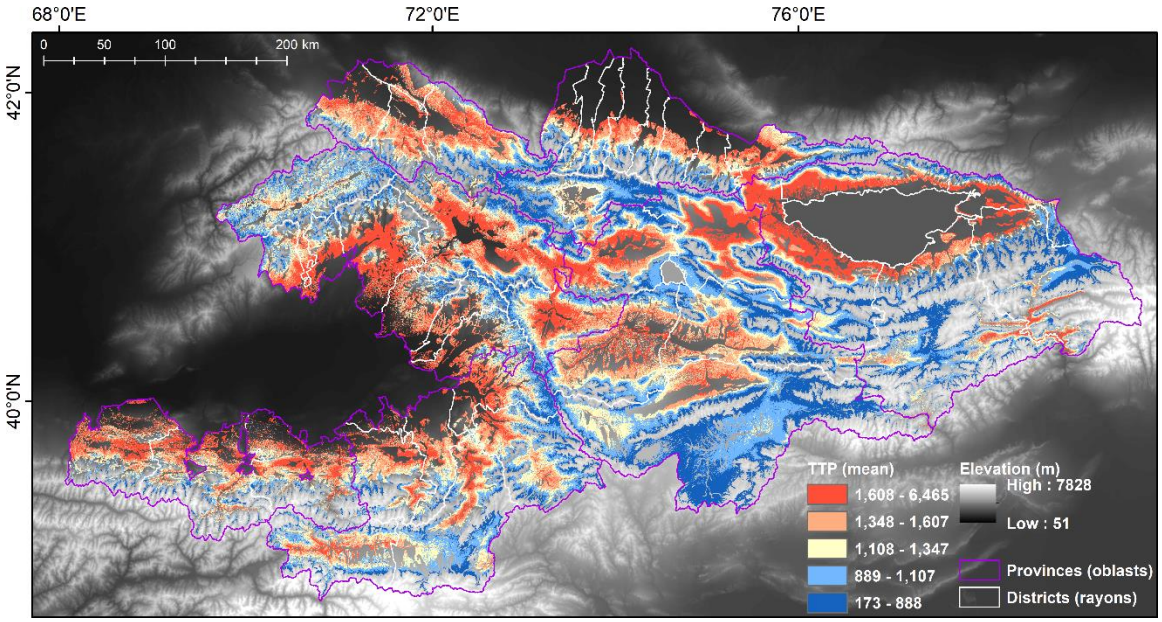

Figure 3.9. (Upper) Mean values of Peak Height (PH), (Bottom) Mean values of Time To Peak (TTP). Maps draped over the SRTM 30 m DEM display data only for pasture land use (Projected coordinate system: Albers Conic Equal Area). Classes based on quintiles.

Figure 3.10 shows the integrated coefficient of variation (CV) over 17 seasons for PH and TTP. We used the median value of CV for each metric (10% for PH and 12% for TTP) as the breakpoint between higher and lower levels of CV. Higher CV for PH and TTP occurs over centrally located lowlands where PH is low and TTP is high, and highlands along the southern border of Kyrgyzstan where PH and TTP are both low. In the western and northern highlands where mean PH is high, lower CV values occur for PH but higher for TTP. The pattern of higher CV for PH and lower CV for TTP occurs over the drier southern regions; whereas, lower CVs for both PH and TTP occur more in the central and northern parts of Kyrgyzstan. Spatial patterns of CV for AUC are muted (as might be expected with an integral measure) with high CV values appearing only in the central valleys (Figure S3.6).

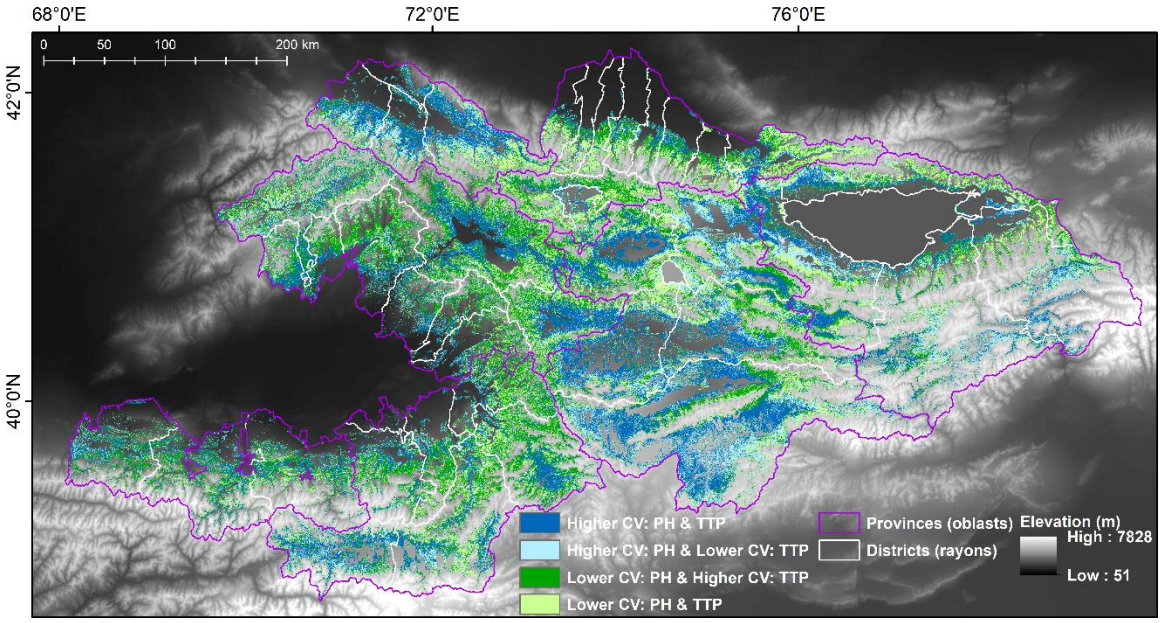

Figure 3.10. Map of integrated Coefficient of Variation for Peak Height (PH) and Thermal Time to Peak (TTP). Median value used as a threshold for higher and lower values (10% for PH, 12% for TTP). In dark blue, higher values for both phenometrics; in light blue, higher CV of PH but lower for TTP; in dark green, lower CV of PH but higher of TTP; and in light green, lower CV for both phenometrics. Map draped over the SRTM 30 m DEM displays data only for pasture land use (Projected coordinate system: Albers Conic Equal Area).

Figures 3.11 and 3.12 map the positive and negative trends of TTP and PH over pasture land use areas. Positive trends of TTP occur mostly over the southern (drier) part of the country and around Issyk-Kul Lake, whereas negative TTP trends appear mostly over central western regions (Figure 3.11). It can be observed that there are no dominant trends in TTP over the study region and the area in significant TTP trends does not exceed 4% of HP or P pastures (Table 3.6). A very different situation appears for PH. The only negative trend occurs on the eastern coast of the Issyk-Kul Lake; whereas, over the remainder of the pasturelands, there are clear positive trends (Figure 3.12), up to 23% of the HP pastures area and 14% of the P pastures (Table 3.6).

Table 3.6. Areal extent (in km^2) and percentage of phenometrics (TTP and PH) with significant positive or negative trends at p-value < 0.01 and p-value < 0.05 for highly persistent (HP) and persistent (P) pastures.

	POSITIVE				***NEGATIVE***			
	p<0.01		**p<0.05**		**p<0.01**		**p<0.05**	
HP (11- 17 yrs) Area=15,261 km^2	km^2	%	km^2	%	km^2	%	km^2	%
TTP	22	0.15	234	1.53	43	0.28	179	1.17
PH	1,188	7.78	3,527	23.11	11	0.07	51	0.33
P (5-10 yrs) Area=53,620 km^2	km^2	%	km^2	%	km^2	%	km^2	%
TTP	41	0.08	476	0.89	68	0.13	535	1.00
PH	1,628	3.04	7,291	13.60	10	0.00	86	0.16

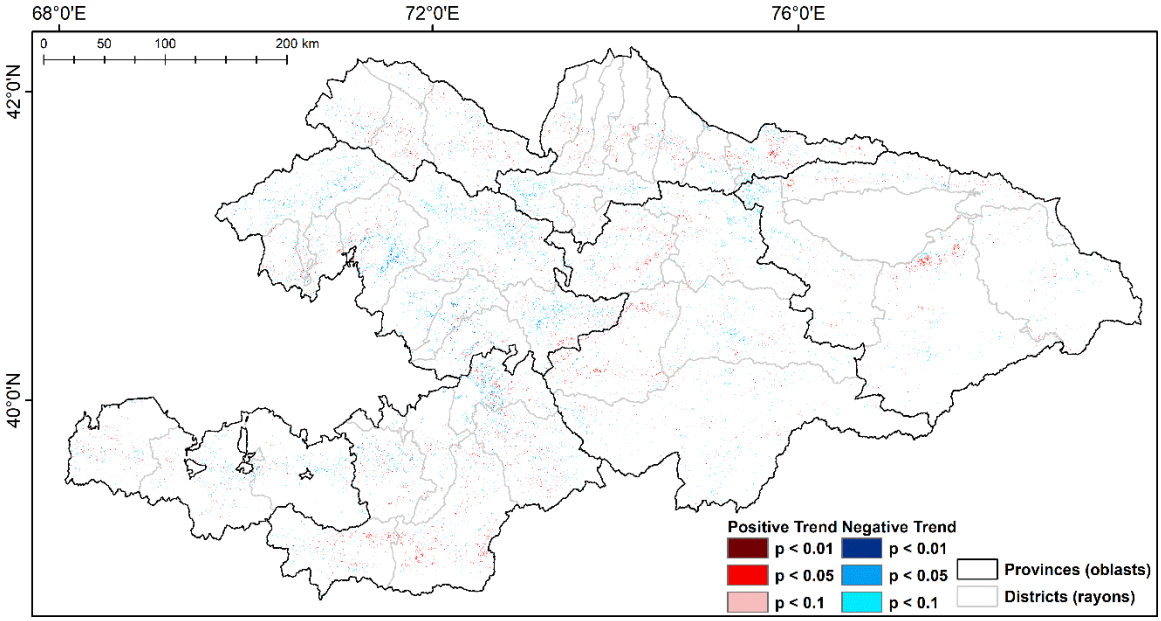

Figure 3.11. Map of significant positive (in red) and negative (in blue) trends of TTP at three significance levels (p<0.01, p<0.05, p<0.1). Map displays data only for pasture land use areas (Projected coordinate system: Albers Conic Equal Area).

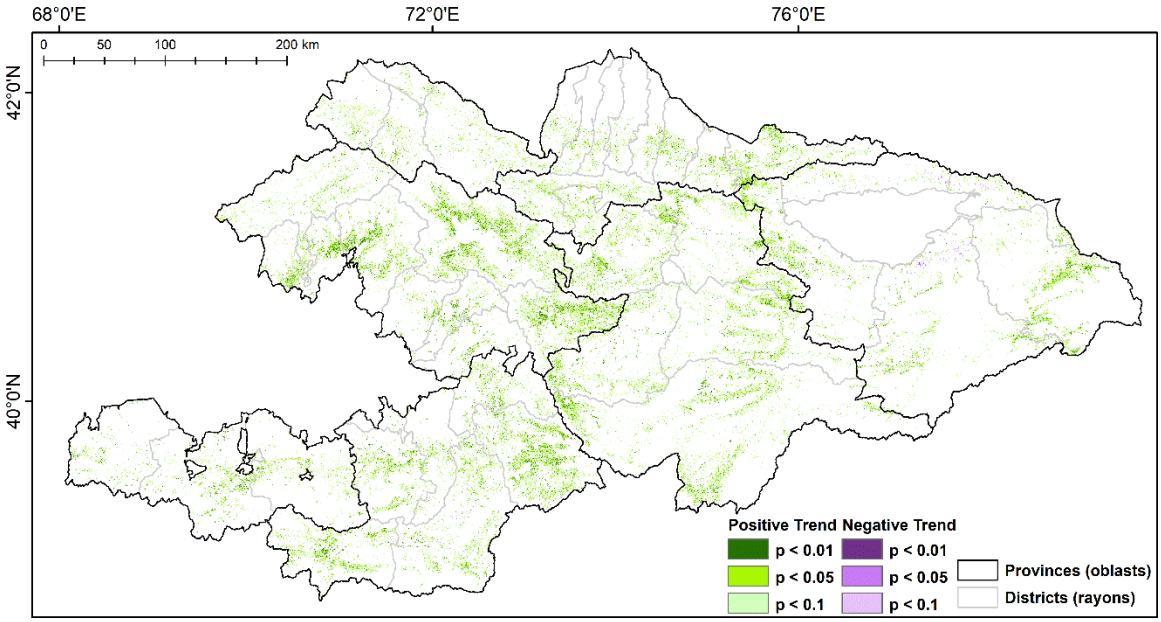

Figure 3.12. Map of significant positive (in green) and negative (in purple) trends of PH at three significance levels ($p<0.01$, $p<0.05$, $p<0.1$). Map displays data only for pasture land use areas (Projected coordinate system: Albers Conic Equal Area).

3.6.4. Linkages between Snow Cover and Land Surface Phenology

3.6.4.1. Correlations among Snow Cover Temporal Metrics

We evaluated the relationships among the snow cover temporal metrics by calculating the areas with significant Spearman correlations. Although both SCD and DoSS are related to FDoS and LDoS, the metrics show different relationships. SCD shows the strongest positive connection with DoSS over 53% of both HP area and P areas at $p<0.05$, and over 31% of both areas at $p<0.01$ (Table 3.7). The significant positive correlation of SCD with LDoS occurs over a greater area at $p<0.05$ (HP: 38%, P: 36%) than the significant negative correlation of SCD with FDoS (HP: 29%, P: 31%). Note that the negative correlation of SCD with FDoS means earlier onset of snow cover, and the positive correlation of SCD with LDoS means later snowmelt. In contrast with SCD, more than 90% of HP and P areas

show a significant negative correlation between DoSS and FDoS at both p-values. The area of significant positive correlation between DoSS and LDoS is just one-third at p<0.01 and over 50% at p<0.05 for HP and slightly lower for P pasture areas (Table 3.7). FDoS exhibits no significant correlation with LDoS (data not shown). Note that the areas of significant positive correlation between SCD and DoSS are nearly identical for HP and P pasture areas. Similar areal coverages over different pasture classes indicate no or, at most, very weak association between pasture availability classes and relationships among the snow cover metrics.

Table 3.7. Areal percentage of snow cover temporal metrics with significant positive or negative correlations at p-value < 0.01 and p-value < 0.05 for highly persistent (HP) and persistent (P) pastures.

	SCD				*DoSS*			
	p< 0.01		**p< 0.05**		**p< 0.01**		**p< 0.05**	
HP (11- 17 yrs) Area=15,261 km^2	**Pos**	**Neg**	**Pos**	**Neg**	**Pos**	**Neg**	**Pos**	**Neg**
FDoS	0.01	13.07	0.12	29.31	<0.01	92.97	<0.01	97.6
LDoS	18.44	<0.01	38.49	0.03	33.34	<0.01	56.66	0.01
DoSS	31.93	<0.01	53.47	0.01	--	--	--	--
P (5-10 yrs) Area=53,620 km^2	**Pos**	**Neg**	**Pos**	**Neg**	**Pos**	**Neg**	**Pos**	**Neg**
FDoS	0.01	13.87	0.08	31.06	<0.01	94.34	<0.01	98.13
LDoS	16.6	<0.01	36.22	0.03	30.46	<0.01	53.22	0.01
DoSS	31.53	<0.01	53.17	0.02	--	--	--	--

3.6.4.2. Correlations between Snow Cover Metrics and Phenometrics

We also used Spearman correlations to explore the relationships between snow cover temporal metrics and phenometrics. Across the 96 correlations (= 4 phenometrics × 4 snow cover temporal metrics × 2 pasture availability classes × 3 significance levels), we focus

here on three phenometrics—PH, TTP, and AUC—at $p < 0.01$ and $p < 0.05$ (Tables 3.7-3.9). Results for the HTV phenometric appear in Table S3.2.

PH exhibits predominant positive correlations with SCD, LDoS, and DoSS and one predominant negative correlation with FDoS (Table 3.8). This pattern holds for HP and P pasture areas at both significance levels. However, spatial predominance is strongest in HP at $p<0.01$ (Table 3.8) and, in terms of elevation, the greatest asymmetry occurs for the 2900-3400 m class. Over P pasture areas, the greatest asymmetry occurs at 3400-4000 m (Table 3.8). For both LDoS and DoSS, the greatest asymmetries occur at 3400-4000 m. In contrast, there is almost no difference between positive and negative correlations of PH with LDoS at the lowest elevation class (<1800 m). The negative relationship with FDoS dominates over the lowest elevation range over both pastures classes and p-values. However, at the highest elevation class (>4000 m) of P pasture areas, the relationship changes to positive; there are no HP pasture areas in the highest elevation class.

Table 3.8. Areal percentage of significant correlations between the snow cover temporal metrics and the phenometric PH and the ratio of positive % area to negative % area at six elevation classes: below 1800 m, 1800-2400 m, 2400-2900 m, 2900-3400 m, 3400-4000 m, above 4000 m, and over total area of each pasture class. In **bold** with grey background, pos%/neg% > 2.0; *in **bold italics**, pos%/neg%* < 0.5.

		PH											
		p<0.01			p<0.05			p<0.01			p<0.05		
		HP (11-17 yrs)						**P (5-10 yrs)**					
		Pos	Neg	Ratio	Pos	Neg	Ratio	Pos	Neg	Ratio	Pos	Neg	Ratio
SCD	< 1800 m	1.56	0.12	**13.07**	6.45	0.62	**10.38**	1.32	0.34	**3.90**	5.00	1.30	**3.86**
	1800-2400 m	2.80	0.33	**8.51**	8.87	1.36	**6.51**	1.60	0.45	**3.53**	5.73	1.69	**3.40**
	2400-2900 m	4.12	0.21	**20.10**	13.27	0.86	**15.47**	2.10	0.37	**5.65**	7.53	1.39	**5.40**
	2900-3400 m	2.80	0.05	**59.37**	10.45	0.29	**35.61**	2.93	0.15	**19.43**	10.00	0.64	**15.75**
	3400-4000 m	2.40	0.06	**37.88**	8.99	0.32	**28.29**	3.53	0.09	**37.88**	12.13	0.38	**32.17**
	> 4000 m	0.00	0.00	NaN	0.00	0.00	NaN	0.72	0.56	1.30	2.87	2.18	1.32
	TOTAL	3.03	0.19	**15.95**	10.27	0.82	**12.52**	2.24	0.30	**7.47**	7.88	1.13	**6.97**
LDoS	< 1800 m	0.46	0.44	1.03	2.28	2.13	1.07	0.62	0.66	0.95	2.40	2.42	0.99
	1800-2400 m	1.20	0.31	**3.91**	4.89	1.45	**3.37**	0.96	0.56	1.72	3.65	2.12	1.72
	2400-2900 m	2.37	0.16	**15.20**	7.62	0.83	**9.17**	1.49	0.44	**3.41**	5.02	1.72	**2.92**
	2900-3400 m	1.29	0.16	**8.19**	5.00	0.85	**5.90**	1.84	0.27	**6.71**	6.16	1.19	**5.18**
	3400-4000 m	2.24	0.15	**15.41**	8.32	0.71	**11.70**	1.61	0.19	**8.45**	5.93	0.86	**6.87**
	> 4000 m	2.07	0.00	NaN	5.52	0.00	NaN	0.58	0.18	**3.26**	3.70	1.27	**2.90**
	TOTAL	1.51	0.24	**6.29**	5.47	1.21	**4.52**	1.33	0.43	**3.09**	4.68	1.69	**2.77**

DoSS	< 1800m	1.49	0.18	**8.36**	5.90	0.91	**6.51**	1.26	0.44	**2.88**	4.68	1.70	**2.76**
	1800-2400 m	1.67	0.27	**6.18**	6.24	1.28	**4.89**	1.14	0.48	**2.37**	4.34	1.91	**2.27**
	2400-2900 m	1.63	0.22	**7.25**	6.17	1.10	**5.60**	1.21	0.47	**2.57**	4.48	1.93	**2.32**
	2900-3400 m	1.51	0.29	**5.18**	5.64	1.39	**4.07**	1.50	0.42	**3.57**	5.36	1.76	**3.04**
	3400-4000 m	1.66	0.17	**9.96**	6.43	0.86	**7.46**	1.45	0.40	**3.59**	5.26	1.60	**3.29**
	> 4000 m	0.00	0.00	NaN	0.00	1.38	***<0.01***	0.86	0.52	1.64	3.86	2.02	1.90
	TOTAL	1.59	0.24	**6.63**	6.04	1.17	**5.16**	1.31	0.45	**2.91**	4.80	1.81	**2.65**
FDoS	< 1800 m	0.14	2.48	***0.06***	0.71	8.51	***0.08***	0.39	1.87	***0.21***	1.42	6.24	***0.23***
	1800-2400 m	0.28	1.48	***0.19***	1.23	5.62	***0.22***	0.45	1.28	***0.35***	1.72	4.68	***0.37***
	2400-2900 m	0.33	1.04	***0.32***	1.51	4.44	***0.34***	0.54	1.02	0.53	2.12	3.90	0.54
	2900-3400 m	0.46	1.06	***0.43***	2.11	4.01	0.53	0.61	0.94	0.65	2.37	3.50	0.68
	3400-4000 m	0.24	0.80	***0.30***	1.29	3.42	***0.38***	0.57	0.96	0.59	2.16	3.46	0.62
	> 4000 m	0.00	0.00	NaN	1.38	0.00	NaN	0.80	0.31	**2.61**	3.16	1.48	**2.14**
	TOTAL	0.31	1.39	***0.22***	1.43	5.30	***0.27***	0.52	1.19	***0.44***	1.98	4.30	***0.46***

The pattern of asymmetries with the TTP phenometric show predominant negative correlations with SCD, LDoS, and DoSS, but no strong asymmetries between TTP and FDoS (Table 3.9). The negative relationship with SCD predominates at the higher elevation belts: 2900-3400 m and 3400-4000 m over both pasture classes and significance levels. The asymmetry of correlations between TTP and LDoS is similar level regardless of elevation at $p < 0.01$, and the greatest at 2400-2900 m at $p<0.05$. Over P pastures, the greatest asymmetry occurs at 2400-2900 m (Table 3.9). The strength of correlation asymmetries between DoSS and TTP are comparable across elevation classes. However, at the highest elevation in HP pastures, there were no pixels at $p<0.01$, and only very few pixels exhibiting a significant negative relationship at $p<0.05$. In P pastures, the differences of relationship direction even out. Contrary to the relationship between FDoS and PH, there are no predominant asymmetries for TTP and FDoS, with the sole exception of a significant positive relationship at 3400-4000 m in P pasture areas (Table 3.9).

Table 3.9. Areal percentage of significant correlations between the snow cover temporal metrics and the phenometric TTP and the ratio of positive % area to negative % area at six elevation classes: below 1800 m, 1800-2400 m, 2400-2900 m, 2900-3400 m, 3400-4000 m, above 4000 m, and over total area of each pasture class. In **bold** with grey background, pos%/neg% > 2.0; *in bold italics, pos%/neg%* < 0.5. NaN means "Not a Number" and results from division by zero.

		TTP											
		p<0.01			p<0.05			p<0.01			p<0.05		
		HP (11-17 yrs)						**P (5-10 yrs)**					
		Pos	Neg	Ratio	Pos	Neg	Ratio	Pos	Neg	Ratio	Pos	Neg	Ratio
SCD	< 1800 m	0.19	0.90	***0.21***	1.01	4.02	***0.25***	0.37	1.18	***0.32***	1.49	4.43	***0.34***
	1800-2400 m	0.15	2.05	***0.07***	0.84	7.32	***0.11***	0.25	1.57	***0.16***	1.05	5.77	***0.18***
	2400-2900 m	0.03	4.18	***0.01***	0.21	14.06	***0.01***	0.21	2.08	***0.10***	0.87	7.61	***0.11***
	2900-3400 m	0.01	6.50	***<0.01***	0.07	18.23	***<0.01***	0.15	3.49	***0.04***	0.58	11.52	***0.05***
	3400-4000 m	0.02	7.11	***<0.01***	0.12	18.92	***0.01***	0.12	3.85	***0.03***	0.48	12.51	***0.04***
	> 4000 m	0.00	4.14	***<0.01***	0.00	13.79	***<0.01***	0.25	2.04	***0.12***	0.88	6.84	***0.13***
	TOTAL	0.08	3.64	***0.02***	0.48	11.63	***0.04***	0.22	2.40	***0.09***	0.89	8.27	***0.11***
LDoS	< 1800 m	0.13	2.88	***0.04***	0.65	9.71	***0.07***	0.31	1.93	***0.16***	1.14	6.62	***0.17***
	1800-2400 m	0.10	3.18	***0.03***	0.57	10.03	***0.06***	0.26	2.00	***0.13***	1.03	6.85	***0.15***
	2400-2900 m	0.06	3.23	***0.02***	0.36	10.62	***0.03***	0.21	2.22	***0.10***	0.85	7.60	***0.11***
	2900-3400 m	0.11	2.65	***0.04***	0.62	8.71	***0.07***	0.25	2.16	***0.12***	1.01	7.35	***0.14***
	3400-4000 m	0.28	0.96	***0.29***	1.25	4.05	***0.31***	0.37	1.48	***0.25***	1.45	5.05	***0.29***
	> 4000 m	0.00	2.07	***<0.01***	1.38	7.59	***0.18***	0.26	0.59	***0.44***	1.36	3.60	***0.38***
	TOTAL	0.10	2.99	***0.03***	0.54	9.76	***0.06***	0.27	2.02	***0.13***	1.05	6.90	***0.15***

DoSS	< 1800 m	0.24	1.32	***0.18***	1.21	5.02	***0.24***	0.46	1.22	***0.38***	1.80	4.55	***0.40***
	1800-2400 m	0.23	1.37	***0.17***	1.17	5.26	***0.22***	0.39	1.39	***0.28***	1.60	5.08	***0.31***
	2400-2900 m	0.22	1.49	***0.15***	1.09	5.63	***0.19***	0.38	1.45	***0.26***	1.55	5.27	***0.29***
	2900-3400 m	0.19	1.56	***0.12***	0.94	5.93	***0.16***	0.34	1.69	***0.20***	1.42	6.12	***0.23***
	3400-4000 m	0.22	0.91	***0.24***	1.16	3.92	***0.29***	0.40	1.37	***0.29***	1.60	5.02	***0.32***
	> 4000 m	0.00	1.38	***<0.01***	0.00	12.41	***<0.01***	0.80	0.66	1.20	3.20	2.77	1.16
	TOTAL	0.22	1.43	***0.15***	1.10	5.46	***0.20***	0.39	1.45	***0.27***	1.57	5.31	***0.30***
FDoS	< 1800 m	0.58	0.59	0.98	2.40	2.72	0.88	0.73	0.74	0.98	2.73	2.72	1.00
	1800-2400 m	0.60	0.50	1.21	2.63	2.16	1.22	0.84	0.60	1.41	3.14	2.32	1.35
	2400-2900 m	0.74	0.52	1.42	3.19	2.27	1.40	0.95	0.58	1.63	3.53	2.28	1.55
	2900-3400 m	0.78	0.55	1.42	3.34	2.29	1.46	1.14	0.59	1.95	4.14	2.17	1.91
	3400-4000 m	0.57	0.33	1.77	2.67	1.58	1.69	1.06	0.49	**2.14**	3.88	1.85	**2.10**
	> 4000 m	0.69	0.00	NaN	6.90	0.00	NaN	0.49	0.87	0.57	2.11	3.16	0.67
	TOTAL	0.68	0.53	1.28	2.93	2.30	1.27	0.95	0.60	1.58	3.51	2.28	1.54

Among the four phenometrics, the relationships between the snow cover temporal metrics and AUC are the weakest, with modest asymmetries for LDoS and FDoS in HP and only LDoS in P pastures. Therefore, we do not report asymmetries by elevation class, but instead over the total area for each pasture availability class (Table 3.10). Similarly, we only report results of HTV for the total area of each pasture availability class (Table S3.2). As expected, the pattern of HTV closely follows PH, but the linkages of HTV with SCD and FDoS exhibit even stronger asymmetries at each combination of pasture availability class and significance level (Table S3.2)

Table 3.10. Areal percentage of significant correlations between the snow cover temporal metrics and the phenometric AUC and the ratio of positive % area to negative % area. In **bold**, pos%/neg% > 2.0; in ***bold italics***, *pos%/neg%* < 0.5.

AUC						
	p<0.01			**p<0.05**		
HP (11- 17 yrs) Area=15,261 km^2	Pos	Neg	Ratio	Pos	Neg	Ratio
SCD	0.32	0.52	0.62	1.75	2.42	0.72
LDoS	0.28	1.04	***0.27***	1.35	4.45	***0.30***
DoSS	0.56	0.51	1.10	2.58	2.33	1.11
FDoS	0.31	0.87	***0.36***	1.52	3.80	***0.40***
P (5 – 10 yrs) Area=53,620 km^2	Pos	Neg	Ratio	Pos	Neg	Ratio
SCD	0.57	0.66	0.86	2.29	2.56	0.89
LDoS	0.42	1.05	***0.40***	1.67	4.00	***0.42***
DoSS	0.60	0.78	0.77	2.39	3.09	0.77
FDoS	0.64	0.80	0.80	2.46	3.06	0.80

3.6.4.3. Influence of Terrain on Relationships between Snow Cover Seasonality and Phenometrics

We conducted eight exact multinomial tests for equivalence for the nine hotspots shown in Figure S3.4. Table 3.11 presents 95% upper bound for $d(p,p_0)$ of five sets of correlations with p-value < 0.05 at nine hotspots. We marked in bold those values below the specified Δ value of 0.025, indicating that H_0 is rejected, thereby leading to the conclusion that there is no evidence of influence by terrain features on the relationship between the snow cover temporal metrics and the phenometrics at that hotspot.

Of the eight equivalence tests, aspect alone and the interaction between aspect and the 5-10° slope class show weaker influence with 13 and 12 instances of equivalence, respectively, out of the possible 45 (=5 correlations × 9 hotspots). In contrast, the tests for slope alone, the interaction of aspect and the >30° slope class, and the overall interaction of aspect and slope each show only three out of 45 occasions of equivalence (Table 3.11). We can conclude, therefore, that within these hotspots, the primary influence of terrain is slope rather than aspect. SCD exhibited equivalence in nearly 20% of the tests. LDoS, in contrast, had just over 8% equivalence, indicating that both are sensitive to terrain features, but LDoS is more sensitive than SCD (Table 3.11). While both PH and TTP have comparable levels of equivalence (13% and 11%, respectively), a full quarter of the HTV tests concluded with a finding of equivalence, indicating that HTV was much less sensitive to terrain features than PH or TTP (Table 3.11).

Over all equivalence tests in the nine hotspots, more terrain sensitivity (fewer cases of equivalence) occurs in hotspots 1, 2, 5, and 9 and less terrain sensitivity in hotspots 4, 7,

and 8. Yet, these sensitivities are relative: each hotspot exhibits some degree of terrain sensitivity in the relationships between snow cover temporal metrics and phenometrics.

Table 3.11. Results of exact multinomial tests for equivalence: values of 95% upper bound for $d(p,p_0)$. In **bold** are values below $\Delta=0.025$, meaning H_o is rejected and we conclude equivalence and no significant terrain effect. Note in hotspot 9, the significant negative correlation between PH and LDoS *is highlighted in italics.* In every other hotspot, the significant correlation between PH and LDoS was positive.

Dataset	Hotspot	Aspect	Slope	0 - 5° × Aspect	5 - 10° × Aspect	10 -15° × Aspect	15 -30° × Aspect	>30° × Aspect	Slope × Aspect
PH SCD pos	HS1	0.025	**0.021**	0.033	**0.021**	0.050	0.047	0.064	**0.022**
PH LDoS pos		0.025	0.091	0.058	0.031	0.045	0.039	0.050	0.091
TTP SCD neg		0.055	0.096	0.027	0.062	0.080	0.058	0.043	0.096
TTP LDoS neg		0.030	0.087	0.029	0.032	0.042	0.037	0.048	0.092
HTV SCD pos		0.050	0.053	**0.016**	0.040	0.077	0.083	0.087	0.053
PH SCD pos	HS2	0.037	0.100	0.043	**0.025**	0.027	0.054	0.051	0.101
PH LDoS pos		**0.024**	0.053	0.042	0.033	0.033	0.032	0.043	0.056
TTP SCD neg		**0.023**	0.084	0.045	0.051	0.050	0.042	0.070	0.086
TTP LDoS neg		0.026	0.080	0.028	0.058	0.046	0.052	0.052	0.080
HTV SCD pos		0.043	0.104	0.055	0.041	0.044	0.060	0.063	0.107
PH SCD pos	HS3	**0.014**	0.038	**0.023**	**0.018**	**0.013**	0.026	0.032	0.040
PH LDoS pos		0.037	0.100	0.034	0.046	0.030	**0.020**	0.066	0.102
TTP SCD neg		0.035	0.089	0.033	0.035	0.079	0.064	0.096	0.094
TTP LDoS neg		0.041	0.184	0.036	0.051	0.057	0.027	0.042	0.184
HTV SCD pos		0.028	0.034	0.027	0.031	0.033	0.042	0.038	0.038
PH SCD pos	HS4	**0.017**	0.028	**0.007**	**0.016**	0.032	0.028	0.032	0.030
PH LDoS pos		0.045	0.050	**0.023**	0.034	0.050	0.072	0.100	0.050
TTP SCD neg		0.027	0.067	**0.021**	0.043	0.070	0.057	0.045	0.069
TTP LDoS neg		0.050	0.128	0.025	0.085	0.109	0.083	0.132	0.132
HTV SCD pos		**0.009**	0.066	**0.009**	**0.016**	**0.019**	**0.023**	0.049	0.066
PH SCD pos	HS5	0.028	0.067	0.050	0.034	**0.020**	0.032	0.047	0.067
PH LDoS pos		0.031	0.033	0.044	**0.024**	0.045	0.027	0.060	0.033

TTP SCD neg		**0.020**	0.025	0.036	0.028	0.052	0.040	0.085	0.025
TTP LDoS neg		0.040	0.099	0.082	0.037	0.050	0.035	0.087	0.105
HTV SCD pos		0.055	0.044	0.039	**0.025**	0.043	0.087	0.088	0.044
PH SCD pos	HS6	0.056	0.083	0.058	0.059	0.075	0.053	0.059	0.084
PH LDoS pos		0.031	0.076	0.044	0.044	0.031	0.034	0.041	0.076
TTP SCD neg		0.026	0.083	**0.022**	**0.024**	**0.018**	0.029	0.037	0.083
TTP LDoS neg		0.046	0.096	**0.021**	**0.024**	0.025	0.052	0.056	0.106
HTV SCD pos		0.055	0.043	0.049	0.050	0.059	0.068	0.055	0.061
PH SCD pos	HS7	0.031	0.029	0.052	0.040	0.045	0.039	0.029	0.030
PH LDoS pos		**0.021**	0.106	0.038	**0.020**	0.029	0.028	0.056	0.106
TTP SCD neg		**0.022**	0.115	0.044	0.038	0.039	**0.022**	0.033	0.117
TTP LDoS neg		0.032	**0.015**	0.032	0.034	0.042	0.035	0.043	0.027
HTV SCD pos		**0.016**	**0.020**	0.069	0.041	0.026	**0.018**	**0.022**	**0.022**
PH SCD pos	HS8	**0.019**	0.078	0.033	0.066	0.048	0.047	**0.020**	0.078
PH LDoS pos		0.040	0.052	0.095	0.087	0.050	0.036	0.035	0.061
TTP SCD neg		**0.015**	0.026	0.068	**0.017**	**0.022**	**0.023**	0.049	0.031
TTP LDoS neg		**0.024**	0.040	0.078	0.031	**0.020**	0.027	0.042	0.040
HTV SCD pos		**0.017**	0.072	0.051	0.051	**0.023**	**0.008**	**0.024**	0.072
PH SCD pos	HS9	0.041	0.046	0.051	0.037	0.036	0.045	0.065	0.050
PH LDoS neg		0.033	0.036	0.036	0.026	0.035	0.047	0.057	0.038
TTP SCD neg		0.059	0.091	0.050	0.054	0.058	0.062	0.129	0.094
TTP LDoS neg		0.026	0.060	0.026	**0.018**	0.026	0.033	0.041	0.060
HTV SCD pos		0.052	0.098	0.045	0.036	0.038	0.054	0.094	0.100

3.7. Discussion

In this study, we have sought to understand the impact of a variable and changing climate on land surface phenology in highland pastures, especially the effects of snow cover seasonality as constrained by terrain. Here we revisit the three research questions articulated in the introduction.

3.7.1. How does snow cover seasonality relates to subsequent land surface phenology in highland pastures?

Both PH and TTP showed strong and prevalent relationships with the snow cover metrics. Positive correlations of PH and SCD covered a greater areal extent than the negative correlations: significant ($p<0.05$) positive correlations in HP pastures covered 1,568 km^2 or 10.3% of total HP pasture area compared to 126 km^2 or 0.8% in significant negative correlations, more than a twelve-fold difference. Similarly, in P pastures significant positive correlations covered 4,225 km^2 or 7.9% of total P pasture area versus significant negative correlations over 607 km^2 or 1.1%, nearly a seven-fold difference (Tables 3.8, 3.12). More days with snow coverage resulted in greater PH in the following growing season, particularly at the higher elevation ranges: 2900-3400 m of HP and 3400-4000 m for P pastures (Tables 3.7, 3.11). A greater areal extent exhibited a significant ($p<0.05$) negative than positive correlations between SCD and TTP: in HP pastures, 1,774 km^2 or 11.6% of the total HP pasture areas compared to 73 km^2 or 0.5%, more than a 24-fold difference; and in P pastures, 4,434 km^2 or 8.3% of the total P pastures had significant negative correlations versus significant positive correlations in 477 km^2 or 0.9%, more than a nine-fold difference (Tables 3.9, 3.12). More snow covered dates translated into fewer

growing degree-days accumulated to reach the thermal time to peak NDVI in the subsequent growing season.

Figure 3.13 presents a false color composite (red=TTP; green=PH; blue=SCD) displaying these relationships averaged over 2001-2017. Red shades indicate higher TTPs and lower values of other metrics and there are mostly located over lower elevations and in valleys. Green shades indicate higher PH values and lower TTP and SCD; whereas, shades of blue indicate more dates with snow cover, and lower values of both TTP and PH. The hues of yellow-orange indicate higher PH and TTP but lower SCD. Cyan shows higher PH and SCD but lower TTP. Purple displays lower PH, higher SCD, and higher TTP over the drier areas in southern Kyrgyzstan (Figure 3.13).

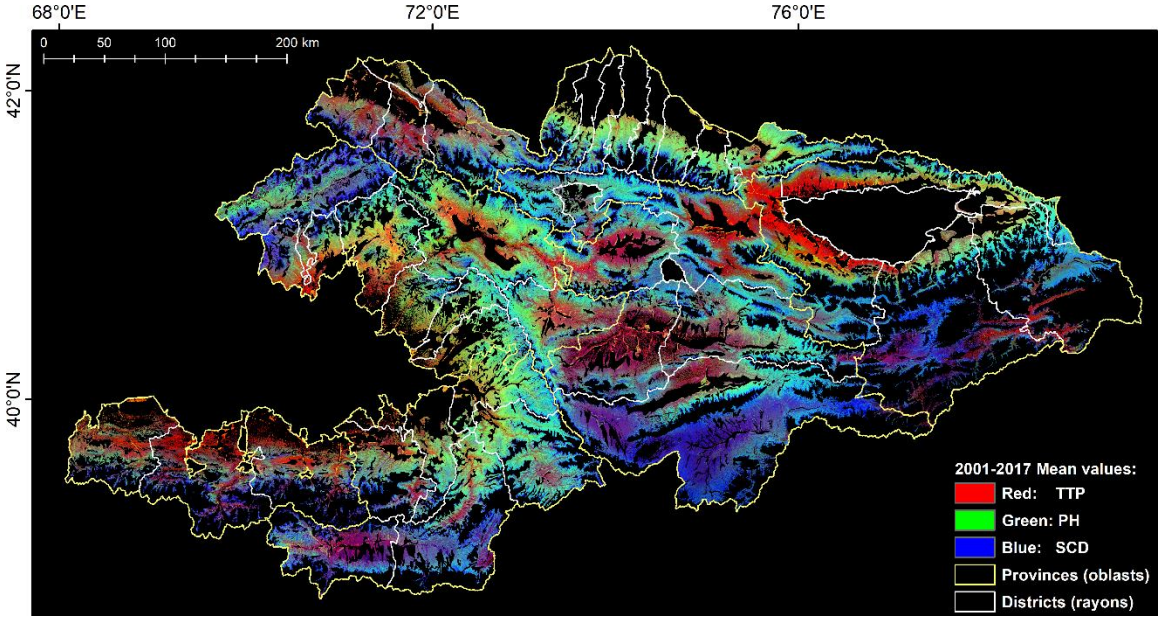

Figure 3.13. False color composite of 2001-2017 average values of Thermal Time to Peak (Red), Peak Height (Green), and Snow Covered Dates (Blue). Map displays data only for pasture land use areas (Projected coordinate system: Albers Conic Equal Area).

Similar relationships occurred with DoSS, but the area of coverage was twice as small (Tables 3.9, 3.12), and the major portion occurs over lower elevation ranges: 1800-2400 m and 2400-2900 m. Later snowmelt also positively influences Peak Height and decreases Thermal Time to Peak, especially at higher elevations. A strong negative relationship was also observed of snowmelt timing and Area Under Curve. For PH, the relationship with FDoS (snow onset in preceding snow season) was negative: earlier snow cover increases Peak Height (Tables 3.9, 3.12), especially at lowest elevations below 1800 m; whereas, above 4000 m the relationship turned to positive in P pastures. This linkage relates to the necessarily positive correlation between the duration of snow cover season and number of snow covered dates within that season, since SCD ≤ DoSS, and SCD is typically fewer than DoSS. In the case of TTP and FDoS, there were no clear asymmetries since the areal coverages of both positive and negative correlations were similar, except for positive relationships evident only in Persistent pasture areas between 3400 m and 4000 m (Table 3.9) over Persistent pastures. Early season AUC showed negative asymmetries with earlier snow onset, but only in HP areas (Table 3.10). In contrast, early season AUC showed negative asymmetries with earlier snowmelt in both HP and P areas (Table 3.10).

The significant trends in PH and TTP showed contrasting spatial patterns. PH showed widespread patches of positive trends (Figure 3.12), which may be related to the lengthening of snow cover duration in some areas (Dietz et al., 2013; Tomaszewska and Henebry, 2018). TTP showed no strong patchiness at the national scale (Figure 3.11) with minimal area affected (not exceeding 4% in HP and P) with no evident directional bias. This result may arise, in part, from the coarser spatial resolution of MODIS LST data relative to the Landsat NDVI data.

Figure 3.14 presents a time-series of mean PH values with 2± SEM (Standard Errors of Mean) calculated from the randomly selected 200 pixels over HP pastures that showed a significant ($p<0.01$) positive trend. In contrast, time-series of the mean TTP values corresponding to the PH values show no evidence of a trend (Figure 3.14b). Mean PH and TTP values of 2001-2003 show high standard error values, which might be due to the lower number of successful fits (low number of pixels from selection) resulted from a limited observations from Landsat 7 ETM+ (*cf.* Table S3.1). The outlier year is 2003, which has the lowest mean PH and the highest TTP, due to dry and hot weather conditions. However, the very high SEM comes from the very low number of successful pixels, which mostly results from the lowest number of possible observations of all 17 years (*cf.* Table S3.1). The strength of the PH trend is visible from 2009, when PH increases and the number of observations available for fitting started to increase, producing a higher number of successful fits (*cf.* Table S3.1). Over the same period, however, TTP shows no predominant trend direction but rather a quasi-sinusoidal pattern. The increasing PH trend without a concomitant TTP trend suggests that the PH trend does not arise from weather conditions but rather pasture conditions.

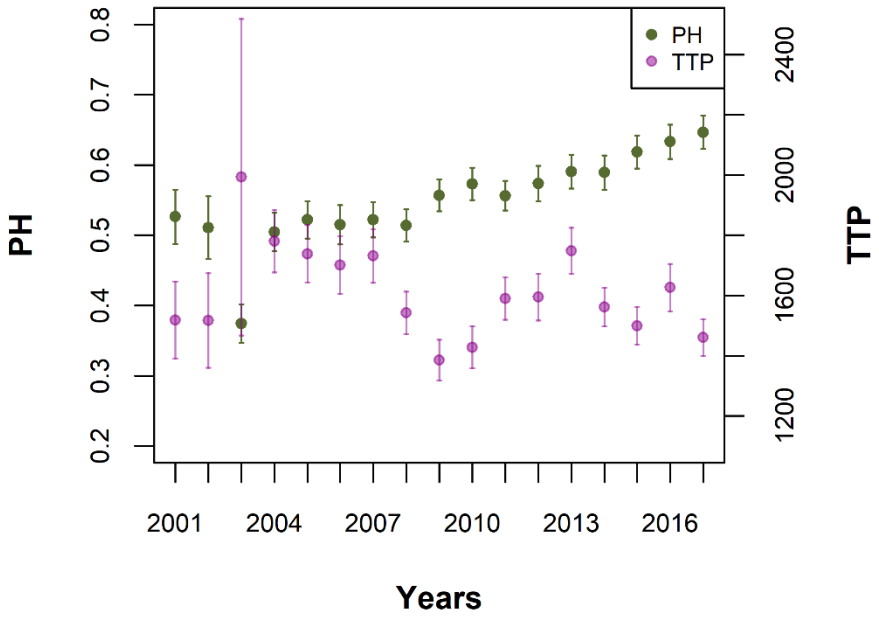

Figure 3.14. Green displays the time-series of mean Peak Height (PH) with ± 2 SEM (Standard Errors of Mean) from 2001-2017 for 200 randomly selected pixels from Highly Persistent (HP) pastures that show a significant positive trend (p-value < 0.01). No significant trend is evident in the time-series of mean Thermal Time to Peak (TTP) values (magenta) that correspond to the PH values.

Table 3.12. Areal extent (km^2) of significant correlations between metrics of snow cover seasonality and phenometrics from the following growing season. TTP is Thermal Time to Peak; PH is Peak Height; SCD is Snow-Covered Dates; LDoS is Last Date of Snow cover; DoSS is Duration of Snow Season; FDoS is First Date of Snow cover; HP indicates highly persistent and P indicates persistent pasture areas. Positive correlations on grey background; negative correlations on white background.

		TTP				**PH**			
		p<0.01		p<0.05		p<0.01		p<0.05	
		HP	P	HP	P	HP	P	HP	P
SCD	< 1800m	22	99	99	368	38	110	158	416
	1800-2400m	85	211	304	774	116	215	368	769
	2400-2900m	210	236	706	861	207	238	666	852
	2900-3400m	215	501	603	1,656	93	422	346	1,437
	3400-4000m	24	238	63	773	8	218	30	750
	> 4000m	<0.01	<0.5	<0.01	2	--	<0.5	--	<1
	TOTAL	556	1,284	1,774	4,434	462	1,202	1,568	4,225
LDoS	< 1800m	71	161	238	550	11	52	56	200
	1800-2400m	132	268	416	919	50	128	203	489
	2400-2900m	162	251	533	860	119	168	383	568
	2900-3400m	88	310	288	1,056	43	265	166	885
	3400-4000m	3	91	13	312	7	100	27	366
	> 4000m	<0.01	<0.5	<0.01	1	<0.01	<0.5	<0.01	<1
	TOTAL	456	1,082	1,489	3,699	230	713	835	2,508

DoSS	< 1800m	32	101	123	378	37	105	145	389
	1800-2400m	57	186	218	681	69	153	259	582
	2400-2900m	75	164	283	596	82	136	310	507
	2900-3400m	52	243	196	880	50	216	187	770
	3400-4000m	3	85	13	310	5	90	21	325
	> 4000m	<0.01	<0.5	<0.5	1	0	<0.5	0	<1
	TOTAL	219	779	833	2,847	243	700	921	2,574
FDoS	< 1800m	14	61	59	227	61	156	209	518
	1800-2400m	25	113	109	421	61	172	233	628
	2400-2900m	37	107	160	400	52	115	223	442
	2900-3400m	26	164	111	594	35	135	133	504
	3400-4000m	2	65	9	240	3	59	11	214
	> 4000m	<0.01	<0.5	<0.01	<0.5	0	<0.1	0	<0.5
	TOTAL	104	510	447	1,883	212	637	809	2,306

How do these findings relate to other studies concerning the influence of snow cover on phenology?

Most studies have focused specific dates, e.g., the beginning (SOS), end (EOS), and length (LOS) of the growing season. Our approach uses model phenometrics and, thus, is not directly comparable with the other studies. Moreover, we discuss here the influence of snow cover on vegetation dynamics.

In a study on the QTP (Qinghai-Tibetan Plateau), Wang et al. (2018) used MODIS 500m NDVI dataset and combined 500 m MODIS daily snow products with IMS (National Snow and Ice Data Center's Interactive Multisensor Snow and Ice Mapping System). The Ice Mapping System provides daily snow and ice cover maps for the Northern Hemisphere from February 1997 to the present at three coarse spatial resolutions: 1 km, 4 km, and 24 km. The IMS products are derived from a variety of data products including satellite imagery (MODIS Terra & Aqua, DMSP, GEOS series, NOAA series, RADARSAT, SUOMI-NPP) and *in situ* data (*cf.* https://nsidc.org/data/g02156). Their results varied strongly by region, biome, and thermal and moisture regime, although they are presented in a way that allows for comparison with our results.

In the eastern QTP, snow cover duration (number of days with snow cover occurrence within a hydrological year) that corresponds to our SCD, showed a positive correlation with start of growing season (SOS), but it was negatively correlated with length of growing season (LOS), suggesting that longer snow cover delays the spring onset date, thereby reducing the duration of the growing season in this very high elevation environment.

In our study, TTP served to indicate the length of green-up period, and we found a substantially greater area of negative than positive relationship of TTP with the number of snow covered dates (SCD) over the study area. Counterintuitively, across the most of the QTP, a longer snow cover duration advanced the SOS and extended the LOS the following year. Alpine steppe communities showed a strong negative correlation between SOS and snow cover duration and a positive correlation between LOS and snow cover duration, from which Wang et al. (2018) concluded that longer snow cover duration led to an earlier SOS and longer growing season.

In terms of the snow cover melting dates, they detected two opposed relationships with SOS: a positive correlation between snow cover melting date and SOS occurred in most areas—except alpine steppe—but a negative correlation appeared over warmer, drier areas where snow melted too early for the vegetation to take advantage of the meltwater (Wang et al. 2018). Further, the loss of insulating effect of the snow cover due to earlier snowmelt may increase the risk of soil exposure to freezing events and decrease soil moisture through evaporative loss. Snow cover melting date was positively correlated with LOS in the eastern and southwestern part of QTP, while negative correlations were observed over much of the central Plateau.

If we consider our LDoS metric as functionally equivalent to their snow cover melting date, a predominantly negative relationship between LDoS and TTP was also evident in our results. Finally, they found the maximum NDVI showed positive correlation with snow cover duration and snow cover melt date, which are findings similar to ours: where we found that PH was been positively correlated with SCD, DoSS, and LDoS, and negatively

correlated with FDoS, meaning that when snow occurred earlier and lasted longer on the ground, the NDVI was higher in the subsequent growing season.

Qiao and Wang (2019) explored relationships between winter snow cover dynamics, climate and spring grassland vegetation phenology in Inner Mongolia, China using AVHRR-NDVI dataset at ~5 km spatial resolution and meteorological station data for precipitation and temperature.

In general, Qiao and Wang (2019) found positive relationships of the start of the growing season with snow cover duration and with snow cover melt date. However, variation in the duration of snow cover and snow depth may affect soil-vegetation interactions. Increased snow cover duration and/or depth could add soil moisture, slow down soil heat exchange, and have crucial effects on soil heat and moisture preservation that might protect over-winter survival of vegetation from low air temperatures and wind damage. It may also affect the activity of soil microbes and the transformation of soil organic matter and nutrients (Groffman et al., 2001; Qiao and Wang, 2019). Deeper snow depths may lead to later SOS dates, which in turn might not be beneficial for soil respiration over winter or the accumulation of heat needed to unfold leaves in spring (Monson et al., 2006; Schimel et al., 2004). However, Welker et al., (2005) showed that deeper snow could alter carbon-to-nitrogen (C:N ratios) leading to increased N in leaves that may result in higher crude protein content in forage. On the other hand, lack of snow cover or just a shallow snowpack may increase the frequency of soil freeze-thaw events and, consequently, alter soil nutrient cycling and aboveground productivity (Choler, 2015). Earlier snow cover could shield vegetation from lower temperatures by keeping the subniveal temperature at a favorable

level and protecting the activity of the soil microorganisms during the winter, which could lead to increased vegetation growth during the following growing season.

While we found a negative relationship between FDoS and PH, meaning earlier FDoS positively influenced PH,, Qiao and Wang (2019) found a negative relationship between snow cover onset date and the start of the growing season,. Variable influence of snow cover depth on SOS was reported by Yu et al. (2013) in the study over China, where increasing snow depth could advance or delay the SOS, depending on elevation, vegetation type, and climatic zone.

Paudel and Andersen (2013) explored responses of rangeland vegetation to snow cover dynamics in Nepal Trans Himalayas using MODIS NDVI data at 250m and MODIS snow cover product at 500 m resolution over the 2000-2009 period. They observed significant positive correlations between SOS and the last snow-free date in drier areas at higher elevations (above 4000 m), while negative or no significant correlations were observed at lower elevations (3000-4000 m). To evaluate the relationship between snow cover duration and vegetation production, they used pre-monsoon NDVI time-integrated from April to June in four elevational belts (<3000 m, 3000-4000 m, 4000-4500 m, and >4500 m), while we used an early season AUC metric, which could be considered comparable to their time-integrated NDVI. They observed strong positive relationships between snow cover duration and the time-integrated NDVI at the driest location over elevation above 3000 m, and the strengthening of that relationship toward higher elevation ($p< 0.01$). In contrast, there was a negative linear relationship at the wetter site in every elevation class ($p<0.05$). They concluded, the declining length of the growing season in the drier eco-zones corresponded with delayed SOS and declining trend of annual snow cover duration in these

regions over their 2000-2009 study period (Paudel and Andersen, 2011). The lengthening of the growing season in the wetter southern regions was attributed to both earlier start and delayed end dates of the growing season. The delayed SOS was attributed to unusual late season snowfall that had occurred in March and early April instead of January and February in nearly every snow season during the second half of the decade they studied (2000-2009). Thus, a delayed SOS might arise from a lag in the responsiveness of NDVI to precipitation, and so they presumed a similar lag effect of the timing of snowmelt (and the duration of snow cover) on the vegetation response. Hence, during years with late snowfall, seeds may not be able to germinate until the soil receives enough moisture from meltwater and, thus, a delay in SOS leads to a delay in the timing of peak NDVI.

In contrast, over relatively wetter study areas, where the soil received sufficient moisture from meltwater and rainfall during the post-winter or early pre-monsoon, the SOS had advanced during the decade they studied. Over these wetter areas, snowmelt was associated with warming conditions and, thus, earlier snowmelt could lead to earlier SOS. The significant influence of elevation on relationship strength observed by Paudel and Andersen (2013) points to strong terrain effects (and related thermal-moisture conditions) on snow cover-vegetation relationships, which we found in our study (*cf.* section 3.6.4.3). We found the correlations of early season AUC with the snow cover metrics to be the weakest in terms of areal extent among the four phenometrics. Moreover, only three correlations exhibited substantial asymmetries, where the ratio of areal extent of positive to negative correlations was lower than our threshold of 0.5 meaning a much greater area of significant negative correlations (*cf.* section 3.6.4.2). This situation appeared in HP

pastures for correlations between AUC and LDoS and AUC and FDoS, but in P pastures only between AUC with LDoS (Table 3.10).

Paudel and Andersen (2013) observed a strong negative relationship of time-integrated NDVI and snow cover duration over rather relatively wetter areas of study sites, but positive over drier regions. In contrast, we found a slightly greater area of the negative correlation between AUC and SCD (*pos%/neg%* = 0.62 for HP and 0.86 for P pastures at $p<0.01$). However, as those asymmetries did not cross our threshold of 0.5, the distributions were deemed not to be substantially different. Further, we integrated NDVI by GDD only up to the fitted PH, thus affecting linkages with the snow cover metrics. Furthermore, the interannual variation of AUC may also have been affected by local factors such as grazing and pasture management practices and disturbance history (*e.g.*, landslides and mudflows). Finally, the threshold values for AGDD (100) and NDVI (0.1) we used for the AUC calculation may have affected the strength of the relationships.

Overall, our study and the others all agreed on the strong influence of snow cover on shaping growing season dynamics, although the patterns differed due to elevation, vegetation community, and climatic characteristics.

3.7.2. How does mountainous terrain modulate snow cover effects?

Highland pasture phenology depends on the thermal regime of growing season. Over mountains, the growing season is shaped by terrain features. Elevation, aspect, and slope all play crucial roles (An et al., 2018), and can have strong effects on vegetation species richness, productivity, and nutrient dynamics (Gong et al., 2008).

Our results show that the longest growing season occurred at the lowest elevations (below 1800 m) showing similar low variability over the years, while with the increasing elevation, the growing season length decreased and interannual variation increased, especially during summer. However, when we divided the data into contrasting aspects, we found greater differences in the length of thermal time on northern aspects than in southern aspects, which might arise from higher variation in soil moisture on steeper slopes. The soil moisture-slope-aspect interaction influences species composition and productivity due to water availability (Armesto and Martinez, 1978; Badano et al., 2005; Måren et al., 2015; Sternberg and Shoshany, 2001). The difference between growing seasons on different slopes increased at higher elevations and became more significant and more pronounced on steeper slopes (Table 3.5). Erosion processes may limit vegetation growth and development on steeper slopes. In addition, soil weathering can be accelerated on south-facing slopes resulting in different soil properties (*e.g.*, changes in organic soil layer) in northern versus southern aspects (Gong et al., 2008; Xue et al., 2018). The aspect of the slope can lead to local environmental conditions unfavorable for plant growth, *e.g.*, where sun exposure might be longer over southern aspects leading to the lower soil moisture and soil nutrient levels. In the recent study in alpine meadows on the QTP, Liu et al. (2019) observed that plant leaves have better growing conditions, the higher moisture content, and the lower dry matter content in the leaves over northern aspects due to higher soil moisture and soil nutrient levels (Sternberg and Shoshany, 2001). On the other hand, the edpahic factors on southern aspects could help to maintain more stress-tolerant and light-demanding flora (Bennie et al., 2006; Liu et al., 2019).

An et al. (2018) explored terrain effects on LSP across the QTP using Landsat data. They found that green-up onset dates were later, but dormancy onset dates were earlier on shaded slopes than on sun-exposed slopes in meadow areas; whereas, in steppe areas where the climate is drier, the green-up onset dates did not show any significant aspect effect. Dormancy onset dates showed a similar response to aspect in steppe and meadow areas. When considering slope steepness across meadow areas, green-up dates were significantly delayed, while dormancy onset dates significantly advanced with the increase of slope on both north and south slopes. The pattern of slope in steppe areas was the opposite: earlier green-up and later dormancy onset. Findings of An et al. (2018) indicate that in complex terrain at high elevation, the temperature-moisture combinations strongly shapes the land surface phenology with slope playing a key role in the vegetation development. Those results are in correspondence with our findings from the exact multinomial tests, which clearly pointed to stronger influence from slope than aspect.

Terrain complexity affects the relationship between snow seasonality and pasture phenology. In general, longer snow cover favors higher peak height, but terrain features can modify that relationship. Results of the Xie et al. (2017) showed the role of snow cover greatly varies due to elevation, vegetation type, and climate. A higher positive correlation between duration and SOS, and higher negative between duration and LOS on slopes facing north or west than on south or east slopes. When considering the influence of elevation, they found that the correlations between duration and LSP varied over low elevation (<1000 m) and mid-elevation (1000-2000 m), while with increasing elevation they weaken and eventually disappear toward the highest elevations. Less than 10% of study sites showed a weak correlation between last snow day and LSP metrics. In our study,

we found different results: the strength of significant correlation asymmetries between snow cover temporal metrics and LSP increased with elevation, for the most part. Also, a greater area of those relationships were reported at higher elevation ranges (Tables 3.8, 3.9, 3.12). This finding indicates a higher sensitivity of vegetation to changes in weather patterns at higher elevations. The exception was the relationship between FDoS and PH, where the area of negative relationship decreased with increasing elevation and became positive relationship above 4000 m, although the areal extent was very small (*cf.* section 3.6.4.2, Table 3.8).

Results from the exact multinomial tests for equivalence (Table 3.11) point to the predominant role of slope in shaping interactions between snow seasonality metrics and phenometrics. Slope alone, the interaction of aspect with the >30° slope class, and the overall interaction of slope and aspect show the lowest number of equivalence occurrences (just three null hypotheses rejected out 45 tests). In contrast, aspect alone show had 29% (13/45) of null hypotheses rejected. Moreover, relationships with LDoS showed overall fewer conclusions of equivalence than relationships with SCD (11 vs. 41, Table 3.11), which may indicate the more sensitive relationship between the timing of the end of snow season and phenology over more complex terrain, and the higher instability of LDoS (*cf.* section 3.7.3).

Terrain effects and elevation gradients may differentially affect vegetation productivity and susceptibility to disturbance. In a study across the Great Basin region in the western United States over Sierra Nevada, Ruby, and Wasatch/Uinta mountain ranges where elevation reaches above 4300 m, Petersky et al. (2019) showed that vegetation types used to have a consistent seasonal snow cover in their historical record were likely to have lower

resilience under a new hydrologic regime resulting from warming trends that generated rain on snow events. This new hydrological regime was supposed to have earlier and more intermittent snowmelt causing a longer but drier growing season. However, the implications of the changes in snow cover persistency and vegetation expected sensitivity varied locally due to elevation and topographic complexity. In addition, those consequences depended on groundwater availability and potential physiological adaptation by the vegetation communities.

3.7.3. What can recent changes in snow cover seasonality tell us about possible futures for highland pasture phenology and productivity?

Snow cover can experience multiple melting episodes over the snow season in the highland pastures of Kyrgyzstan.

The positive correlation between SCD and DoSS was significant but relatively low: just over 30% of each pasture availability class at $p< 0.01$ and up to 53% at $p< 0.05$. Annual high variation of snow cover duration, especially in southeastern Kyrgyzstan, has also been reported by Dedieu et al. (2014) based on MOD10 snow products. DoSS showed more than 90% of area negatively correlated with FDoS at both significance levels, and only 30% to 50% of positive correlation with LDoS. That higher correlation of DoSS and FDoS than DoSS with LDoS, would suggest a greater dependence of snow cover duration on the snow onset date than on end date. However, the much smaller area of negative correlation between SCD and FDoS, and positive relationship between SCD and LDoS means high variation of snow cover over the season, especially at a beginning of snow cover season when the depth is still small and snowmelt can easily occur. Of the four snow metrics, SCD played a leading role in influencing pasture phenology, and a similar conclusion reached

by Xie et al. (2018) in their study of alpine LSP. The negative relationship between TTP and snow metrics may mean more days for pasture vegetation to grow. The connection of soil moisture and growth rate could also be explained by the large area of positive correlation between of SCD and PH more days with snow cover may add moisture to soil, and have crucial effects on soil heat and moisture preservation due to the insulating properties of the snowpack (Groffman et al., 2001; Qiao and Wang, 2019). HTV, which occurs earlier in the season, follows the correlation patterns of PH, and also shows positive relationships with SCD and DoSS. As Chapter 2 reproduces a published article, it would not be appropriate to edit its content. Since SCD, which was not examined in Chapter 2, showed the strongest relationship with the LSP metrics, we ran trend analysis for the SCD metric to compare with the other snow cover seasonality metrics (Figure 3.15).

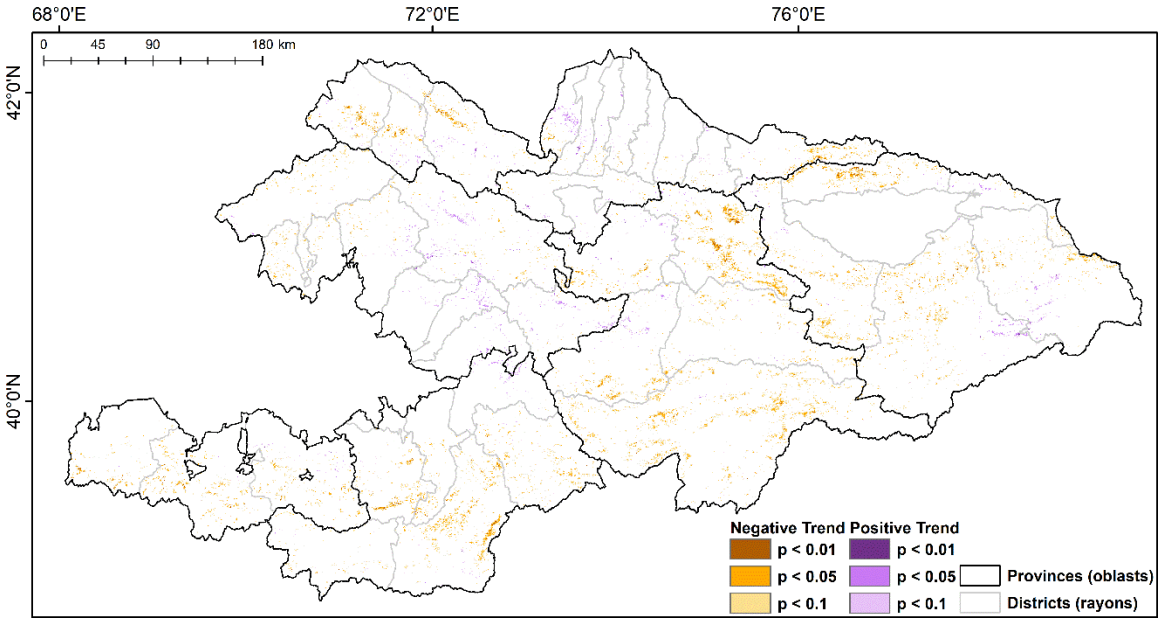

Figure 3.15. Map of significant negative (in orange) and positive (in purple) trends of SCD at three significance levels ($p<0.01$, $p<0.05$, $p<0.1$). Map displays data only for pasture land use areas with successful LSP fits (Projected coordinate system: Albers Conic Equal Area).

Negative trends in SCD predominated over positive trends across the pastures of Kyrgyzstan, especially in the central and southern parts of the country. Since PH showed a positive relationship with SCD and the retrospective SCD trend analysis showed decreasing SCD, a potential decrease in PH might be expected, arising from lower moisture availability due to fewer SCD.

The most important consequence of the shifts in the snow cover seasonality for mountainous vegetation is the alteration of the timing and rates of water availability and snow-insulation benefits. Shifts in vegetation structure and composition in response to new thermal and hydrological regimes (Telwala et al., 2013; Xie et al., 2018) in semiarid regions are likely to have cascading implications on large-scale water, carbon budgets, and susceptibility to disturbance (Petersky et al., 2019).

Here, we found the strongest response of LSP metrics to changes in snow cover temporal metrics occurred at higher elevations. A study over the Himalayas (Telwala et al., 2013) showed, that over higher elevations the stronger warming-driven range shift of vegetation distribution was evident and vegetation composition richness had been declining. They concluded that the continued trend of warming was likely to result in ongoing shifts in elevational range distributions and, eventually, species extinctions, particularly at mountaintops due to compression of suitable habitat. In study over the Alps in France, where mean elevation was about 2600, and ranged between 1000-4000 m, (Choler, 2015) showed that the length of the snow-free period was the primary determinant at productivity in temperate montane grasslands, and later snowmelt dates had a strong negative impact on the grassland productivity. We found a greater area of significant negative correlation between LDoS and AUC, meaning a later snowmelt translated into a lower AUC.

3.7.4. Limitations, uncertainties, and paths forward

Remote sensing studies of snow effects on vegetation are limited by the relatively short duration of most sensor archives and by the rather coarse spatial resolution of pixels relative to the spatial heterogeneity encountered in mountainous terrain. Within the area of a 500 m pixel it is not possible to state snow spatial distribution or its condition, while the use of higher spatial resolution data (*i.e.*, ≤30 m) may deliver more detailed information, especially in terms of the spatial distribution of snow cover. However, the temporal resolution of most sensors does not allow for observations at a tempo to characterize well the changes in a melting snowfield. Thus, while remote sensing datasets may be well suited for landscape scale research, they may be not appropriate for local field studies where the objects of interest are particular species or plant communities. In addition, frequent cloudiness lowers the number of clear observations and generates uncertainty in the differentiation of snow from clouds (Ackerman et al., 2008; Crane and Anderson, 1984). Our use of 8-day snow cover composites may introduce some temporal imprecision into the study, but the use of composites also provides consistent statistical power for trend analyses. In the 8-day composites, the maximum snow extent occurs where snow was observed on at least one day during the 8-day period. Therefore, a pixel may be marked as snow in two consecutive composites, but there might be no actual snow coverage on the land between the beginning of the first period and the end of the second period. This situation may lead to uncertainty in the determination of snow cover duration. However, these products have undergone extensive evaluation and validation, with additional screening in V006, so we concluded it was a suitable product for our study despite its limitations. Although we used the snow cover product from Terra satellite (MOD10A2)

because of longer data archive, a comparable snow cover product is available from the MODIS on the Aqua satellite as MYD10A2 dataset starting in 2002. In our previous study (Tomaszewska and Henebry, 2018; *cf.* Chapter 2), we used both 8-day snow cover products (MOD10A2, MYD10A2) for snow cover metrics trends comparison, and found that significant trends apparent in the Aqua data were less prevalent, indicating a discrepancy between those products. We speculated that this discrepancy may have resulted arise from the early afternoon overpass of Aqua, when imaging geometry, cloudiness, terrain shadows, and surface temperatures may differ from late morning overpass of Terra. The discrepancy is important as it may extend into the future since the presumptive sensor for post-MODIS snow cover continuity products is the Visible Infrared Imaging Radiometer Suite (VIIRS; Justice et al., 2013), currently in an early afternoon orbit on the Suomi National Polar-orbiting Partnership (S-NPP; https://www.jpss.noaa.gov/mission_and_instruments.html) satellite. Small differences may be caused by differences in bands, viewing geometry, and spatial resolution (VIIRS 375m, MODIS 500m). Larger differences may be caused by use of different cloud-mapping algorithms, and actual cloud differences due to time of acquisition; although, the snow detection algorithms and data products are designed to be as similar as possible (Riggs et al., 2017).

One potential option for longer-term observations could the ESA DUE (European Space Agency Data User Element) Global Snow Monitoring for Climate Research (GlobSnow) product (Luojus et al., 2010), which provides information on snow coverage retrieved from ERS-2 ATSR-2 and Envisat AATSR from 1995 until the present. There are three temporal resolutions (daily, weekly aggregated, and monthly aggregated). However, the spatial resolution is approximately 1 km, which is substantially coarser than in the case of MOD10

products, and there are discontinuities in the archive, different product versions for specific periods, and known issues of missing swaths (Luojus et al., 2010). The relatively new Theia snow collection is a high-resolution operational snow cover mapping system based on Sentinel-2 and Landsat-8 datasets (Gascoin et al., 2019) at 20 m spatial resolution, which may offer new possibilities for snow-vegetation interaction studies at local scales moving forward. Studies of the influence of snow cover on phenology are complicated by local interactions between terrain, vegetation, and microclimate; thus, synergistic analysis with higher spatial resolution image time series from digital cameras (Liu et al., 2017; Melaas et al., 2016; Rossi et al., 2019; Watson et al., 2019; Yan et al., 2019) might provide an avenue for balancing spatial and temporal resolutions (Julitta et al., 2014; Westergaard-Nielsen et al., 2017).

Our study is built around using the CxQ model to filter the NDVI time series. Despite using a great many Landsat images (*viz*., 13,285), data limitations remain in our analysis, as can be seen in the map of successful fits (Figure S3.1) where the evident stripes indicate greater numbers of observations. With the advent of the Sentinel-2 data streams in the late 2010s, the combination with Landsat observations into a harmonized surface reflectance product offers a much richer source of observations for moving forward (Claverie et al., 2018), but does not necessarily produce better characterization of LSPs (Nguyen and Henebry, 2019). We based our quantitative analyses on pasture classes related to the number of successful fits over 17 years. However, successful LSP fitting is strongly related to a sufficient number of high quality observations (Zhang et al., 2017). We did not run correlation analyses over the Rarely Available pasture class since only up to four years of successful fits were available. Using our specified conditions for fitting and additional filtering of observations

surely reduced the number of available pixels for subsequent analyses. That data reduction potentially introduces additional uncertainties into the analysis of pasture phenologies, *e.g.*, by influencing the shape of the parabola. However, a similar analytical approach has been used successfully in the study of LSP across Central Asia, albeit at a coarser spatial resolution (de Beurs et al., 2018).

We are aware, that the data inhomogeneity and an uneven distribution of clear observations over a year may well affect modeling results. Furthermore, an uneven distribution of successful fits over years in time-series may affect the interpretation of trend analyses in PH (Figure 3.14) and TTP, especially over Persistent pastures with lower number of successful fits.

Finally, we did not account for human impacts on pasture phenology that can arise from stocking rates, herd management, pasture maintenance, and control of invasive species, each of which may add to uncertainties that may affect some findings of this study (Eddy et al., 2017; Karnieli et al., 2013; Zhumanova et al., 2018, 2016). However, our study focused primarily on the early season green-up dynamics when differential effects from grazing management are expected to be minimal.

3.8. Conclusion

We investigated the effects of snow cover timing and duration on the land surface phenology during the following growing season across the highland pastures of Kyrgyzstan. Our results show strong interactions between snow cover timing and metrics of land surface phenology and these interactions differ due to location, elevation, and terrain characteristics. We found a positive relationship between the number of composite dates with snow cover (SCD) and the amplitude of the fitted phenological curve (PH). We

also found that later timing of snowmelt (LDoS) also increased the amplitude of the fitted phenological curve. On the other hand, a negative correlation was found between the onset of snow cover (FDoS) and the amplitude of the fitted phenological curve. Relationships of the snow cover temporal metrics with the amount of thermal time needed to reach the peak amplitude of the fitted curve were negative, with the strongest relationship between the number of snow covered composites (SCD) and the amount of thermal time needed to reach the peak amplitude (TTP).

We further demonstrated that the mountainous terrain affected linkages between snow cover and pasture phenology. The most pronounced effects were on the timing of snowmelt (LDoS) with slope being more influential than aspect, and the strongest interaction being aspect on steeper slopes. Over the highest elevations, the interplay of steep slopes and aspects strongly decreased growing season duration. We also observed a slight increase in areal extent asymmetries of positive and negative correlations between snow cover temporal metrics and LSP toward higher elevations (up to 4000 m).

While this paper has focused on establishing linkages between snow cover seasonality and metrics of land surface phenology in highland pastures, there is a need to zoom out from the landscape to see the broader biospheric context. One direction for future research is to explore how the modes of climate oscillations affect local weather patterns and, thus, potentially snow cover seasonality and LSP (Alemu and Henebry, 2013; de Beurs et al., 2018; de Beurs and Henebry, 2010b; Gonsamo and Chen, 2016; Pervez and Henebry, 2015; Viña and Henebry, 2005; Wright et al., 2014; Yeo et al., 2017). There is also need to analyze both snow cover seasonality and pasture phenology over particular colder/drier and warmer/wetter years to describe in detail how the phenometrics behave under different

weather sequences, and if the behaviors vary due to the terrain features. Eventually, the introduction of additional datasets with higher spatial and temporal resolutions could improve the precision and accuracy of the analyses, especially over the challenging terrain of montane Central Asia.

3.9. Acknowledgements

This research was supported, in part, by the NASA Land Cover / Land Use Change Program (NNX15AP81G) *How Environmental Change in Central Asian Highlands Impacts High Elevation Communities*. We appreciate the assistance and feedback from A.A. Aidaraliev, K. Kelgenbaeva, and P. Maatkarimov. We thank J. Frey of Villanova University for sharing his expertise and code that enabled us to run the exact multinomial test for equivalence.

3.10. References

Ackerman, S.A., Holz, R.E., Frey, R., Eloranta, E.W., Maddux, B.C., McGill, M., 2008. Cloud Detection with MODIS. Part II: Validation. J. Atmos. Ocean. Technol. 25, 1073–1086. https://doi.org/10.1175/2007JTECHA1053.1

Aizen, V.B., Aizen, E.M., Melack, J.M., 1995. Climate, snow cover, glaciers, and runoff in the Tien Shan. J. Am. Water Resour. Assoc. 31, 1113–1129. https://doi.org/10.1111/j.1752-1688.1995.tb03426.x

Akimaliev, D.A., Zaurov, D.E., Eisenman, S.W., 2013. The Geography, Climate and Vegetation of Kyrgyzstan, in: Medicinal Plants of Central Asia: Uzbekistan and Kyrgyzstan. Springer New York, New York, NY, pp. 1–4. https://doi.org/10.1007/978-1-4614-3912-7_1

Alemu, W.G., Henebry, G.M., 2013. Land surface phenologies and seasonalities using cool earthlight in mid-latitude croplands. Environ. Res. Lett. 8, 045002. https://doi.org/doi:10.1088/1748-9326/8/4/045002

Allen, T.R., 2000. Topographic Normalization of Landsat Thematic Mapper Data in Three Mountain Environments. Geocarto Int. Geocarto Int. Centre, G.P.O. Box 15.

An, S., Zhang, X., Chen, X., Yan, D., Henebry, G.M., 2018. An Exploration of terrain effects on Land Surface Phenology across the Qinghai–Tibet Plateau using Landsat ETM+ and OLI Data. Remote Sens. 10, 1069. https://doi.org/10.3390/rs10071069

Apel, H., Abdykerimova, Z., Agalhanova, M., Baimaganbetov, A., Gavrilenko, N., Gerlitz, L., Kalashnikova, O., Unger-Shayesteh, K., Vorogushyn, S., Gafurov, A., 2018. Statistical forecast of seasonal discharge in Central Asia using observational records: development of a generic linear modelling tool for operational water resource management. Hydrol. Earth Syst. Sci 22, 2225–2254. https://doi.org/10.5194/hess-22-2225-2018

Armesto, J.J., Martinez, J.A., 1978. Relations Between Vegetation Structure and Slope Aspect in the Mediterranean Region of Chile. J. Ecol. 66, 881. https://doi.org/10.2307/2259301

Asian Development Bank, 2010a. Central Asian Countries Initiative for Land Management (CACILM) Multicountry Partnership Framework Support Project [WWW Document]. URL https://www.adb.org/projects/38464-012/main

Asian Development Bank, 2010b. Central Asia Atlas of Natural Resource. Central Asian Countries Initiative for Land Management and Asian Development Bank, Manila, Philippines.

Azykova, E.K., 2002. Geographyical and landscape characteristics of mountain territories, in: Aidaraliev, A.A. (Ed.), Mountains of Kyrgyzstan. Technology, Bishkek.

Badano, E.I., Cavieres, L.A., Molina-Montenegro, M.A., Quiroz, C.L., 2005. Slope aspect influences plant association patterns in the Mediterranean matorral of central Chile. J. Arid Environ. 62, 93–108. https://doi.org/10.1016/J.JARIDENV.2004.10.012

Bai, J., Shi, H., Yu, Q., Xie, Z., Li, L., Luo, G., Jin, N., Li, J., 2019. Satellite-observed vegetation stability in response to changes in climate and total water storage in Central Asia. Sci. Total Environ. 659, 862–871. https://doi.org/10.1016/J.SCITOTENV.2018.12.418

Bennie, J., Hill, M.O., Baxter, R., Huntley, B., 2006. Influence of slope and aspect on long-term vegetation change in British chalk grasslands. J. Ecol. 94, 355–368. https://doi.org/10.1111/j.1365-2745.2006.01104.x

Bernauer, T., Siegfried, T., 2012. Climate change and international water conflict in Central Asia. J. Peace Res. 49, 227–239. https://doi.org/10.1177/0022343311425843

Bohovic, R., Dobrovolny, P., Klein, D., 2016. The Spatial and Temporal Dynamics of Remotely-sensed Vegetation Phenology in Central Asia in the 1982–2011 Period. Eur. J. Remote Sens. 49, 279–299. https://doi.org/10.5721/EuJRS20164916

Chen, Y., Li, W., Deng, H., Fang, G., Li, Z., 2016. Changes in Central Asia's Water Tower: Past, Present and Future. Sci. Rep. 6, 35458. https://doi.org/10.1038/srep35458

Choler, P., 2015. Growth response of temperate mountain grasslands to inter-annual variations in snow cover duration. Biogeosciences 12, 3885–3897. https://doi.org/10.5194/bg-12-3885-2015

Christensen, J.H., Kumar, K.K., Aldrian, E., An, S., Cavalcanti, I.F.A., De Castro, M., Dong, W., Goswami, P., Hall, A., Kanyanga, J.K., Kitoh, A., Kossin, J., Lau, N.C.,

Renwick, J., Stephenson, D.B., Xie, S.P., Zhou, T., 2013. Climate Phenomena and their Relevance for Future Regional Climate Change. In: Climate Change 2013: The Physical Sci- ence Basis. Contribution of Working Group I to the Fifth Assessment Report of the Intergovernmental Panel on Climate Change Coordinating L.

Claverie, M., Ju, J., Masek, J.G., Dungan, J.L., Vermote, E.F., Roger, J.-C., Skakun, S. V., Justice, C., 2018. The Harmonized Landsat and Sentinel-2 surface reflectance data set. Remote Sens. Environ. 219, 145–161. https://doi.org/10.1016/J.RSE.2018.09.002

Crane, R.G., Anderson, M.R., 1984. Satellite discrimination of snow/cloud surfaces. Int. J. Remote Sens. 5, 213–223. https://doi.org/10.1080/01431168408948799

Danielson, J.J., Gesch, D.B., 2011. Global multi-resolution terrain elevation data 2010 (GMTED2010). https://doi.org/https://doi.org/10.3133/ofr20111073

de Beurs, K.M., Henebry, G.M., 2010a. Spatio-Temporal Statistical Methods for Modelling Land Surface Phenology, in: Hudson I., K.M. (Ed.), Phenological Research. Springer Netherlands, Dordrecht, pp. 177–208. https://doi.org/10.1007/978-90-481-3335-2_9

de Beurs, K.M., Henebry, G.M., 2010b. A land surface phenology assessment of the northern polar regions using MODIS reflectance time series. Can. J. Remote Sens. 36, S87–S110. https://doi.org/10.5589/m10-021

de Beurs, K.M., Henebry, G.M., 2008a. Northern annular mode effects on the land surface phenologies of northern Eurasia. J. Clim. 21, 4257–4279. https://doi.org/10.1175/2008JCLI2074.1

de Beurs, K.M., Henebry, G.M., 2008b. War, Drought, and Phenology: Changes in the land surface phenology of Afghanistan since 1982. J. Land Use Sci. 3, 95–111. https://doi.org/10.1109/IGARSS.2006.630

de Beurs, K.M., Henebry, G.M., 2005. Land surface phenology and temperature variation in the International Geosphere-Biosphere Program high-latitude transects. Glob. Chang. Biol. 11, 779–790. https://doi.org/10.1111/j.1365-2486.2005.00949.x

de Beurs, K.M., Henebry, G.M., 2004. Land surface phenology, climatic variation, and institutional change: Analyzing agricultural land cover change in Kazakhstan. Remote Sens. Environ. 89, 497–509. https://doi.org/10.1016/J.RSE.2003.11.006

de Beurs, K.M., Henebry, G.M., Owsley, B.C., Sokolik, I., 2015. Using multiple remote sensing perspectives to identify and attribute land surface dynamics in Central Asia 2001-2013. Remote Sens. Environ. 170, 48–61. https://doi.org/10.1016/j.rse.2015.08.018

de Beurs, K.M., Henebry, G.M., Owsley, B.C., Sokolik, I.N., 2018. Large scale climate oscillation impacts on temperature, precipitation and land surface phenology in Central Asia. Environ. Res. Lett. 13, 065018. https://doi.org/10.1088/1748-9326/aac4d0

de Beurs, K.M., Wright, C.K., Henebry, G.M., 2009. Dual scale trend analysis for

evaluating climatic and anthropogenic effects on the vegetated land surface in Russia and Kazakhstan. Environ. Res. Lett. 4, 045012. https://doi.org/10.1088/1748-9326/4/4/045012

Dedieu, J.P., Lessard-Fontaine, A., Ravazzani, G., Cremonese, E., Shalpykova, G., Beniston, M., 2014. Shifting mountain snow patterns in a changing climate from remote sensing retrieval. Sci. Total Environ. 493, 1267–1279. https://doi.org/10.1016/J.SCITOTENV.2014.04.078

Delbart, N., Le Toan, T., Kergoat, L., Fedotova, V., 2006. Remote sensing of spring phenology in boreal regions: A free of snow-effect method using NOAA-AVHRR and SPOT-VGT data (1982–2004). Remote Sens. Environ. 101, 52–62. https://doi.org/10.1016/J.RSE.2005.11.012

Diaz, H.F., Grosjean, M., Graumlich, L., 2003. Climate Variability and Change in High Elevation Regions: Past, Present and Future. Clim. Change 59, 1–4. https://doi.org/10.1023/A:1024416227887

Dietz, A.J., Kuenzer, C., Conrad, C., 2013. Snow-cover variability in central Asia between 2000 and 2011 derived from improved MODIS daily snow-cover products. Int. J. Remote Sens. 34, 3879–3902. https://doi.org/10.1080/01431161.2013.767480

Eddy, I.M.S., Gergel, S.E., Coops, N.C., Henebry, G.M., Levine, J., Zerriffi, H., Shibkov, E., 2017. Integrating remote sensing and local ecological knowledge to monitor rangeland dynamics. Ecol. Indic. 82, 106–116. https://doi.org/10.1016/J.ECOLIND.2017.06.033

FAO, 2015. FAOStats: Statistics page of the Food and Agriculture Organisation (FAO) [WWW Document]. URL http://www.fao.org/faostat/en/#data/RL

Fieller, E.C., Hartley, H.O., Pearson, E.S., 1957. Tests for Rank Correlation Coefficients. I. Biometrika 44, 470. https://doi.org/10.2307/2332878

Fisher, J.I., Mustard, J.F., Vadeboncoeur, M.A., 2006. Green leaf phenology at Landsat resolution: Scaling from the field to the satellite. Remote Sens. Environ. 100, 265–279. https://doi.org/10.1016/J.RSE.2005.10.022

Foody, G.M., 2009. Classification accuracy comparison: Hypothesis tests and the use of confidence intervals in evaluations of difference, equivalence and non-inferiority. Remote Sens. Environ. 113, 1658–1663. https://doi.org/10.1016/J.RSE.2009.03.014

Frey, J., 2009. An exact multinomial test for equivalence. Can. J. Stat. / La Rev. Can. Stat. https://doi.org/10.2307/25653460

Gascoin, S., Grizonnet, M., Bouchet, M., Salgues, G., Hagolle, O., 2019. Theia Snow collection: high-resolution operational snow cover maps from Sentinel-2 and Landsat-8 data. Earth Syst. Sci. Data 11, 493–514. https://doi.org/10.5194/essd-11-493-2019

Gong, X., Brueck, H., Giese, K.M., Zhang, L., Sattelmacher, B., Lin, S., 2008. Slope aspect has effects on productivity and species composition of hilly grassland in the Xilin River Basin, Inner Mongolia, China. J. Arid Environ. 72, 483–493.

https://doi.org/10.1016/J.JARIDENV.2007.07.001

Gonsamo, A., Chen, J.M., 2016. Circumpolar vegetation dynamics product for global change study. Remote Sens. Environ. 182, 13–26. https://doi.org/10.1016/j.rse.2016.04.022

Goodin, D.G., Henebry, G.M., 1997. A technique for monitoring ecological disturbance in tallgrass prairie using seasonal NDVI trajectories and a discriminant function mixture model. Remote Sens. Environ. 61, 270–278. https://doi.org/10.1016/S0034-4257(97)00043-6

Goslee, S.C., 2011. Analyzing Remote Sensing Data in R : The landsat Package. J. Stat. Softw. 43, 1–25. https://doi.org/10.18637/jss.v043.i04

Groffman, P.M., Driscoll, C.T., Fahey, T.J., Hardy, J.P., Fitzhugh, R.D., Tierney, G.L., 2001. Colder soils in a warmer world: A snow manipulation study in a northern hardwood forest ecosystem. Biogeochemistry 56, 135–150. https://doi.org/10.1023/A:1013039830323

Hall, D.K., Riggs, G.A., Salomonson, V. V., DiGirolamo, N.E., Bayr, K.J., 2002. MODIS snow-cover products. Remote Sens. Environ. 83, 181–194. https://doi.org/10.1016/S0034-4257(02)00095-0

Henebry, G.M., 2003. Phenologies of North American Grasslands and Grasses, in: Schwartz, M.D. (Ed.), Phenology: An Integrative Environmental Science. Springer Netherlands, Dordrecht, pp. 197–210. https://doi.org/10.1007/978-94-007-6925-0

Henebry, G.M., de Beurs, K.M., 2013. Remote Sensing of Land Surface Phenology: A Prospectus, in: Phenology: An Integrative Environmental Science. Springer Netherlands, Dordrecht, pp. 385–411. https://doi.org/10.1007/978-94-007-6925-0_21

Henebry, G.M., de Beurs, K.M., Gitelson, A.A., 2005. Land surface phenologies of Uzbekistan and Turkmenistan between 1982 and 1999. Arid Ecosyst. 11, 25–32.

Hijioka, Y., Lin, E., Jacqueline Pereira, J., Pereira, J.J., Corlett, R.T., Cui, X., Insarov, G.E., Lasco, R.D., Lindgren, E., Surjan, A., 2014. Asia.

Hirsch, R.M., Slack, J.R., Smith, R.A., 1982. Techniques of trend analysis for monthly water quality data. Water Resour. Res. 18, 107–121. https://doi.org/10.1029/WR018i001p00107

Huete, A., Justice, C., Van Leeuwen, W., 1999. MODIS vegetation index (MOD13) algorithm theoretical basis document, Ver. 3.

Immerzeel, W.W., van Beek, L.P.H., Bierkens, M.F.P., 2010. Climate Change Will Affect the Asian Water Towers. Science (80-.). 328, 1382–5. https://doi.org/10.1126/science.1183188

Julitta, T., Cremonese, E., Migliavacca, M., Colombo, R., Galvagno, M., Siniscalco, C., Rossini, M., Fava, F., Cogliati, S., Morra di Cella, U., Menzel, A., 2014. Using digital camera images to analyse snowmelt and phenology of a subalpine grassland. Agric. For. Meteorol. 198–199, 116–125.

https://doi.org/10.1016/J.AGRFORMET.2014.08.007

Justice, C.O., Román, M.O., Csiszar, I., Vermote, E.F., Wolfe, R.E., Hook, S.J., Friedl, M., Wang, Z., Schaaf, C.B., Miura, T., Tschudi, M., Riggs, G., Hall, D.K., Lyapustin, A.I., Devadiga, S., Davidson, C., Masuoka, E.J., 2013. Land and cryosphere products from Suomi NPP VIIRS: Overview and status. J. Geophys. Res. Atmos. 118, 9753–9765. https://doi.org/10.1002/jgrd.50771

Kariyeva, J., Van Leeuwen, W.J.D., 2011. Remote Sensing Environmental Drivers of NDVI-Based Vegetation Phenology in Central Asia. Remote Sens 3, 203–246. https://doi.org/10.3390/rs3020203

Karnieli, A., Bayarjargal, Y., Bayasgalan, M., Mandakh, B., Dugarjav, C., Burgheimer, J., Khudulmur, S., Bazha, S.N., Gunin, P.D., 2013. Do vegetation indices provide a reliable indication of vegetation degradation? A case study in the Mongolian pastures. Int. J. Remote Sens. 34, 6243–6262. https://doi.org/10.1080/01431161.2013.793865

Kendall, M.G., 1938. A new measure of rank correlation. Biometrika 30, 81. https://doi.org/10.2307/2332226

Krehbiel, C., Henebry, G.M., 2016. A Comparison of Multiple Datasets for Monitoring Thermal Time in Urban Areas over the U.S. Upper Midwest. Remote Sens. 8, 297. https://doi.org/10.3390/rs8040297

Krehbiel, C., Zhang, X., Henebry, G., 2017. Impacts of Thermal Time on Land Surface Phenology in Urban Areas. Remote Sens. 9, 499. https://doi.org/10.3390/rs9050499

Kulikov, M., Schickhoff, U., 2017. Vegetation and climate interaction patterns in Kyrgyzstan: spatial discretization based on time series analysis. Erdkunde 71, 143–165. https://doi.org/10.3112/erdkunde.2017.02.04

Lehmann, E.L., D'Abrera, H.J.M., 2006. Nonparametrics : statistical methods based on ranks. Springer.

Lioubimtseva, E., Henebry, G.M., 2009. Climate and environmental change in arid Central Asia: Impacts, vulnerability, and adaptations. J. Arid Environ. 73, 963–977. https://doi.org/10.1016/j.jaridenv.2009.04.022

Liu, M., Che, Y., Jiao, J., Li, L., Jiang, X., 2019. Exploring the community phylogenetic structure along the slope aspect of subalpine meadows in the eastern Qinghai–Tibetan Plateau, China. Ecol. Evol. 9, 5270–5280. https://doi.org/10.1002/ece3.5117

Liu, Y., Hill, M.J., Zhang, X., Wang, Z., Richardson, A.D., Hufkens, K., Filippa, G., Baldocchi, D.D., Ma, S., Verfaillie, J., Schaaf, C.B., 2017. Using data from Landsat, MODIS, VIIRS and PhenoCams to monitor the phenology of California oak/grass savanna and open grassland across spatial scales. Agric. For. Meteorol. 237–238, 311–325. https://doi.org/10.1016/J.AGRFORMET.2017.02.026

Lu, L., Guo, H., Kuenzer, C., Klein, I., Zhang, L., Li, X., 2014. Analyzing phenological changes with remote sensing data in Central Asia. IOP Conf. Ser. Earth Environ. Sci. 17, 012005. https://doi.org/10.1088/1755-1315/17/1/012005

Luo, M., Liu, T., Meng, F., Duan, Y., Bao, A., Frankl, A., De Maeyer, P., 2018. Spatiotemporal characteristics of future changes in precipitation and temperature in Central Asia. Int. J. Climatol. https://doi.org/10.1002/joc.5901

Luojus, K., Pulliainen, J., Takala, M., Derksen, C., Rott, H., Nagler, T., Solberg, R., Wiesmann, A., Metsamaki, S., Malnes, E., Bojkov, B., 2010. Investigating the feasibility of the globsnow snow water equivalent data for climate research purposes, in: 2010 IEEE International Geoscience and Remote Sensing Symposium. IEEE, pp. 4851–4853. https://doi.org/10.1109/IGARSS.2010.5741987

Mannig, B., Müller, M., Starke, E., Merkenschlager, C., Mao, W., Zhi, X., Podzun, R., Jacob, D., Paeth, H., 2013. Dynamical downscaling of climate change in Central Asia. Glob. Planet. Change 110, 26–39. https://doi.org/10.1016/J.GLOPLACHA.2013.05.008

Måren, I.E., Karki, S., Prajapati, C., Yadav, R.K., Shrestha, B.B., 2015. Facing north or south: Does slope aspect impact forest stand characteristics and soil properties in a semiarid trans-Himalayan valley? J. Arid Environ. 121, 112–123. https://doi.org/10.1016/J.JARIDENV.2015.06.004

Matsushita, B., Yang, W., Chen, J., Onda, Y., Qiu, G., 2007. Sensitivity of the Enhanced Vegetation Index (EVI) and Normalized Difference Vegetation Index (NDVI) to Topographic Effects: A Case Study in High-density Cypress Forest. Sensors 7, 2636–2651. https://doi.org/10.3390/s7112636

Melaas, E.K., Friedl, M.A., Zhu, Z., 2013. Detecting interannual variation in deciduous broadleaf forest phenology using Landsat TM/ETM + data. Remote Sens. Environ. 132, 176–185. https://doi.org/10.1016/J.RSE.2013.01.011

Melaas, E.K., Sulla-Menashe, D., Gray, J.M., Black, T.A., Morin, T.H., Richardson, A.D., Friedl, M.A., 2016. Multisite analysis of land surface phenology in North American temperate and boreal deciduous forests from Landsat. Remote Sens. Environ. 186, 452–464. https://doi.org/10.1016/j.rse.2016.09.014

Monson, R.K., Lipson, D.L., Burns, S.P., Turnipseed, A.A., Delany, A.C., Williams, M.W., Schmidt, S.K., 2006. Winter forest soil respiration controlled by climate and microbial community composition. Nature 439, 711–714. https://doi.org/10.1038/nature04555

Moreira, E.P., Valeriano, M., Sanches, I., Formaggio, A.R., 2016. Topographic effect on spectral vegetation indices from Landsat TM data: is topographic correction necessary? Bol. Ciências Geodésicas 22, 95–107. https://doi.org/10.1590/S1982-21702016000100006

Moritz, S., Bartz-Beielstein, T., 2017. imputeTS: Time Series Missing Value Imputation in R [WWW Document]. R J. 9.1. URL https://journal.r-project.org/archive/2017/RJ-2017-009/RJ-2017-009.pdf

NASA JPL, 2013. NASA Shuttle Radar Topography Mission Global 1 arc second [Data set] [WWW Document]. NASA EOSDIS L. Process. DAAC.

https://doi.org/10.5067/MEaSUREs/SRTM/SRTMGL1.003

Nguyen, L.H., Henebry, G.M., 2019. Characterizing Land Use/Land Cover Using Multi-Sensor Time Series from the Perspective of Land Surface Phenology. Remote Sens. 11, 1677. https://doi.org/10.3390/rs11141677

Nguyen, L.H., Joshi, D.R., Clay, D.E., Henebry, G.M., 2018. Characterizing land cover/land use from multiple years of Landsat and MODIS time series: A novel approach using land surface phenology modeling and random forest classifier. Remote Sens. Environ. https://doi.org/10.1016/J.RSE.2018.12.016

Paudel, K.P., Andersen, P., 2013. Response of rangeland vegetation to snow cover dynamics in Nepal Trans Himalaya. Clim. Change 117, 149–162. https://doi.org/10.1007/s10584-012-0562-x

Paudel, K.P., Andersen, P., 2011. Monitoring snow cover variability in an agropastoral area in the Trans Himalayan region of Nepal using MODIS data with improved cloud removal methodology. Remote Sens. Environ. 115, 1234–1246. https://doi.org/10.1016/j.rse.2011.01.006

Pepin, N., Bradley, R.S., Diaz, H.F., Baraer, M., Caceres, E.B., Forsythe, N., Fowler, H., Greenwood, G., Hashmi, M.Z., Liu, X.D., Miller, J.R., Ning, L., Ohmura, A., Palazzi, E., Rangwala, I., Schöner, W., Severskiy, I., Shahgedanova, M., Wang, M.B., Williamson, S.N., Yang, D.Q., 2015. Elevation-dependent warming in mountain regions of the world. Nat. Clim. Chang. 5, 424–430. https://doi.org/10.1038/nclimate2563

Pervez, M.S., Henebry, G.M., 2015. Spatial and seasonal responses of precipitation in the Ganges and Brahmaputra river basins to ENSO and Indian Ocean dipole modes: Implications for flooding and drought. Nat. Hazards Earth Syst. Sci. 15, 147–162. https://doi.org/10.5194/nhess-15-147-2015

Petersky, R.S., Shoemaker, K.T., Weisberg, P.J., Harpold, A.A., 2019. The sensitivity of snow ephemerality to warming climate across an arid to montane vegetation gradient. Ecohydrology 12, e2060. https://doi.org/10.1002/eco.2060

Qiao, D., Wang, N., 2019. Relationship between Winter Snow Cover Dynamics, Climate and Spring Grassland Vegetation Phenology in Inner Mongolia, China. ISPRS Int. J. Geo-Information 8, 42. https://doi.org/10.3390/ijgi8010042

Reyer, C.P.O., Otto, I.M., Adams, S., Albrecht, T., Baarsch, F., Cartsburg, M., Coumou, D., Eden, A., Ludi, E., Marcus, R., Mengel, M., Mosello, B., Robinson, A., Schleussner, C.F., Serdeczny, O., Stagl, J., 2017. Climate change impacts in Central Asia and their implications for development. Reg. Environ. Chang. 17, 1639–1650. https://doi.org/10.1007/s10113-015-0893-z

Rhoades, A.M., Ullrich, P.A., Zarzycki, C.M., Johansen, H., Margulis, S.A., Morrison, H., Xu, Z., Collins, W.D., 2018. Sensitivity of Mountain Hydroclimate Simulations in Variable-Resolution CESM to Microphysics and Horizontal Resolution. J. Adv. Model. Earth Syst. 10, 1357–1380. https://doi.org/10.1029/2018MS001326

Riaño, D., Chuvieco, E., Salas, J., Aguado, I., 2003. Assessment of Different Topographic Corrections in Landsat-TM Data for Mapping Vegetation Types. IEEE Trans. Geosci. Remote Sens. 41. https://doi.org/10.1109/TGRS.2003.811693

Riggs, G.A., Hall, D.K., 2015. MODIS Snow Products Collection 6 User Guide.

Riggs, G.A., Hall, D.K., 2004. Snow Mapping with the MODIS Aqua Instrument. 61st East. Snow Conf.

Riggs, G.A., Hall, D. K., Román, M.O., 2017. Overview of NASA's MODIS and Visible Infrared Imaging Radiometer Suite (VIIRS) snow-cover Earth System Data Records. Earth Syst. Sci. Data 9, 765–777. https://doi.org/10.5194/essd-9-765-2017

Rossi, M., Niedrist, G., Asam, S., Tonon, G., Tomelleri, E., Zebisch, M., Rossi, M., Niedrist, G., Asam, S., Tonon, G., Tomelleri, E., Zebisch, M., 2019. A Comparison of the Signal from Diverse Optical Sensors for Monitoring Alpine Grassland Dynamics. Remote Sens. 11, 296. https://doi.org/10.3390/rs11030296

Roy, D.P., Kovalskyy, V., Zhang, H.K., Vermote, E.F., Yan, L., Kumar, S.S., Egorov, A., 2016. Characterization of Landsat-7 to Landsat-8 reflective wavelength and normalized difference vegetation index continuity. Remote Sens. Environ. 185, 57–70. https://doi.org/10.1016/J.RSE.2015.12.024

Schillhorn Van Veen, T.W., 1995. The Kyrgyz Sheep Herders at a Crossroads. Overseas Dev. Institute. Pastor. Dev. Netw. Ser.

Schimel, J.P., Bilbrough, C., Welker, J.M., 2004. Increased snow depth affects microbial activity and nitrogen mineralization in two Arctic tundra communities. Soil Biol. Biochem. 36, 217–227. https://doi.org/10.1016/J.SOILBIO.2003.09.008

Sorg, A., Bolch, T., Stoffel, M., Solomina, O., Beniston, M., 2012. Climate change impacts on glaciers and runoff in Tien Shan (Central Asia). Nat. Clim. Chang. 2. https://doi.org/10.1038/NCLIMATE1592

Sternberg, M., Shoshany, M., 2001. Influence of slope aspect on Mediterranean woody formations: Comparison of a semiarid and an arid site in Israel. Ecol. Res. 16, 335–345. https://doi.org/10.1046/j.1440-1703.2001.00393.x

Still, C.J., Pau, S., Edwards, E.J., 2014. Land surface skin temperature captures thermal environments of C 3 and C 4 grasses. Glob. Ecol. Biogeogr. 3, 286–296. https://doi.org/10.1111/geb.12121

Stocker, T.F., Qin, D., Plattner, G.-K., Tignor, M.M.B., Allen, S.K., Boschung, J., Nauels, A., Xia, Y., Bex, V., Midgley, P.M., 2013. Climate Change 2013 The Physical Science Basis Working Group I Contribution to the Fifth Assessment Report of the Intergovernmental Panel on Climate Change. Cambridge University Press, Cambridge, United Kingdom and New York, NY, USA.

Telwala, Y., Brook, B.W., Manish, K., Pandit, M.K., 2013. Climate-induced elevational range shifts and increase in plant species richness in a Himalayan biodiversity epicentre. PLoS One 8, e57103. https://doi.org/10.1371/journal.pone.0057103

Thompson, L.G., 2000. Ice core evidence for climate change in the Tropics: implications for our future. Quat. Sci. Rev. 19, 19–35.

Tomaszewska, M.A., Henebry, G.M., 2018. Changing snow seasonality in the highlands of Kyrgyzstan. Environ. Res. Lett. 13, 065006. https://doi.org/10.1088/1748-9326/aabd6f

USGS EROS, 2017. Landsat Collection 1 Level 1 Product Definition. Sioux Falls, SD.

Vázquez-Jiménez, R., Romero-Calcerrada, R., Ramos-Bernal, R., Arrogante-Funes, P., Novillo, C., 2017. Topographic Correction to Landsat Imagery through Slope Classification by Applying the SCS + C Method in Mountainous Forest Areas. ISPRS Int. J. Geo-Information 6, 287. https://doi.org/10.3390/ijgi6090287

Viña, A., Henebry, G.M., 2005. Spatio-temporal change analysis to identify anomalous variation in the vegetated land surface: ENSO effects in tropical South America. Geophys. Res. Lett. 32, 1–5. https://doi.org/10.1029/2005GL023407

Walker, J.J., de Beurs, K.M., Henebry, G.M., 2015. Land surface phenology along urban to rural gradients in the U.S. Great Plains. Remote Sens. Environ. 165, 42–52. https://doi.org/10.1016/J.RSE.2015.04.019

Wan, Y., Gao, Q., Li, Y., Qin, X., Zhang, W., Ma, X., Liu, S., 2014. Change of Snow Cover and Its Impact on Alpine Vegetation in the Source Regions of Large Rivers on the Qinghai-Tibetan Plateau. Arctic, Antarct. Alp. Res. 46, 632–644. https://doi.org/10.1657/1938-4246-46.3.632

Wan, Z., Hook, S., Hulley, G., 2015. MOD11A2 MODIS/Terra Land Surface Temperature/Emissivity 8-Day L3 Global 1km SIN Grid V006.

Wang, L., Li, Z., Wang, F., Edwards, R., 2014. Glacier shrinkage in the Ebinur lake basin, Tien Shan, China, during the past 40 years. J. Glaciol. 60, 245–254. https://doi.org/10.3189/2014JoG13J023

Wang, X., Wu, C., Peng, D., Gonsamo, A., Liu, Z., 2018. Snow cover phenology affects alpine vegetation growth dynamics on the Tibetan Plateau: Satellite observed evidence, impacts of different biomes, and climate drivers. Agric. For. Meteorol. 256–257, 61–74. https://doi.org/10.1016/J.AGRFORMET.2018.03.004

Watson, C.J., Restrepo-Coupe, N., Huete, A.R., 2019. Multi-Scale Phenology of Temperate Grasslands: Improving Monitoring and Management With Near-Surface Phenocams. Front. Environ. Sci. 7, 14. https://doi.org/10.3389/fenvs.2019.00014

Welker, J.M., Fahnestock, J.T., Sullivan, P.F., Chimner, R.A., 2005. Leaf mineral nutrition of Arctic plants in response to warming and deeper snow in northern Alaska. Oikos 109, 167–177. https://doi.org/10.1111/j.0030-1299.2005.13264.x

Wellek, S., 2010. Testing Statistical Hypotheses of Equivalence and Noninferiority, Second Edition, 2nd ed. Chapman and Hall/CRC, New York City . https://doi.org/10.1201/EBK1439808184

Westergaard-Nielsen, A., Lund, M., Pedersen, S.H., Schmidt, N.M., Klosterman, S.,

Abermann, J., Hansen, B.U., 2017. Transitions in high-Arctic vegetation growth patterns and ecosystem productivity tracked with automated cameras from 2000 to 2013. Ambio 46, 39–52. https://doi.org/10.1007/s13280-016-0864-8

WorldBank, 2018. Kyrgyzstan; Population 2017 [WWW Document]. URL https://data.worldbank.org/country/kyrgyz-republic

Wright, C.K., de Beurs, K.M., Henebry, G.M., 2014. Land surface anomalies preceding the 2010 Russian heat wave and a link to the North Atlantic oscillation. Environ. Res. Lett. 9, 124015. https://doi.org/10.1088/1748-9326/9/12/124015

Xenarios, S., Gafurov, A., Schmidt-Vogt, D., Sehring, J., Manandhar, S., Hergarten, C., Shigaeva, J., Foggin, M., 2018. Climate change and adaptation of mountain societies in Central Asia: uncertainties, knowledge gaps, and data constraints. Reg. Environ. Chang. 1–14. https://doi.org/10.1007/s10113-018-1384-9

Xie, J., Kneubühler, M., Garonna, I., de Jong, R., Notarnicola, C., De Gregorio, L., Schaepman, M.E., 2018. Relative influence of timing and accumulation of snow on alpine land surface phenology. J. Geophys. Res. 123, 561–576. https://doi.org/10.1002/2017JG004099

Xie, J., Kneubühler, M., Garonna, I., Notarnicola, C., De Gregorio, L., De Jong, R., Chimani, B., Schaepman, M.E., 2017. Altitude-dependent influence of snow cover on alpine land surface phenology. J. Geophys. Res. Biogeosciences 122, 1107–1122. https://doi.org/10.1002/2016JG003728

Xu, Y., Zhou, B., Wu, Ji, Han, Z., Zhang, Y., Wu, J, 2017. Asian climate change under 1.5–4 °C warming targets. Adv. Clim. Chang. Res. 8, 99–107. https://doi.org/10.1016/J.ACCRE.2017.05.004

Xue, R., Yang, Q., Miao, F., Wang, X., Shen, Y., 2018. Slope aspect influences plant biomass, soil properties and microbial composition in alpine meadow on the Qinghai-Tibetan plateau. J. soil Sci. plant Nutr. 18, 0–0. https://doi.org/10.4067/S0718-95162018005000101

Yan, D., Scott, R.L., Moore, D.J.P., Biederman, J.A., Smith, W.K., 2019. Understanding the relationship between vegetation greenness and productivity across dryland ecosystems through the integration of PhenoCam, satellite, and eddy covariance data. Remote Sens. Environ. 223, 50–62. https://doi.org/10.1016/j.rse.2018.12.029

Yeo, S., Kim, W., Kim, K., 2017. Eurasian snow cover variability in relation to warming trend and Arctic Oscillation. Clim. Dyn. 48, 499–511. https://doi.org/10.1007/s00382-016-3089-4

Yu, X., Zhao, Y., Ma, X., Yao, J., Li, H., 2018. Projected changes in the annual cycle of precipitation over central Asia by CMIP5 models. Int. J. Climatol. 38, 5589–5604. https://doi.org/10.1002/joc.5765

Yu, Z., Liu, S., Wang, J., Sun, P., Liu, W., Hartley, D.S., 2013. Effects of seasonal snow on the growing season of temperate vegetation in China. Glob. Chang. Biol. 19, 2182–2195. https://doi.org/10.1111/gcb.12206

Yuan-An, J., Ying, C., Yi-Zhou, Z., Peng-Xiang, C., Xing-Jie, Y., Jing, F., Su-Qin, B., 2013. Analysis on Changes of Basic Climatic Elements and Extreme Events in Xinjiang, China during 1961–2010. Adv. Clim. Chang. Res. 4, 20–29. https://doi.org/10.3724/SP.J.1248.2013.020

Zhang, X., Wang, J., Gao, F., Liu, Y., Schaaf, C., Friedl, M., Yu, Y., Jayavelu, S., Gray, J., Liu, L., Yan, D., Henebry, G.M., 2017. Exploration of scaling effects on coarse resolution land surface phenology. Remote Sens. Environ. 190, 318–330. https://doi.org/10.1016/J.RSE.2017.01.001

Zhumanova, M., Mönnig, C., Hergarten, C., Darr, D., Wrage-Mönnig, N., 2018. Assessment of vegetation degradation in mountainous pastures of the Western Tien-Shan, Kyrgyzstan, using eMODIS NDVI. Ecol. Indic. 95, 527–543. https://doi.org/10.1016/j.ecolind.2018.07.060

Zhumanova, M., Wrage-Mönnig, N., Darr, D., 2016. Farmers' Decision-making and Land Use Changes in Kyrgyz Agropastoral Systems. Mt. Res. Dev. 36, 506–517. https://doi.org/10.1659/MRD-JOURNAL-D-16-00030.1

3.11. Supplementary materials

3.11.1. Exploratory Analysis of Topographic Corrections on NDVI Data with the Study Area

We used two Landsat-8 OLI tiles from Collection 1 Tier 1 Level-1 Precision and Terrain (L1TP) corrected product acquired on 07 July 2017 (Path 150 Row 030) and on 30 July 2017 (Path 152 Row 032), to which we applied seven topographic correction methods (Goslee, 2011). There are two families of topographic correction methods. The first is Lambertian method, which assumes that the reflectance of all wavelengths is constant and independent of viewing angle, and for which the correction factor is identical for all bands. In addition, only the direct part of the irradiance is modeled. The second family is composed of the non-Lambertian methods that consider surface roughness, which means the interaction of incident and view angles influences the observed radiance (Riaño et al., 2003).

At two locations where the topography corrections were performed, the results of four Lambertian methods—Cosine, Improved Cosine, Gamma, and Sun-Canopy-Sensor (SCS)—showed that the difference between the NDVI calculated from the original and corrected bands was minimal, regardless of terrain. The higher differences were generated using the three non-Lambertian methods (Minnaert, Minnaert + Slope, and C-Correction), which showed that differences reached up to 4% over the steepest slopes (>30°) when the NDVI values were lower (~0.2-0.3). At the peak summer, when the Landsat data were collected, NDVI values of 0.2 to 0.3 would indicate sparse vegetation than values typical of pasture at that time of year. We concluded that topographic corrections were unnecessary for our study because the magnitude of the correction to the NDVI was so much smaller than the seasonal NDVI signal. Moreira et al. (2016) also concluded that the NDVI was robust to topographic effects.

Table S3.1. Landsat tiles for each sensor and year. Paths from 147 to 155, rows from 30 to 33.

	LT5		*LE7*		*LC8*		
	Unique	**Total**	**Unique**	**Total**	**Unique**	**Total**	
2001	5	18	33	312	-	-	
2002	3	3	33	286	-	-	
2003	0	0	33	273	-	-	
2004	0	0	33	432	-	-	
2005	0	0	33	457	-	-	
2006	11	44	33	451	-	-	
2007	9	54	33	512	-	-	
2008	32	228	32	488	-	-	
2009	33	533	33	455	-	-	
2010	33	451	33	425	-	-	
2011	33	406	33	433	-	-	
2012	0	0	33	581	-	-	
2013	-	-	33	621	33	518	
2014	-	-	33	633	33	685	
2015	-	-	33	643	33	678	
2016	-	-	33	622	33	682	
2017	-	-	33	653	33	708	
TOTAL		1,737		8,277		3,271	**13,285**

Table S3.2. Areal percentage of significant correlations between snow cover temporal metrics and the phenometric HTV and the ratio of positive % area to negative % area. In **bold**, pos%/neg% > 2.0; *in* ***bold italics***, *pos%/neg%* < 0.5.

HTV						
	p< 0.01			**p< 0.05**		
HP (11- 17 yrs) Area=15,261 km^2	Pos	Neg	Ratio	Pos	Neg	Ratio
SCD	2.87	0.11	**26.09**	10.63	0.51	**20.84**
LDoS	1.36	0.22	**6.18**	5.30	1.12	**4.73**
DoSS	1.71	0.22	**7.77**	6.37	1.07	**5.95**
FDoS	0.27	1.47	***0.18***	1.30	5.60	***0.23***
P (5 – 10 yrs) Area=53,620 km^2	Pos	Neg	Ratio	Pos	Neg	Ratio
SCD	2.45	0.25	**9.80**	8.46	0.97	**8.72**
LDoS	1.25	0.43	**2.91**	4.38	1.76	**2.49**
DoSS	1.40	0.42	**3.33**	5.05	1.71	**2.95**
FDoS	0.47	1.30	***0.36***	1.81	4.65	***0.39***

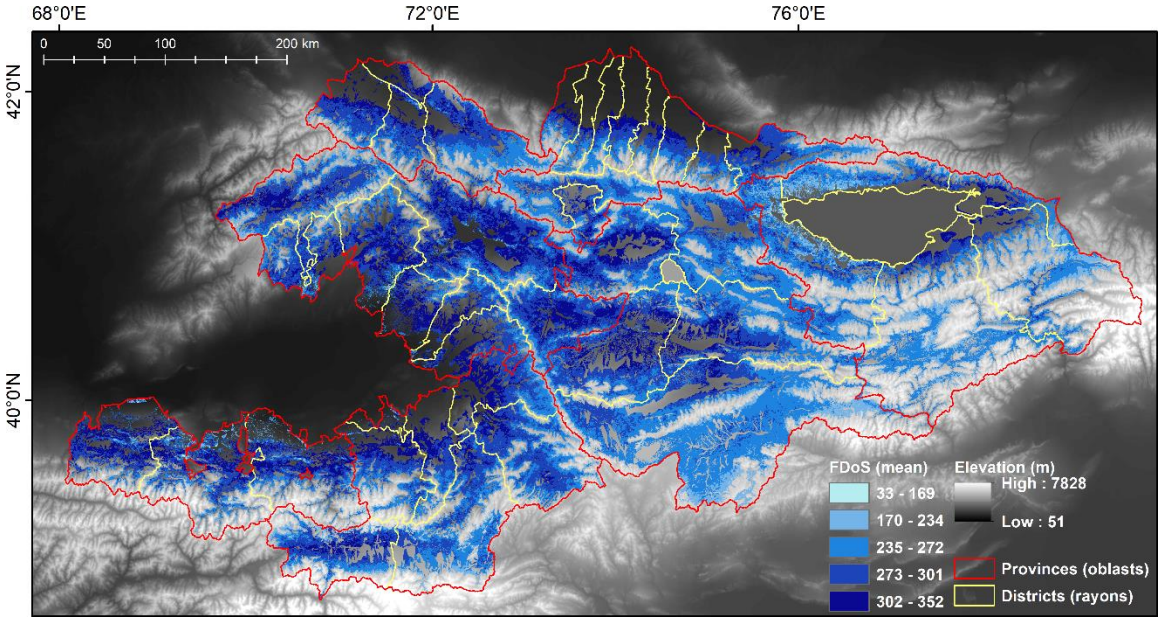

Figure S3.1. Mean values of First Day of Snow (FDoS). Map draped over the SRTM 30 m DEM display data only for pasture land use (Projected coordinate system: Albers Conic Equal Area).

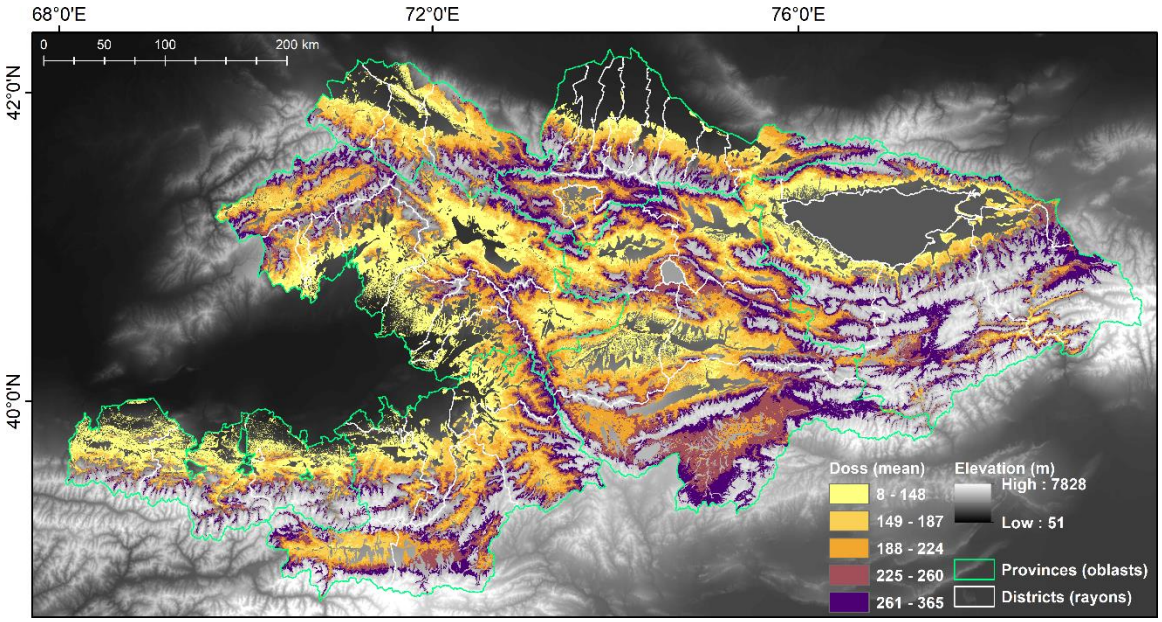

Figure S3.2. Mean values of Duration of Snow Season (DoSS). Map draped over the SRTM 30 m DEM display data only for pasture land use (Projected coordinate system: Albers Conic Equal Area).

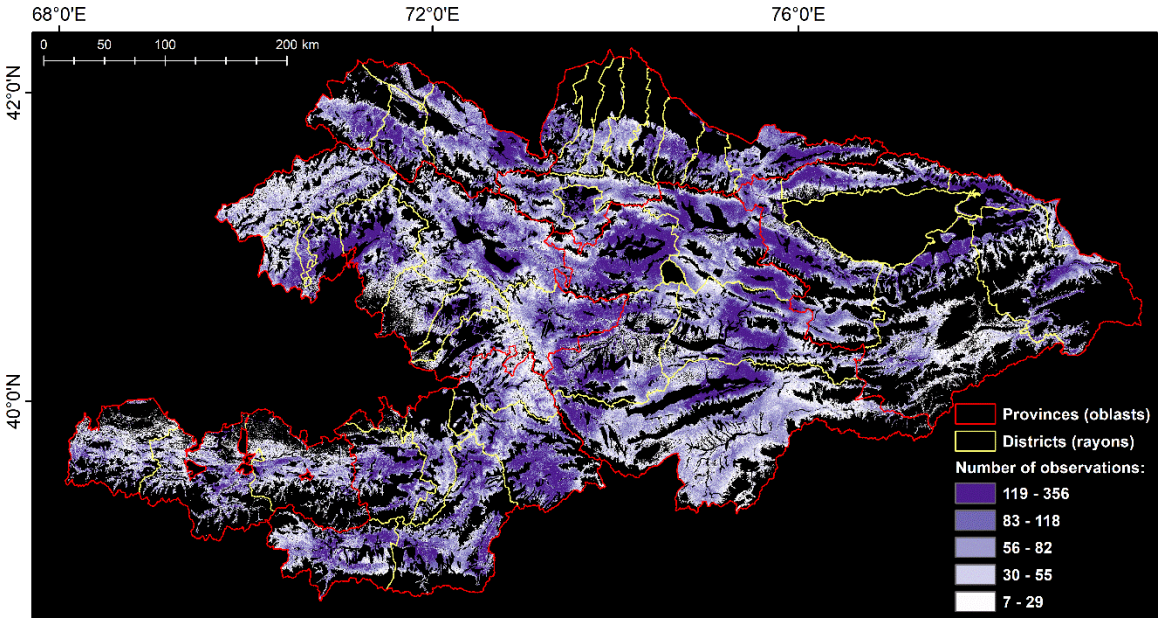

Figure S3.3. Total number of data observations used for successful LSP fits over pasturelands. Classes based on quintiles. Map displays data only for pasture land use (Projected coordinate system: Albers Conic Equal Area).

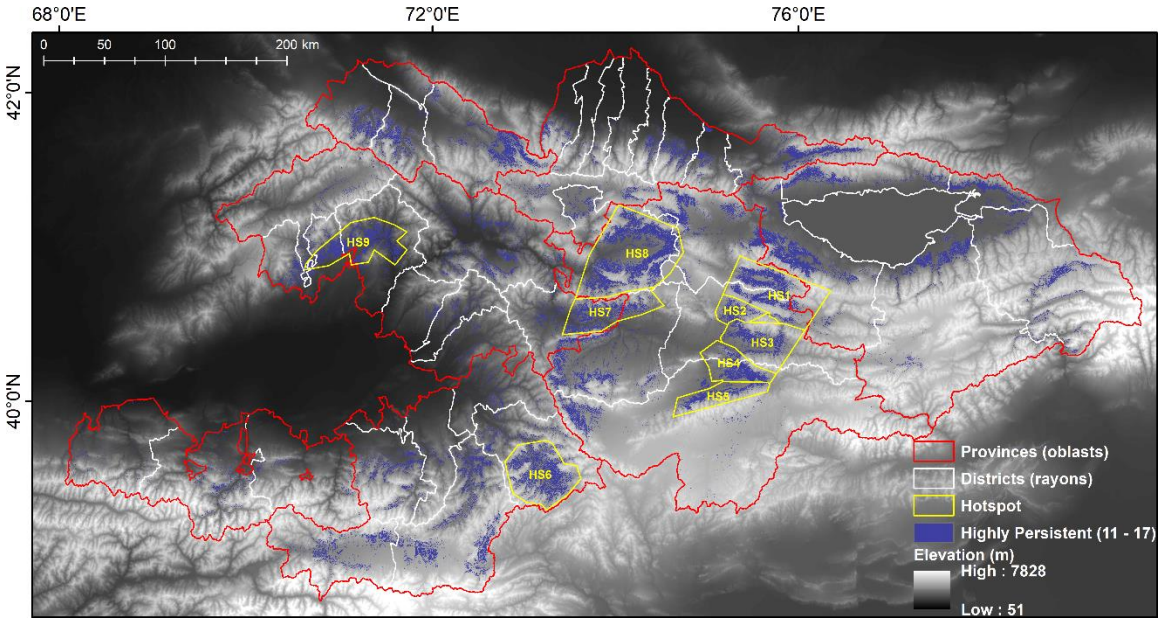

Figure S3.4. Nine hotspot areas (in purple) selected based on Spearman's rank correlation results draped over the SRTM 30 m DEM (Projected coordinate system: Albers Conic Equal Area).

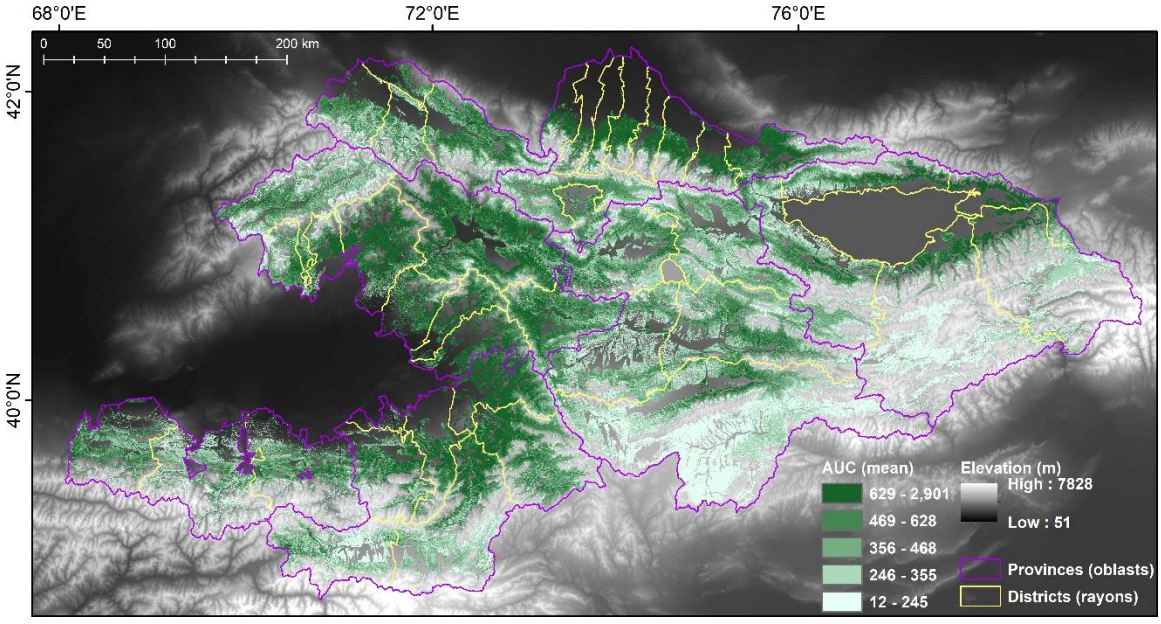

Figure S3.5. Mean values of Area Under the Curve (AUC) for pasture land use areas draped over the SRTM 30 m DEM (Projected coordinate system: Albers Conic Equal Area). Classes based on quintiles.

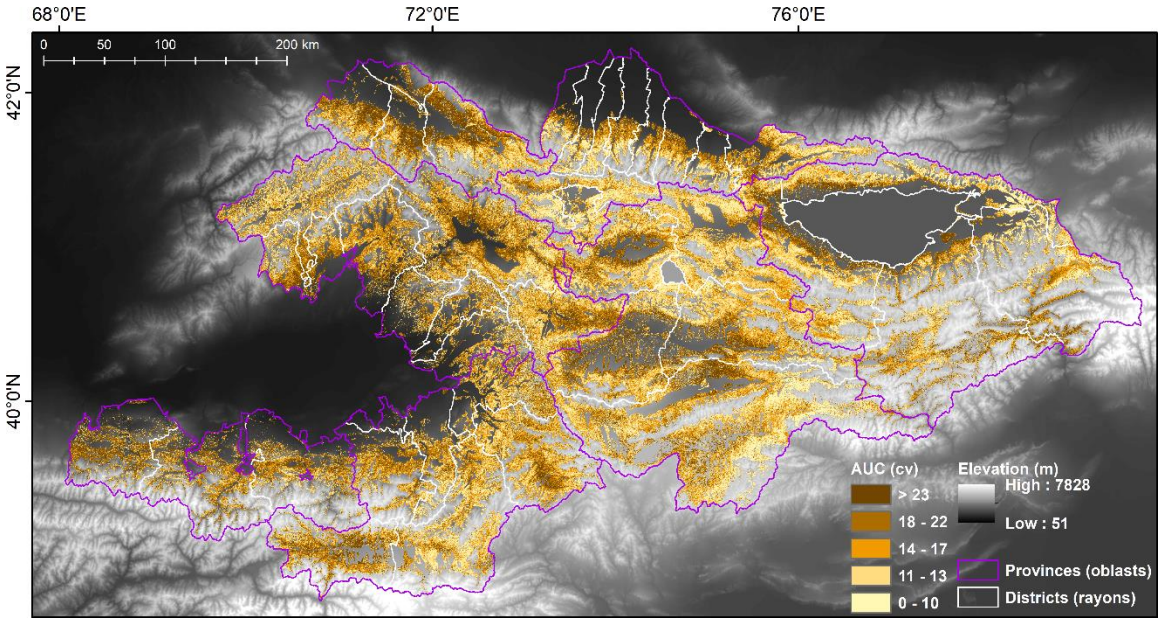

Figure S3.6. Mean Coefficient of Variation (%) of Area Under the Curve (AUC) for pasture land use areas draped over the SRTM 30 m DEM (Projected coordinate system: Albers Conic Equal Area). Classes based on quintiles.

CHAPTER 4

HOW MUCH VARIATION IN LAND SURFACE PHENOLOGY CAN CLIMATE OSCILLATION MODES EXPLAIN AT THE SCALE OF MOUNTAIN PASTURES IN KYRGYZSTAN?

Paper #3:

Tomaszewska, M.A., Henebry, G.M., *In review following revision*. How much variation in land surface phenology can climate oscillations explain at the scale of mountain pastures in Kyrgyzstan? *International Journal of Applied Earth Observation and Geoinformation* (revision submitted 25NOV2019, JAG-2019-1051-R1).

4.0. Abstract

Climate oscillation modes can shape weather across the globe due to atmospheric teleconnections. We built on the findings of a recent study to assess whether the impacts of teleconnections are detectable and significant in the early season dynamics of highland pastures across five rayons in Kyrgyzstan. Specifically, since land surface phenology (LSP) has already shown to be influenced by snow cover seasonality and terrain, we investigated here how much more explanatory and predictive power information about climatic oscillation modes might add to explain variation in LSP. We focused on seasonal values of five climate oscillation indices that influence vegetation dynamics in Central Asia. We characterized the phenology in highland pastures with metrics derived from LSP modeling using Landsat NDVI time series together with MODIS land surface temperature (LST) data: Peak Height (PH), the maximum modeled NDVI and Thermal Time to Peak (TTP), the quantity of accumulated growing degree-days based on LST required to reach PH. Next, we calculated two metrics of snow cover seasonality from MODIS snow cover composites: last date of snow (LDoS), and the number of snow covered dates (SCD). For terrain features, we derived elevation, slope, and TRASP index as linearization of aspect.

First, we used Spearman's rank correlation to assess the geographical differentiation of land surface phenology metrics responses to environmental variables. PH showed weak correlations with TTP (positive in western but negative in eastern rayons), and moderate relationships with LDoS and SCD only in one northeastern rayon. Slope was weakly related to PH, while TRASP showed a consistent moderate negative correlation with PH. A significant but weak negative correlation was found between PH and SCAND JJA, and a significant weak positive correlation with MEI MAM. TTP showed consistently strong negative relationships with LDoS, SCD, and elevation. Very weak positive correlations with TTP were found for EAWR DJF, AMO DJF, and MEI DJF in western rayons only. Second, we used Partial Least Squares regression to investigate the role of oscillation modes altogether. PLS modelling of TTP showed that thermal time accumulation could be explained mostly by elevation and snow cover metrics, leading to reduced models explaining 55 to 70% of observed variation in TTP. Variable selection indicated that NAO JJA, AMO JJA and SCAND MAM had significant relationships with TTP, but their input of predictive power was neglible. PLS models were able to explain up to 29% of variability in PH. SCAND JJA and MEI MAM were shown to be significant predictors, but adding them into models did not influence modeling performance. The impacts of climate oscillation anomalies were not detectable or significant in mountain pastures using LSP metrics at fine spatial resolution. Rather, at a 30 m resolution, the indirect effects of seasonal climatic oscillations are overridden by terrain influences (mostly elevation) and snow cover timing. Whether climate oscillation mode indices can provide some new and useful information about growing season conditions remains a provocative question,

particularly in light of the multiple environmental challenges facing the agropastoralism livelihood in montane Central Asia.

4.1. Introduction

Kyrgyzstan (aka the Kyrgyz Republic) spans multiple climatic regimes, from arid/semi-arid deserts to hot, humid continental climates (Peel et al., 2007). Strong spatial variation in precipitation and temperature exists due to orography (Böhner, 2006; Bothe et al., 2012), as the mountain ranges of Tien Shan, Pamir, and Alatau cover more than 90% of the country's land area (Azykova, 2002). Moreover, Central Asia (Kazakhstan, Kyrgyzstan, Tajikistan, Turkmenistan, and Uzbekistan) has been identified as a "climate change hot-spot", a region where climate is especially responsive to global change (Bothe et al., 2012; Giorgi, 2006). This "hot-spot" might arise from regional and local feedbacks (e.g., snow-ice albedo feedback and/or soil moisture-precipitation feedback) or to changes in intrinsic variability of atmospheric circulation patterns and oscillation modes (Giorgi, 2006). Interaction of atmosphere and oceans plays an essential role in shaping climate and its variability, including naturally-occurring dynamical modes (Wang et al., 2004; Wang and Schimel, 2003), which may also be changing as a result of global warming (Yeh et al., 2018). Large-scale climatic variability is often dominated by a few modes resulting in teleconnections—correlated weather patterns between remote locations (Horel and Wallace, 1981). Teleconnections can play significant roles in determining seasonal weather anomalies, whether warm and dry or wet and cold (Casanueva et al., 2014). The most well-known mode of interannual climatic variability is ENSO (El Niño-Southern Oscillation; (Wang et al., 2004)), which is generated through coupled interactions between the ocean and atmosphere in the tropical Pacific and alternates between anomalously warm (El Niño)

and cold (La Niña) sea surface temperature (SST) conditions (Bjerksen, 1969). Over the Northern Hemisphere during wintertime, the most influential mode is the North Atlantic Oscillation (NAO) (Hurrell, 1995; Hurrell et al., 2003; Rodwell et al., 1999).

Over Central Asia, there are many studies describing the linkages between weather patterns anomalies and climatic oscillations (Barlow et al., 2002; Bothe et al., 2012; Gerlitz et al., 2018). For example, Syed et al., (2006) showed that a positive precipitation anomaly over southwestern Central Asia had been triggered by warm ENSO phase and positive phase of North Atlantic Oscillation. Yin et al., (2014) highlighted the effects of the polar–Eurasian (POL/EUR), and East Atlantic–Western Russia (EAWR) patterns on Central Asian winter climate, which enhanced moisture fluxes. In addition, the EA mode has been shown to be strongly related to ENSO, which makes the investigation of its nature and the independence of its influence more complex (Gerlitz et al., 2018; Iglesias et al., 2014). Li et al., (2008) indicated that the warm phase of the Atlantic Multidecadal Oscillation (AMO) could significantly affect the Indian monsoon rainfall, which could, in turn, affect southern Central Asia (de Beurs et al., 2018).

The agropastoralism, which is the basis of the economy in montane Central Asia, depends critically on precipitation. Herders of the highlands have been practising vertical transhumance—the annual cycle of livestock movement to higher elevation pastures (Schillhorn Van Veen, 1995)—to take advantage of seasonally available forage resources. Dependency on pasture resource availability during the short montane growing season makes pastoral livelihoods especially vulnerable to variation and change in environmental conditions and weather patterns. In this semi-arid region where most of the precipitation falls outside of the growing season, changes in precipitation patterns may shift forage

availability and shorten growing season (Hoppe et al., 2016; Vetter, 2005; Zhumanova et al., 2018, 2016).

Assessment of changes in local to regional environmental conditions in the highlands of Kyrgyzstan are impeded due to the remoteness of much of the area, a paucity of ground-level data, and the siting of most weather stations in inhabited valleys far from the pasture zones of interest. One solution is to use satellite remote sensing as a source of information. Pasture phenology has often been tracked through modelling of land surface phenology (LSP), which describes the temporal pattern of the vegetated land surface as observed using remote sensing (de Beurs and Henebry, 2004, 2010; Henebry and de Beurs, 2013). A commonly used indicator of green vegetation, the Normalized Difference Vegetation Index (NDVI) is the difference between near-infrared and red reflectance divided (or normalized) by the sum of the reflectances: [NIR−Red]/[NIR+Red] (Buermann et al., 2003; Myneni et al., 1995; Tucker, 1979).

Variability in the timing of LSP and the seasonal amplitude of the NDVI has been linked to changes in weather and climate within Central Asia (Bohovic et al., 2016; de Beurs et al., 2015, 2018; de Beurs and Henebry, 2008; Jiang et al., 2017; Kariyeva et al., 2012; Kariyeva and van Leeuwen, 2011; Lu et al., 2014). Studies have shown that fluctuations in LSP can be related to large scale climate oscillations at various extents over Central Asia and other regions (Buermann et al., 2003; Cook et al., 2005; de Beurs et al., 2009; Gong and Shi, 2003; Li et al., 2016; Menzel et al., 2005; Viña and Henebry, 2005; Wright et al., 2014). de Beurs and Henebry (2008) showed the Arctic Oscillation (AO) appears to affect the NDVI peak (modelled seasonal maximum of the NDVI index) over the Asian part of northern Eurasia more strongly than the NAO. Wright et al., (2014) found that early season

vegetation productivity measured using NDVI over the Eurasian wheat belt is linked to both the winter (December–February) and early summer (April–June) phases of the NAO. Their results have shown that land surface anomalies preceding the Russian heatwave in 2010 were consistent with highly negative anomalies of NAO. More recently, de Beurs et al., (2018) analyzed the importance of five climate modes (NAO, EAWR, AMO, Scandinavian [SCAND], and ENSO), both together and separately, on precipitation, temperature, and land surface phenology to discover where each climate index had more influence across the Central Asian region. They used a downward-arching convex quadratic (CxQ) function to model the observed land surface phenology and to derive, as a phenological metric, the Peak Height (PH) – the maximum modelled NDVI. Then, they linked this phenometric with seasonal (winter, spring, and summer) values of five oscillation indices. As a result, they reported a percentage of land area in Central Asia that exhibited a significant correlation between each seasonal mode index and PH over at least 10% of the study area. Their maps that show multivariate climate oscillation impacts on land surface phenology and weather (seasonal temperature and precipitation). Across Kyrgyzstan, they reported a significant R^2 around 0.4.

While de Beurs et al. (2018) found indications of significant teleconnected influence on precipitation in montane Central Asia, the scale of analysis was spatially coarse. The precipitation and temperature data they used were gridded to 0.5° and the NDVI data were nominally 100 times finer (0.05°) in area. Here, we aim to test whether the linkages identified in de Beurs et al. (2018) as important for explaining observed temperature and precipitation anomalies at the regional scale translated to the scale of mountain pastures using finer resolution remote sensing data and, thus, might be able to inform decision-

making by herders and pasture committees. Specifically, our question is whether the impacts of oscillation anomalies are detectable and significant in the mountain pastures using LSP metrics based on much finer spatial resolution data. We have already shown that land surface phenology is influenced by snow cover seasonality and terrain (Tomaszewska et al., 2019). Thus, we investigate here how much more explanatory power some information about oscillation modes might add to explain LSP in mountain pastures of Kyrgyzstan. The time frame of this study extends from 2000/01 to 2017.

4.2. Study Area

The area of the study focuses on pasturelands spanning over five districts (called rayons): Chong-Alay (4,850 km^2), Alay (7,554 km^2), Kara-Kulja (5,739 km^2), At-Bashy (19,030 km^2), and Naryn (7,872 km^2) in the highlands of Kyrgyzstan in montane Central Asia. We selected these rayons because they represent a range of climatic conditions due to geographic location and elevation (*cf.* Figure 4.1). According to the Köppen-Geiger climate classification system (Peel et al., 2007): Chong-Alay and Alay are under the cold desert climate (BWk), while the eastern part of Alay is also impacted by cold semi-arid climate (BSk) and warm continental/humid continental climate (Dfa). Most of Kara-Kulja lies under warm continental climate (Dsa). The large extent of At-Bashy includes temperate continental climate/Mediterranean continental climate (Dsb), temperate continental/humid continental climate (Dfb), cold semi-arid climate (BSk) and, at the very southern part, cold desert climate (BWk). Naryn is a mixture of temperate continental/humid continental climate (Dfb) and cold semi-arid climate (BSk).

In addition, we visited four of these rayons during two field campaigns: Naryn and At-Bashy in July 2016, and Chong-Alay and Alay in July 2017. Information about the extent

of pasture land use was acquired from Soviet-era land use map that had been updated in 2008 within the CACILM project (Asian Development Bank, 2010a, 2010b) using remote sensing data from Landsat 7 ETM+ and MODIS.

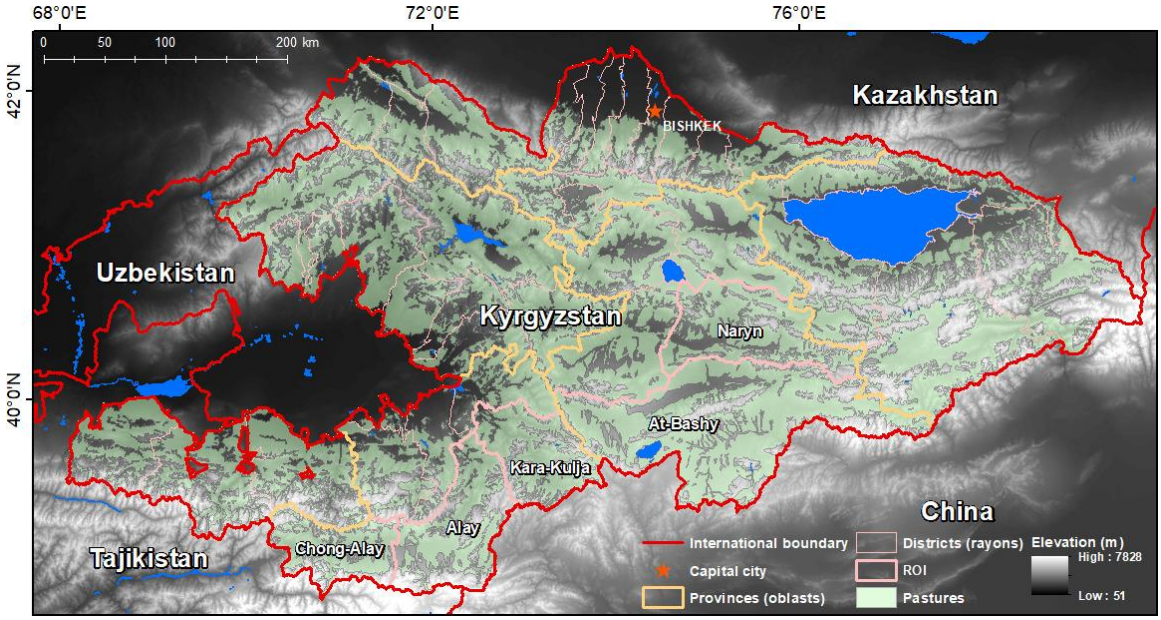

Figure 4.1. The study area is the pasture land use area in Kyrgyzstan; it is displayed in light green (from Asian Development Bank, 2010a, 2010b) and draped over the SRTM 30 m DEM (Projected coordinate system: Albers Conic Equal Area). Selected rayons of interest (ROI) are labelled and marked in light pink.

4.3. Data

We used multiple geospatial datasets and climate oscillation mode information.

4.3.1. Geospatial data

Metrics of land surface phenology, snow seasonality, and terrain information were supplied by the previous work (Tomaszewska et al., 2019; Tomaszewska and Henebry, 2018, *cf.* Chapter 2 & 3).

Metrics of snow seasonality were generated using 500m MODIS (MOD10A2) Terra snow cover 8-day composites (Riggs and Hall, 2015) distributed by the National Snow and Ice Data Center (https://nsidc.org/). Using the Normalized Difference Snow Index (NDSI) (Hall et al., 2002; Riggs and Hall, 2004), the MOD10A2 product reports the maximum snow cover extent observed during 8-day period by compositing observations from the MODIS/Terra Snow Cover Daily L3 Global 500 m Grid product (MOD10A1 V006). We downloaded two MODIS tiles (h23v04 and h23v05) from the middle of 2000 to the end of 2017, where each annual dataset consisted of 46 8-day composites. After tile merging, we projected them into the Albers Conic Equal Area coordinate system to 30 m pixel resolution using nearest neighbor resampling. We then extracted in each composite all pixels flagged as “snow” (i.e., pixel value = "200").

To generate the metrics of land surface phenology, we used two groups of products: (1) MODIS Land Surface Temperature, and (2) Landsat Surface Reflectance.

MODIS/Terra and MODIS/Aqua Land Surface Temperature/Emissivity (MOD11A2/MYD11A2 V006) products at 1 km spatial resolution provided an average 8-day land surface temperature (LST) from all MOD11A1/MYD11A1 LST pixels collected within the 8-day period (Wan et al., 2015). We downloaded two MODIS tiles (h23v04 and h23v05) from 2001 for MODIS/Terra and from 2002 for MODIS/Aqua through the end of 2017. After merging, we removed poor quality pixels using the quality bits provided in each product, converted land surface temperature from Kelvin to °C, and projected the data into the Albers Conic Equal Area coordinate system with 30 m pixel resolution using bilinear resampling.

We used the Landsat Collection 1 Tier 1 Level-1 Precision and Terrain (L1TP) corrected product from 2001 to the end of 2017. The Collection contains Level-1 data products generated from Landsat 5 Thematic Mapper (TM), Landsat 7 Enhanced Thematic Mapper Plus (ETM+), and Landsat 8 Operational Land Imager (OLI) (USGS EROS, 2017). Surface reflectance NDVI data were obtained by downloading 13,285 images in 33 unique tiles (WRS-2 Paths 147 to 155 and Rows 30 to 33) from the USGS Earth Resources Observation and Science (EROS) Center Science Processing Architecture (ESPA) On Demand Interface (https://espa.cr.usgs.gov/). After masking out poor quality pixels using quality bits delivered with each product, we projected the data into the Albers Conic Equal Area coordinate system. Further, to adjust Landsat 5 TM surface NDVI and Landsat 7 ETM+ surface NDVI to the surface Landsat 8 OLI NDVI, which showed to have higher surface reflectance values, we applied the inter-calibration equation from Roy et al., (2016) to both surface NDVI from Landsat 5 TM and Landsat 7 ETM+ scenes. The same equation was used with both datasets because differences between those data were very small (Fisher et al., 2006; Melaas et al., 2013).

For the terrain representation, we downloaded 133 tiles of SRTMGL1, the NASA Shuttle Radar Topography Mission Global 1 arc second (~30 m) V003 product (NASA JPL, 2013) from USGS Earth Explorer (https://earthexplorer.usgs.gov/). Tiles were merged and projected into the Albers Conic Equal Area coordinate system using bilinear resampling to 30 m spatial resolution. Further, we generated two layers of terrain features: slope (in degrees) and aspect (in degrees). Because aspect is a circular measure, we used a linear transformation to get a continuous measure from 0 to 1, where ‘0’ is assigned to the aspect facing a north-northeast direction—typically, the coolest and wettest orientation in this

landscape—and a value of ‘1’ for the hotter, drier south-southwesterly slopes [4.1]. That measure, called Topographic Solar Radiation Aspect Index (TRASP) (Roberts and Cooper, 1989), is calculated:

$$TRASP = [1 - \cos((\pi/180) \times (a - 30))]/2 \quad \text{(Equation 4.1)}$$

where a is aspect in degrees. If there was no aspect (flat area = ‘-1’), then the value of TRASP was set to 0.5. In addition, we reclassified elevation into six classes (<1800 m, 1800–2400 m, 2400–2900 m, 2900–3400 m, 3400–4000 m, and >4000 m).

4.3.2. Oscillation data

Following de Beurs et al. (2018), we examined standardized anomaly time series of five climate oscillation indices to capture two regional (SCAND, EAWR) and three global (NAO, AMO, MEI) patterns that were found important in Central Asia.

SCAND The Scandinavia (SCAND) regional pattern, also known as Eurasia-1 (Barnston and Livezey, 1987), consists of a primary circulation center over Scandinavia with weaker centers of the opposite sign over western Europe and eastern Russia/western Mongolia. The positive phase of SCAND is associated with positive 500-hPa geopotential height anomalies sometimes reflecting anticyclones (a weather system with high atmospheric pressure in the center) over Scandinavia and western Russia. Geopotential heights approximate the actual height of a pressure surface above mean sea-level. Colder air masses have lower heights; warmer air masses have higher heights. Positive phase of SCAND is linked to below-average temperatures across central Russia and western Europe, and also associated with above-average precipitation across central and southern

Europe, but below-average precipitation across Scandinavia (Barnston and Livezey, 1987; CPC-NOAA, 2019; Liu et al., 2014).

EAWR The East Atlantic/West Russia (EAWR) pattern aka Eurasia-2 (Barnston and Livezey, 1987) consists of four main anomaly centers. The positive phase is associated with positive 500-hPa geopotential height anomalies located over Europe and northern China, and negative 500-hPa geopotential height anomalies located over central North Atlantic and north of the Caspian Sea (40°-50°N, 50°-60°E). The positive phase of EAWR exhibits above-average temperatures over eastern Asia and below-average temperatures over large portions of western Russia and northeastern Africa, as well as above-average precipitation in eastern China and below-average precipitation across central Europe (Barnston and Livezey, 1987; CPC-NOAA, 2019; Liu et al., 2014).

NAO The North Atlantic Oscillation (NAO) consists of a north-south dipole of anomalies, with one center located over Greenland and the other center of opposite sign spanning the central latitudes of the North Atlantic between 35°N and 40°N (centered on the Azores). The positive phase of the NAO indicates below-average 500-hPa geopotential height and surface pressure across the high latitudes of the North Atlantic and above-average heights and pressure over the central North Atlantic, eastern United States, and western Europe. Together they generate a larger-than-average meridional pressure gradient, causing stronger-than-average midlatitude surface westerlies across the Atlantic onto Europe (Wang et al., 2004). Strong positive phases of the NAO tend to produce above-average temperatures in the eastern United States and across northern Europe, and below-average temperatures in Greenland as well as across southern Europe and the Middle East. They are also associated with above-average precipitation over northern Europe and

Scandinavia during the winter, and below-average precipitation over southern and central Europe (Hurrell et al., 2003; National Weather Service, 2019; Wang et al., 2004).

AMO The Atlantic Multi-Decadal Oscillation (AMO) is a series of long-duration changes in the sea surface temperature of the North Atlantic, composed of alternating cool and warm phases that may last for 20-40 years at a time. In general, during positive AMO phases, sea surface temperature (SST) is anomalously warm over most of the North Atlantic ocean, low pressure extends over the Atlantic between 20°S-50°N, wind speeds are reduced over the tropical Atlantic, and precipitation is enhanced in the eastern tropical Atlantic (Alexander et al., 2014; Kerr, 2000).

MEI Multivariate ENSO Index (MEI) describes the status of the El Niño/Southern Oscillation. It combines five oceanic and atmospheric variables: sea level pressure (SLP), sea surface temperature (SST), zonal and meridional components of surface winds, and outgoing longwave radiation (OLR) over the tropical Pacific basin (30°S-30°N, 100°E-70°W). Anomalously positive MEI events (El Niño) include (1) anomalously warm SSTs across the east-central equatorial Pacific, (2) anomalously high SLP over Indonesia and the western tropical Pacific and low SLP over the eastern tropical Pacific, (3) reduction or even reversal of tropical Pacific easterly winds (trade winds), (4) suppressed tropical convection (positive OLR anomalies) over Indonesia and Western Pacific and enhanced convection (negative OLR anomalies) over the central Pacific (ERL-NOAA, 2019; Kobayashi et al., 2015; Wolter and Timlin, 2011, 1993). During anomalously negative phases (La Niña), roughly opposite conditions occur.

From the National Oceanographic and Atmospheric Administration (NOAA) Climate Prediction Center (https://www.cpc.ncep.noaa.gov/data/teledoc/teleindcalc.shtml), we

obtained monthly values of SCAND, EAWR, and NAO from 2000 through 2017. From the NOAA Earth Research Laboratory, we downloaded for 2000 through 2017, monthly AMO values (https://www.esrl.noaa.gov/psd/data/timeseries/AMO/) and bimonthly MEI values (https://www.esrl.noaa.gov/psd/enso/mei.old/table.html). Each index was then summarized into seasonal average value of standardized anomaly for winter (DJF), spring (MAM), and summer (JJA). In our study, we did not include the autumn season (SON), following de Beurs et al. (2018). Based on Tables 3 and 4 in de Beurs et al. (2018), we selected those nine of 15 seasonal indices (five oscillation indices × three seasons) that exhibited significant (p-value< 0.1) Spearman correlations with the Peak Height phenometric or seasonal (spring or summer) precipitation or temperature across at least 10% of Central Asia (Table 4.1). Figure 4.2 presents seasonal oscillation annual values of these selected indices.

Table 4.1. Oscillation indices shown in de Beurs et al. (2018) to be significant at p-value < 0.1 across at least 10% of Central Asia area, and the direction of their Spearman correlations with the Peak Height phenometric and with spring or summer precipitation or temperature. **Pos is positive**, Neg is negative, *ns is not significant*, and — is not selected.

Index	**Season**	**PH**	**Precipitation**		**Temperature**	
			MAM	**JJA**	**MAM**	**JJA**
SCAND	DJF	neg	neg	*ns*	*ns*	*ns*
SCAND	MAM	**pos**	**pos**	**pos**	*ns*	neg
SCAND	JJA	neg	—	neg	—	*ns*
EAWR	DJF	**pos**	*ns*	*ns*	*ns*	neg
AMO	DJF	**pos**	**pos**	**pos**	*ns*	*ns*
AMO	JJA	neg	—	*ns*	—	**pos**
NAO	JJA	**pos**	—	neg	—	neg
MEI	DJF	**pos**	**pos**	**pos**	*ns*	*ns*
MEI	MAM	**pos**	**pos**	*ns*	*ns*	*ns*

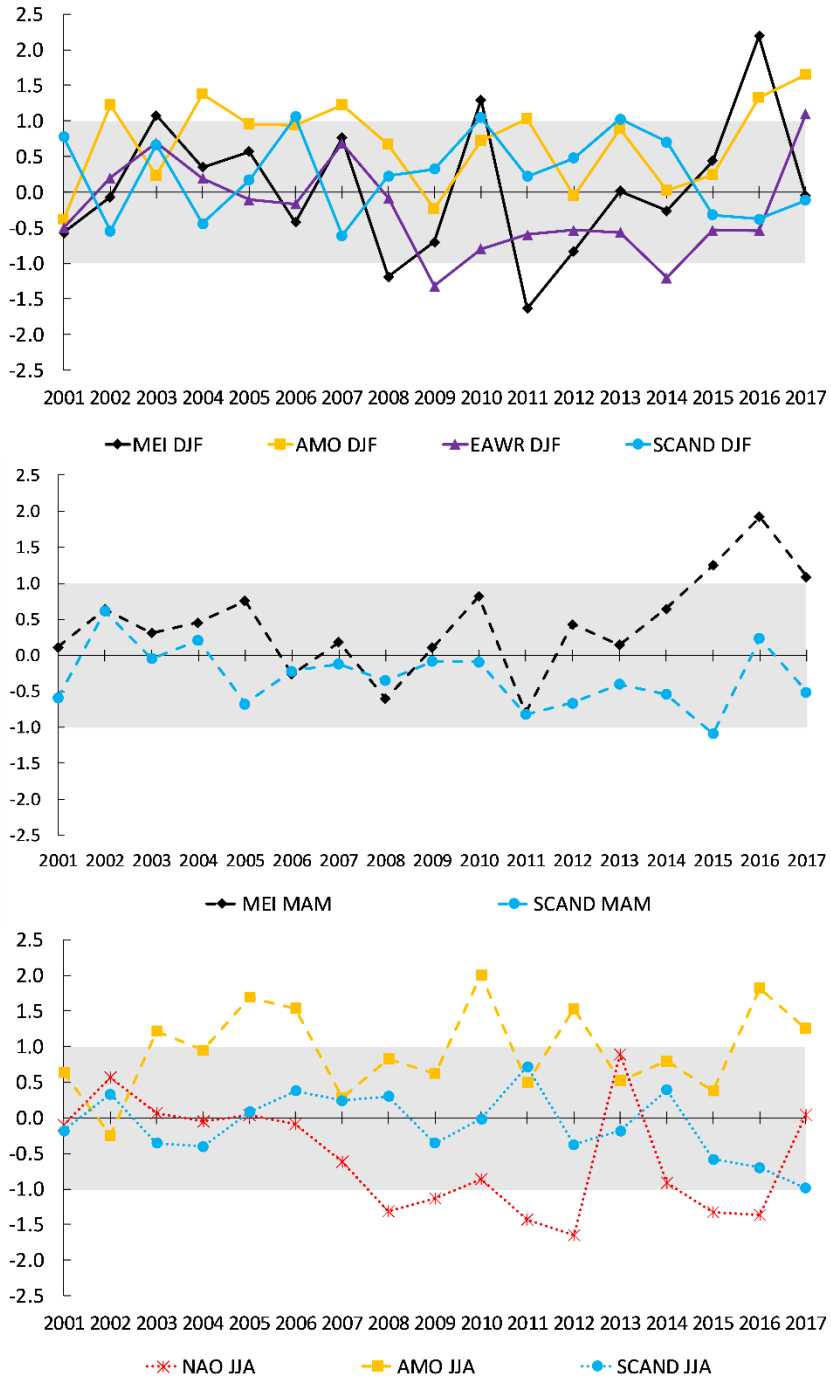

Figure 4.2. Annual seasonal values of selected indices. Upper left: December to February; upper right: March to May; bottom: June to August. Values reflect standardized anomalies of variables used for indices calculation; values between -1 to 1 on grey background. Positive values indicate a positive phase; negative values indicate a negative phase.

4.4. Methods

The approaches to generate land surface phenology metrics and snow cover seasonality metrics has been detailed elsewhere (Tomaszewska et al., 2019; Tomaszewska and Henebry, 2018; *cf.* Chapter 2 & 3). Here, we provide a general but concise description of those techniques.

4.4.1. Snow cover seasonality metrics

We defined the snow observation period from day of year (DOY) 169—approximately the summer solstice and aligns with MODIS composite dates—and extends to DOY 168 in the following year (i.e., $DOY169_{year}$ through $DOY168_{year+1}$). For each snow observation period, we calculated four temporal metrics: the First Date of Snow (FDoS) as the first composite during the snow observation period in which snow cover is detected; the Last Date of Snow (LDoS) as the last composite during the snow observation period in which snow cover is detected; the Duration of Snow Season (DoSS) as the timespan between the FDoS and LDoS; and the number of Snow-Covered Dates (SCD) as the number of times snow cover was detected within the snow season. Further, we multiplied the number of composites with snow detected by 8 since the compositing period is composed of 8 days, although we realize that this count may be an overestimate. For this study, we have focused only on SCD and LDoS since they have shown stronger relationships with the phenometrics (Tomaszewska et al., 2019; *cf.* Chapter 3).

4.4.2. Land Surface Phenology

To characterize land surface phenology, we used a downward-arching convex quadratic (CxQ) function (de Beurs and Henebry, 2004; Henebry and de Beurs, 2013) that captures

well the seasonal course of insolation at the middle to higher latitudes (de Beurs and Henebry, 2004; Henebry and de Beurs, 2013; Krehbiel et al., 2017; Krehbiel and Henebry, 2016; Nguyen et al., 2018). The model used Landsat surface reflectance data to calculate the NDVI as a proxy for active green vegetation and MODIS LST to calculate accumulated growing degree-days (AGDD) as a proxy for insolation. Land surface temperature during the growing season is highly correlated with insolation in extratropical regions, and grassland plants experience the thermal environment close to the ground (Henebry, 2013; Still et al., 2014). First, we calculated the mean MODIS LST of two daytime and nighttime observations from Terra and Aqua into mean MODIS LST based on [4.2]:

$$\text{mean LST} = [\max(\text{LST@1030}, \text{LST@1330}) + \min(\text{LST@2230}, \text{LST@0130})]/2 \quad \text{(Equation 4.2)}$$

We further filtered out mean MODIS LST below 0°C and calculated the growing degree-days GDD [4.3] at compositing period t as the maximum of mean LST and T_{base}, which was set to 0 °C (Goodin and Henebry, 1997; Henebry and de Beurs, 2013). Next, we multiplied by 8 each of 46 GDD composites to account for the 8-day compositing period of the MODIS product and accumulated them across the year [4.4]. AGDD was set to zero at the start of each year. These steps generated 17 annual time series of AGDD in °C.

$$GDD_t = \max((\text{mean } LST_t - T_{base}), 0) \quad \text{(Equation 4.3)}$$

$$AGDD_t = AGDD_{t-1} + (GDD_t \times 8) \quad \text{(Equation 4.4)}$$

Having prepared the AGDD and NDVI, we proceeded to model LSP at each pixel and for each year from 2001 to 2017 as a quadratic function shown in [4.5]:

$$NDVI = \alpha + \beta \times AGDD + \gamma \times AGDD^2 \quad \text{(Equation 4.5)}$$

For each pixel in the study area, we used the fitted parameter coefficients—intercept (α), slope (β), and quadratic (γ)—to calculate two LSP metrics (or phenometrics): Peak Height [PH = $\alpha - (\beta^2/4\gamma)$], the maximum modeled NDVI; and Thermal Time to Peak [TTP = $-\beta/2\gamma$], the quantity of AGDD required to reach PH, corresponds to duration of modeled green–up phase In the model fitting process, we used set of quality criteria and iterative data filtering to obtain optimal model fits (Tomaszewska et al., 2019). We accepted the fitted model only when it passed all six of the following criteria: (i) the quadratic parameter (γ) was less than 0; (ii) the TTP greater than the AGDD of the first observation; (iii) the adjusted R^2 greater than 0.7; (iv) the Root Mean Square Difference (RMSD) less than 0.08; (v) the PH below 1.0; and (vi) at least three observations were distributed before and at least three after the PH.

If any criterion was not fulfilled during the fitting, then the last observation was removed from the dataset, and the model fitting was rerun over the filtered dataset. We then summarized each annual fit by a binary variable (i.e., 0=no fit, 1=fit) to generate a final map of the total number of years with successful fits for each pixel. We then arbitrarily divided the modeling results into three groups based on the data distribution: (i) Highly Persistent (HP) pastures with 11-17 years of successful fits out of 17 years of observations, (ii) Persistent (P) pastures with 5-10 years, and (iii) Rarely Available (RA) pastures with just 1-4 years of successful fits. Here, we focused only on Highly Persistent (HP) and Persistent (P) pastures (Figure 4.3, Table 4.2).

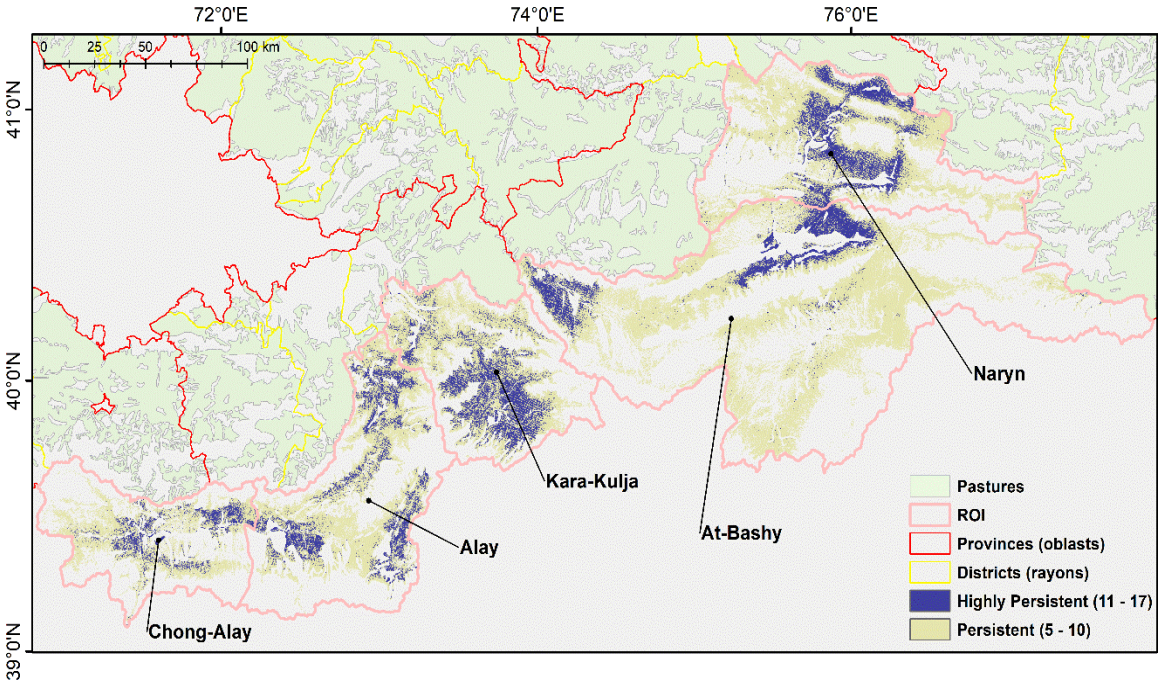

Figure 4.3. Study area: all pasturelands in Kyrgyzstan displayed in light green (from Asian Development Bank, 2010a, 2010b), selected rayons of interest (ROI) are labelled, and marked in light pink. In dark purple are pixels from Highly Persistent (HP) pastures, in yellow Persistent (P) pastures. Other pasture classes and land uses within the ROIs not shown.

Table 4.2. Combined area of HP and P pastures (km^2) within each rayon.

HP + P Elevation Class	Chong-Alay	Alay	Kara-Kulja	At-Bashy	Naryn	TOTAL
< 1800 m	–	100	241	–	4	345
1800-2400 m	45	605	845	381	628	2,504
2400-2900 m	522	529	968	898	1,352	4,269
2900-3400 m	743	1,166	844	2,743	1,548	7,044
3400-4000 m	354	839	212	2,505	230	4,140
> 4000 m	9	4	<1	5	–	18
TOTAL	1,674	3,243	3,108	6,532	3,763	18,320

Because of the limited or absent area of pastures below 1800 m and above 4000 m in some rayons, we restricted our focus to pixels located in the four elevation classes between 1800 m and 4000 m, which constitutes more than 98% (17,957km^2) of the pasture area pixels across the five rayons.

4.4.3. Spearman's Rank Correlation Analysis

We analyzed the connections between variables using the non-parametric Spearman's correlation coefficients to assess the geographical differentiation of land surface phenology metrics in response to environmental variables. Spearman's rank correlation method assesses whether a monotonic relationship exists, it works for data showing non-normality, and is robust against outliers (Fieller et al., 1957; Lehmann and D'Abrera, 2006).

4.4.4. Partial Least Squares Regression Modeling

4.4.4.1. Partial Least Squares Regression

To analyze how much of variation in land surface phenology metrics can be added to its explanation by the climate oscillation patterns at the scale of mountain pastures, we used the Partial Least Squares (PLS) regression model (Wold, 1966). PLS aims to predict Y variables—in our case, the phenometrics PH and TTP—from X variables (snow cover seasonality metrics, climate oscillation mode standardized anomalies, and terrain variables) and describe their common structure (Geladi and Kowalski, 1986; Wold et al., 2001). It is a technique that generalizes and combines features from principal component analysis (PCA) and multiple linear regression (MLR) (Abdi, 2003). Multiple linear regression aims to minimize sample response prediction error by seeking a linear function of the X variables that explains the variation in response Y; it works well when the X variables are relatively few and mutually uncorrelated. To eliminate the problem of high intercorrelation between variables X (multicollinearity), one of many approaches is a principal component regression, which performs PCA on the X matrix. This statistical procedure uses an orthogonal transformation to find new variables, called principal components, that are linear functions of those in the original dataset, which successively

maximize variance and are uncorrelated with each other (Jolliffe and Cadima, 2016; Wold, 1987). Further, PCA approach uses the principal components of X as predictors on response Y. However, this method does not solve the problem of finding an optimal subset of predictors X, because they are chosen to explain X rather than Y. Hence, it does not assure that the principal components that "explain" X are relevant for Y (Abdi, 2003). Therefore, a combination of MLR and PCA seeks to solve that problem.

PLS regression finds components from X that are also relevant for Y. Because correlation has been shown to exist between seasonal oscillations (de Beurs et al., 2018) and between snow metrics—since SCD is determined based on LDoS (Tomaszewska et al., 2019; Tomaszewska and Henebry, 2018), we decided that PLS regression would be a beneficial approach. Specifically, PLS searches for a set of components (also called latent vectors) that performs a simultaneous decomposition of X and Y with the constraint that these components explain as much of the covariance between X and Y as possible (Abdi, 2003). That step generalizes the PCA approach and is followed by a regression step where the decomposition of X is used to predict Y (Abdi, 2003; Wold et al., 2001). However, PLS has no implementation for variable selection, since it aims to find a relevant linear subspace of the predictor variables X, not the variables themselves (Mehmood et al., 2012). In other words, when the dominant source of variation is not related to Y, the maximization of the explained X variance is likely to bring irrelevant information into the PLS model (Tran et al., 2014).

Variable selection methods help to select a small set of highly relevant predictor variables X that are correlated to the response variable Y. Hence, variable selection can improve the estimation accuracy by effectively identifying the subset of important predictors and can

enhance the model interpretability (Farrés et al., 2015). Here, we based our study on three widely used methods for variable selection to investigate which of the X variables (snow cover seasonality metrics, standardized anomalies of climate oscillation modes, and terrain features) have more significant impact on predicting the phenometrics PH and TTP.

4.4.4.2. Variable Selection Methods for PLS Modeling

The first variable selection method is called "variable influence on projection" or "variable importance in projection" (Wold et al., 1993) usually abbreviated as VIP. The VIP score is a combined measure of how much a variable X contributes to describe the two sets of data: the response variable Y and the predictor variables X. It reflects not only the covariance between X and Y variables but also describes how important that information is for the model of the X variables. The average of the square VIP scores equals to unity, so that value is generally accepted as a threshold value (Andersen and Bro, 2010; Chong and Jun, 2005; Farrés et al., 2015; Mehmood et al., 2012; Rajalahti et al., 2009a; Tran et al., 2014), and we used it here as well.

The second method called the "Selectivity Ratio" (SR) is calculated as the ratio of explained variance to residual variance of X variables on the Y target-projected component. In other words, the method ranks the X variables in relation to their explanation of Y variance. An F-test has been proposed to define the threshold value (Rajalahti et al., 2009b). In order to determine which variable has a high discriminatory ability and to reject the null hypothesis (that explained and residual variances are the same), the calculated F value (F_{calc}), which is equal to SR of variable, has to exceed the critical value for the F distribution, (F_{crit}) = F(1-α, N-2, N-3), where α is the significance level, and N is sample size. The number of degrees of freedom for the numerator (i.e., explained variance) is equal

to sample size N minus two degrees of freedom, one because of the calculation of the variable's mean and one because of the introduction of the target-projected component. For the denominator (i.e., residual variance), one additional degree of freedom is lost when the explained variance is subtracted from the original variance of the variable (Farrés et al., 2015; Rajalahti et al., 2009b). Another approach is to set a limit based on explained variance, e.g., for 75% of explained variance, the cut-off value is 3, i.e., 75% of explained to 25% of unexplained variance (Rajalahti et al., 2009a).

The third method of variable selection is to use the classical technique of statistical significance testing that aims to eliminate variables for which the regression coefficient (β) (a single measure of association between each variable X and the response Y) is not significant. To determine significant coefficients, bootstrapping or jackknifing methods (Efron and Tibshirani, 1993; Faber, 2002) are often used (Andersen and Bro, 2010; Mehmood et al., 2012). Based on that method, variables that are not significant at a chosen significance level might be excluded from the model. Additionally, Rajalahti et al. (2009a) propose to use a rule of ±2 standard deviations calculated from the spread of all regression coefficients (if the X variables have the same units). Variables that are within this range can be also excluded.

We employed all three variable selection methods because each of them conveys a bit different information about the variables and the model, and so those methods are expected to yield slightly different results due to the data characteristics (Farrés et al., 2015).

To conduct PLS regression and variable selection, we used mdatool package v. 0.9.6 in R (Kucheryavski, 2019).

4.4.4.3. Sampling and Variables Preparation for PLS Modeling

First, we merged HP and P pasture masks into one, and cropped it based on the area of each rayon. For each rayon, we randomly selected 400 pixels for each of the four elevation classes (1600 pixels in total) to create a new elevation-based mask. Using each elevational-based mask, we extracted pixels from PH, TTP, LDoS, and SCD for each year (17 in total). Further, we removed pixels with unsuccessful CxQ fits (that yielded no values for PH and TTP), to create a complete dataset. We repeated that procedure four times, once for each elevation class. Then, we divided the datasets into modelling (70%) and testing (30%) subsets (Table 4.3). Finally, we combined each elevational-based modelling and testing datasets to construct the final datasets, so elevation would serve as a variable X for prediction.

Table 4.3. Number of pixels for modelling and testing (split 70:30) over 17 years within each of five studied rayons based on elevation class. **In bold, number of pixels used for modeling**.

Elevation class	**Chong-Alay**		**Alay**		**Kara-Kulja**		**At-Bashy**		**Naryn**	
	Model	*Test*	*Model*	*Test*	*Model*	*Test*	*Model*	*Test*	*Model*	*Test*
1800 – 2400 m	**2,508**	836	**2,960**	986	**2,734**	911	**2,899**	966	**2,608**	869
2400 – 2900 m	**2,526**	842	**2,489**	829	**2,962**	987	**3,006**	1,002	**2,848**	949
2900 – 3400 m	**2,453**	817	**2,647**	882	**2,691**	897	**2,196**	732	**2,524**	841
3400 – 4000 m	**2,301**	766	**2,457**	819	**2,322**	774	**1,968**	656	**2,064**	688
TOTAL	**9,788**	3,261	**10,553**	3,516	**10,709**	3569	**10,069**	3,356	**10,044**	3,347

We used 14 metrics as predictor variables X: elevation (m), slope (in degrees), TRASP index (linearized aspect), LDoS, SCD, and the z-scores for each of the following seasonal climate oscillation modes, SCAND DJF, SCAND MAM, SCAND JJA, EAWR DJF, AMO DJF, AMO JJA, NAO JJA, MEI DJF, and MEI MAM.

The PLS regression models were run on standardized data using auto-scaling approach: (1) each variable is scaled to unit variance by dividing them by their standard deviations, and (2) centered by subtracting their averages (Wold et al., 2001), although the final estimated regression coefficients are provided in the original values (Table S4.1-S4.2). We modeled the PH and TTP response variables separately.

Prior to run PLS regression modelling, for each rayon separately, we estimated the association of variables Y and X using Spearman's rank correlation method.

4.4.4.4. PLS Regression Sequence

The modeling for each phenometric was carried out in four steps: (1) build the initial model using all variables, (2) select fewer but significantly important variables, (3) build three reduced models based on the different variables selected, and (4) compare the results. This procedure was run separately for the two phenometrics in each of five rayons.

It was essential to determine in step one of modeling, the appropriate model complexity to avoid "over-fitting" that would limit generality. The cross-validation (CV) method is a standard procedure to determine a number of significant components (Wold, 1982; Wold et al., 2001, 1984). During CV part, after developing a model, differences between actual and predicted Y-values are calculated for the withheld data. The sum of squares of these differences is computed and collected from all the parallel models to form the predictive residual sum of squares (PRESS), which estimates the predictive ability of the model (Bulut and Alma, 2012; Wold et al., 2001). Then, we applied Wold's R criterion to find the optimal number of significant components based on the specific threshold (0.95) for

the ratio of PRESS values between two consecutive components (Abdi, 2003; Bulut and Alma, 2012; Tenenhaus, 1998; Wold et al., 1993).

We used three variable selectors: VIP score with '1' as the threshold; Selectivity Ratio (SR) with '1.5' as threshold (ratio of 60% variance explained to 40% of unexplained variance), and 'regression coefficients' method using p-value < 0.05 obtained from jack-knifing and plus or minus one standard deviation—from the mean of all standardized (using auto-scaling) regression coefficients—a slightly less conservative approach compared to Rajalahti et al., (2009a) in the case of cut-offs for the Selectivity Ratio and standard deviation.

4.5. Results

4.5.1. Spearman's Rank Correlation

Figures 4.4, 4.5, and S4.1-S4.3 show a matrix of Spearman's rho coefficients for the X variables (PH and TTP) and the Y variables (two snow cover seasonality metrics, three terrain characteristics, and nine seasonal oscillations) calculated based on the final training (model) dataset for each rayon across elevation classes. Figure 4 shows the matrix for Chong-Alay, the most southwestern of the five rayons and Figure 5 shows the correlation matrix for Naryn, the most northeastern rayon (Alay, Kara-Kulja, and At-Bashy appear as Figures S1-S3, respectively).

Peak Height (PH) was effectively decoupled from Thermal Time to Peak (TTP), exhibiting weakly positive correlation in Chong-Alay (Figure 4.4), Alay (Figure S4.1), and At-Bashy (Figure S4.3), weakly negative in Kara-Kulja (Figure S4.2), and modestly negative in Naryn (Figure 4.5). In Naryn rayon, PH showed a moderate positive relationship with both

LDoS and SCD (Figure 4.5), but not in any other rayon. PH also exhibited moderate negative relationships with elevation, except in Naryn, where it was moderately positive. Slope was weakly related to PH, except in Alay where it showed a moderate positive relationship (Figure S4.1). The pattern between PH and TRASP provided a consistent signal across rayons: weak to moderate negative correlation, meaning higher PH on northern and eastern slopes. With respect to the seasonal oscillation indices, there were two patterns consistent across the rayons: weak negative correlation with SCAND JJA and weak positive correlation with MEI MAM. TTP showed consistently strong to very strong negative relationships with LDoS, SCD, and elevation The relationship of TTP with slope was moderately negative except in Alay, where it was weakly positive. TTP showed weak positive correlations with EAWR DJF, AMO DJF, and MEI DJF in the western rayons.

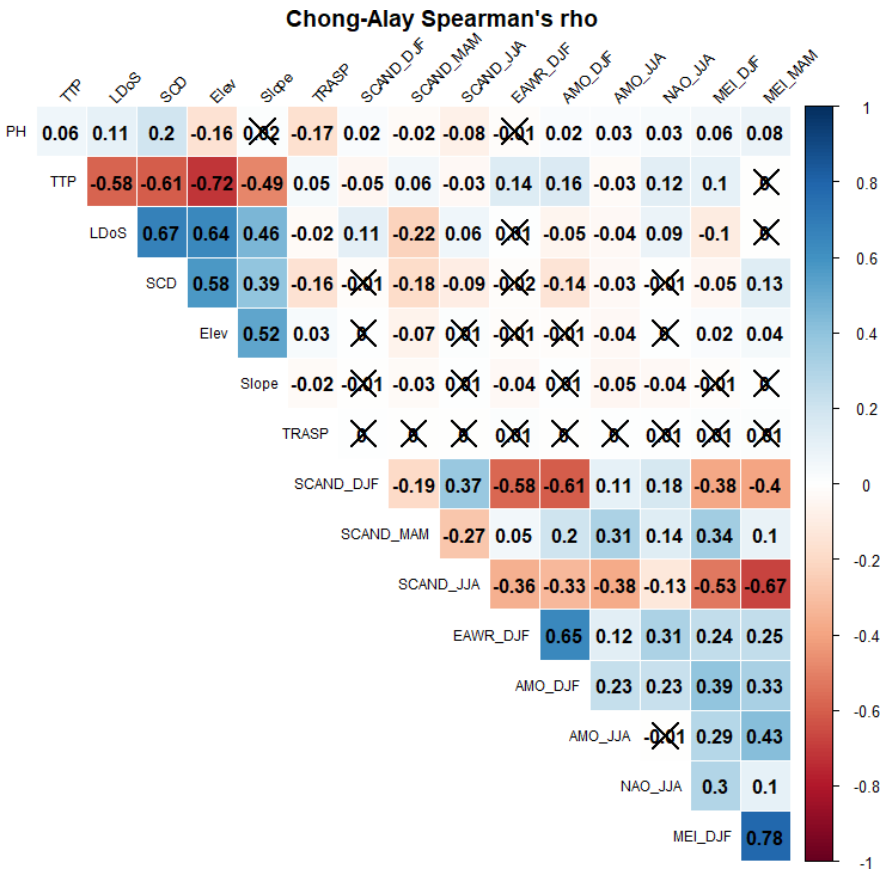

Figure 4.4. Spearman's rho coefficient of correlation for Chong–Alay rayon. Significant level at p-value < 0.05 Correlation coefficients with p > 0.05 are crossed out. In reds, negative values of rho; in blues, positive values.

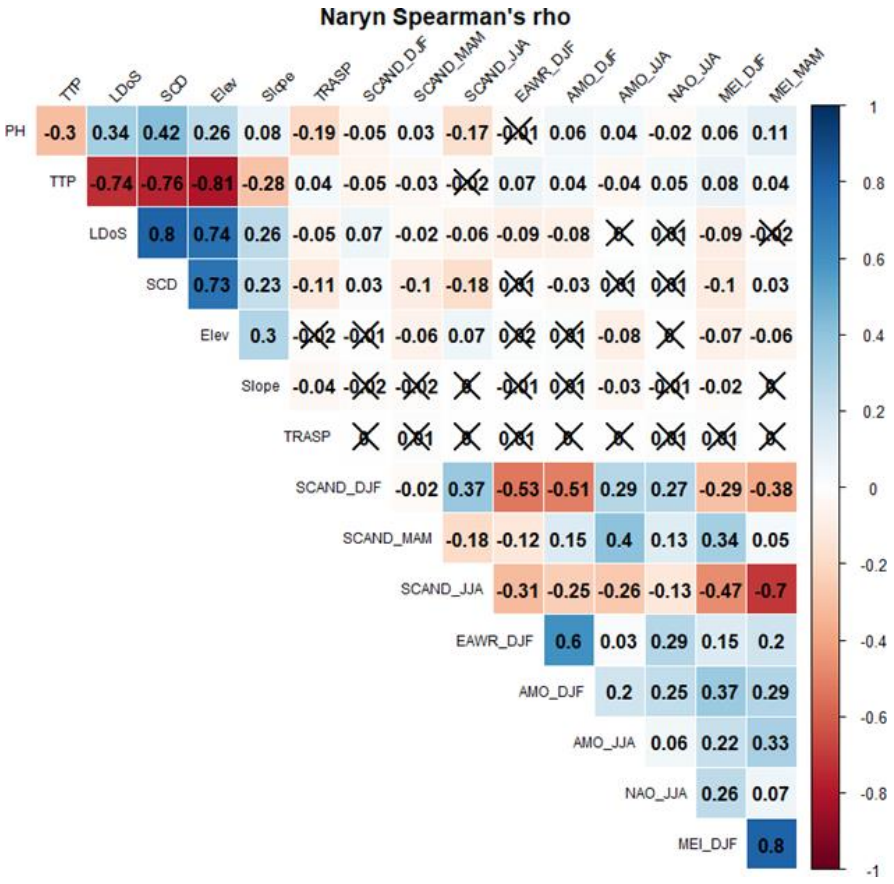

Figure 4.5. Spearman's rho coefficient of correlation for Naryn rayon. Significant level at p-value < 0.05 Correlation coefficients with p > 0.05 are crossed out. In reds, negative values of rho; in blues, positive values.

The snow cover seasonality metrics were positively correlated, as expected given that LDoS was used in the determination of SCD. Both snow cover metrics also showed strong positive relationships with elevation and moderate positive relationships with slope (except in Alay, where slope is weakly negative). Relationships with TRASP were weakly negative with SCD (except in At-Bashy were it was not significant) meaning that snow cover stayed

longer on northern aspects. For the seasonal climatic oscillation indices, there were weakly negative relationships for both LDoS and SCD with SCAND MAM and AMO DJF (except in At-Bashy and Kara-Kulja) and with SCD only for SCAND JJA in the western rayons of Chong-Alay and Alay.

An interesting feature of each of the correlation matrices was the prevalence of moderately strong to strong positive and negative correlations between the seasonal oscillation mode values. While some of these correlations were not surprising, such as between subsequent seasons of the same oscillation mode index, there were also strong connections—both positive and negative—across different oscillation modes, and their values were not identical across rayons. Note that what is displayed in the correlation matrices constitutes random sample of those pixels that were successful fitted by the CxQ LSP model for some number of years. Thus, each rayon sample was a spatially and temporally random subset of those pixels within the population of pasture land use that were successfully fitted by with the LSP models. In other words, the correlations between seasonal oscillation modes have been "filtered" by a biased spatio-temporal sample within each rayon based on the pixels showing years of good pasture growth.

Table 4.4 displays the effects of this filtering. The reference correlations are those reported in Table 1 of de Beurs et al. (2018). There was some slight variation in correlation strength across rayons, but all these correlations were significant, even when the reference correlation is not, e.g., SCAND DJF and MEI DJF. Indeed, an effect of the filtering appeared to enhance the signal to noise ratio between the oscillation mode pairs.

Table 4.4. Spearman correlations between selected pairs of seasonal oscillation modes. The reference correlation is from de Beurs et al. (2018). Rayon specific correlations are extracted from Figures 4.4, 4.5, and S4.1-S4.3. Superscripts after reference correlations: ns= p>0.10; ◊ = p<0.10; * = p<0.05. All rayon specific correlations are significant at p<0.05.

Oscillation Mode Pair	Reference Correlation	Chong-Alay	Alay	Kara-Kulja	At-Bashy	Naryn
SCAND DJF + EAWR DJF	-0.43◊	-0.58	-0.58	-0.56	-0.54	-0.53
SCAND DJF + AMO DJF	-0.59*	-0.61	-0.56	-0.55	-0.55	-0.51
SCAND DJF + MEI DJF	-0.20ns	-0.38	-0.32	-0.32	-0.34	-0.29
SCAND DJF + MEI MAM	-0.27ns	-0.40	-0.42	-0.39	-0.38	-0.38
SCAND JJA + MEI MAM	-0.46◊	-0.67	-0.69	-0.68	-0.69	-0.70
EAWR DJF + AMO DJF	+0.36ns	+0.65	+0.57	+0.57	+0.61	+0.60

4.5.2. Partial Least Squares Regression

Table 4.5 shows the results of PLS modelling of TTP using R^2 and RMSE based on the testing datasets (30% of the randomly selected pixels and not used for modeling), and the number of components used in the PLS model. In general, the differences between models were small, R^2 ranged from 0.56 to 0.71 across rayons using the initial model. When variable selection methods were applied, it resulted in marginal decreases in R^2 and increases in RMSE. In two instances the variable selection methods yielded the same model: in Alay, SR and RC generated the same model; while in Kara-Kulja, all three variable selection methods resulted in the same outcome. The number of components varied between one and two depending on the rayon. The number of components changed in Alay and At-Bashy after application of variable selection.

Table 4.6 shows standardized regression coefficients of final models based on three different variable selection methods. Note that values are in decreasing order of coefficient strength. The strongest, elevation was the strongest negative effect on TTP over all methods and rayons, except in Kara-Kulja, where rank order of components is SCD, then LDoS and

elevation, all with nearly the same coefficient values. The second coefficient in the other rayons was SCD, generally followed by LDoS. The selectivity ratio method yielded no model with a climatic oscillation index showing any significant impact on TTP. While the RC selection approach indicated moderate to weak positive relationship with NAO JJA in Chong-Alay, At-Bashy, and Naryn. The VIP score pulled in a negligible weak correlation with AMO JJA in Alay and weak negative correlations with SCAND MAM in At-Bashy and Naryn.

Table 4.5. Comparison of TTP modelling performance using value of R^2 and Root Mean Square Error (RMSE) based on initial model without variable selection ("Initial"), and three models using different variable selection methods: VIP score ("VIP"), Selectivity Ratio ("SR"), and Regression Coefficients ("RC"). **Same models in bold**.

TTP by Rayon	**R^2**				**RMSE**				**No. of components**			
	Initial	**VIP**	**SR**	**RC**	**Initial**	**VIP**	**SR**	**RC**	**Initial**	**VIP**	**SR**	**RC**
Chong-Alay	0.57	0.56	0.55	0.57	252.4	257.1	259	252	2	2	2	2
Alay	0.66	0.64	0.64	0.64	190.6	197.4	197.9	197.9	2	1	1	1
Kara-Kulja	0.56	0.55	0.55	0.55	206.3	208.6	208.6	208.6	1	1	1	1
At-Bashy	0.71	0.70	0.70	0.67	202.6	206.5	205.5	214.7	2	2	2	1
Naryn	0.66	0.66	0.66	0.66	208.8	209.9	210.5	210.7	2	2	2	2

Table 4.6. Standardized (using auto-scaling) regression coefficients for TTP modelling for each rayon based on different variable selection methods. **Same models in bold.** *Positive values in underlined italics.*

VS	Chong-Alay		Alay		Kara-Kulja		At-Bashy		Naryn	
VIP score	Elev	-0.49	Elev	-0.30	**SCD**	**-0.28**	Elev	-0.49	Elev	-0.43
	SCD	-0.23	SCD	-0.30	**LDoS**	**-0.26**	SCD	-0.24	SCD	-0.26
	Slope	-0.09	LDoS	-0.26	**Elev**	**-0.26**	LDoS	-0.21	LDoS	-0.22
	LDoS	-0.06	AMO	-0.01			SCAND	-0.16	SCAND	-0.12
			JJA				MAM		MAM	
Selectivity Ratio	Elev	-0.53	**Elev**	**-.030**	**SCD**	**-0.28**	Elev	-0.59	Elev	-0.53
	SCD	-0.22	**SCD**	**-0.29**	**LDoS**	**-0.26**	SCD	-0.19	SCD	-0.22
	LDoS	-0.08	**LDoS**	**-0.26**	**Elev**	**-0.26**	LDoS	-0.14	LDoS	-0.15
Regression Coefficient	Elev	-0.42	**Elev**	**-0.30**	**SCD**	**-0.28**	Elev	-0.49	Elev	-0.45
	SCD	-0.24	**SCD**	**-0.29**	**LDoS**	**-0.26**	SCD	-0.41	SCD	-0.25
	NAO	*0.22*	**LDoS**	**-0.26**	**Elev**	**-0.26**	*NAO*	*0.02*	LDoS	-0.19
	JJA						*JJA*		*NAO*	*0.13*
	LDoS	-0.17							*JJA*	

For the PLS modeling of PH, Table 4.7 shows the performance results. In general, R^2 was very low not exceeding 0.2 except in Alay, where the initial model has R^2=0.34 and R^2=0.29 for reduced models using either VIP or RC for variable selection. Over the four rayons other than Naryn, the SR method did not indicate any variable to be significant; thus, no model was built. Differences in RMSE between initial and reduced models were negligible. Higher R^2 in Alay is related to the higher number of components selected (four components rather than one or two for other rayons) for the initial model. Although in the case of TTP modelling, a higher number of components did not really improve R^2, for PH in Alay and At-Bashy where there were two components used (after variable selection), the R^2 was much higher than in Chong-Alay, Kaka-Kulja and slightly higher in Naryn where only one component was selected.

Table 4.7. Comparison of PH modelling performance using value of R^2 and Root Mean Square Error (RMSE) based on: initial model without variable selection ("Initial"), and three models using different variable selection methods: VIP score ("VIP"), Selectivity Ratio ("SR"), and Regression Coefficients ("RC"), "—" no model built.

PH by Rayon	R^2				RMSE				No. of components			
	Initial	VIP	SR	RC	Initial	VIP	SR	RC	Initial	VIP	SR	RC
Chong-Alay	0.12	0.12	—	0.13	0.157	0.157	—	0.156	1	1	—	1
Alay	0.34	0.29	—	0.29	0.142	0.148	—	0.148	4	2	—	2
Kara-Kulja	0.16	0.12	—	0.14	0.149	0.153	—	0.151	2	1	—	1
At-Bashy	0.18	0.20	—	0.20	0.17	0.167	—	0.168	2	2	—	2
Naryn	0.17	0.16	0.16	0.17	0.149	0.150	0.150	0.149	1	1	2	1

Table 4.8 provides the standardized regression coefficients for the PH modelling. Across rayons, the strongest effects are elevation interchanging with SCD, except in Kara-Kulja where TRASP has a negative effect. Elevation negatively affects PH, except in Naryn where its value is positive; whereas, SCD (and LDoS, where selected) shows a positive influence. Slope does not appear in any reduced model. The VIP score method resulted models with negative influence of SCAND JJA in three rayons (Chong-Alay, Kara-Kulja, and At-Bashy) and positive influence of MEI MAM in Chong-Alay and in Kara-Kulja. The SR method selected significant variables only in Naryn: the two snow cover metrics. Note, that using only those two variables, the R^2 is comparable to other models for Naryn; moreover, the RMSE is slightly lower than in case of VIP score or RC models.

Table 4.8. Standardized (using auto-scaling) regression coefficients for PH modelling for each rayon based on different variable selection methods. *Positive values in underlined italics*.

VS	Chong-Alay		Alay		Kara-Kulja		At-Bashy		Naryn	
VIP score	Elev. *SCD* TRASP SCAND JJA *MEI* *MAM*	-0.18 *0.17* -0.16 -0.10 *0.10*	Elev. *LDoS* *SCD*	-0.86 *0.47* *0.19*	TRASP Elev. SCAND JJA *MEI* *MAM*	-0.20 -0.14 -0.12 *0.12*	*SCD* Elev. TRASP SCAND JJA	*0.46* -0.46 -0.19 -0.07	*SCD* *LDoS* *Elev.* TRASP	*0.17* *0.14* *0.11* -0.08
Selectivity Ratio	--		--		--		--		*SCD* *LDoS*	*0.39* *0.01*
Regression Coefficient	Elev. *SCD* TRASP SCAND JJA	-0.20 *0.21* -0.20 -0.12	Elev. *SCD*	-0.82 0.60	TRASP Elev. *MEI* *MAM* *SCD*	-0.26 -0.19 *0.16* *0.04*	*SCD* Elev. TRASP	*0.47* -0.46 -0.21	*SCD* *LDoS* *Elev.* TRASP SCAND JJA	0.17 0.14 0.11 -0.08 -0.07

4.6. Discussion

In this study, we sought to confirm the findings of de Beurs et al. (2018) regarding linkages between seasonal climate oscillation modes, regional weather, and land surface phenology in Central Asia. Specifically, we focused on the explanatory and predictive power of seasonal climatic oscillations on land surface phenology in highland pastures in Kyrgyzstan from 2001 to 2017. Our question was whether the impacts of oscillation anomalies are detectable and significant in these mountain pastures using LSP metrics based on much finer spatial resolution data. In order to build models that could describe PH and TTP, we included both snow cover seasonality metrics and terrain characteristics, which have already shown to influence on the land surface phenology of highland pastures (Tomaszewska et al., 2019; Chapter 3).

The very weak correlations of PH with TTP and PH with snow cover metrics may result in part from calculating the correlations by rayons and across elevation classes. Pasture area

in Kyrgyzstan is characterized by complex mountainous terrain that has led to spatially heterogeneous soils and vegetation communities blending into each other (Zhumanova et al., 2018). Thus, at different elevations belts, pasture vegetation types may vary in their NDVI response and their response to snow cover seasonality. For example, the southern part of Alay rayon is an extensive and flat valley bottom traversed by tributaries of the Kyzyl-Suu River, while the northern part is a combination of mountain ridges and intervening valleys along the Gulcha River. Furthermore, given the coarse (1 km) spatial resolution of MODIS LST product relative to the terrain, as a result, any effects of aspect and slope that may be evident at 30m were blurred across the complex topography at 1 km. The southwestern rayons of Chong-Alay and Alay showed weak positive relationships between TTP and winter values of EAWR and AMO, but these relationships dissipate moving eastward.

Figure 4.6 visualizes the mutual relationships among PH, TTP, and SCD by elevation class for Naryn rayon, and Table 4.9 reports the R^2 values of the simple linear fits illustrated in Figure 4.6 for each elevation class alone and considering all classes together. The amount of scatter within each elevation class is substantial, and the effects of elevation on TTP and SCD are clear from Figures 4.6B and 4.6C, respectively. The relatively tight negative relationship between TTP and SCD is not unexpected (Figure 4.6C), but note that the slope of the relationship across elevation classes is much steeper than the roughly parallel slopes for the four elevation classes. The relationships between PH and SCD are also notable in that the elevation classes between 2400 m and 3400 m exhibit similar steeper slopes; whereas, the other two classes 1800-2400 m and 3400-4000 m have similar shallower slopes (Figure 4.6B). The overall slope splits the difference, but the elevations between

2400 m and 3400 m comprise more than 77% of the pasture land use areas with successful LSP model fits (*cf.* Table 4.2). The relationships of PH and TTP show an unexpected positive relationship between 1800 m and 2400 m, but negative relationships at higher elevations. The overall slope is also negative with a slope comparable to 2400 m to 2900 m, but shallower than at the higher elevations (Figure 4.6A). The negative relationship between TTP and the number of snow cover days can be understood in terms of higher albedo associated with snow cover reducing the net radiation at the surface and limiting sensible heat flux. The positive relationship of PH with snow cover days arises from the dependence of the pastures on precipitation that falls outside of the growing season. Most of the annual precipitation falls during the winter and the meltwater from the accumulated snow provides the moisture for the beginning of the growing season. Also, the snowpack insulates the soil surface and retains moisture; thus, having a later snowmelt date, suggesting a larger snowpack, provides more soil moisture enabling greater plant growth (Groffman et al., 2001; Qiao and Wang, 2019).

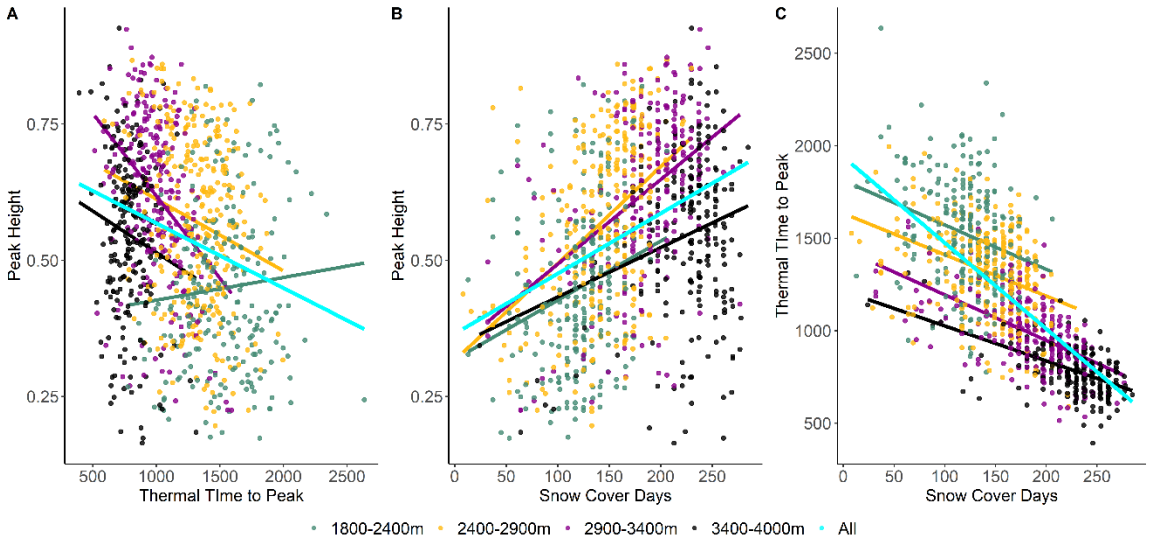

Figure 4.6. Randomly sampled 1000 pixels from modeling dataset over Naryn rayon. (A) PH vs TTP, (B) PH vs SCD, (C) TTP vs SCD. Colored circles and corresponding lines of slope show different elevation classes: in green 1800 – 2400 m, in orange 2400 – 2900 m, in magenta 2900 – 3400 m, in black 3400 – 4000 m. The cyan line show the slope across all pixels without stratification by elevation class.

Table 4.9. R^2 values of linear fits based on 1000 randomly sampled pixels that compose the modeling dataset for Naryn rayon.

Elevation class	PH x TTP	PH x SCD	TTP x SCD
1800-2400 m	0.006	0.061	0.075
2400-2900 m	0.039	0.201	0.139
2900-3400 m	0.146	0.211	0.332
3400-4000 m	0.018	0.051	0.281
1800-4000 m	0.067	0.138	0.517

Given these results, it would be fair to inquire why not model the phenometrics by elevation class. We had three reasons for the approach we took. First, any division of elevation into classes is arbitrary and we wanted to avoid developing "optimized classifications" for each rayon and, thus, increase the possibility of overfitting the data. Second, since terrain complexity is very high in each rayon resulting in variation in phenometrics (sometimes in counterintuitive ways) and so we expected to improve model performance by including a broad range of conditions, especially as TTP follows an elevational gradient. Third, our primary interest was to evaluate the impact of the climate oscillation indices on potentially increasing both explanatory and predictive power.

The PLS modeling of TTP showed that thermal time accumulation was modulated by elevation and snow cover metrics. Those variables alone produced models using SR variable selection that explained 55-70% of the observed variation in TTP (Table 6). Overall, variable selection brought almost no change in modeling performance; thus, the

reduction in variables eliminated those variables that had marginal explanatory and prediction power at the scale of mountainous pastures. VIP score and RC methods showed that specific seasonal oscillation indices could add to model performance, but the differences in R^2 and RMSE were negligible. Recall the VIP score reflects both the covariance between X and Y variables and the importance of each X variable for predicting Y. Therefore, while a variable may add explanatory power of the model itself, it does not necessarily improve the predictive power of the model.

VIP scores indicated that AMO JJA and SCAND MAM had significant negative relationships with TTP in Alay and in the two eastern rayons, respectively. According to de Beurs et al. (2018) AMO JJA showed positive Spearman's correlation with summer temperature. However, the standardized AMO JJA regression coefficient is minimal, and so that impact might be potentially overlooked in the modelling. In our findings SCAND MAM showed a stronger negative relationship with TTP, while in the reference paper, SCAND MAM exhibited a positive relationship with spring and summer precipitation and negative relationship with spring temperature. We may speculate that since high SCAND MAM values were associated with positive precipitation anomalies and negative temperature decreases during spring season (de Beurs et al., 2018), the TTP would decrease during these years with wetter springs.

The RC variable selection methods indicated only NAO JJA to be significant and have a positive regression coefficient with TTP (*cf.* Table 4.6); whereas, de Beurs et al., (2018) found a negative relationship with summer temperature (*cf.* Table 4.1). It is important to keep in mind that de Beurs et al. (2018) analyzed all five countries of Central Asia, and so

our findings for selected rayons in Kyrgyzstan might not have been captured in the broader scale analysis.

In terms of PH, the PLS models after variable selection were able to explain up to 29% of variability in PH. The SR approach, which emphasizes explaining variability in Y, indicated no significant variables X in every rayon other than Naryn where only snow cover metrics were significant. Using VIP score and RC, in the three western rayons, terrain features drove PH; whereas, in the two eastern rayons (At-Bashy and Naryn), the stronger effect appeared from snow cover metrics. It should be mentioned that PH may be influenced by abiotic factors (climate, terrain, recent weather), biotic influences (vegetation community, grazing pressure, unpalatable species), and disturbance history (time since landslide, time since grazing, time since drought) (Henebry, 2019, 2013). Thus, modeling PH is not as straightforward as TTP, which is influenced by temperature and moisture lapse rates.

Again, only two seasonal oscillations were selected as significant: SCAND JJA and MEI MAM. SCAND JJA, according to de Beurs et al. (2018), showed negative correlation with summer precipitation, meaning that more negative values of the index are associated with increased precipitation. In our results, SCAND JJA was shown to have a negative relationship with PH as well, meaning more precipitation would be linked with higher PH, likely resulting from more soil moisture. However, that effect may be only evident at particular elevation belts, since in alpine and subalpine areas, precipitation may not correlate with NDVI, probably because vegetation activity is limited by low temperatures (Zhumanova et al., 2018). MEI MAM was shown in de Beurs et al. (2018) to have a positive relationship with summer precipitation. Here we found a positive relationship

between MEI MAM with PH: higher MEI MAM index was linked to more summer precipitation and higher PH. Moreover, we can speculate that this increased summer precipitation could yield additional later season forage. Finally, SCAND JJA and MEI MAM were shown to be significantly negatively correlated (Table 4.4), which may explain why they were selected through different methods as significant influences on PH.

We also ran PLS modelling across all five rayons at two elevation classes: 2400-2900 m and 2900–3400 m. The results yielded that R^2 of TTP modelling dropped to ~0.27 and ~0.31 respectively (data not shown). The only significant variables, regardless of variable selection method, were snow cover metrics and slope. No seasonal oscillation index value appeared significant. In terms of PH, R^2 values were ~0.21 and ~0.27 for 2400-2900 m and 2900-3400 m, respectively (data not shown). For PH, snow cover metrics and terrain features (both slope and TRASP) were significant, but no climate oscillation index.

We posed in the introduction the question of whether the impacts of oscillation anomalies are detectable and significant in the mountain pastures using LSP metrics based on much finer spatial resolution data. Our results point to an answer of "no": at a finer spatial scale, the indirect effects of seasonal climatic oscillations are evidently overridden by terrain influences (mostly elevation) and snow cover timing. Although, while it is beyond the scope of this study, we note that changes in vegetation communities characteristics (Zhumanova et al., 2018) can result in high interannual variability in phenometrics, that in turn, may impede modeling of the linkages with oscillation modes. Moreover, the specific approach to phenometrics calculation might have introduced additional uncertainties in the analysis (Tomaszewska et al., 2019). Nevertheless, while at the fine spatial resolution of 30m, we have not detected the indirect impacts of climate oscillations, our results do not

mean that climatic teleconnections have no influence on shaping weather patterns in the region.

4.7. Conclusion

Although studies on much coarser scale show links between NDVI and climatic oscillation modes, and their strong influence on regional biomes (Dahlin and Ault, 2018), we did not find a significant effect at the local scale. Using much finer spatial resolution and limited spatial extent, we found overriding effects of terrain complexity, and snow cover metrics upon land surface phenology. Differences between coarser and finer spatial resolution observations increase over heterogeneous areas, and so that scale effect plays a significant role in modeling process (Liu et al., 2017; Zhang et al., 2017). Within the highland pasture land use areas of Kyrgyzstan, the heterogeneity of plant communities can be very high (Zhumanova et al., 2018) but appear homogeneous at the scale of even 30 m, which may influence land surface phenology in subtle ways. For instance, de Beurs et al., (2009) ran trend analyses of NDVI retrieved from two MODIS products at ~5.6 km and 500 m over Kazakhstan, and found that coarser scale analysis was relevant to atmospheric boundary layer processes, while the finer scale data revealed trends that were more relevant to human decision-making and regional economics. Similar cross-scale trend findings were reported using NDVI and EVI in the vegetated land surfaces of the Western Hemisphere (Heck et al., 2019).

We conclude the potential role of climatic oscillation indices informing outlooks for favorable pasture conditions in Kyrgyzstan is not feasible. One alternative approach might include focusing on those years with extreme climate oscillation values and analyze seasonal weather conditions over region to determine if those anomalies were transmitted

into the phenometrics. A second alternative would be to focus on those pixels that failed LSP modelling to investigate whether those failed fits resulted from unfavorable environmental conditions and climatic anomalies.

Whether climate oscillation mode indices can provide some new and useful information about growing season conditions remains a provocative question, particularly in light of the multiple environmental challenges facing the agropastoralism livelihood in montane Central Asia.

4.8. Acknowledgements

This research was supported, in part, by the NASA Land Cover / Land Use Change Program (NNX15AP81G) How Environmental Change in Central Asian Highlands Impacts High Elevation Communities. We appreciate the assistance and feedback from A.A. Aidaraliev, K. Kelgenbaeva, and P. Maatkarimov. We thank the two anonymous reviewers for their helpful feedback to improve the clarity of this manuscript.

4.9. References

Abdi, H., 2003. Partial least squares (PLS) regression, in: Lewis-Beck, M., Bryman, A., Futing, T. (Eds.), Encyclopedia of Social Sciences Research Methods. SAGE Publications.

Alexander, M.A., Halimeda Kilbourne, K., Nye, J.A., 2014. Climate variability during warm and cold phases of the Atlantic Multidecadal Oscillation (AMO) 1871–2008. J. Mar. Syst. 133, 14–26. https://doi.org/10.1016/J.JMARSYS.2013.07.017

Andersen, C.M., Bro, R., 2010. Variable selection in regression-a tutorial. J. Chemom. 24, 728–737. https://doi.org/10.1002/cem.1360

Asian Development Bank, 2010a. Central Asia Atlas of Natural Resource. Central Asian Countries Initiative for Land Management and Asian Development Bank, Manila, Philippines.

Asian Development Bank, 2010b. Central Asian Countries Initiative for Land Management (CACILM) Multicountry Partnership Framework Support Project [WWW Document]. URL https://www.adb.org/projects/38464-012/main

Azykova, E.K., 2002. Geographyical and landscape characteristics of mountain territories, in: Aidaraliev, A.A. (Ed.), Mountains of Kyrgyzstan. Technology, Bishkek.

Barlow, M., Cullen, H., Lyon, B., 2002. Drought in Central and Southwest Asia: La Niña, the Warm Pool, and Indian Ocean Precipitation. J. Clim. 15, 697–700. https://doi.org/10.1175/1520-0442(2002)015<0697:DICASA>2.0.CO;2

Barnston, A.G., Livezey, R.E., 1987. Classification, Seasonality and Persistence of Low-Frequency Atmospheric Circulation Patterns. Mon. Weather Rev. https://doi.org/10.1175/1520-0493

Bjerksen, J., 1969. Atmospheric teleconnections from the equatorial pacific. Mon. Weather Rev. 97, 163–172. https://doi.org/10.1175/1520-0493(1969)097<0163:ATFTEP>2.3.CO;2

Böhner, J., 2006. General climatic controls and topoclimatic variations in Central and High Asia. Boreas 35, 279–295. https://doi.org/10.1111/j.1502-3885.2006.tb01158.x

Bohovic, R., Dobrovolny, P., Klein, D., 2016. The Spatial and Temporal Dynamics of Remotely-sensed Vegetation Phenology in Central Asia in the 1982–2011 Period. Eur. J. Remote Sens. 49, 279–299. https://doi.org/10.5721/EuJRS20164916

Bothe, O., Fraedrich, K., Zhu, X., 2012. Precipitation climate of Central Asia and the large-scale atmospheric circulation. Theor. Appl. Climatol. 108, 345–354. https://doi.org/10.1007/s00704-011-0537-2

Buermann, W., Anderson, B., Tucker, C.J., Dickinson, R.E., Lucht, W., Potter, C.S., Myneni, R.B., 2003. Interannual covariability in Northern Hemisphere air temperatures and greenness associated with El Niño-Southern Oscillation and the Arctic Oscillation. J. Geophys. Res. Atmos. 108, n/a-n/a. https://doi.org/10.1029/2002JD002630

Bulut, E., Alma, Ö., 2012. A Performance Assessment of Model Selection Criteria When the Number of Objects Is Much Larger than the Number of Variables in PLSR. Eur. J. Appl. Sci. 4, 257–264. https://doi.org/10.5829/idosi.ejas.2012.4.6.1111

Casanueva, A., Rodríguez-Puebla, C., Frías, M.D., González-Reviriego, N., 2014. Variability of extreme precipitation over Europe and its relationships with teleconnection patterns. Hydrol. Earth Syst. Sci. 18, 709–725. https://doi.org/10.5194/hess-18-709-2014

Chong, I., Jun, C., 2005. Performance of some variable selection methods when multicollinearity is present. Chemom. Intell. Lab. Syst. 78, 103–112. https://doi.org/10.1016/J.CHEMOLAB.2004.12.011

Cook, B.I., Smith, T.M., Mann, M.E., 2005. The North Atlantic Oscillation and regional phenology prediction over Europe. Glob. Chang. Biol. 11, 919–926. https://doi.org/10.1111/j.1365-2486.2005.00960.x

CPC-NOAA, 2019. National Oceanographic and Atmospheric Administration (NOAA) Climate Prediction Center (CPC) [WWW Document]. URL

https://www.cpc.ncep.noaa.gov/data/teledoc/telecontents.shtml

Dahlin, K.M., Ault, T.R., 2018. Global linkages between teleconnection patterns and the terrestrial biosphere. Int. J. Appl. Earth Obs. Geoinf. 69, 56–63. https://doi.org/10.1016/J.JAG.2018.02.017

de Beurs, K.. M., Wright, C.K., Henebry, G.M., 2009. Dual scale trend analysis for evaluating climatic and anthropogenic effects on the vegetated land surface in Russia and Kazakhstan. Environ. Res. Lett. 4, 045012. https://doi.org/10.1088/1748-9326/4/4/045012

de Beurs, K.M., Henebry, G.M., 2010. Spatio-Temporal Statistical Methods for Modelling Land Surface Phenology, in: Hudson, I.L., Keatley, M.R. (Eds.), Phenological Research. Springer Science+Business Media B.V., Dordrecht, pp. 177–208. https://doi.org/10.1007/978-90-481-3335-2_9

de Beurs, K.M., Henebry, G.M., 2008. Northern annular mode effects on the land surface phenologies of northern Eurasia. J. Clim. 21, 4257–4279. https://doi.org/10.1175/2008JCLI2074.1

de Beurs, K.M., Henebry, G.M., 2004. Land surface phenology, climatic variation, and institutional change: Analyzing agricultural land cover change in Kazakhstan. Remote Sens. Environ. 89, 497–509. https://doi.org/10.1016/J.RSE.2003.11.006

de Beurs, K.M., Henebry, G.M., Owsley, B.C., Sokolik, I.N., 2018. Large scale climate oscillation impacts on temperature, precipitation and land surface phenology in Central Asia. Environ. Res. Lett. 13, 065018. https://doi.org/10.1088/1748-9326/aac4d0

de Beurs, K.M., Henebry, G.M., Owsley, B.C., Sokolik, I.N., 2015. Using multiple remote sensing perspectives to identify and attribute land surface dynamics in Central Asia 2001-2013. Remote Sens. Environ. 170, 48–61. https://doi.org/10.1016/j.rse.2015.08.018

Efron, B., Tibshirani, R.., 1993. An Introduction to the Bootstrap. Chapman and Hall/CRC.

ERL-NOAA, 2019. NOAA Earth Research Laboratory [WWW Document].

Faber, N.M., 2002. Uncertainty estimation for multivariate regression coefficients. Chemom. Intell. Lab. Syst. 64, 169–179. https://doi.org/10.1016/S0169-7439(02)00102-8

Farrés, M., Platikanov, S., Tsakovski, S., Tauler, R., 2015. Comparison of the variable importance in projection (VIP) and of the selectivity ratio (SR) methods for variable selection and interpretation. J. Chemom. 29, 528–536. https://doi.org/10.1002/cem.2736

Fieller, E.C., Hartley, H.O., Pearson, E.S., 1957. Tests for Rank Correlation Coefficients. I. Biometrika 44, 470. https://doi.org/10.2307/2332878

Fisher, J.I., Mustard, J.F., Vadeboncoeur, M.A., 2006. Green leaf phenology at Landsat resolution: Scaling from the field to the satellite. Remote Sens. Environ. 100, 265–

279. https://doi.org/10.1016/J.RSE.2005.10.022

Geladi, P., Kowalski, B.R.R., 1986. Partial least-squares regression: a tutorial. Anal. Chim. Acta, 185, 1–17.

Gerlitz, L., Steirou, E., Schneider, C., Moron, V., Vorogushyn, S., Merz, B., Gerlitz, L., Steirou, E., Schneider, C., Moron, V., Vorogushyn, S., Merz, B., 2018. Variability of the Cold Season Climate in Central Asia. Part I: Weather Types and Their Tropical and Extratropical Drivers. J. Clim. 31, 7185–7207. https://doi.org/10.1175/JCLI-D-17-0715.1

Giorgi, F., 2006. Climate change hot-spots. Geophys. Res. Lett. 33, 1–4. https://doi.org/10.1029/2006GL025734

Gong, D., Shi, P., 2003. Northern hemispheric NDVI variations associated with large-scale climate indices in spring. Int. J. Remote Sens. 24, 2559–2566. https://doi.org/10.1080/0143116031000075107

Goodin, D.G., Henebry, G.M., 1997. A technique for monitoring ecological disturbance in tallgrass prairie using seasonal NDVI trajectories and a discriminant function mixture model. Remote Sens. Environ. 61, 270–278. https://doi.org/10.1016/S0034-4257(97)00043-6

Groffman, P.M., Driscoll, C.T., Fahey, T.J., Hardy, J.P., Fitzhugh, R.D., Tierney, G.L., 2001. Colder soils in a warmer world: A snow manipulation study in a northern hardwood forest ecosystem. Biogeochemistry 56, 135–150. https://doi.org/10.1023/A:1013039830323

Hall, D.K., Riggs, G.A., Salomonson, V. V., DiGirolamo, N.E., Bayr, K.J., 2002. MODIS snow-cover products. Remote Sens. Environ. 83, 181–194. https://doi.org/10.1016/S0034-4257(02)00095-0

Heck, E., de Beurs, K.M., Owsley, B.C., Henebry, G.M., 2019. Evaluation of the MODIS collections 5 and 6 for change analysis of vegetation and land surface temperature dynamics in North and South America. ISPRS J. Photogramm. Remote Sens. 156, 121–134. https://doi.org/10.1016/J.ISPRSJPRS.2019.07.011

Henebry, G.M., 2019. Methodology II: Remote sensing of change in grasslands, in: Gibson, D.., Newman, J. (Eds.), Grasslands and Climate Change. Cambridge University Press, pp. 40–64. https://doi.org/10.1017/9781108163941.005

Henebry, G.M., 2013. Phenologies of North American Grasslands and Grasses, in: Schwartz, M.D. (Ed.), Phenology: An Integrative Environmental Science. Springer Netherlands, Dordrecht, pp. 197–210. https://doi.org/10.1007/978-94-007-6925-0

Henebry, G.M., de Beurs, K.M., 2013. Remote Sensing of Land Surface Phenology: A Prospectus, in: Phenology: An Integrative Environmental Science. Springer Netherlands, Dordrecht, pp. 385–411. https://doi.org/10.1007/978-94-007-6925-0_21

Hoppe, F., Zhusui Kyzy, T., Usupbaev, A., Schickhoff, U., 2016. Rangeland degradation assessment in Kyrgyzstan: vegetation and soils as indicators of grazing pressure in

Naryn Oblast. J. Mt. Sci. 13, 1567–1583. https://doi.org/10.1007/s11629-016-3915-5

Horel, J.D., Wallace, J.M., 1981. Planetary-Scale Atmospheric Phenomena Associated with the Southern Oscillation. Mon. Weather Rev. 109, 813–829. https://doi.org/10.1175/1520-0493(1981)109<0813:PSAPAW>2.0.CO;2

Hurrell, J.W., 1995. Decadal trends in the north atlantic oscillation: regional temperatures and precipitation. Science (80-.). 269, 676–9. https://doi.org/10.1126/science.269.5224.676

Hurrell, J.W., Kushnir, Y., Ottersen, G., 2003. An overview of the North Atlantic Oscillation, in: Hurrell, J.W., Kushnir, Y., Ottersen, G., Visbeck, M., Visbeck, M.H. (Eds.), The North Atlantic Oscillation: Climatic Significance and Environmental Impact. AGU, Washington, D.C, pp. 1–35. https://doi.org/10.1029/134GM01

Iglesias, I., Lorenzo, M.N., Taboada, J.J., 2014. Seasonal Predictability of the East Atlantic Pattern from Sea Surface Temperatures. PLoS One 9, e86439. https://doi.org/10.1371/journal.pone.0086439

Jiang, L., Guli·J., Bao, A., Guo, H., Ndayisaba, F., 2017. Vegetation dynamics and responses to climate change and human activities in Central Asia. Sci. Total Environ. 599–600, 967–980. https://doi.org/10.1016/J.SCITOTENV.2017.05.012

Jolliffe, I.T., Cadima, J., 2016. Principal component analysis: a review and recent developments. Philos. Trans. R. Soc. A Math. Phys. Eng. Sci. 374, 20150202. https://doi.org/10.1098/rsta.2015.0202

Kariyeva, J., van Leeuwen, W.J.D., 2011. Environmental Drivers of NDVI-Based Vegetation Phenology in Central Asia. Remote Sens. 3, 203–246. https://doi.org/10.3390/rs3020203

Kariyeva, J., van Leeuwen, W.J.D., Woodhouse, C.A., 2012. Impacts of climate gradients on the vegetation phenology of major land use types in Central Asia (1981–2008). Front. Earth Sci. 6, 206–225. https://doi.org/10.1007/s11707-012-0315-1

Kerr, R.A., 2000. A north atlantic climate pacemaker for the centuries. Sci. 288, 1984–5. https://doi.org/10.1126/science.288.5473.1984

Kobayashi, S., Ota, Y., Harada, Y., Ebita, A., Moriya, M., Onoda, H., Onogi, K., Kamahori, H., Kobayashi, C., Endo, H., Miyaoka, K., Takahashi, K., 2015. The JRA-55 Reanalysis: General Specifications and Basic Characteristics. J. Meteorol. Soc. Japan. Ser. II 93, 5–48. https://doi.org/10.2151/jmsj.2015-001

Krehbiel, C., Henebry, G.M., 2016. A Comparison of Multiple Datasets for Monitoring Thermal Time in Urban Areas over the U.S. Upper Midwest. Remote Sens. 8, 297. https://doi.org/10.3390/rs8040297

Krehbiel, C., Zhang, X., Henebry, G., 2017. Impacts of Thermal Time on Land Surface Phenology in Urban Areas. Remote Sens. 9, 499. https://doi.org/10.3390/rs9050499

Kucheryavski, S., 2019. mdatool.

Lehmann, E.L., D'Abrera, H.J.M., 2006. Nonparametrics : statistical methods based on ranks. Springer.

Li, J., Fan, K., Xu, Z., 2016. Links between the late wintertime North Atlantic Oscillation and springtime vegetation growth over Eurasia. Clim. Dyn. 46, 987–1000. https://doi.org/10.1007/s00382-015-2627-9

Li, S., Perlwitz, J., Quan, X., Hoerling, M.P., 2008. Modelling the influence of North Atlantic multidecadal warmth on the Indian summer rainfall. Geophys. Res. Lett. 35, L05804. https://doi.org/10.1029/2007GL032901

Liu, Y., Hill, M.J., Zhang, X., Wang, Z., Richardson, A.D., Hufkens, K., Filippa, G., Baldocchi, D.D., Ma, S., Verfaillie, J., Schaaf, C.B., 2017. Using data from Landsat, MODIS, VIIRS and PhenoCams to monitor the phenology of California oak/grass savanna and open grassland across spatial scales. Agric. For. Meteorol. 237–238, 311–325. https://doi.org/10.1016/J.AGRFORMET.2017.02.026

Liu, Y., Wang, L., Zhou, W., Chen, W., 2014. Three Eurasian teleconnection patterns: spatial structures, temporal variability, and associated winter climate anomalies. Clim. Dyn. 42, 2817–2839. https://doi.org/10.1007/s00382-014-2163-z

Lu, L., Guo, H., Kuenzer, C., Klein, I., Zhang, L., Li, X., 2014. Analyzing phenological changes with remote sensing data in Central Asia. IOP Conf. Ser. Earth Environ. Sci. 17, 012005. https://doi.org/10.1088/1755-1315/17/1/012005

Mehmood, T., Liland, K.H., Snipen, L., Sæbø, S., 2012. A review of variable selection methods in Partial Least Squares Regression. Chemom. Intell. Lab. Syst. 118, 62–69. https://doi.org/10.1016/J.CHEMOLAB.2012.07.010

Melaas, E.K., Friedl, M.A., Zhu, Z., 2013. Detecting interannual variation in deciduous broadleaf forest phenology using Landsat TM/ETM + data. Remote Sens. Environ. 132, 176–185. https://doi.org/10.1016/J.RSE.2013.01.011

Menzel, A., Sparks, T.H., Estrella, N., Eckhardt, S., 2005. "SSW to NNE" - North Atlantic Oscillation affects the progress of seasons across Europe. Glob. Chang. Biol. 11, 909–918. https://doi.org/10.1111/j.1365-2486.2005.00954.x

Myneni, R.B., Hall, F.G., Sellers, P.J., Marshak, A.L., 1995. The interpretation of spectral vegetation indexes. IEEE Trans. Geosci. Remote Sens. 33, 481–486. https://doi.org/10.1109/TGRS.1995.8746029

NASA JPL, 2013. NASA Shuttle Radar Topography Mission Global 1 arc second [Data set] [WWW Document]. NASA EOSDIS L. Process. DAAC. https://doi.org/10.5067/MEaSUREs/SRTM/SRTMGL1.003

National Weather Service, 2019. Climate Prediction Center, Teleconnection Index Calculation Procedures [WWW Document]. URL https://www.cpc.ncep.noaa.gov/data/teledoc/teleindcalc.shtml

Nguyen, L.H., Joshi, D.R., Clay, D.E., Henebry, G.M., 2018. Characterizing land cover/land use from multiple years of Landsat and MODIS time series: A novel

approach using land surface phenology modeling and random forest classifier. Remote Sens. Environ. https://doi.org/10.1016/J.RSE.2018.12.016

Peel, M.C., Finlayson, B.L., McMahon, T.A., 2007. Updated world map of the Köppen-Geiger climate classification. Hydrol. Earth Syst. Sci. 11, 1633–1644. https://doi.org/10.5194/hess-11-1633-2007

Qiao, D., Wang, N., 2019. Relationship between Winter Snow Cover Dynamics, Climate and Spring Grassland Vegetation Phenology in Inner Mongolia, China. ISPRS Int. J. Geo-Information 8, 42. https://doi.org/10.3390/ijgi8010042

Rajalahti, T., Arneberg, R., Berven, F.S., Myhr, K., Ulvik, R.J., Kvalheim, O.M., 2009a. Biomarker discovery in mass spectral profiles by means of selectivity ratio plot. Chemom. Intell. Lab. Syst. 95, 35–48. https://doi.org/10.1016/J.CHEMOLAB.2008.08.004

Rajalahti, T., Arneberg, R., Kroksveen, A., Berle, M., Myhr, K., Kvalheim, O., 2009b. Discriminating Variable Test and Selectivity Ratio Plot: Quantitative Tools for Interpretation and Variable (Biomarker) Selection in Complex Spectral or Chromatographic Profiles. Anal. Chem. 81, 2581–2590. https://doi.org/10.1021/ac802514y

Riggs, G.A., Hall, D.K., 2015. MODIS Snow Products Collection 6 User Guide.

Riggs, G.A., Hall, D.K., 2004. Snow Mapping with the MODIS Aqua Instrument. 61st East. Snow Conf.

Roberts, D.W., Cooper, S. V., 1989. Concepts and techniques of vegetation mapping. In Land Classifications Based on Vegetation:: Applications for Resource Management. Ogden, UT.

Rodwell, M.J., Rowell, D.P., Folland, C.K., 1999. Oceanic forcing of the wintertime North Atlantic Oscillation and European climate. Nature 398, 320–323. https://doi.org/10.1038/18648

Roy, D.P., Kovalskyy, V., Zhang, H.K., Vermote, E.F., Yan, L., Kumar, S.S., Egorov, A., 2016. Characterization of Landsat-7 to Landsat-8 reflective wavelength and normalized difference vegetation index continuity. Remote Sens. Environ. 185, 57–70. https://doi.org/10.1016/J.RSE.2015.12.024

Schillhorn Van Veen, T.W., 1995. The Kyrgyz Sheep Herders at a Crossroads. Overseas Dev. Institute. Pastor. Dev. Netw. Ser.

Still, C.J., Pau, S., Edwards, E.J., 2014. Land surface skin temperature captures thermal environments of C 3 and C 4 grasses. Glob. Ecol. Biogeogr. 3, 286–296. https://doi.org/10.1111/geb.12121

Syed, F.S., Giorgi, F., Pal, J.S., King, M.P., 2006. Effect of remote forcings on the winter precipitation of central southwest Asia part 1: observations. Theor. Appl. Climatol. 86, 147–160. https://doi.org/10.1007/s00704-005-0217-1

Tenenhaus, M., 1998. La regression PLS. Technip, Paris.

Tomaszewska, M.A., Henebry, G.M., 2018. Changing snow seasonality in the highlands of Kyrgyzstan. Environ. Res. Lett. 13, 065006. https://doi.org/10.1088/1748-9326/aabd6f

Tomaszewska, M.A., Nguyen, L.N., Henebry, G.M., 2019. Land Surface Phenology in the Highland Pastures of Montane Central Asia: Interactions with Snow Cover Seasonality and Terrain Characteristics. Remote Sens. Environ. In review.

Tran, T.N., Afanador, N.L., Buydens, L.M.C., Blanchet, L., 2014. Interpretation of variable importance in Partial Least Squares with Significance Multivariate Correlation (sMC). Chemom. Intell. Lab. Syst. 138, 153–160. https://doi.org/10.1016/J.CHEMOLAB.2014.08.005

Tucker, C.J., 1979. Red and photographic infrared linear combinations for monitoring vegetation. Remote Sens. Environ. 8, 127–150. https://doi.org/10.1016/0034-4257(79)90013-0

USGS EROS, 2017. Landsat Collection 1 Level 1 Product Definition. Sioux Falls, SD.

Vetter, S., 2005. Rangelands at equilibrium and non-equilibrium: recent developments in the debate. J. Arid Environ. 62, 321–341. https://doi.org/10.1016/J.JARIDENV.2004.11.015

Viña, A., Henebry, G.M., 2005. Spatio-temporal change analysis to identify anomalous variation in the vegetated land surface: ENSO effects in tropical South America. Geophys. Res. Lett. 32, 1–5. https://doi.org/10.1029/2005GL023407

Wan, Z., Hook, S., Hulley, G., 2015. MOD11A2 MODIS/Terra Land Surface Temperature/Emissivity 8-Day L3 Global 1km SIN Grid V006.

Wang, C., Xie, S., Carton, J.A., 2004. A global survey of ocean-atmosphere interaction and climate variability, in: Wang, C., Xie, S., Carton, J. (Eds.), Earth's Climate: The Ocean-Athmosphere Interaction. AGU, Washington, D. C, pp. 1–19. https://doi.org/10.1029/147GM01

Wang, G., Schimel, D., 2003. Climate change, climate modes, and climate impacts. Annu. Rev. Environ. Resour. 28, 1–28. https://doi.org/10.1146/annurev.energy.28.050302.105444

Wold, H.O.A., 1982. Soft Modeling: The Basic Design and Some Extensions, in: Jöreskog, K.G., Wold, H.O.A. (Eds.), Systems under Indirect Observations: Part II. North-Holland, Amsterdam, pp. 1–54.

Wold, H.O.A., 1966. Estimation of principal components and related models by iterative least squares, in: Krishnajah, P.R. (Ed.), Multivariate Analysis. Academic Press., New York, NY, pp. 391–420.

Wold, S., 1987. Principal Component Analysis. Chemom. Intell. Lab. Syst. 2, 37–52.

Wold, S., Johansson, E., Cocchi, M., 1993. PLS: Partial Least Squares Projections to Latent Structures, in: Kubinyi, H. (Ed.), 3D QSAR in Drug Design. Volume 1: Theory Methods and Applications. Springer Netherlands, pp. 523–550.

Wold, S., Ruhe, A., Wold, H., Dunn, III, W.J., 1984. The Collinearity Problem in Linear Regression. The Partial Least Squares (PLS) Approach to Generalized Inverses. SIAM J. Sci. Stat. Comput. 5, 735–743. https://doi.org/10.1137/0905052

Wold, S., Sjöström, M., Eriksson, L., 2001. PLS-regression: a basic tool of chemometrics. Chemom. Intell. Lab. Syst. 58, 109–130. https://doi.org/10.1016/S0169-7439(01)00155-1

Wolter, K., Timlin, M.S., 2011. El Niño/Southern Oscillation behaviour since 1871 as diagnosed in an extended multivariate ENSO index (MEI.ext). Int. J. Climatol. 31, 1074–1087. https://doi.org/10.1002/joc.2336

Wolter, K., Timlin, M.S., 1993. Monitoring ENSO in COADS with a Seasonally Adjusted Principal Component Index, in: Proceedings of the 17th Climate Diagnostics Workshop. Norman, OK, pp. 52–57.

Wright, C.K., de Beurs, K.M., Henebry, G.M., 2014. Land surface anomalies preceding the 2010 Russian heat wave and a link to the North Atlantic oscillation. Environ. Res. Lett. 9, 124015. https://doi.org/10.1088/1748-9326/9/12/124015

Yeh, S., Cai, W., Min, S., McPhaden, M., Dommenget, D., Dewitte, B., Collins, M., Ashok, K., An, S., Yim, B., Kug, J., 2018. ENSO Atmospheric Teleconnections and Their Response to Greenhouse Gas Forcing. Rev. Geophys. 56, 185–206. https://doi.org/10.1002/2017RG000568

Yin, Z., Wang, H., Liu, X., 2014. A Comparative Study on Precipitation Climatology and Interannual Variability in the Lower Midlatitude East Asia and Central Asia. J. Clim. 27, 7830–7848. https://doi.org/10.1175/JCLI-D-14-00052.1

Zhang, X., Wang, J., Gao, F., Liu, Y., Schaaf, C., Friedl, M., Yu, Y., Jayavelu, S., Gray, J., Liu, L., Yan, D., Henebry, G.M., 2017. Exploration of scaling effects on coarse resolution land surface phenology. Remote Sens. Environ. 190, 318–330. https://doi.org/10.1016/J.RSE.2017.01.001

Zhumanova, M., Mönnig, C., Hergarten, C., Darr, D., Wrage-Mönnig, N., 2018. Assessment of vegetation degradation in mountainous pastures of the Western Tien-Shan, Kyrgyzstan, using eMODIS NDVI. Ecol. Indic. 95, 527–543. https://doi.org/10.1016/j.ecolind.2018.07.060

Zhumanova, M., Wrage-Mönnig, N., Darr, D., 2016. Farmers' Decision-making and Land Use Changes in Kyrgyz Agropastoral Systems. Mt. Res. Dev. 36, 506–517. https://doi.org/10.1659/MRD-JOURNAL-D-16-00030.1

4.10. Supplementary materials

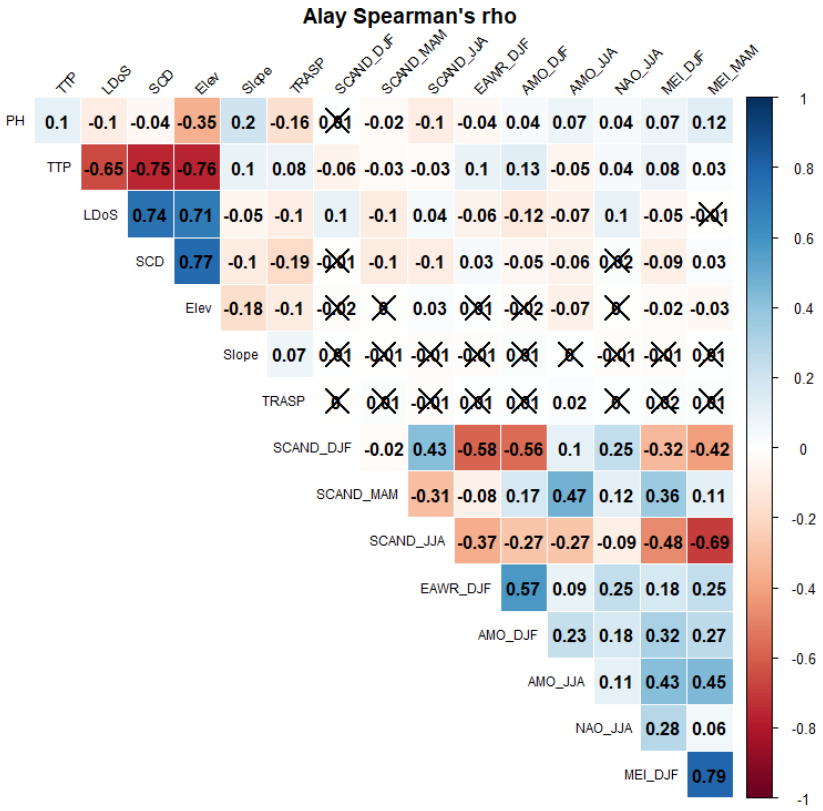

Figure S4.1. Spearman's rho coefficient of correlation for Alay rayon. Significant level at p-value < 0.05 Correlation coefficients with p > 0.05 are crossed out. In reds, negative values of rho; in blues, positive values.

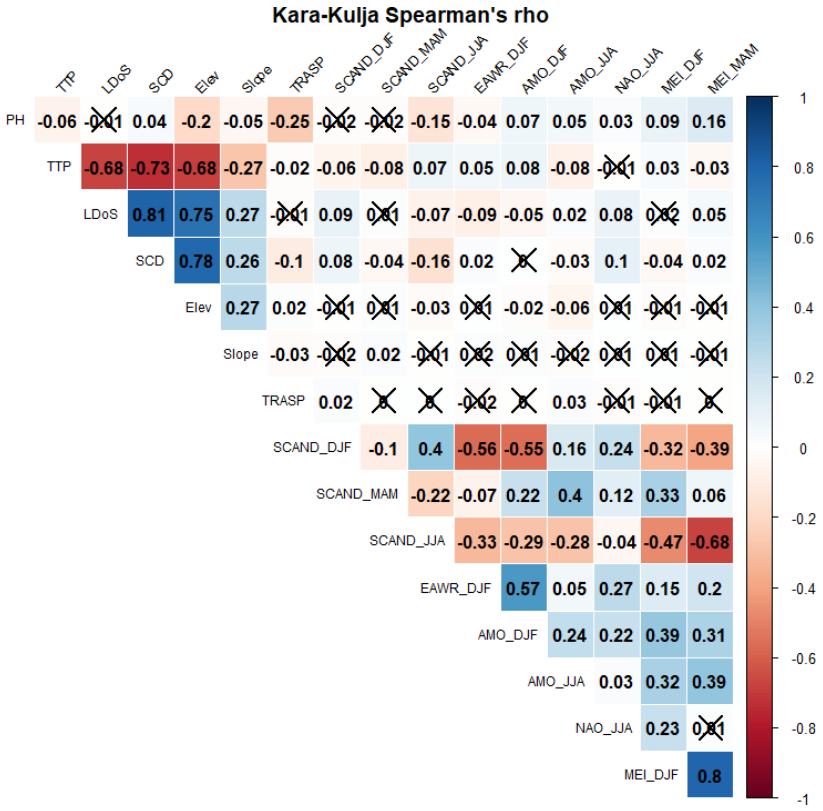

Figure S4.2. Spearman's rho coefficient of correlation for Kara-Kulja rayon. Significant level at p-value < 0.05 Correlation coefficients with p > 0.05 are crossed out. In reds, negative values of rho; in blues, positive values.

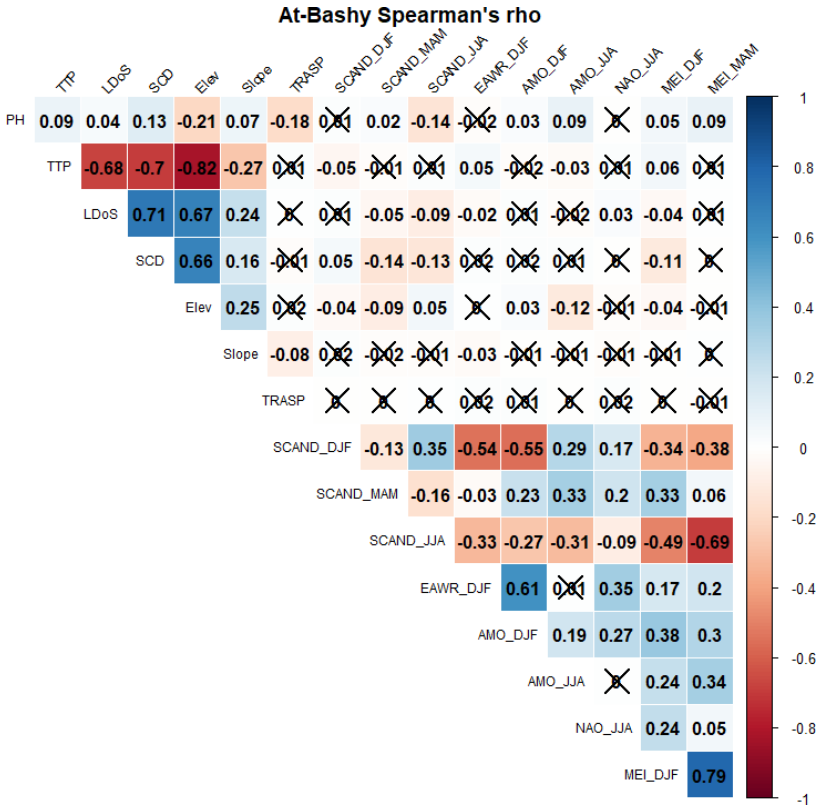

Figure S4.3. Spearman's rho coefficient of correlation for At-Bashy rayon. Significant level at p-value < 0.05 Correlation coefficients with p > 0.05 are crossed out. In reds, negative values of rho; in blues, positive values.

Table S4.1. Final TTP models based on different variable selection (VS) methods. **The same models in bold;** *positive values in italics***.**

TTP	**VS method**	**Final model**
Chong Alay	VIP	3211.4 - 0.39 × Elevation - 2.15 × SCD - 3.03 × Slope - 0.93 × LDoS
	SR	3335.5 - 0.42 × Elevation - 2.08 × SCD - 1.21 × LDoS
	RC	3590.3 - 0.34 × Elevation - 2.19 × SCD + *108.5* × *NAO JJA* - 2.51 × LDoS
Alay	VIP	3114.7 - 0.17 × Elevation - 2.21 × SCD - 3.07 × LDoS -6.07 × AMO JJA
	SR	**3103.9 - 0.17 × Elevation - 2.20 × SCD - 3.06 × LDoS**
	RC	**3103.9 - 0.17 × Elevation - 2.20 × SCD - 3.06 × LDoS**
Kara-Kulja	VIP	**2874.3 - 1.86 × SCD - 2.98 × LDoS - 0.15 × Elev**
	SR	**2874.3 - 1.86 × SCD - 2.98 × LDoS - 0.15 × Elev**
	RC	**2874.3 - 1.86 × SCD - 2.98 × LDoS - 0.15 × Elev**
At-Bashy	VIP	3412.9 - 0.35 × Elevation -1.92 × SCD - 2.96 × LDoS - 153.6 × SCAND MAM
	SR	3306.2 - 0.42 × Elevation - 1.52 × SCD - 1.99 × LDoS
	RC	2779.1 - 0.36 × Elevation - 3.24 × SCD + *15.33* × *NAO JJA*
Naryn	VIP	3226.3 - 0.33 × Elevation - 1.83 × SCD - 2.69 × LDoS - 120.25 × SCAND MAM
	SR	3180.9 - 0.41 × Elevation - 1.56 × SCD - 1.83 × LDoS
	RC	3267.2 - 0.35 × Elevation - 1.74 × SCD - 2.4 × LDoS + *70.4* × *NAO JJA*

Table S4.2. Final PH models based on different variable selection (VS) methods. "—" = no model built. *Positive values in italics*.

PH	VS method	Final model
Chong-Alay	VIP	$0.50 - 6.0 \times 10^{-5} \times \text{Elevation} + \textit{0.0006} \times \textit{SCD} - \textit{0.07} \times \textit{TRASP} - 0.03 \times \text{SCAND JJA} + \textit{0.02} \times \textit{MEI MAM}$
	SR	—
	RC	$0.54 - 7.0 \times 10^{-5} \times \text{Elevation} + \textit{0.0008} \times \textit{SCD} - 0.09 \times \text{TRASP} - 0.03 \times \text{SCAND JJA}$
Alay	VIP	$0.62 - 2.5 \times 10^{-4} \times \text{Elevation} + \textit{0.001} \times \textit{LDoS} + \textit{0.001} \times \textit{SCD}$
	SR	—
	RC	$0.86 - 2.4 \times 10^{-4} \times \text{Elev} + \textit{0.002} \times \text{SCD}$
Kara-Kulja	VIP	$0.79 - 0.1 \times \text{TRASP} - 4.0 \times 10^{-5} \times \text{Elevation} - 0.04 \times \text{SCAND JJA} + \textit{0.02} \times \textit{MEI MAM}$
	SR	—
	RC	$0.82 - 0.13 \times \text{TRASP} - 6.0 \times 10^{-5} \times \text{Elevation} + \textit{0.03} \times \textit{MEI MAM} + \textit{0.0001} \times \textit{SCD}$
At-Bashy	VIP	$0.71 + \textit{0.001} \times \textit{SCD} - 1.0 \times 10^{-4} \times \text{Elevation} - 0.11 \times \text{TRASP} - 0.02 \times \text{SCAND JJA}$
	SR	—
	RC	$0.72 + \textit{0.001} \times \textit{SCD} - 1.0 \times 10^{-4} \times \text{Elevation} - 0.12 \times \text{TRASP}$
Naryn	VIP	$0.12 + \textit{0.0005} \times \textit{SCD} + \textit{0.0007} \times \textit{LDoS} + \textit{3.0} \times \textit{10}^{-5} \times \textit{Elevation} - 0.04 \times \text{TRASP}$
	SR	$0.32 + \textit{0.0012} \times \textit{SCD} + \textit{0.00007} \times \textit{LDoS}$
	RC	$0.12 + \textit{0.0005} \times \textit{SCD} + \textit{0.0007} \times \textit{LDoS} + \textit{3.0} \times \textit{10}^{-5} \times \textit{Elevation} - 0.04 \times \text{TRASP} - 0.24 \times \text{SCAND JJA}$

CHAPTER 5

RESEARCH SUMMARY AND RECOMMENDATIONS

5.1. Research summary and key findings

Remote sensing investigations of variability in montane pastures phenology and the impacts of snow cover in Central Asia have been frequently carried out (i) on regional base i.e. across Central Asia, with no specific focus on Kyrgyzstan, (ii) by using rather coarse spatial resolution datasets (at least 500m), or (iii) if using higher spatial resolution datasets, the focal areas have been limited to specific parts of the Kyrgyzstan as case studies. Therefore, in the light of lacking extensive spatial and temporal studies over Kyrgyzstan, I recognized the need for a comprehensive approach that would aim to evaluate the temporal phenology variability of pasturelands, which serve as the basis of the economy and livelihoods in rural Kyrgyzstan.

In this study, first, I analyzed changes in snow cover seasonality metrics across Kyrgyzstan over 2002-2016. Then, I described changes in land surface phenology (LSP) metrics of highland pastures across Kyrgyz Republic between 2001 to 2017. Further, I investigated the impact of snow cover seasonality on LSP of pastures, and how that influence differs depending on the terrain characteristic. Finally, I analyzed whether the large and regional scale climate oscillation mode influences can be detectable and captured by changes in LSP at large scale. Those five aspects have been addressed in three research studies and translated into three peer-reviewed manuscripts submitted to scientific journals, of which one is already published in *Environmental Research Letters*, the second is in revision

following review at *Remote Sensing of Environment*, and the third in review following revision at the *International Journal of Applied Earth Observation and Geoinformation*.

I summarize the key findings of my research as follows.

Chapter 2, Research Study #1: In this study, my goal was to analyze various aspects of snow cover seasonality to detect where significant changes had occurred in Kyrgyzstan over 2002-2016 and, if they occurred, how were they linked to terrain features. I used 500m MODIS 8-day snow cover composites to calculate snow cover seasonality metrics: First Date of Snow (FDoS) and snowmelt (Last Date of Snow, LDoS), and duration of snow cover season (DoSS). I found that (i) more territory has been experiencing earlier onset of snow than earlier snowmelt, and around equivalent areas have been experiencing longer and shorter duration of snow seasons; (ii) significant shifts toward earlier snow onset that occurred in western and central Kyrgyzstan, while significant shifts toward earlier snow departure appeared in eastern part; (iii) a significant duration of the snow season shortening across western and eastern Kyrgyzstan and a significant extension over northern and southwestern parts. Moreover, duration was significantly longer where the snow onset occurred significantly earlier or the snowmelt significantly later; (iv) a general trend of significantly earlier snowmelt below 3400m, and the area of earlier snowmelt was 15 times greater in eastern than western rayons.

Chapter 3, Research Study #2: In this study, I focused on land surface phenology of highland pastures and its interactions with snow cover seasonality from 2001 through 2017; namely, to characterize how snow cover seasonality relates to subsequent land surface phenology, and how much mountainous terrain shapes those relationships. Using more than 13K Landsat images at 30 m to model land surface phenology as a function of thermal

time based on from 1 km MODIS 8-day Land Surface Temperature (LST) products, and 500m MODIS 8-day snow cover composites for snow cover seasonality metrics, viz., the same three (FDoS, LDoS, DoSS) as in research study #1 and one additional metric: the number of snow covered dates (SCD). Analysis of the data revealed the following patterns: (i) predominant trends of increasing peak NDVI in highland pastures; (ii) positive relationships between snow covered dates and modeled peak NDVI (PH) over more than 8% of the 68,881 km^2 of analyzed pasturelands; (iii) more negative correlations between snow cover onset and PH, and more positive correlations between snowmelt timing and PH, thereby producing a longer snow season, which can positively influence PH; (iv) significant negative correlations between Thermal Time to Peak (TTP) and SCD over more than 11% of analyzed pasturelands, and a comparable but smaller area of negative correlations between TTP and snowmelt date and, thus, more snow covered dates translated into fewer growing degree-days accumulated to reach the thermal time to peak NDVI in the subsequent growing season; and (v) stronger influence of terrain on the timing of snowmelt than on the number of snow covered dates, wherein slope was more important than aspect, and the strongest effect appeared from the interaction of aspect and the steepest slopes.

Chapter 4, Research Study #3: In this study, I followed up the findings of de Beurs et al., (2018), who found significant correlations of land surface phenology metrics and climate oscillation modes over Central Asia using coarse spatial resolution datasets (~5km MODIS NDVI and ~50km for precipitation and temperature). Here I re-used many datasets from research study #2: (i) two LSP metrics of the Peak Height (PH) and the Thermal Time to Peak (TTP); (ii) two snow cover seasonality metrics of the Last Date of Snow (LDoS) and

the number of Snow Cover Dates (SCD); and (iii) three terrain features based on the 30 m DEM. I found that: (i) thermal time accumulation could be explained mostly by elevation and snow cover metrics, leading to reduced models via Partial Least Squares (PLS) regression, explaining 55 to 70% of observed variation in TTP; (ii) significant relationships of spring SCAND and summer NAO and AMO with TTP, but their respective contributions to predictive power were negligible; (iii) only up to 29% of PH variability was captured by any PLS model; (iv) spring MEI and summer SCAND were significant predictors for PH, but they had no influence on modeling performance; (v) indirect effects of seasonal climate oscillations were overridden by terrain influences (primarily elevation) and snow cover timing. In short, climate oscillation modes did not manifest significant impacts in mountain pastures using LSP metrics when observed at fine spatial resolution. Rather, terrain and snow cover effects predominated.

5.2. Recommendations and future directions

Although, in this study I concentrated strictly on environmental and climate-induced impacts on pasture vegetation, human activities play a role in influencing pasture phenology, primarily through grazing management, which can lead to increased pasture degradation. According to official data, about 70% of natural pastures may be degraded (Sabyrbekov, 2019) due to environmental and anthropogenic factors—through encroachment of invasive and unpalatable species that, in turn, could affect pasture phenology. Studies have shown that unpalatable vegetation can increase vegetation indices (Eddy et al., 2017; Karnieli et al., 2013; Zhumanova et al., 2018). This situation may lead to uncertainties since I used NDVI time series as proxies for pasture productivity. To alleviate this issue, I focused on the early season green-up phase, when environmental

effects are most evident and management effects are minimal. However, results from Research Study #2 (c.f. Chapter 3, Tomaszewska et al., 2019) show significant increasing trends of peak NDVI over pasture areas, which might be interpreted as a result of vegetation degradation rather than improvement. Zhumanova et al. (2018) suggested that usage of enhanced vegetation index (EVI; Huete et al., 2002) would allow for better capturing semi desert pastures phenology. EVI is more NIR sensitive and responsive to canopy structural variations and canopy type, in contrast to NDVI that is more sensitive to chlorophyll and responds more strongly to variation in the red band. Comparison of different vegetation indices performance would be a reasonable step in the future studies of pasture phenology dynamics. Using a combination of Sentinel-2 and Landsat observations would enrich the number of observations and, potentially, decrease the number of unsuccessful fits.

However, a recent study has shown in a simpler agricultural settings, using multiple sensors does not necessarily produce better characterization of the LSP metrics (Nguyen and Henebry, 2019). Moreover, a thorough investigation of the pixels in which the model fitting failed due to unfavorable environmental conditions or weather anomalies could be an alternative approach to link pasture phenology to climate oscillation modes. A further approach might focus on those years with extreme climate oscillation index values and analyze seasonal weather conditions over region to determine if the anomalous conditions were detectable through the phenometrics. Another option would be to extend the study in Chapter 4 to explore the potential roles of the Siberian High (Yihui, 1990) and the Indian Ocean dipole (Saji et al., 2006), on influencing regional weather patterns in Kyrgyzstan. Further, the selection of specific years, e.g., colder/drier and warmer/wetter, would allow describing in detail: (i) how the phenometrics behave under different weather sequences;

(ii) if the behaviors vary due to the terrain features; and (iii) whether interactions between snow cover seasonality and pasture phenology diverges or converge.

In this research, I have focused only on optical and thermal data. An interesting complementary approach for snow-phenology studies would be to use microwave data, which could allow retrieval of other snow parameters such as snow depth and density or snow water equivalent (water content obtained from melting snow). Wang et al. (2018) using 8 km Global Inventory Modeling and Mapping Studies (GIMMS) NDVI from 1981 through 2011 and daily snow water equivalent (SWE) observations at 25 km for the 1982–2011 from GlobSnow SWE product, showed that winter snow accumulation can strongly affect vegetation productivity, but increased winter snow accumulation did not proportionally translate into delayed snowmelt. Thus, vegetation may take advantage of the greater snow accumulation during winter season, which may not always be reflected in the snowmelt timing, through increased soil moisture conditions in growing season. Moreover, in some regions, Wang et al., (2018) found that spring onset dates were not always synchronized with snowmelt date (due to insufficient heat accumulation after snowmelt and light limitation).

Eventually, the introduction of additional datasets with higher spatial, temporal resolutions could improve the precision and accuracy of the analyses, especially over the challenging terrain of montane Kyrgyzstan and beyond.

5.3. References

de Beurs, K.M., Henebry, G.M., Owsley, B.C., Sokolik, I.N., 2018. Large scale climate oscillation impacts on temperature, precipitation and land surface phenology in Central Asia. Environ. Res. Lett. 13, 065018. https://doi.org/10.1088/1748-9326/aac4d0

Eddy, I.M.S., Gergel, S.E., Coops, N.C., Henebry, G.M., Levine, J., Zerriffi, H., Shibkov, E., 2017. Integrating remote sensing and local ecological knowledge to monitor rangeland dynamics. Ecol. Indic. 82, 106–116. https://doi.org/10.1016/J.ECOLIND.2017.06.033

Huete, A., Didan, K., Miura, T., Rodriguez, E.P., Gao, X., Ferreira, L.G., 2002. Overview of the radiometric and biophysical performance of the MODIS vegetation indices. Remote Sens. Environ. 83, 195–213. https://doi.org/10.1016/S0034-4257(02)00096-2

Karnieli, A., Bayarjargal, Y., Bayasgalan, M., Mandakh, B., Dugarjav, C., Burgheimer, J., Khudulmur, S., Bazha, S.N., Gunin, P.D., 2013. Do vegetation indices provide a reliable indication of vegetation degradation? A case study in the Mongolian pastures. Int. J. Remote Sens. 34, 6243–6262. https://doi.org/10.1080/01431161.2013.793865

Nguyen, L.H., Henebry, G.M., 2019. Characterizing Land Use/Land Cover Using Multi-Sensor Time Series from the Perspective of Land Surface Phenology. Remote Sens. 11, 1677. https://doi.org/10.3390/rs11141677

Sabyrbekov, R., 2019. Income diversification strategies among pastoralists in Central Asia: Findings from Kyrgyzstan. Pastoralism 9. https://doi.org/10.1186/s13570-019-0152-x

Saji, N.H., Xie, S.-P., Yamagata, T., 2006. Tropical Indian Ocean Variability in the IPCC Twentieth-Century Climate Simulations. J. Clim. 19, 4397–4417. https://doi.org/10.1175/JCLI3847.1

Tomaszewska, M.A., Nguyen, L.N., Henebry, G.M., 2019. Land surface phenology in the highland pastures of montane Central Asia: Interactions with snow cover seasonality and terrain characteristics. Remote Sens. Environ. In revision following review.

Wang, X., Wang, T., Guo, H., Liu, D., Zhao, Y., Zhang, T., Liu, Q., Piao, S., 2018. Disentangling the mechanisms behind winter snow impact on vegetation activity in northern ecosystems. Glob. Chang. Biol. 24, 1651–1662. https://doi.org/10.1111/gcb.13930

Yihui, D., 1990. Build-up, air mass transformation and propagation of Siberian high and its relations to cold surge in East Asia. Meteorol. Atmos. Phys. 44, 281–292. https://doi.org/10.1007/BF01026822

Zhumanova, M., Mönnig, C., Hergarten, C., Darr, D., Wrage-Mönnig, N., 2018. Assessment of vegetation degradation in mountainous pastures of the Western Tien-Shan, Kyrgyzstan, using eMODIS NDVI. Ecol. Indic. 95, 527–543. https://doi.org/10.1016/j.ecolind.2018.07.060